Alkyl-heteroatom Bond Forming Reactions from the Late Transition Metals

Tyler Eugene Stevens

A dissertation submitted

in partial fulfillment of the

requirements for the degree

Doctor of Philosophy

University of Washington

2016

Reading Committee:

Karen I. Goldberg, Chair

Brandi M Cossairt

D. Michael Heinekey

Program Authorized to Offer Degree:

Chemistry

University of Washington

Abstract

Alkyl-heteroatom Bond Forming Reactions from the Late Transition Metals

Tyler Eugene Stevens

Chair of the Supervisory Committee:

Professor Karen I. Goldberg

Department of Chemistry

$C(sp^3)$-N bond formation is a potential high value reaction in transition metal catalysis, however, only a handful of examples of this fundamental coupling reaction step have been reported. Presented in this thesis are new efforts to promote this challenging reaction. Group 9 and 10 metals bound by the pincer ligands Pybox and PCP, respectively, were initially investigated. Evidence suggests the Ir-Et complex ([(^{dm}Pybox)Ir(Et)(OAc)][PF_6] (**12**)) undergoes a β-H deprotonation, similar to an E2 type elimination in organic chemistry, rather than the desired S_N2 nucleophilic attack. Use of strong nucleophiles, i.e. sulfur nucleophiles, resulted in the ring opening of the pybox ligand. Ir-Et complexes bound by the ^{Me}BPA ligand ([(^{Me}BPA)Ir(OOCR)Et][PF_6] (**20** and **21**)), however, did undergo the desired reaction to form C-N bonds upon reaction with neutral nitrogen nucleophiles. A computational investigation of the mechanism revealed that rather than the direct attack at the Ir-Et (generally observed for high

valent Pd and Pt) the complex first undergoes β-hydrogen elimination to form an Ir ethylene complex. Nucleophilic attack by amine at the olefin then forms the C-N bond. In the final chapter the synthesis and characterization of new a new Rh-Me complex ((DPEphos)RhMe$(I)_2$ (**25**)), which undergoes C(sp^3)-I reductive elimination, is described. A kinetic investigation of the mechanism indicated two competing mechanisms involving S_N2 attack by iodide at both cationic and neutral Rh-Me species. The demonstration of bond formation via nucleophilic attack at the Rh-Me allowed for the room temperature functionalization of the methyl ligand with both nitrogen and sulfur nucleophiles.

Table of Contents

List of Figures

List of Tables

Numbering Scheme

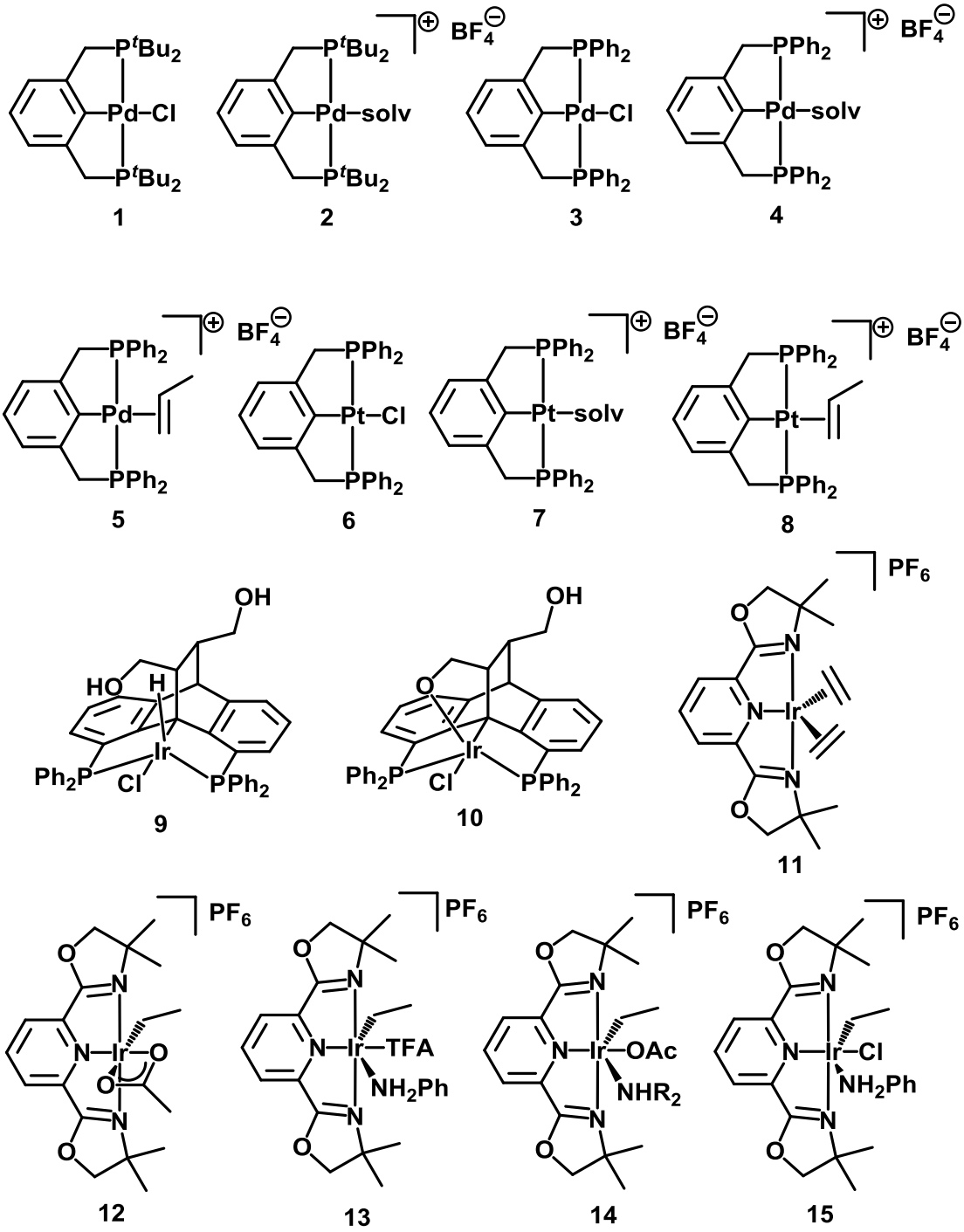

x

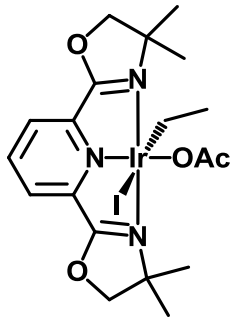

16

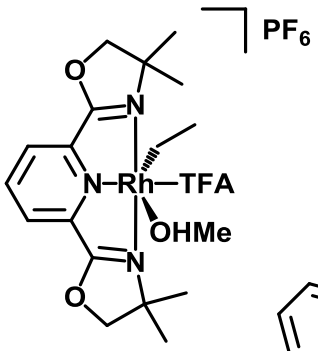

17

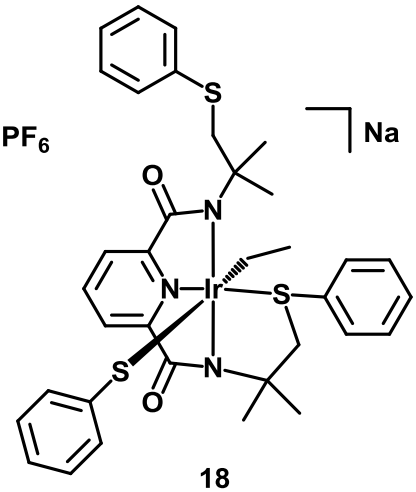

18

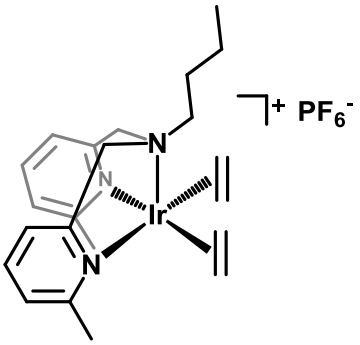

19

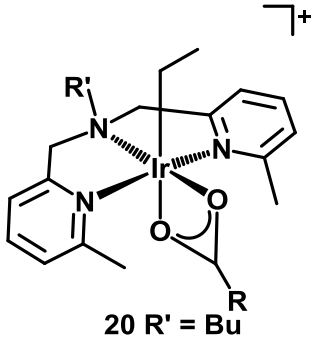

20 R' = Bu

21 R' = Me

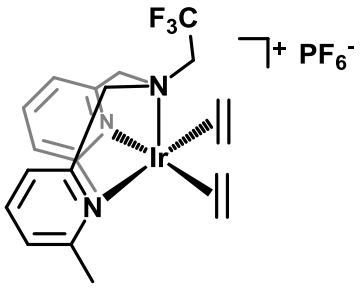

22

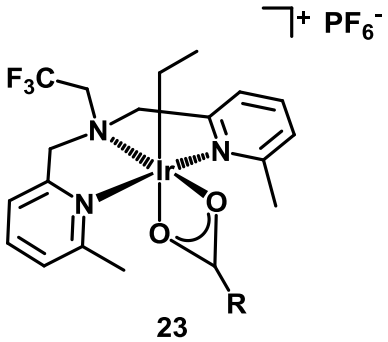

23

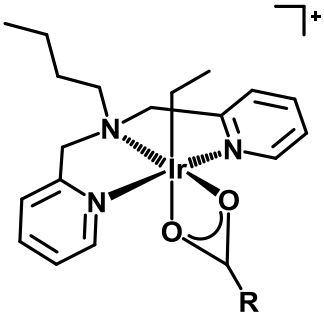

24

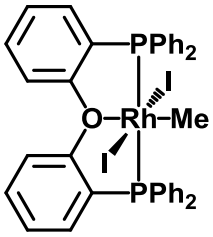

25

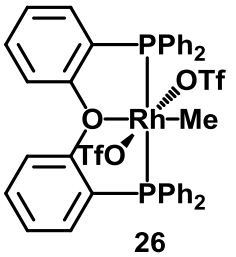

26

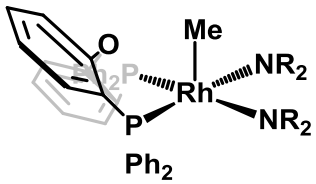

27

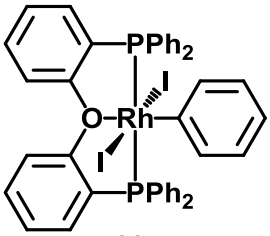

28

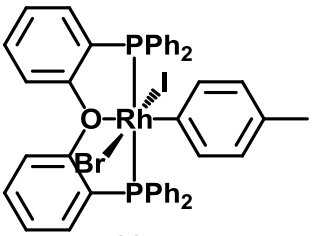

29

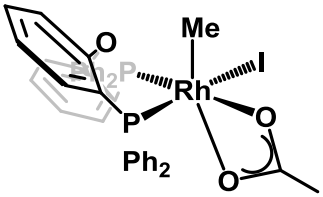

30

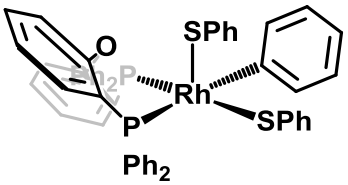

31

Glossary

9-BBN:	9-borabicyclo[3.3.1]nonane
anthraphos	1,8-*bis*-(diphenylphosphino)anthracene
BAr^F_4:	$[B(3,5\text{-}(CF_3)_2C_6H_3)_4]$
BPA:	*N*,*N*-bis(2-pyridylmethyl)butylamine)
^{Me,Me}BPA:	*N*,*N*-bis(6-methyl-2-pyridylmethyl)methylamine)
$^{Me,n\text{-}Bu}$BPA:	*N*,*N*-bis(6-methyl-2-pyridylmethyl)butylamine)
COD:	1,5-cyclooctadiene
COE:	*cis*-cyclooctene
DPEphos:	(Oxydi-2,1-phenylene)bis(diphenylphosphine)
dppbz:	1,2-bis(diphenylphosphino)benzene
IPr:	1,3-bis(2,6-diisopropylphenyl)-1,3-dihydro-2*H*-imidazole-2--ylidene
OAc:	acetate
OBz:	benzoate
OTf:	triflate
^{Ph}PCP:	1,3-bis-(di-phenyl-phosphinomethyl)benzene
^{dm}Pybox:	2,6-bis[4',4'-dimethyloxazolin-2'-yl]pyridine
(*S*)-DTBM-Segphos:	(*S*)-(+)-5,5'-Bis[di(3,5-di-*tert*-butyl-4-methoxyphenyl)phosphino]4,4'-bi-1,3-benzodioxole
TFA:	trifluoroacetate
THF:	tetrahydrofuran
TPA:	*N*,*N*,*N*(tri-2-pyridylmethyl)amine)
^{Me}TPA:	*N*,*N*,*N*-tri(6-methyl-2-pyridylmethyl)amine
TPP:	tetraphenylporphyrin

Acknowledgements

Karen, thank you for the support and encouragement you provided throughout my time in graduate school. I appreciate the high standards you hold people to and feel that it has made me a better scientist. It is obvious that you care not only for the success of your students, but also their well-being. As such, you have created an excellent atmosphere for expanding knowledge (and fun!). It has truly been inspiring to work with you and I thoroughly enjoyed our many discussions about kinetics.

Thank you, Mike, for teaching me about NMR spectroscopy. I owe much of my understanding of the subject to you. Brandi, Gojko, Jim, and Ron, thank you for everything you taught me along the way. You all contributed greatly to my knowledge.

Chapter 4 would not have been possible without the help of Tom Cundari. Thank you, Tom, for teaching me how to setup and run computations.

Todd, thank you your guidance as an undergraduate student. You were an excellent mentor and really sparked my excitement for chemistry (and skiing!). I appreciate all of your help and advice as I considered graduate school options. Dr. Kemp and Dr. Whalen were also crucial in this decision (as well as my interest in chemistry).

The students and post-docs in the Goldberg lab made it a great place to be. I have had the opportunity to work with some exceptional people over the years and I thank them for everything they taught me. I would especially like to thank Alex, Gene, Joe, Kate, Magnus, and Margaret for their help and guidance. Thank you to Karena, Jon, Wilson, and Zuzana for many helpful discussions and for making lab a thoroughly enjoyable experience. To the newer members of the Goldberg group: Alex, Amy, Braden, Byongjoo, Hannah, Jessica, Natalie, Sophia, and Zoha, I have enjoyed working with you and know you all will excel.

I am thankful both for my long-time friends, and the new friends I have made in Seattle. Ariel, Bob, Erika, Jackie, Jean, Jody, Kieran, Kim, Kris, Kristen, Lisa, Patricia and Todd: thank you for always being supportive. Ben, Caroline, Carolyn, Cecily, Erica, Jon, Karena, Kim, Louise, Mike, Sophia (Cherry and Sidhu), Travis, Wilson, and Zuzana: Thank you for making Seattle feel like home, and to many of the same people, for the extreme kindness when I broke my femur attempting STP. On that note, I thoroughly enjoyed cycling around the Seattle area with Ben, Carolyn, Wilson, and Zuzana, and "powering" up hills with Caroline. Thank you to Carolyn and Erica for getting coffee with me- it got me through some long afternoons.

I could not have done this without the support of all of my wonderful family. Sadly, my grandma Betty and grandpa Gene are no longer with us, but I would not be here without them. Thank you, grandma Lolo, for checking in on me weakly and for sending care packages (I know you often drove through many feet of snow to do so). Thank you, Danielle, mom, and dad for everything- words cannot express my gratitude!

Chapter 1

Hydroamination Catalyzed by the Late Transition Metals

1.1 Introduction

The terminal amine is a common industrially important functional group used in the synthesis of both pharmaceuticals and commodity chemicals.[1] For example, Nylon 6,6 is produced on a 2 million ton scale annually. This important polymer is synthesized from adipic acid and hexamethylene diamine. Currently, most terminal alkylamines are produced by a multi-step process;[2] First, terminal alcohols are synthesized by reduction of aldehydes obtained via the oxo process (catalyzed by Co or Rh). Reaction of amines (or ammonia) with these alcohols (Figure 1.1) (catalyzed by a solid state catalyst) yields the desired alkylamines, however, over amination (reaction of the product amine with the terminal alcohol to form secondary and tertiary amines) is a common problem.

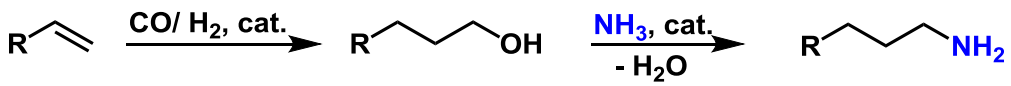

Figure 1.1. Current method for synthesis of terminal amines.

As the demand for linear alkyl amines is high, improved synthetic methods that are both efficient and selective would be of great utility. Hydroamination, the direct addition of a N-H bond across a C-C multiple bond (Figure 1.2), is an attractive alternative, as it meets both the aforementioned criteria. This single-step process is 100 % atom efficient and utilizes readily available chemical feedstocks. This process is calculated to have a ΔG of -3.5 kcal mol^{-1} for the reaction of ethylene and ammonia, however a high activation barrier due to electrostatic repulsion between the amine and olefin necessitates the use of a catalyst.[3] Hartwig et al. directly measured the thermodynamics for the Pd catalyzed hydroamination of vinyl arenes to be quite close to the calculated value above. It was shown that the reaction was slightly more favorable for the addition of electron rich anilines, such as m-anisidine ($\Delta G = -3.54 \pm 0.01$) to styrene than for aniline ($\Delta G = -0.18 \pm 0.01$ kcal mol^{-1}).[4]

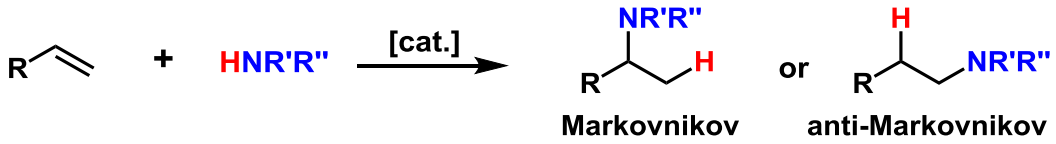

Figure 1.2. Hydroamination of olefins.

In hydroamination, there are two possible regioisomers, the Markovnikov and anti-Markovnikov products (Figure 1.2). Obtaining the anti-Markovnikov selectivity represents a particularly difficult challenge, and was listed as one of the "Ten Challenges in Catalysis" in 1993.[5] Despite significant advances in the field, this still remains a challenge today.

Hydroamination reactions catalyzed by rare earth and early metals have largely been used for intramolecular cyclizations of aminoalkenes. Early work by Marks showed the Cp'_2Ln based catalysts effectively catalyzed the hydroamination of aminoalkenes to form 5 –

7 member rings with Markovnikov selectivity.[6] Mechanistic studies indicated the C-N bond was formed by insertion of the olefin into the Ln-amido. Subsequent protonolysis yielded the cyclized product (Figure 1.3).

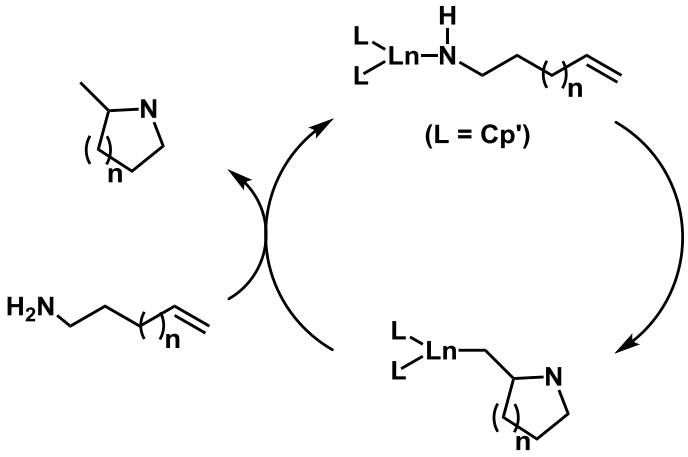

Figure 1.3. Proposed catalytic cycle for intermolecular hydroamination using Ln complexes. Figure reproduced from reference 10b.

Hydroamination catalyzed by the early metals was reported by the laboratories of Bergman[7] and Livinghouse.[8] It was shown that the early metals were effective catalysts for the addition of amines to alkynes. Mechanistic studies by Doye et al.[9] indicated the C-N bond was formed by a 2 + 2 cycloaddition. Protonolysis yielded the product (Figure 1.4).

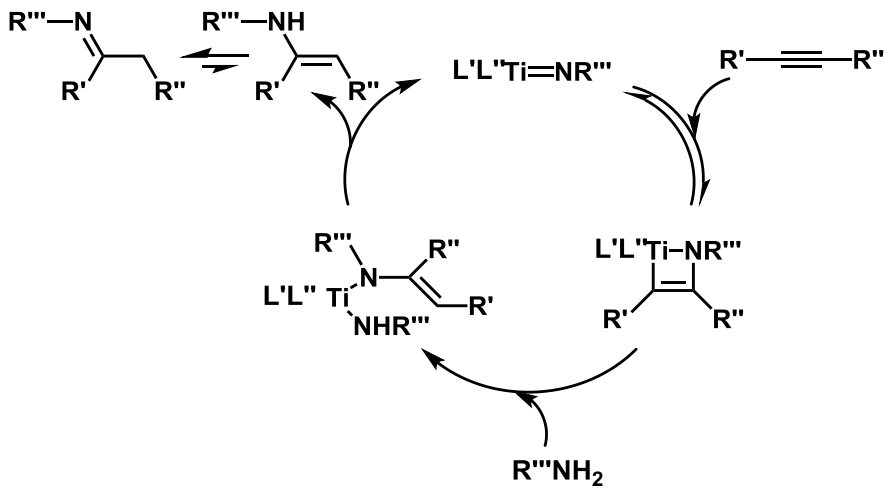

Figure 1.4. Proposed catalytic cycle for hydroamination of alkynes catalyzed by Ti complexes. Figure reproduced from reference 10b.

While the early metals and rare earths have proved to be effective catalysts for the hydroamination of alkynes and intramolecular hydroamination of alkenes, intermolecular hydroamination of alkenes is much more challenging.[10] The late transition metals generally have better functional group tolerance and higher stability toward oxygen. Thus this dissertation will focus on late metal catalyzed hydroamination with emphasis on the C-N coupling step.

1.2 Intermolecular late metal catalyzed hydroamination.

In 1971, Coulson reported the first example of homogeneously catalyzed hydroamination of ethylene and secondary amines catalyzed by Rh and Ir salts.[11] Strongly nucleophilic and sterically unencumbered amines were most effective under these conditions (Amine:Ethylene:$RhCl_3 \cdot 3H_20$ = 350:100:1, THF, 200 ˚C), with piperidine giving the highest

yield (70 %). Homologues of ethylene showed no reactivity. In a later report Diamond, Mares et al. showed $RhCl_3$ was also capable of the hydroamination of ethylene with the primary amine aniline.[12] Since these initial reports, numerous catalysts have emerged and have been extensively reviewed.[10b,13] Despite these advances, the hydroamination of unactivated olefins higher than ethylene has proven to be particularly challenging. As such, examples of the addition of amines to higher olefins are relatively scarce.

Burnet et. al. reported the hydroamination of 1-hexene with aniline catalyzed by Pt salts with high selectivity (95% yield) for the Markovnikov product (Figure 1.5).[14] Notably, yields were not affected when the reaction was performed in air. This reaction was performed in the ionic solvent *n*-Bu_4PBr and the bromide was thought to increase the basicity of the Pt center. This could lead to a more facile proton transfer to the Pt facilitating the last step in the catalytic cycle (see, Figure 1.11, step c.).

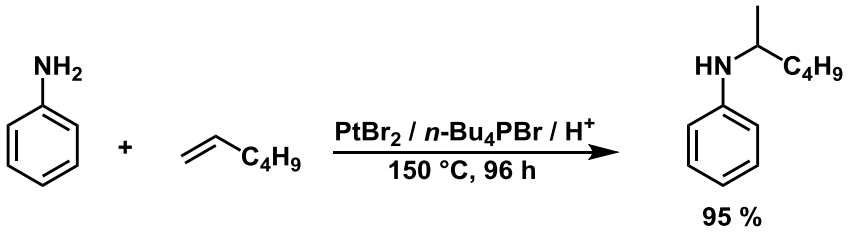

Figure 1.5. Pt catalyzed hydroamination of 1-hexene.[14]

Research from the Tilley laboratory later showed (COD)$Pt(OTf)_2$ or Ziese's dimer/ $AgBF_4$ could hydroaminate olefins with sulfonamides (Figure 1.6).[15] Norbornene, *cis*-2-butene, propylene, cyclopentene, and cyclohexene were all hydroaminated to form the corresponding alkyl sulfonamide in greater than 95 % yield under relatively mild conditions (less than 90 ˚C). Markovnikov selectivity was observed for propylene. Mechanistic studies

showed nucleophilic attack by the amine on the coordinated olefin was likely the rate determining step.

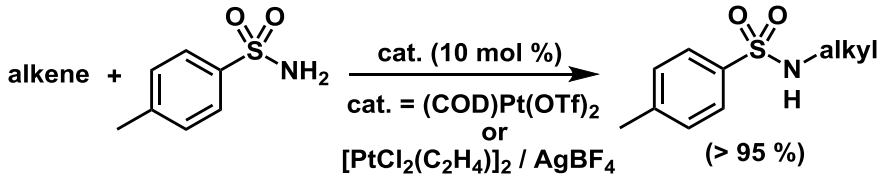

Figure 1.6. Pt catalyzed hydroamination of olefins with sulfonamides.[15]

Au^{I} catalysts were reported to catalyze both inter- and intramolecular hydroamination of several olefins with sulfonamides by He et al .[16] 1-octene was hydroaminated to give a 2:1 mixture of *N*-(1-methylheptyl)-*p*-toluenesulfonamide and *N*-(1-ethylhexyl)-*p*-toluenesulfonamide, respectively in the prescence of a the Au^{I} catalyst, PPh_3AuOTf, (5 mol %) (Figure 1.7.). Widenhoefer et al. subsequently reported that Au^{I}, in the presence of *bis*-phosphine ligands, catalyzed the hydroamination of olefins with ureas.[17] Notably, 1-octene was hydroaminated to give the Markovnikov product as the only regioisomer, in contrast to the system reported by He.

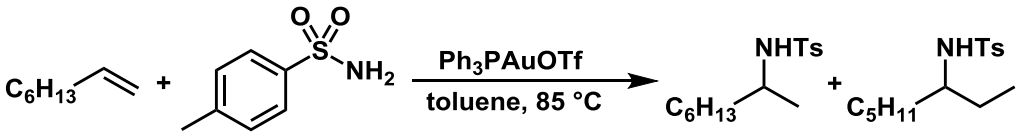

Figure 1.7. Au catalyzed hydroamination of olefins with sulfonamides.[16]

Hartwig et. al. have reported the Ir catalyzed hydroamination of olefins with amides and sulfonamides.[18] Several *bis*-phosphine ligands were screened with (S)-DTBM-Segphos giving the highest yield (up to 92 %) (Figure 1.8). This same system was also found to catalyze the enantioselective hydroamination of norbornene with amides (up to 93 % ee). In a

subsequent publication, they reported the addition of indoles to olefins under similar conditions.[19]

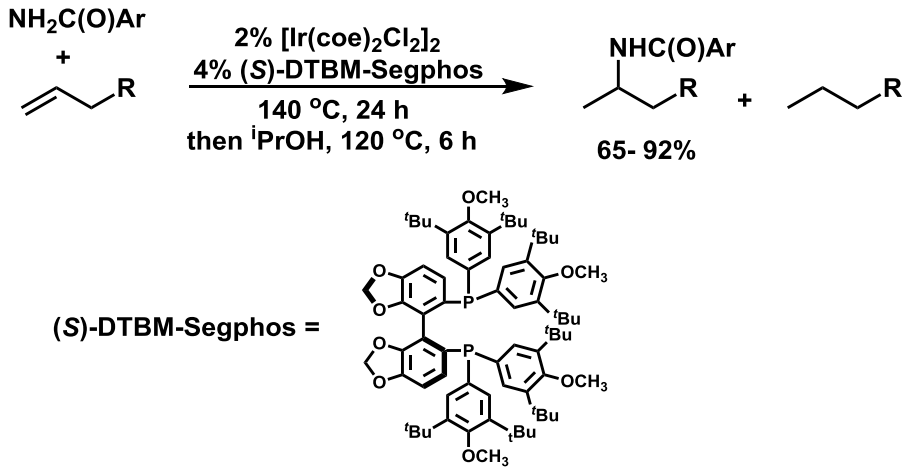

Figure 1.8. Ir catalyzed hydroamination of olefins with sulfonamides/ amides.[18]

Recent efforts have focused on hydroamination (or formal hydroamination) of unactivated internal olefins to give enantiopure products. Cu based catalysts have largely been used to realize this transformation.[20] For example, Buchwald et al. reported the Cu catalyzed enantioselective hydroamination of internal olefins with hydroxylamine esters (Figure 1.9).[20a] Notably unsymmetrical olefins were hydroaminated with both high regioselectivity and high enantioselectivity.

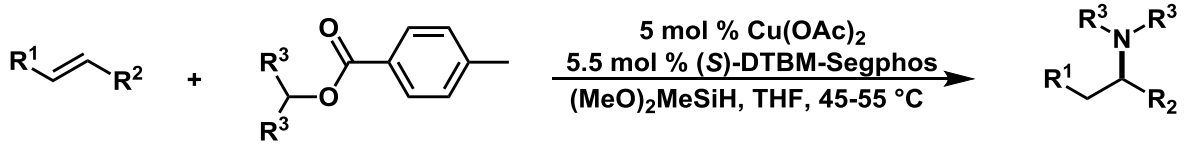

Figure 1.9. Enantioselective Cu catalyzed hydroamination of olefins with hydroxylamine esters.[20a]

1.3 Mechanisms for late transition metal catalyzed hydroamination

Two mechanisms are generally proposed for late transition metal catalyzed hydroaminations. These can be classified as the amine activation mechanism (Figure 1.10) and the olefin activation mechanism (Figure 1.11). In the amine activation mechanism, first reported by Casalnuovo, Calabrese, and Milstein for the Ir catalyzed hydroamination of norbornene with aniline,[21] N-H oxidative addition occurs at a low-valent metal to form a metal hydrido amido. This is followed by olefin insertion into the metal amido. C-H reductive elimination releases the product. Alternatively, olefin insertion into the hydride to form a metal alkyl amido (not pictured), followed by C-N reductive elimination is also possible.

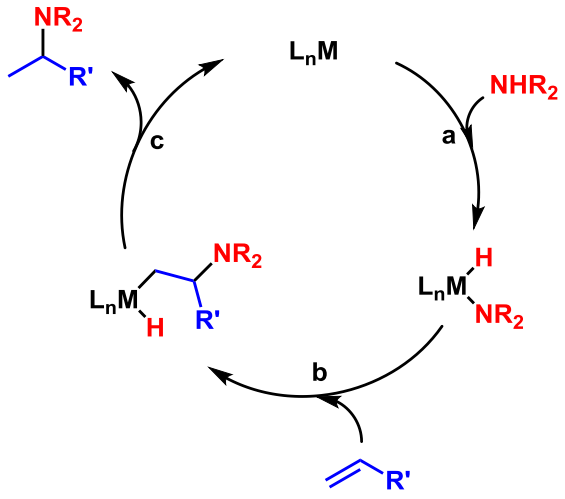

Figure 1.10. Amine activation mechanism.

In the olefin activation mechanism (Figure 1.11), initial coordination of an olefin to a low-valent metal renders the olefin electrophilic. Nucleophilic attack by the amine at the olefin results in the C-N bond formation. Direct protonolysis, or protonation at the metal center followed by C-H reductive elimination, releases the product.

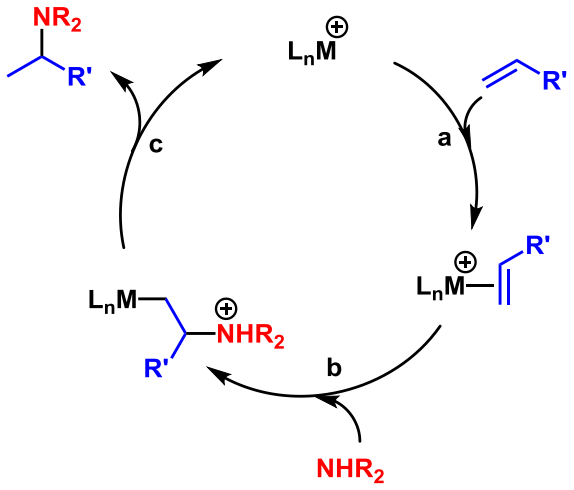

Figure 1.11. Olefin activation mechanism.

Markovnikov selectivity is generally obtained for both of these mechanisms. In the amine activation mechanism, insertion of the olefin into the metal amide to place the bulky R group away from the metal is likely more favorable (Figure 1.10, step b). However, under certain conditions, such as having an electron withdrawing group adjacent to the olefin, insertion to obtain anti-Markovnikov selectivity may be possible.[22]

In the olefin activation mechanism, nucleophilic attack at the bound olefin dictates the selectivity. Calculations by Eisenstein and Hoffmann have shown that the olefin must first slip to η^1 coordination. If the olefin is not symmetric, slippage occurs to the unsubstituted carbon. The nucleophile subsequently attacks at the substituted carbon to give the Markovnikov metal alkyl (Figure 1.12.).[23]

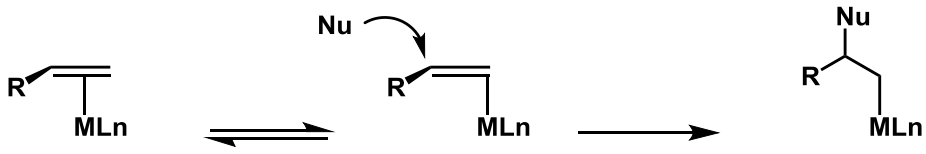

Figure 1.12. Olefin slippage from η^2 to η^1 followed by nucleophilic attack.[23]

1.4 Anti-Markovnikov hydroamination

Only a handful of examples of catalysts for anti-Markovnikov hydroamination have emerged and these examples are generally limited to vinyl arenes. Beller et. al. reported the Rh catalyzed anti-Markovnikov hydroamination of vinyl pyridine with amines.[24] Oxidative amination and hydroamination products were both observed. Optimizing the reaction conditions allowed for the hydroamination product to be formed in up to 97 % yield. Through stoichiometric studies, it was shown that activation of the vinyl arene likely occurs by coordination of the pyridine nitrogen to the cationic Rh.

Hartwig et. al. reported the anti-Markovnikov hydroamination of styrene with morpholine catalyzed by Rh *bis*-phosphine complexes.[25] Several ligands were screened with DPEphos giving the highest yield (71 %) (Figure 1.13). The enamine (oxidative amination) and ethyl arene were formed as side products. Higher amine:eneamine ratios were obtained at increased styrene loading, indicating two vinyl arenes may be involved in the selectivity determining transition state.

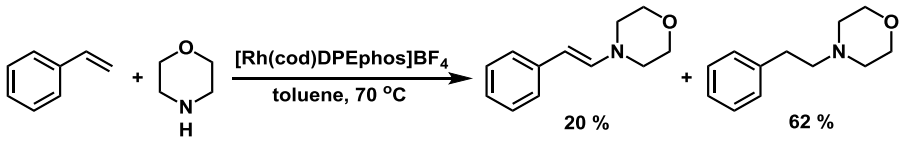

Figure. 1.13. Rh catalyzed anti-Markovnikov hydroamination of styrene with morpholine.[25]

The Rh catalyzed hydroamination of vinyl arenes with morpholine has recently been investigated computationally by Ujaque et al.[26] The N-H oxidative addition pathway had high energy transition states (up to 56.8 kcal mol^{-1}) and was thus ruled out. The olefin activation pathway had much more reasonable barriers (Figure 1.14). Nucleophilic attack at

coordinated styrene had a Gibbs energy barrier of 16.5 kcal mol^{-1}. The highest energy transition state for this pathway was proton transfer from the amine to the metal at 22.5 kcal mol^{-1}. Notably, nucleophilic attack at styrene to give the anti-Markovnikov addition was 5.9 kcal mol^{-1} lower than the Markovnikov addition. The difference became much smaller for unactivated olefins, such as propylene (0.8 kcal mol^{-1}), shedding some insight onto one possibility for why anti-Markovnikov hydroamination is most often observed for vinyl arenes.

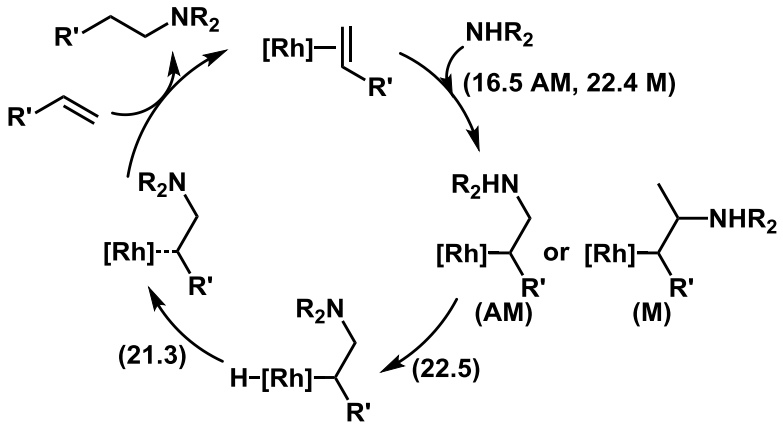

Figure 1.14. Mechanism for Rh catalyzed anti-Markovnikov hydroamination of styrene. Computed barriers are listed in kcal mol^{-1}.[26]

Hartwig et. al. later reported the anti-Markovnikov hydroamination of styrene and morpholine to give exclusively the hydroamination product (96 %) catalyzed by ruthenium complexes.[27] This system was proposed to go by a mechanism involving vinyl arene coordination to the Ru center followed by nucleophilic attack of morpholine on styrene (Figure 1.15). Vinyl arene exchange liberates the product and completes the catalytic cycle.[28]

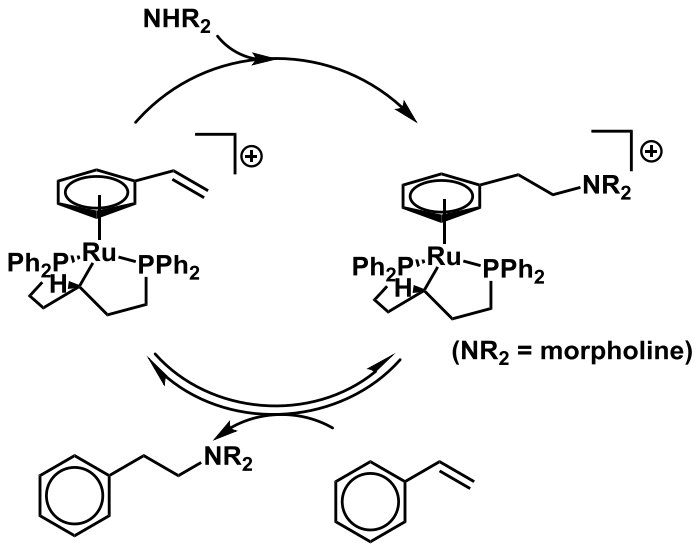

Figure 1.15. Proposed mechanism for Ru catalyzed anti-Markovnikov hydroamination of styrene with morpholine.[28]

Research from the Gunnoe laboratory showed that NHC copper amido complexes were capable of the anti-Markovnikov hydroamination of styrenes with aniline derivatives.[29] They proposed nucleophilic attack at the vinyl arene by a Cu amido (Figure 1.16). Coordination of an amine to the Cu center followed by proton transfer yields the product.

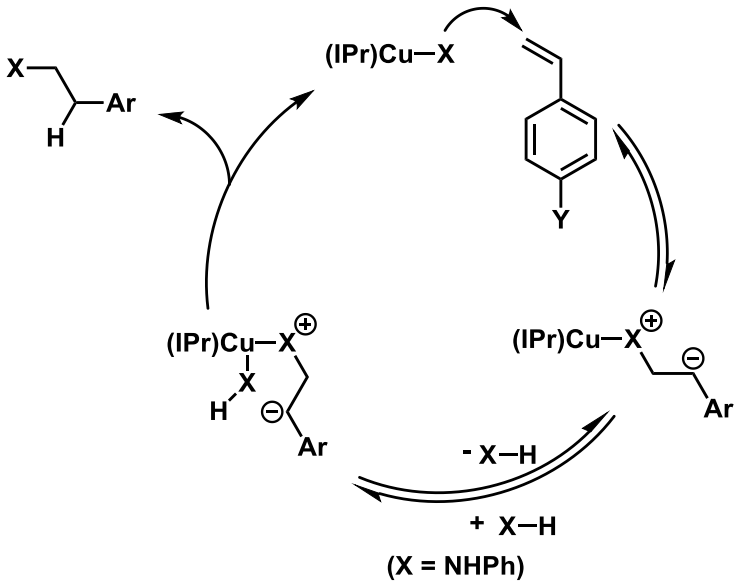

Figure 1.16. Cu catalyzed anti-Markovnikov hydroamination of vinyl arenes.[29]

A stoichiometric anti-Markovnikov hydroamination was reported by Sanford and Groves.[30] It was found that olefins inserted into the Rh hydride complex (TPP)RhH to form stable Rh alkyls (Figure 1.17). Intramolecular nucleophilic attack resulted in anti-Markovnikov cyclization. Protonolysis released the product and regenerated (TPP)RhH. Unfortunately, the individual reaction steps were performed under different conditions and the system was not catalytic.

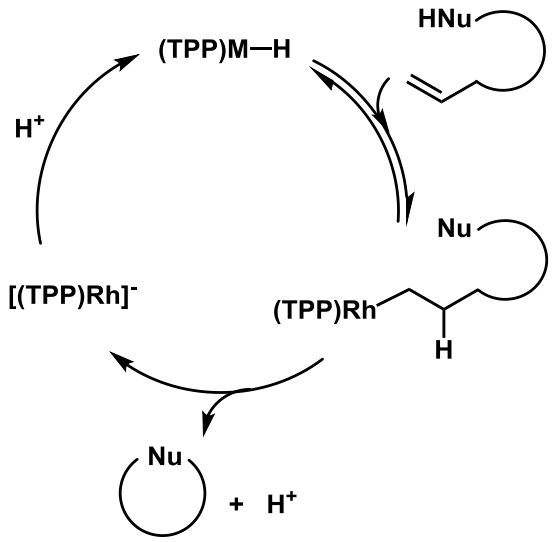

Figure 1.17. Intramolecular anti-Markovnikov hydroamination of olefins.[30]

Recent approaches have focused on multi-step one pot reactions to facilitate an overall anti-Markovnikov hydroamination. Cu,[31] Pd,[32] and Zr[33] have successfully been employed in this strategy. For example, Lalic et al. reported the formal anti-Markovnikov hydroamination by a reaction pathway involving hydroboration and then amination (Figure 1.18.) Notably this reaction sequence allowed for the formation of tertiary alkyl amines.

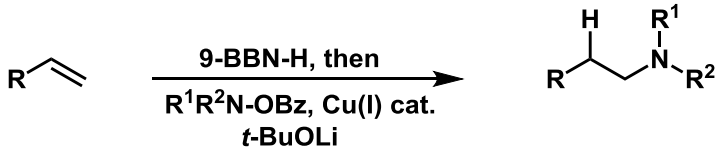

Figure 1.18. Hydroamination/ amination reaction to yield alkyl amines form olefins.[31]

1.5 Design of a new system to promote anti-Markovnikov hydroamination

As a part of the Center for Enabling New Technologies through Catalysis (CENTC), we proposed to achieve anti-Markovnikov hydroamination by amine nucleophilic attack at high-valent late metal alkyls. In the proposed catalytic cycle (Figure 1.19), we hypothesized

that sterically bulky ligands would favor formation of the *n*-alkyl upon protonation of a M-olefin precursor. This could be a direct protonation at the M-olefin or a protonation at the metal to forma a M-H followed by olefin insertion into the hydride. Subsequent nucleophilic attack by amine at the α-carbon should yield the desired product.

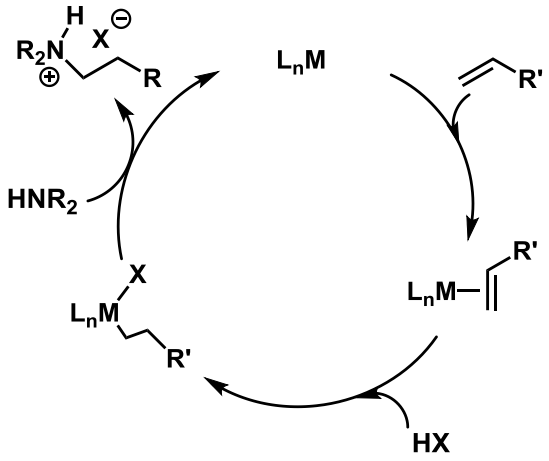

Figure 1.19. Proposed catalytic cycle for anti-Markovnikov hydroamination.

Early efforts focused on (^{Me}TPA)Rh propylene complexes. Gal et. al. reported the protonation of (TPA)Rh(ethylene)$^+$ (TPA = *N*,*N*,*N*(tri-2-pyridylmethyl)amine) with HCl to form (TPA)Rh(Et)(Cl)$^+$ (Figure 1.20).[34]

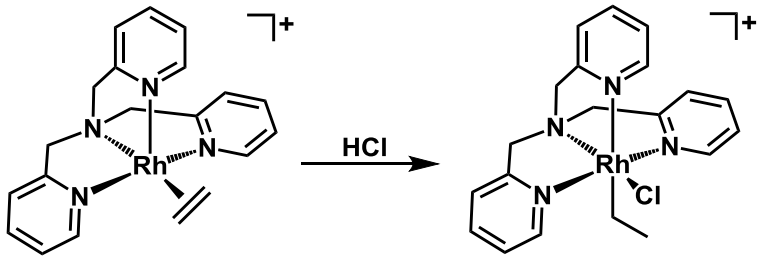

Figure 1.20. Protonation of (TPA)Rh(ethylene)$^+$ to yield (TPA)Rh(Et)(Cl)$^+$.[34]

We found that protonation of the propylene complex, (TPA)Rh-propyl$^+$ with acetic acid yielded (TPA)Rh(^{i}Pr)(OAc)$^+$ (Figure 1.21.). Gratifyingly, addition of methyl groups to

the ligand added sufficient steric bulk to favor the selective formation of linear (^{Me}TPA)Rh-propyl^{+} (^{Me}TPA = *N*,*N*,*N*-tri(6-methyl-2-pyridylmethyl)amine) via protonation of [(^{Me}TPA)Rh-propylene][BPh_4][35] with anilinium triflate (Figure 1.21). Nucleophilic attack at the alkyl group should generate the desired linear alkylamine. However, thermolysis of (^{Me}TPA)Rh-propyl^{+} and amine (or amide) did not promote C-N coupling. Instead, β-hydride elimination was observed resulting in [(^{Me}TPA)RhH]$^{2+}$.[35] Presumably this decomposition occurs via loss of triflate to generate an open site. The facially coordinating TPA ligand dictates that the open site is cis to the alkyl ligand, which is not the proper orientation required for S_N2 nucleophilic attack. Although, this tetradentate ligand enforced the correct regiochemistry for the olefin insertion, C-N coupling could not be achieved.

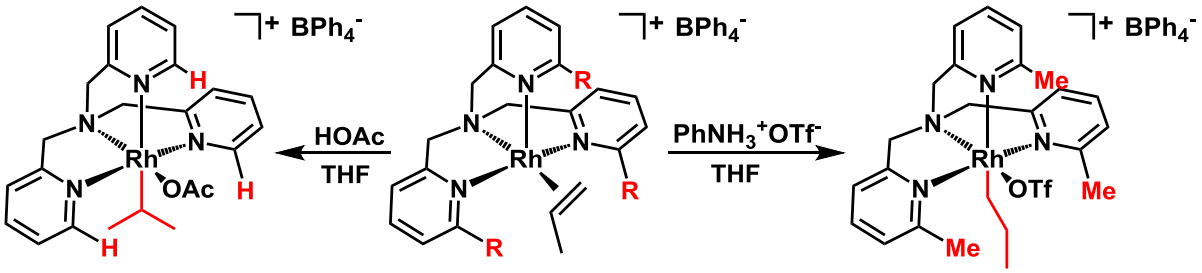

Figure 1.21. Steric control of selectivity: protonation of (TPA)Rh-propylene^{+}.[35]

Since the pyridine moiety trans to the alkyl was proposed to inhibit the desired reactivity, the tridentate version of the ligand was synthesized (where a phenyl or alkyl replaced the axial pyridine). Unfortunately, the Rh-olefin complexes were not thermally robust and attempts to protonate at low temperature led to decomposition.[35]

Through the addition of steric bulk to the ligand, we were able to control the selectivity to favor the n-propyl complex (^{Me}TPA)Rh-propyl^{+} upon protonation of

(^{Me}TPA)Rh-propylene^{+}. Significantly, this represents the first two steps in our proposed catalytic cycle (Figure 1.19). However, the last step, C-N coupling, has proven to be challenging.

While C(sp^2)-N couplings reported by the laboratories of Buchwald[36] and Hartwig[37] to form aryl amines have become prevalent and widely used, C(sp^3)-N couplings have only been observed a handful of times. We therefore focused our efforts on developing a fundamental understanding of this rarely reported reaction. This could lead to new and improved methods for the functionalization of alkanes and olefins.

1.6 C(sp^3)-N reductive elimination

Early examples of C(sp^3)-N reductive elimination were reported by Hillhouse et al. from Ni.[38] They showed by deuterium labeling studies that aziridines were added to Ni^0 by S_N2 oxidative addition to form the corresponding Ni^{II} azanickelacyclobutane (Figure 1.22). Reaction with O_2 promoted the oxidatively induced reductive elimination to regenerate the original aziridine. This last step in 1.22 is a rare example of C(sp^3)-N reductive elimination.

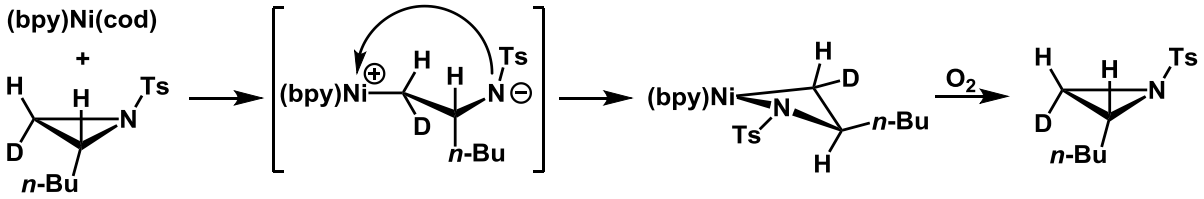

Figure 1.22. Oxidatively induce reductive elimination from Ni.[38]

C(sp^3)-N reductive elimination was later reported from Pt^{IV} methyl sulfonamides by Goldberg et al.[39] Thermolysis of the complex *fac*-(dppbz)$PtMe_3(NHSO_2R)$ resulted in the

reductive elimination of methyl sulfonamide (Figure 1.23). C-N reductive elimination was favored (over C-C reductive elimination) in non-polar solvents and could be obtained exclusively in the presence of excess sulfonamide. Mechanistic studies indicated that initial sulfonamide dissociation to forma a five-coordinate intermediate was followed by nucleophilic attack at the Pt^{IV}-Me to form the methyl sulfonamide and (dppbz)$Pt^{II}Me_2$.

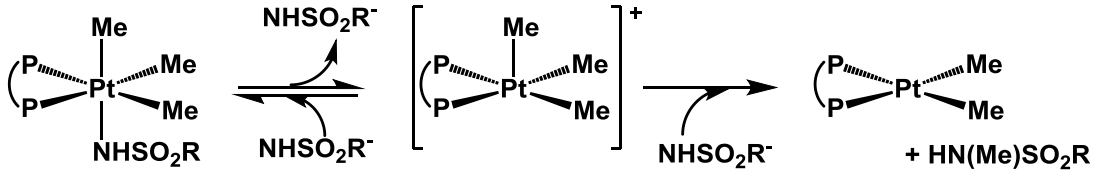

Figure 1.23. Reductive elimination of methyl sulfonamides from Pt^{IV}.[39]

Bis-phosphine ligated benzyl Pd^{II} amido complexes were reported to undergo C(sp^3)-N reductive elimination by Hartwig et al. (Figure 1.24).[40] Through mechanistic studies (kinetic and sterochemical) they proposed a pathway involving initial dissociation of the diarylamido ligand followed by attack on the benzyl Pd intermediate. Notably, in contrast to Hillhouse's Ni example, oxidation was not required and reductive elimination occurred from Pd^{II}.

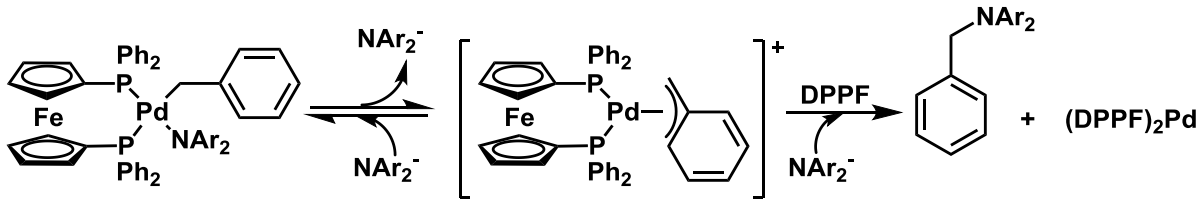

Figure 1.24. Reductive elimination of benzyl diarylamidos from Pd^{II}.[40]

In a subsequent publication, Hartwig et al. reported the C(sp^3)-N reductive elimination from NHC ligated Pd alkyl amido complexes (Figure 1.25).[41] In contrast to the

previous system, this system was found to undergo reductive elimination by a concerted pathway, implicated by the sterochemical configuration of the norbornyl amine product. Furthermore computed barriers were consistent with experimentally determined barriers for a concerted reductive elimination from three-coordinate Pd^{II}.

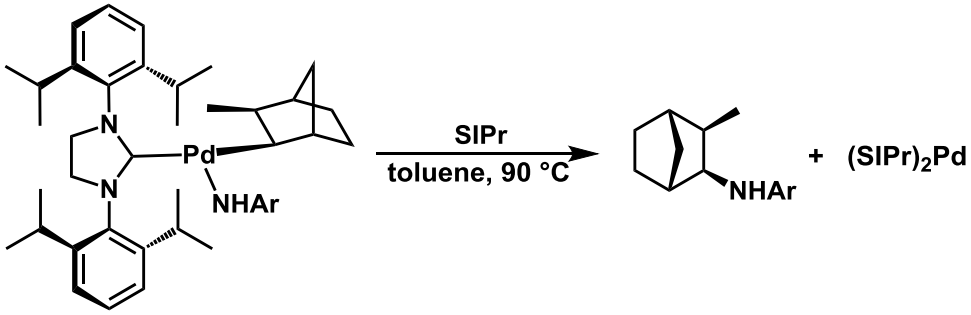

Figure 1.25. Reductive elimination of alkyl amines from Pd^{II}.[41]

Sanford et. al. reported $C(sp^3)$-N reductive elimination from Pd^{IV}.[42] In this system $C(sp^3)$-N reductive elimination was found to compete with $C(sp^3)$-F reductive elimination. $C(sp^3)$-F reductive elimination was the dominate reaction; however, C-N reductive elimination could be favored by the addition of excess sulfonamide. It was proposed that initial dissociation of the sulfonamide to five-coordinate intermediate preceded nucleophilic attack (or concerted C-F reductive elimination), similar to the Pt system above (Figure 1.26).

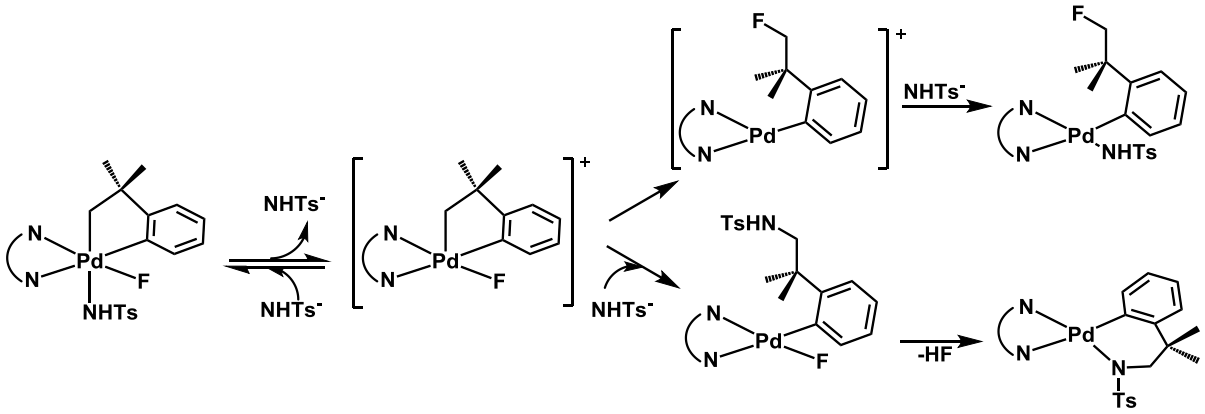

Figure 1.26. Reductive elimination of alkyl sulfonamides from Pd^{IV}.[42]

Sanford et al. have recently reported C(sp^3)-X coupling from Ni^{IV}.[43] In this system C-O, C-N, and C-S coupling reactions were possible (Figure 1.27). It was found that the initial rates of reductive elimination correlated with the Swain-Scott nucleophilicity values, indicating an S_N2 type mechanism was likely operative.

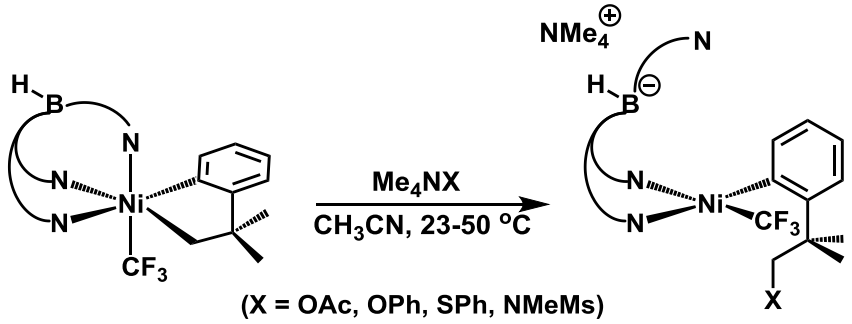

Figure 1.27. C(sp^3)-X coupling to form alkyl heteroatoms from Ni^{IV}.[43]

Through these examples, the importance of unsaturated species (three-coordinate M^{II} and five-coordinate M^{IV}) in C(sp^3)-N reductive elimination reactions has become evident. Mechanistic studies have shown that S_N2[38,39,40,42,43] and concerted reductive elimination are both possible for C-N coupling reactions.[41]

Dissertation statement.

Described in the following chapters are experimental and mechanistic studies on the reactivity of metal alkyls with nucleophiles. Chapter 2 focuses on the synthesis and characterization of Pd and Pt olefin complexes. Protonation of these complexes was expected to generate the corresponding alkyls. Chapter 3 explores the reactivity of (Pybox)Ir ethyl complexes toward nucleophiles and the synthesis and reactivity of Rh analogues. In Chapter 4, the synthesis and reactivity of (BPA)Ir ethyl complexes is explored both experimentally and computationally. C-N coupling was observed and mechanistic implications are discussed. Chapter 5 explores the $C(sp^3)$-I redctuive elimination and $C(sp^3)$-X (X = N, S) coupling from Rh^{III}. C-I reductive elimination is proposed to occur by a two-path mechanism. Kinetic studies support the direct attack at the Rh^{III}-Me by amines and thiolates.

Notes to Chapter 1.

(1) (a) Fischer, A.; Mallat, T.; Baiker, A. *Catal. Today* **1997**, *37*, 167. (b) Lawrence, S. A. Amines: *Synthesis, Properties and Applications*; Cambridge University Press, New York, **2004**.

(2) Eller, K.; Henkes, E.; Rossbacher, R.; & Hoke, H. "Aliphatic Amines" in Ullmann's Encyclopedia of Industrial Chemistry, Wiley-VCH, Weinheim, **2012**, pp647-692.

(3) Taube, R. **2002**, In: Cornils B, Herrmann WA (eds) Applied homogeneous catalysis with organometallic compounds, vol 1, 2nd edn. Wiley-VCH, Weinheim, p 507–520.

(4) Johns, A. M.; Sakai, N.; Ridder, A.; Hartwig, J. F. *J. Am. Chem. Soc.* **2006**, *128*, 9306.

(5) Haggins, J. *Chem. Eng. News* **1993**, *71*, 23.

(6) Gagné, M. R.; Stern, C. L.; Marks, T. J. *J. Am. Chem. Soc.* **1992**, *114*, 275.

(7) (a) Walsh, P. J.; Baranger, A. B.; Bergman, R. G. *J. Am. Chem. Soc.* **1992**, *114*, 1708. (b) Baranger, A. M.; Walsh, P. J.; Bergman, R. G. *J. Am. Chem. Soc.* **1993**, *115*, 2753.

(8) McGrane, P. L.; Jensen, M.; Livinghouse, T. *J. Am. Chem. Soc.* **1992**, *114*, 5459.

(9) Pohlki, F.; Doye, S. *Angew. Chem. Int. Ed.* **2001**, *40*, 2305.

(10) (a) Hong, S.; Marks, T. J. *Acc. Chem. Res.* **2004**, *37*, 673. (b) Muller, T. M.; Hultzch, K. C.; Yus, M.; Foubelo, F.; Tada, M. *Chem. Rev*. **2008**, *108*, 3795. (c) Reznichenko, A. L.; Hultzsch, K. C. *Top. Organomet. Chem*. **2013**, *43*, 51.

(11) Coulson, D. R. *Tetrahedron Lett*. **1971**, *5*, 429.

(12) Diamond, S. E.; Szalkiewicz, A.; Mares, F. *J. Am. Chem. Soc.* **1979**, *101*, 490.

(13) (a) Hartwig, J. F. *Pure Appl. Chem*. **2004**, *76*, 507. (b) Hesp, K. D.; Stradiotto, M. *ChemCatChem* **2010**, *2*, 1192. (c) Nishina, N.; Yamamoto, Y. *Top. Organomet. Chem*. **2012**, *43*, 115. (d) Huang, L.; Arndt, M.; Gooßen, K.; Heydt, H.; Gooßen, L. J. *Chem. Rev*. **2015**, *115*, 2596.

(14) Brunet, J.-J.; Chu, N. C.; Diallo, O. *Organometallics* **2005**, *24*, 3104.

(15) Karshtedt, D.; Bell, A. T.; Tilley, T. D. *J. Am. Chem. Soc.* **2005**, *127*, 12640.

(16) Zhang, J.; Yang, C.-G.; He, C. *J. Am. Chem. Soc*. **2006**, *128*, 1798.

(17) Zhang, Z.; Lee, S. D.; Widenhoefer, R. A. *J. Am. Chem. Soc.* **2009**, *131*, 5372.

(18) Sevov, C. S.; Zhou, J.; Hartwig, J. F. *J. Am. Chem. Soc.* **2012**, *134*, 11960.

(19) Sevov, C. S.; Zhou, J.; Hartwig, J. F. *J. Am. Chem. Soc.* **2014**, *136*, 3200.

(20) (a) Yang, Y.; Shi, S.-L.; Niu, D.; Liu, P.; Buchwald, S. L. Science 2015, 349, 62. (b) Xi, Y.; Butcher, T. W.; Zhang, J.; Hartwig, J. F. Angew. Chem. Int. Ed. 2016, 55, 776.

(21) Casalnuovo, A. L.; Calabrese, J. C.; Milstein, D. *J. Am. Chem. Soc*. **1988**, *110*, 6738.

(22) Jiao, Y.; Evans, M. E.; Morris, J.; Brennessel, W. W.; Jones, W. D. *J. Am. Chem. Soc.* **2013**, *135*, 6994.

(23) (a) Eisenstein, O.; Hoffmann, R. *J. Am. Chem. Soc.* **1980**, *102*, 6149. (b)Eisenstein, O.; Hoffmann, R. *J. Am. Chem. Soc.* **1981**, *103*, 4308.

(24) Beller, M.; Trauthwein, H.; Eichberger, M.; Breindl, C.; Müller, T. E. *Eur. J. Inorg. Chem.* **1999**, 1121.

(25) Utsunomiya, M.; Kuwano, R.; Kawatsura, M.; Hartwig, J. F. *J. Am. Chem. Soc.* **2003,** 125, 5608.

(26) Couce-Rios, A.; Lledós, A.; Ujaque, G. *Chem. Eur. J.* **2016**, *22*, 9311.

(27) Utsunomiay, M.; Hartwig, J. F. *J. Am. Chem. Soc.* **2004**, *126*, 2702.

(28) Takaya, J.; Hartwig, J. F. *J. Am. Chem. Soc.* **2005**, *127*, 5756.

(29) Munro-Leighton, C.; Delp, S. A.; Alsop, N. M.; Blue, E. D.; Gunnoe, T. B. *Chem. Commun.* **2008**, *111*, 111.

(30) Sanford, M. S.; Groves, J. T. *Angew. Chem. Int. Ed.* **2004**, *43*, 588.

(31) Rucker, R. P.; Whittaker, A. M.; Dang, H.; Lalic, G. *J. Am. Chem. Soc.* **2012**, *134*, 6571.

(32) Bronner, S. M.; Grubbs, R. H. *Chem. Sci.* **2014**, *4*, 101.

(33) Strom, A. E.; Hartwig, J. F. *J. Org. Chem.* **2013**, *78*, 8909.

(34) de Bruin, B.; Boerakker, M. J.; Verhagen, J. A. W.; de Gelder, R.; Smitts, J. M. M.; Ga. A. W. *Chem. Eur. J.* **2000**, *6*, 298.

(35) St. John, Anthony. PhD. Dissertation, University of Washington, **2011**.

(36) Wolfe, J. P.; Wagaw, S.; Marcoux, J.-F.; Buchwald, S. L. *Acc. Chem. Res.* **1998**, *31*, 805.

(37) Hartwig, J. F. *Acc. Chem. Res.* **1998**, *31*, 852.

(38) Lin, B. L.; Clough, C. R.; Hillhouse, G. L. *J. Am. Chem. Soc.* **2002**, *124*, 2890.

(39) Pawlikowski, A. V.; Getty, A. D.; Goldberg, K. I. *J. Am. Chem. Soc.* **2007**, *129*, 10382.

(40) Marquard, S. L.; Rosenfeld, D. C.; Hartwig, J. F. *Angew. Chem.* **2010**, *122*, 805.

(41) Hanley, P. S.; Marquard, S. L.; Cundari, T. R.; Hartwig, J. F. *J. Am. Chem. Soc.* **2012**, *134*, 15281.

(42) Pérez-Temprano, M. H.; Racowski, J. M.; Kampf, J, W.; Sanford, M. S. *J. Am. Chem. Soc.* **2014**, *136*, 4097.

(43) Camasso, N. M.; Sanford, M. S. *Science* **2015**, *347*, 1218.

Chapter 2

Synthesis and reactivity of (PCP)M based olefin complexes

2.1 Introduction

Metal olefin complexes are important species, often invoked as intermediates in catalytic reactions. For example, the oxo process, which is carried out industrially on the scale of 10.4 million tons/ year,[1] involves coordination of an olefin to a Co or Rh catalyst followed by insertion into the Co or Rh hydride.[2] The selectivity of this system has been optimized to generate both Markovnikov and anti-Markovnikov products.

Metal olefin complexes are also proposed as intermediates in hydroamination reactions, however, Markovnikov selectivity is generally obtained.[3] As outlined in Chapter 1, we hypothesized that the selectivity could be controlled to favor formation of anti-Markovnikov products if protonation of the M^n-olefin to form a M^{n+2}-alkyl precedes C-N bond formation. In this case, sterically bulky ligands are predicted to favor formation of the linear alkyl upon protonation.

Group 10 metal olefin species were targeted as $C(sp^3)$-N reductive elimination reaction has been reported from these metals.[4] Mechanistic studies have shown that high

valent group 10 metals undergo C(sp^3)-N reductive elimination by nucleophilic attack at the M^{IV}-alkyl. Concerted C(sp^3)-N reductive elimination has been observed from low valent Pd^{II}-(alkyl)(amido) complexes.[4]

The PCP ligand was an ideal candidate as it offers great control over the steric environment about the metal center. Small steric differences in the substituents on the phosphine moieties (i.e ^{t}Bu vs ^{i}Pr) have been shown to have dramatic effects on the reactivity. For example, Milstein et al. showed that they could promote reductive elimination of methyl iodide from a naphthyl-based (PCP)Rh^{III} complex with the more bulky ^{t}Bu variant.[5] Furthermore, Goldberg, Heinekey, et al. found that metalation of ^{R}POCOP onto Ir resulted in Ir^{III} when R = ^{i}Pr whereas Ir^I was formed when R = ^{t}Bu .[6]

While Ir ethylene complexes reported by Brookhart, Goldman, et al. with several variations of this ligand framework (i.e. PCP, PCOP, anthraphos) are known,[7] isolable group 10 (PCP) metal olefin complexes are much less common. Milstein et al. reported observation of [(^{Ph}PCP)Pd(norbornene)][BF_4], however this complex was not isolable and the norbornene ligand was easily displaced by solvents such as THF.[8] Vitagliano et al. reported the synthesis of the related dicationic PNP variant, [(^{Ph}PNP)Pd(olefin)][BF_4]$_2$, with a variety of olefins, although, nucleophilic attack at the olefin resulted in Markovnikov selectivity.[9]

As the dicationic PNP variant would likely be challenging to protonate, we focused our efforts on the PCP ligand. Thus, group 10 propylene complexes bearing this ligand were targeted. The reactivity of both the ^{t}Bu variant and Ph variant of the PCP ligand were investigated with Pd and Pt.

2.2 Synthesis of [(PCP)Pd(propylene)][BF_4]

As steric control of the protonation step is key to our proposed catalytic cycle (Figure 2.1, step b), we hypothesized complexes bearing the ^{t}Bu variant of PCP would be more likely to yield the n-propyl moiety upon protonation of the propylene complex. Previous studies from the Goldberg lab found control over the protonation of Rh propylene complex to favor *n*-propyl over *i*-propyl was possible by adding more steric bulk to the ligand.[10] Similar to reported procedures,[11] we targeted propylene complexes by silver abstraction from (PCP)Pd-Cl in the presence of propylene. ($^{t\text{-Bu}}$PCP)PdCl (**1**) was prepared according to a published procedure.[12] Upon addition of $AgBF_4$ to a solution of **1** in CD_2Cl_2, complete disappearance of the ^{31}P NMR resonance of **1** (73 ppm) was observed along with the appearance of a new ^{31}P NMR resonance (77.4 ppm) consistent with [($^{t\text{-Bu}}$PCP)Pd-solv][BF_4] (**2**). Furthermore the methylene resonance in the ^{1}H NMR spectrum was shifted from 3.25 to 3.18 ppm, consistent with the formation of **2**. While methylene chloride is generally considered a poor ligand, related complexes (with methylene chloride coordinated) have been reported by Milstein.[7] Upon pressurization of the sample with propylene (5 atm), no change in the ^{31}P NMR spectrum was observed, indicating that coordination of propylene to the metal center had not occurred. Furthermore, only free propylene and resonances corresponding to **2** were observed in the ^{1}H NMR spectrum. One possibility for the lack of reactivity toward propylene could be that the bulky ^{t}Bu groups inhibit binding of the olefin. Considering $P(Ph)_3$ has a significantly smaller cone angle[13] (145˚) than both $P(^tBu)_3$ (182 ˚) and $P(^iPr)_3$ (160 ˚), the reactivity of the analogues ^{Ph}PCPPd was explored to test this hypothesis.

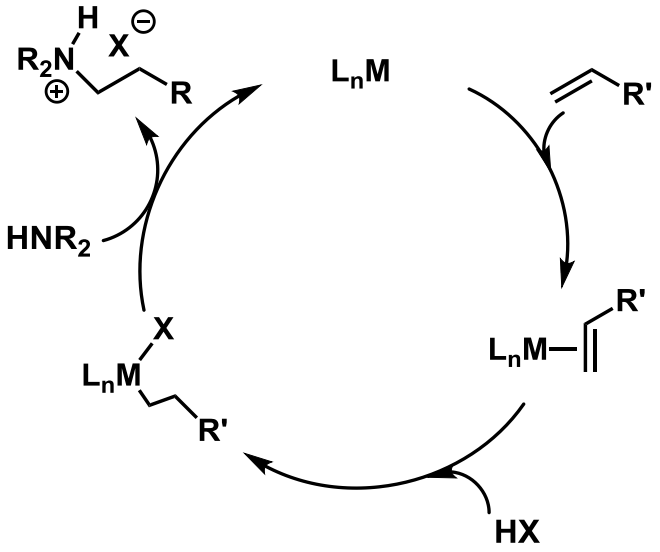

Figure 2.1. Proposed catalytic cycle for anti-Markovnikov hydroamination.

(^{Ph}PCP)PdCl (**3**) was prepared from $PdCl_2(NCPh)_2$ and 1,3-*bis*[methyldiphenylphosphine]benzene according to a published procedure.[14] Upon addition of $AgBF_4$ to a solution of **3** in CD_2Cl_2, complete disappearance of the ^{31}P NMR resonance attributed to **3** (36.1 ppm) was observed along with the appearance of a new ^{31}P NMR resonance (40.3 ppm) consistent with [(^{Ph}PCP)Pd-solv][BF_4] (**4**). This was accompanied by a shift in the resonance corresponding to the methylene ligand protons from 4.01 to 3.99 ppm in the ^{1}H NMR spectrum. The sample was then pressurized with propylene (5 atm). Gratifyingly, complete disappearance of the ^{31}P NMR resonance attributed to **4** was observed, along with the appearance of a new ^{31}P NMR resonance (49.2 ppm) consistent with [(^{Ph}PCP)Pd-propylene][BF_4] (**5**) (Figure 2.2). Signals for bound propylene in the ^{1}H NMR were likely obscured by the large excess of free propylene. Upon removal of excess propylene two broad peaks were observed in the ^{31}P NMR spectrum at c.a. 50 ppm and c.a. 40 ppm (Figure 2.3, spectrum 4). This result suggests **4** and **5** exist as an equilibrium mixture in the absence of excess propylene. The room temperature ^{1}H NMR spectrum, after the

removal of excess propylene, shows well resolved coupling for the aromatic peaks, but all other peaks are broad, likely due to exchange of propylene. This data suggests that the smaller phenyl substituents allow enough access to the Pd center for propylene to coordinate, consistent with our prediction.

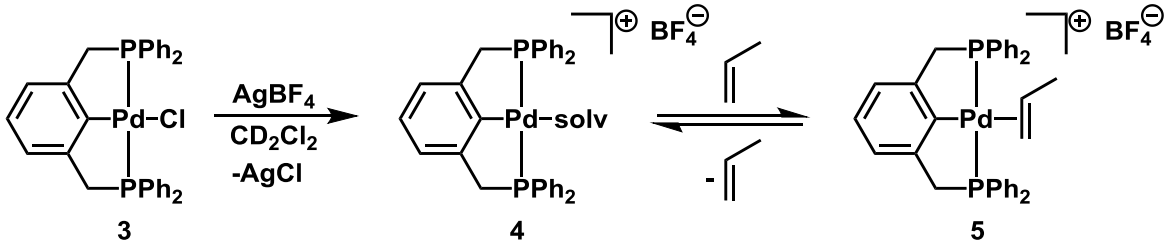

Figure 2.2. Synthesis of **5**.

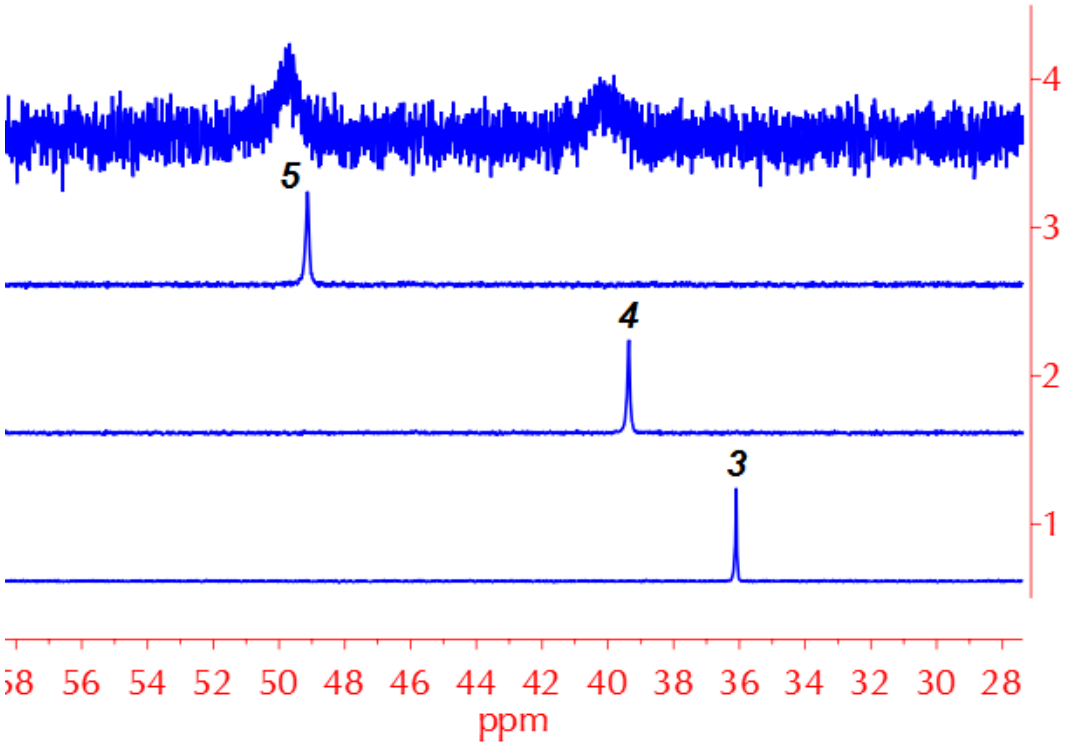

Figure 2.3. $^{31}P\{^{1}H\}$ NMR spectra (202 MHz, CD_2Cl_2, 298 K) supporting the formation of the propylene complex, **5**. Spectrum 1: Complex **3** in CD_2Cl_2. Spectrum 2: Reaction of complex **3** + $AgBF_4$ to form **4**. Spectrum 3: Reaction of complex **4** with propylene (5 atm) to form complex **5**. Spectrum 4: Excess propylene removed.

In order to gain more insight into the exchange process, variable temperature NMR studies were performed. Cooling a mixture of complex **4** & **5** (after removing excess propylene) to < 260 K revealed a sharp peak at 49.6 ppm in the ^{31}P NMR spectrum corresponding to **5** (Figure 2.4) and a well resolved ^{1}H NMR spectrum (Figure 2.5). If the solution was warmed back up to room temperature, broad signals corresponding to **4** and **5** were both observed in the ^{31}P NMR spectrum. Notably, if only 0.5 equivalents propylene were added, only **5** was observed at low temperature (< 260 K). One possibility is that **4** precipitates out of solution at low temperature. To test this, a solution of **4** in CD_2Cl_2 was cooled to 260 K. Approximately 60 % of **4** remained in solution by ^{1}H NMR spectroscopy. The fact that not all of 4 remained in solution explains why only 5 was observed at low temp when only 0.5 equivalents of propylene were added. Overall, the broadness in the NMR spectra suggests that a dynamic process exists on the NMR timescale at room temperature and **4** and **5** are in equilibrium. At low temperatures, the equilibrium is shifted toward **5**.

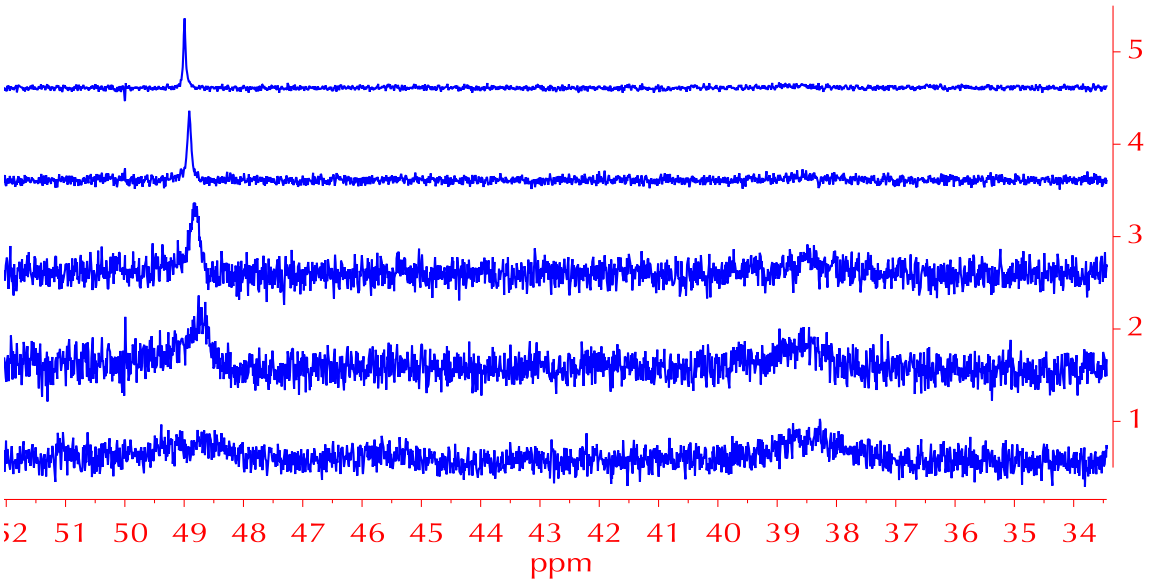

Figure 2.4. $^{31}P\{^{1}H\}$ NMR (202 MHz, CD_2Cl_2) of **4** and **5** after removing excess propylene. Spectrum 1, T =298 K. Spectrum 2, T = 288 K. Spectrum 3, T = 278 K. Spectrum 4, T = 268 K. Spectrum 5, T = 260 K. (bottom spectrum) cooled to 241 K (top spectrum)

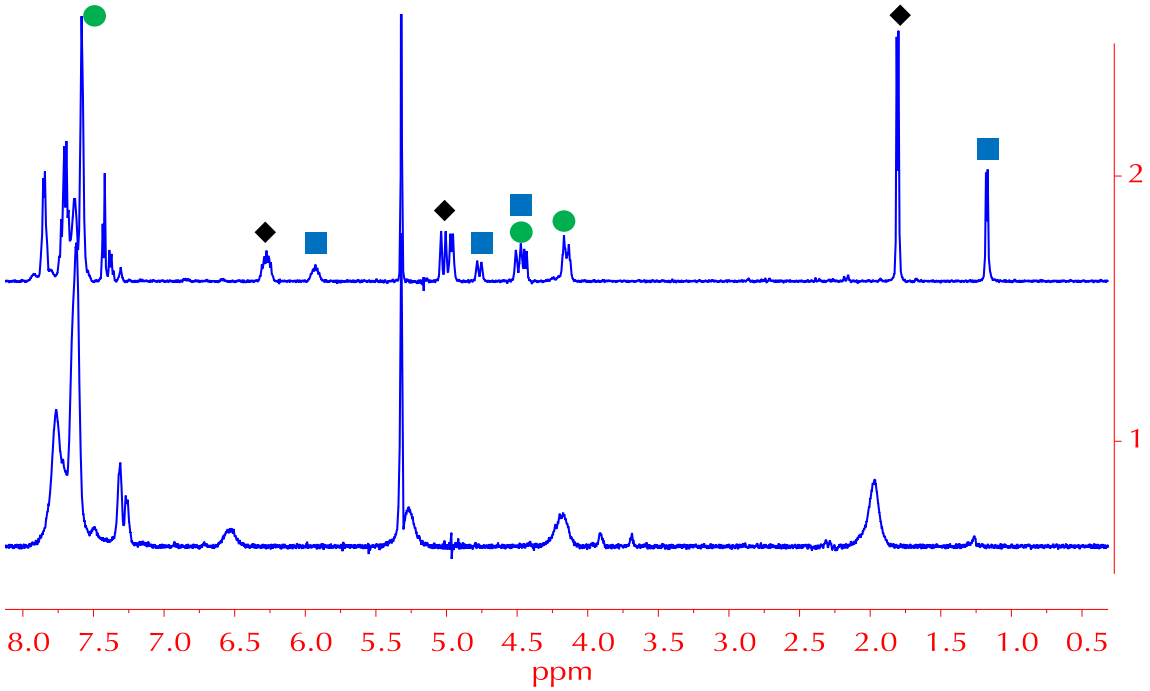

Figure 2.5. ^{1}H NMR (500 MHz, CD_2Cl_2) of **4/5** at 298 K (spectrum 1) and **5** at 200K (spectrum 2). Ligand resonances for **5** = ● , propylene resonances for **5** =■ , free propylene =◆ .

2.3 Attempted Protonation of [(PCP)Pd(propylene)][BF_4]

The next step in the catalytic cycle would involve formation of a Pd-propyl complex by reaction of **5** with an acid (Figure 2.1, step c). The addition of one equivalent of triflic acid to a solution of **5** in CD_2Cl_2 resulted in no new phosphorus containing species. Addition of excess triflic acid led to multiple intractable products by ^{1}H NMR spectroscopy. No peaks were observed in the ^{31}P NMR spectrum. However, upon addition of one equivalent of $HBF_4 \cdot Et_2O$ to a solution of **5** in methylene chloride, a new ^{31}P resonance was observed at 50.2 ppm. The signal corresponding to **5** was still observed, thus additional $HBF_4 \cdot Et_2O$ was added. This again led to multiple intractable products by ^{1}H NMR spectroscopy and the disappearance of signals in the ^{31}P NMR spectrum. Based on the success of anilinium salts with the (^{Me}TPA)Rh system,[9] anilinium triflate and anilinium tetrafluoroborate were prepared

and in separate experiments added to **5** in methylene chloride. The triflate and tetrafluoroborate salts of aniline are insoluble in methylene chloride and no reaction was observed. Complex **5** was heated to 60˚C with one equivalent of anilinium tetrafluoroborate. Complete disappearance of the ^{31}P resonance of **5** was observed along with the appearance of a new ^{31}P resonance corresponding to the Pd-Cl complex **3**, suggesting that heating causes the olefin to dissociate and, in the presence of chlorinated solvent, regenerate complex **3**. To increase solubility of anilinium in methylene chloride, anilinium $B(Ar^F)_4$ was prepared. Addition of anilinium $B(Ar^F)_4$ to a solution of **5** in methylene chloride resulted in the formation of an insoluble solid as well as what appears to be Pd black. In all cases, [(PCP)Pd(propyl)][BF_4][X] was not observed.

2.4 Synthesis of [(PCP)Pt(propylene)][BF_4]

While there are many examples of organometallic complexes with an oxidation state of Pt^{IV}, accessing the Pd^{IV} oxidation state in organometallic complexes has proven to be more challenging.[15] With that notion in mind we targeted the analogous $(PCP)Pt^{II}(propylene)^+$ complex with the idea that protonation to yield the Pt^{IV}-$propyl^+$ should be more feasible. As synthesis of a propylene complex with the $^{t\text{Bu}}$PCP ligand was not achievable with the Pd system, ($^{\text{Ph}}$PCP)Pt complexes were explored. ($^{\text{Ph}}$PCP)PtCl (**6**) was synthesized according to a published procedure.[16] Addition of $AgBF_4$ to a solution of ($^{\text{Ph}}$PCP)PtCl in CD_2Cl_2 resulted in a downfield shift and broadening of the ^{31}P NMR resonance, similar to the Pd system. The ^{31}P NMR signal for ($^{\text{Ph}}$PCP)PtCl at 34.4 ppm ($J_{Pt\text{-}P}$ = 2957 Hz) was replaced by a signal at 43.7 ppm corresponding to [($^{\text{Ph}}$PCP)Pt-solv][BF_4] (**7**). Addition of propylene to this sample resulted in further downfield shift to 44.3 ppm ($J_{Pt\text{-}P}$ = 2709 Hz) and a well resolved ^1H NMR spectrum. In contrast to the Pd system, no change was observed upon removal of excess

propylene. Furthermore, [(^{Ph}PCP)Pt(propylene)][BF_4] (**8**) could be prepared on a larger scale in high yield (87 %) by bubbling propylene through a methylene chloride solution of the Pt-Cl complex **6** and $AgBF_4$ (Figure 2.6). The Pt-propylene complex **8** is stable both in the solid state and in solution; however, propylene is displaced upon addition of donor ligands and solvents, such as THF.

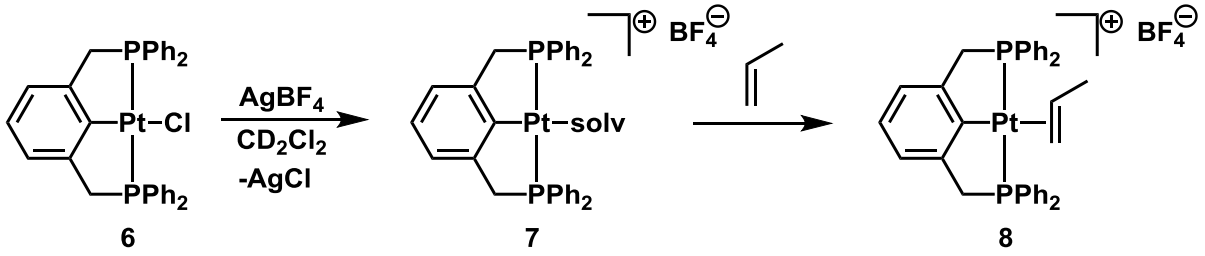

Figure 2.6 Synthesis of **8.**

2.5 Attempted protonation of [PCP)Pt(propylene)][BF_4]

The reaction of the Pt propylene complex **8** with acid was investigated. Addition of one equivalent of HCl·Et_2O to a CD_2Cl_2 solution of **8** resulted in complete disappearance of the ^{31}P resonance corresponding to **8** and the concomitant appearance of a new ^{31}P resonance consistent with (^{Ph}PCP)PtCl. Furthermore, free propylene was observed in the ^{1}H NMR spectrum. Addition of triflic acid resulted in the formation of intractable Pt products and *iso*-propyl triflate. Triflic acid and propylene reacted in the absence of Pt. No reaction was observed between **8** with HBF_4·Et_2O or HOAc. In all cases, [(PCP)Pt-propyl][BF_4][X] was not observed by ^{1}H NMR spectroscopy.

2.6 Synthesis and reactivity of PC(sp^3)PIrHCl

Due to the unsuccessful reactions between the Pd and Pt propylene complexes, **5** and **8**, respectively with acids, we explored a variant of the PCP ligand (PC(sp^3)P) with Ir (Figure 2.7). Ir mono-hydride complexes bearing this ligand have been shown to extrude dihydrogen upon heating, **9** → **10** (Figure 2.7), with one hydrogen coming from the ligand and one from the metal.[17] We hypothesized that we may be able to exploit this M-L cooperativity to form a five-coordinate Ir-alkyl as shown in Figure 2.8. This could facilitate the desired nucleophilic attack by nitrogen nucleophiles to form C-N bonds.

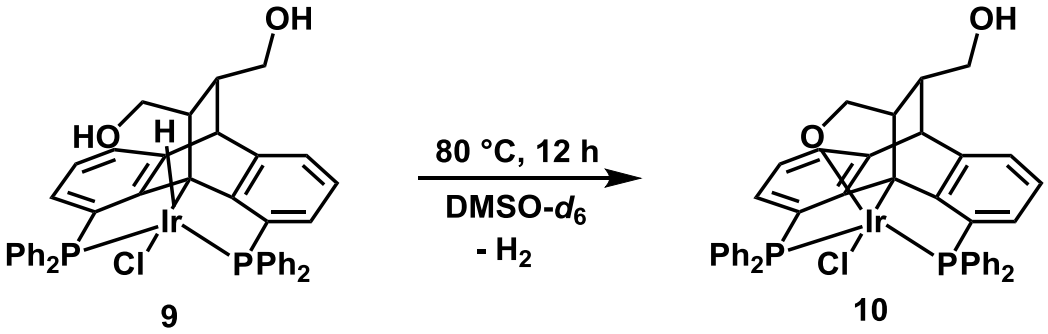

Figure 2.7: Extrusion of dihydrogen by MLC.[13]

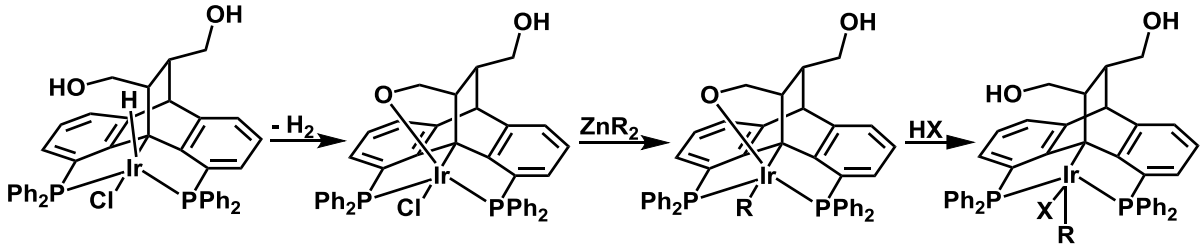

Figure 2.8. Potential synthetic route to a five-coordinate Ir-alkyl.

The reported synthesis for the (PC(sp^3)P) ligand involves a Diels Alder reaction between 1,8-*bis*-(diphenylphosphino)anthracene (anthraphos) and diethyl fumarate.[13] While

the synthesis for anthraphos has been reported,[18] we found many of the reported procedures failed to give the desired product. The most successful strategy, in our laboratory, was reported by Virgili et. al.[19] In short, 1,8-dibromoanthraquinone was synthesized by halide exchange from 1,8-dichloroanthraquinone. This reaction resulted in only partial substitution, as reported. To achieve exclusively 1,8-dibromoanthraquinone, the product mixture was isolated and then subjected to the halide exchange reaction conditions once again (Figure 2.9). This was done until complete conversion to 1,8-dibromoanthraquinone was obtained. Although the reported synthesis required two times, it was often necessary to repeat up to four times to get complete conversion. Reduction with $NaBH_4$ (Figure 2.10)followed by reaction with $KPPh_2$[20] (Figure 2.11) resulted in anthraphos. Reaction of anthraphos with diethyl fumarate followed by reduction to obtain the desired $PC(sp^3)P$ ligand, as well as the metalation with $[IrCl(COE)_2]_2$, were straight forward and synthesized according to the published procedure.[13]

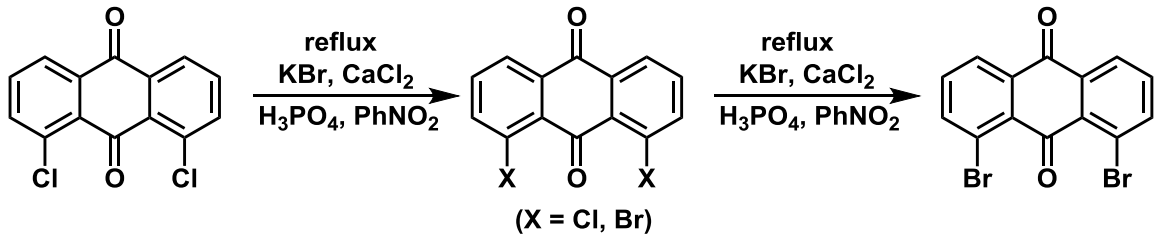

Figure 2.9. Halide exchange to form 1,8-dibromoanthraquinone. Typically it was necessary to subject mixture of halides (middle species) to the reaction conditions 3 times.

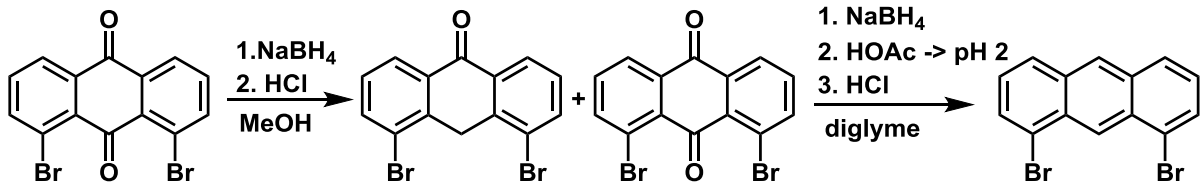

Figure 2.10. Reduction of 1,8-dibromoanthraquinone to form 1,8-dibromoanthracene.

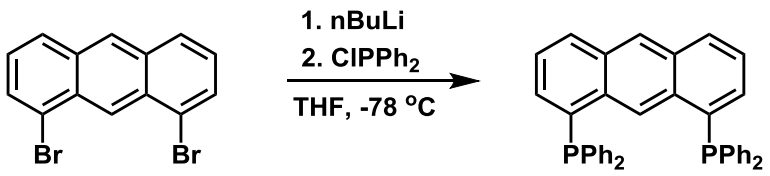

Figure 2.11. Synthesis of anthraphos from 1,8-drbromoanthracene.

As the C-N coupling reactions would likely require heat, we explored thermolysis of (PC(sp^3)P)IrHCl (**9**). We expected that the complex would extrude dihydrogen when heated to 80˚C in DMSO-d_6, as reported, however the complex did not undergo any reactivity at this temperature. At 100 ˚C the complex reacted to generate a new containing a singlet in the ^{31}P NMR spectrum at 21.0 ppm and a hydride in the ^{1}H NMR spectrum at -18.1 ppm. Upon removing the volatiles and vac-transferring C_6D_6 into the tube the singlet in the ^{31}P NMR spectrum (20.9 ppm) and the hydride in the ^{1}H NMR spectrum at -18.5 ppm remained, however all other signals, aside from the aromatic signals, were now gone. Thus we propose the product is (anthraphos)IrHCl, presumably formed by a retro-Diels Alder reaction of the ligand. Due to this shortcoming, this complex was not investigated further.

2.7 Summary

The importance of sterics in the formation of group 10 propylene complexes was highlighted by the difference in reactivity $^{t\text{-Bu}}$PCP vs ^{Ph}PCP ligated Pd complexes toward propylene. Whereas [($^{t\text{-Bu}}$PCP)Pd-solv][BF_4] (**2**) showed no reactivity toward propylene, [(^{Ph}PCP)Pd-solv][BF_4] (**4**) (with smaller phenyl substituents on P) reacted with an excess of propylene, as demonstrated by a 10 ppm downfield shift in the ^{31}P NMR resonance of the ligand, to form [(^{Ph}PCP)Pd-propylene][BF_4] (**5**). The propylene ligand was labile at room temperature and in equilibrium with **4**. As expected, moving down the group resulted in

increased stability and allowed for the synthesis of an isolable group 10 PCP propylene complex, [(^{Ph}PCP)Pt-propylene][BF_4] (**8**). Attempts to protonate **5** and **8** were unsuccessful, thus other systems were explored.

Although a promising potential route to Ir alkyls was proposed starting from complex **9**, the challenge of the synthesis as well as the fact that **9** decomposed via a retro-Diels Alder reaction upon heating, rendered this system unviable for our target reaction.

Experimental

General considerations. All manipulations were carried out in a nitrogen filled glove box, using standard Schlenk techniques, or on a high vacuum manifold, unless otherwise noted. Propylene pressurizations were performed by transferring an appropriate amount of propylene to a known volume bulb on a high vacuum manifold. The propylene was then condensed into a J. Young style NMR tube. Deuterated solvents were purchased from Cambridge Isotope Laboratories and dried over calcium hydride (methylene chloride-d_2, chloroform-d_3, and acetonitrile-d_3), sodium/benzophenone (THF-d_8 and benzene-d_6), or indicator drierite (acetone-d_6). THF, methylene chloride, ether, benzene, and toluene were dried by passage through columns containing activated alumina and molecular sieves. All other solvents were dried over molecular sieves. All other reagents were purchased from Aldrich or Strem and used as received. NMR spectra were recorded on Bruker AV 300, DRX 499, and AV 500 spectrometers. ^{1}H NMR chemical shifts were referenced to residual solvent signals and are reported relative to TMS as 0 ppm. ^{31}P chemical shifts were referenced to an

85% H_3PO_4 external standard set to 0 ppm. (^{Ph}PCP)PdCl (**3**),[21] (^{Ph}PCP)PtCl (**6**),[22] and (PC(sp^3)P)IrHCl (**9**)[13] were prepared according to published procedures.

[(^{Ph}PCP)Pd-propylene][BF4] (5). This procedure was modified from a published procedure.[11]**Error! Bookmark not defined.** In a 4 mL vial, (^{Ph}PCP)PdCl (4 mg, 0.007 mmol) and $AgBF_4$ (1.4 mg, 0.0072 mmol) were dissolved in CH_2Cl_2 (2 mL). The solution was stirred for 20 minutes during which a grey precipitate formed. The solution was filtered through celite into a NMR tube fitted with a Teflon valve. The tube was pressurized with 5 atm of propylene. After 20 minutes, the volatiles were removed and CD_2Cl_2 was added by vacuum transfer to give a pale yellow solution. ^{1}H NMR (CD_2Cl_2, 500 MHz, 298 K): δ 1.88 - 2.16 (broad), 4.08 - 4.55 (broad), 5.27 (broad), 6.40 - 6.75 (broad), 7.26 (1H, m, Ar-*H*), 7.32 (2H, d, J_{HH} = 6.8 Hz, Ar-*H*), 7.52 - 7.88 (m, P-Ph). ^{31}P{^{1}H} NMR (CD_2Cl_2, 298 K): δ 39.89 (br s, Pd-solv), 49.73 (br s, Pd-propylene). ^{1}H NMR (CD_2Cl_2, 500 MHz, 200 K): δ 1.18 (2.3H, d, J_{H-H} = 6.1 Hz, -CH_3), 4.15 (2H, d vt, J_{H-H} = 16.8 Hz, J_{H-P}= 5.6 Hz, Ar-C*H*$_2$-P), 4.47 (2.6H, m, Ar-C*H*$_2$-P), 4.77 (0.7H, m, -CH_2), 5.93 (0.7H, m, -CH), 7.37 (1H, t, J_{H-H} = 7.5, Ar-*H*), 7.43 (2H, d, J_{H-H} = 7.5, Ar-*H*), 7.52 – 7.88 (20H, m, P-Ph). ^{31}P{^{1}H} NMR (202 MHz, CD_2Cl_2, 200 K): δ 49.6.

Example of attempted protonation of 5. To a solution of **5** (4.6 mg, 0.0065 mmol) in CD_2Cl_2, approximately one equivalent of triflic acid (c.a. 0.9 μL, 0.01 mmol) or $HBF_4 \cdot Et_2O$ (c.a. 1 μL, 0.007 mmol) was added by micro syringe. Additional acid (5 equivalents) was added. ^{1}H and ^{31}P NMR spectra were recorded after addition of more acid. At least six species were observed by ^{31}P NMR spectroscopy and no evidence of a Pd-propyl moiety was observed in the ^{1}H NMR spectrum.

Example of attempted protonation of 5 with anilinium salts. To a solution **5** (4.6 mg, 0.0065 mmol) of in CD_2Cl_2, one equivalent of anilinium triflate (1.6 mg, 0.0065 mmol), anilinium tetrafluoroborate (1.2 mg, 0.0065 mmol), or anilinium $B(Ar^F)_4$ (6.3 mg, 0.0065 mmol) was added to the tube and ^1H and ^{31}P NMR spectra were recorded. Multiple intractable products were observed by ^{31}P and ^1H NMR spectroscopy along with the formation of Pd black.**[(^{Ph}PCP)Pt-propylene][BF_4] (8).** In a 50 mL sealable glass vessel, (^{Ph}PCP)PtCl (**6**) (51 mg, 0.72 mmol) and $AgBF_4$ (15.5 mg, 0.079 mmol) were dissolved in CH_2Cl_2 (10 mL). The solution was stirred at room temperature for 20 min resulting in a light brown suspension. Propylene was bubbled through the suspension for 20 min. The suspension was filtered through celite and the volatiles removed in vacuo. The resulting yellow solid was washed with pentane (3 x 5 mL) (50.9 mg, 87 % yield). ^1H NMR, (CD_2Cl_2, 500 MHz, 298 K): δ 1.15 (3H, d, J_{H-H} = 6.1 Hz, J_{Pt-H} = 18.4 Hz, Pt-CH_2CHCH_3), 3.99 (1H, d, J_{H-H} = 8.3 Hz, J_{Pt-H} = 40.7 Hz, Pt-CH_2CHCH_3), 4.12 (2H, dvt, J_{H-H} = 16.9 Hz, J_{P-H} = 4.9 Hz,Ar-CH_2-P), 4.26 (2H, dt, J_{H-H} = 16.7 Hz, J_{P-H} = 3.7 Hz, Ar-CH_2-P), 4.38 (1H, dvt, J_{H-H} = 13.7 Hz, J_{P-H} = 3.5 Hz, Pt-CH_2CHCH_3), 5.45 (1H, m, Pt-CH_2CHCH_3), 7.22 (1H, t, J_{H-H} = 7.4 Hz, Ar), 7.3 (d, J_{H-H} = 7.5 Hz, Ar), 7.52 – 7.81 (20H, m, P-Ph). $^{31}P\{^1H\}$ NMR (202 MHz, 298 K, CD_2Cl_2) δ 44.2 (s, J_{Pt-P} = 2709 Hz).

Reaction of 8 with HCl. 8 (0.35 mg, 0.0044 mmol) was weighed into a NMR tube fitted with a Teflon valve. CD_2Cl_2 was vacuum transferred into the tube. HCl (2.2 μL, 2 M solution in Et_2O) was added. ^{31}P and ^1H NMR spectra were consistent with (PCP)PtCl and free propylene.

Reaction of 8 with triflic acid. To a solution of **8** (4.5 mg, 0.0057 mmol) in CD_2Cl_2 triflic acid (c.a. 1μL, 0.01 mmol) was added. After 24 h, the appearance of a minor species was

observed at 42.9 ppm in the ^{31}P NMR spectrum. An additional 1 μL of triflic acid was added resulting in the disappearance of **8**, but no new species by ^{31}P NMR spectroscopy, indicating possible decomposition. ^{i}PrOTf was observed in the ^{1}H NMR spectrum.

Reaction of 8 with $HBF_4{\cdot}Et_2O$. To a solution of **8** (4.5 mg, 0.0057 mmol) in CD_2Cl_2 $HBF_4{\cdot}Et_2O$ (c.a. 1μL, 0.006 mmol) was added. No reaction was observed after 24 h. An additional 1μL was added. Still no reaction was observed. Heating to 60 ˚C also did not result in a reaction.

Thermolysis of 9. 9 (4 mg, 0.0046 mmol) was weighed into a NMR tube fitted with a Teflon valve. DMSO-d_6 (c.a. 4 mL) was added. The tube was heated at 80 ˚C for 24 h. No reaction was observed. Heating up to 140 ˚C resulted in the proposed (anthraphos)IrHCl. The volatiles were removed and C_6D_6 was vacuum transferred in to the tube. ^{1}H NMR, (C_6D_6, 500 MHz, 298 K) δ -15.3 (1H, t J_{P-H} = 15.3 Hz). $^{31}P\{^{1}H\}$ NMR (202 MHz, 298 K, C_6D_6) δ 20.9 (s).

Notes to Chapter 2

(1) Franke, R.; Selent, D.; Börner, A. Chem. Rev. 2012, 112, 5675.

(2) Bhaduri, S.; Mukesh, D. *Homogeneous Catalysis: Mechanisms and Industrial Applications,* New York. **2000**.

(3) Müller, T. E.; Hultzsch, K. C. Yus, M.; Foubelo, F.; Tada, M. *Chem. Rev*. **2008**, *108*, 3795.

(4) (a) Lin, B. L.; Clough, C. R.; Hillhouse, G. L. *J. Am. Chem. Soc*. **2002**, *124*, 2890. (b) Pawlikowski, A. V.; Getty, A. D.; Goldberg, K. I. *J. Am. Chem. Soc*. **2007**, *129*, 10382. (c)

Marquard, S. L.; Rosenfeld, D. C.; Hartwig, J. F. *Angew. Chem.* **2010**, *122*, 805. (d) Hanley, P. S.; Marquard, S. L.; Cundari, T. R.; Hartwig, J. F. *J. Am. Chem. Soc.* **2012**, *134*, 15281. (e) Pérez-Temprano, M. H.; Racowski, J. M.; Kampf, J. W.; Sanford, M. S. *J. Am. Chem. Soc.* **2014**, *136*, 4097. (f) Camasso, N. M.; Sanford, M. S. *Science*, **2015**, *347*, 1218.

(5) Frech, C. M.; Milstein, D. *J. Am. Chem. Soc.* **2006**, *128*, 12434.

(6) Goldberg, J. M.; Wong, G. W.; Barstow, K. E.; Kaminsky, W.; Goldberg, K. I.; Heinekey, D. M. *Organometallics*, **2015**, *34*, 753.

(7) Ahuja, R.; Punji, B.; Findlater, M.; Supplee, C.; Schinski, W.; Brookhart, M.; Goldman, A. S. *Nature Chemistry* **2011**, *3*, 167.

(8) Kraatz, H-B.; Milstein, D. *J. Organomet. Chem.* **1995**, *488*, 223.

(9) Hahn, C.; Morvillo, P.; Vitagliano, A. *Eur. J. Inorg. Chem.* **2001**, 419.

(10) St. John, A. Investigations in Chemical Hydrogen Storage and the anti-Markovnikov Hydroamination of Alkenes. Ph.D. Dissertation, University of Washington Seattle, WA. **2011**.

(11) Kimmich, B. F.M.; Marshal, W. J.; Fagan, P. J.; Hauptman, E.; Bullock, R. M. *Inorganica Chimica Acta.* **2002**, 330, 52.

(12) Moulton, C. J.; Shaw, B. L. *J. Chem. Soc., Dalton Trans.* **1976**, 1020.

(13) Tolman, C. A. *Chem. Rev.* **1977**, *77*, 313.

(14) Hughes, R. P.; Williamson, A.; Incarvito, C. D.; Rheingold, A. L. *Organometallics* **2001**, 20, 4741.

(15) Sehnal, P.; Taylor, R. J. K.; Fairlamb, J. S. *Chem. Rev.* **2010**, *110*, 824.

(16) Bennett, M. A.; Jin, H.; Willis, A. C. *J. Organomet. Chem.* **1993**, *451*, 249.

(17) Musa, A.; Shaposhnikov, I.; Cohen, S.; Gelman, D. *Angew. Chem. Int. Ed.* **2011**, *50*, 3533.

(18) Haenel, M. W.; Jakubik, D.; Krueger, C.; Betz, P. Chem. Ber. 1991, 124, 333.

(19) Pérez-Trujillo, M.; Maestre, I.; Jaime, C.; Alvarez-Larena, A.; Piniella, J. F.; Virgili, A. *Tetrahedron: Asymmetry* **2005**, *16*, 3084.

(20) Romero, P. E.; Whited, M. T.; Grubbs, R. H. *Organometallics* **2008**, *27*, 3422.

(21) Duncan, D.; Hope, E. G.; Singh, K.; Stuart, A. M. *Dalton Trans.* **2011**, 40, 1998.

(22) Dorta, R.; Goikhman, R.; Milstein, D. *Organometallics* **2003**, 22, 2806.

Chapter 3

Synthesis and reactivity of (Pybox)Ir and (Pybox)Rh complexes

3.1 Introduction

In Chapter 2, protonation of group 10 olefin complexes to form the corresponding alkyl complexes was targeted, however the complexes investigated were either not protonated upon addition of acid or reacted with acid to form intractable products. Examples of tridentate group 9 olefin complexes are much more prevalent in the literature, and notably, protonation of cationic group 9 olefin complexes has been shown.[1,2,3] $^{i\mathrm{Pr}}$Pybox (Pybox = (*S*,*S*)-2,6-Bis(4-isopropyl-2-oxazolin-2-yl)pyridine) ligated group 9 ethylene complexes reported by Gamasa et. al. were of particular interest.[3] Notably, [(*S*,*S*-$^{i\mathrm{Pr}}$Pybox)Ir(C_2H_4)$_2$][PF_6] was prepared in methanol solvent, with no displacement of the ethylene ligands by methanol, a potential donor ligand. The ethylene ligands could however be displaced by stronger π-acids, such as alkynes and CO.[1]

It was reported that [(*S*,*S*-$^{i\mathrm{Pr}}$pybox)Ir(C_2H_4)$_2$][PF_6] reacted cleanly with HCl in THF to retain one of the ethylene ligands and form the Ir^{III} complex, [(*S*,*S*-$^{i\mathrm{Pr}}$pybox)Ir(C_2H_4)H(Cl)][PF_6].[1] In a subsequent report, it was shown that [(*S*,*S*-

$^{i\mathrm{Pr}}$pybox)Ir(C_2H_4)$_2$][PF_6] could be protonated by acetic acid to form the ethyl complex, [(*S*,*S*-$^{i\mathrm{Pr}}$pybox)Ir(Et)(OAc)][PF_6].[3] It was proposed that the initial formation of a mono olefin hydride subsequently undergoes insertion to give the alkyl moeity. κ^1 to κ^2 coordination of the acetate ligand presumably traps out the Ir-ethyl.

Numerous examples of C(sp^3)-X (X = N, O, I) reductive elimination have shown that nucleophilic attack occurs at the alkyl, trans to an open site.[4] We hypothesized that having a strong *trans* labilizing ligand (ethyl) *trans* to the acetate may assist in the formation of a five-coordinate species by κ^2 to κ^1 coordination of the acetate ligand. Described in this chapter is the synthesis of Pybox ligated Ir-Et and Rh-Et complexes and their reactivity with nucleophiles.

3.2 Synthesis of [(^{dm}Pybox)Ir(Et)(OAc)][PF_6] (12)

The complex [(*S*,*S*-^{iPr}Pybox)Ir(Et)(OAc)][PF_6] can be prepared by protonation of the *bis*-ethylene precursor, [(*S*,*S*-^{iPr}Pybox)Ir(C_2H_4)$_2$][PF_6].[3] To simplify NMR studies, the dimethyl analogue, [(^{dm}Pybox)Ir(Et)(OAc)][PF_6] (^{dm}Pybox = 2,6-bis[4',4'-dimethyloxazolin-2'-yl]pyridine)[5] (**12**), was prepared by protonation of [(^{dm}Pybox)Ir(C_2H_4)$_2$][PF_6] (**11**). Unlike [(*S*,*S*-^{iPr}Pybox)Ir(Et)(OAc)][PF_6], complex **12** does not contain diastereotopic protons, thus has a much simpler ^{1}H NMR spectrum. The ^{1}H NMR spectrum for complex **12** exhibited a triplet and quartet (in CD_2Cl_2) for the ethyl ligand at 0.39 ($J_{H\text{-}H}$ = 7.4 Hz) and 1.05 ($J_{H\text{-}H}$ = 7.4 Hz) ppm, respectively, and a singlet for the acetate ligand at 2.11 ppm. These values are quite close to [(^{dm}Pybox)Ir(Et)(OAc)][PF_6] for which the corresponding resonances (in CD_2Cl_2) show up at 0.36, 1.05 (multiplet), and 2.10 ppm, respectively.

3.3 Synthesis and reactivity of [(^{dm}Pybox)Ir(Et)(TFA)(NH_2Ph)][PF_6] (13)

The fact that the ^{dm}PyboxIr *bis*-ethylene complex **11** is protonated by acetic acid, a weak acid, is ideal for our proposed catalytic cycle for anti-Markovnikov hydroamination (Figure 3.1). This implies that the ammonium salts generated may be strong enough acids to protonate the metal olefin complexes (Figure 3.1, step b'). This would make the overall process catalytic in acid.

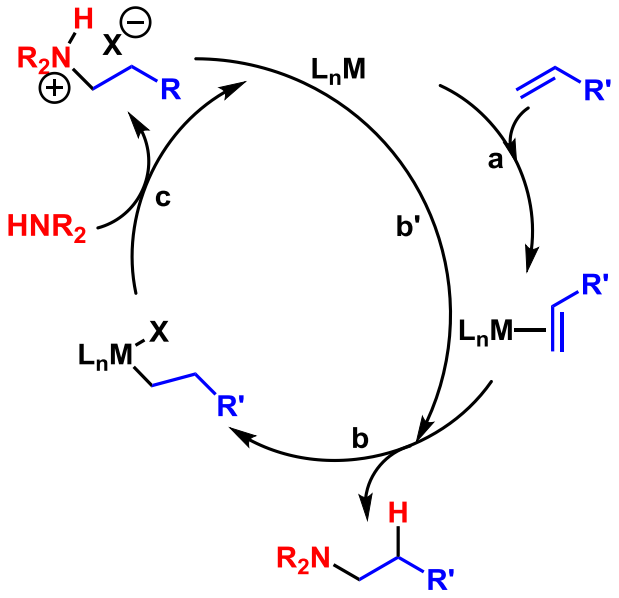

Figure 3.1. Proposed catalytic cycle for anti-Markovnikov hydroamination.

Notably, **11** was also protonated by anilinium trifluoroacetic acid to form [(^{dm}Pybox)Ir(Et)(TFA)(NH_2Ph)][PF_6] (**13**) (Figure 3.2). The ^{1}H NMR resonances corresponding to **13** were significantly shifted compared to **12.** The ethyl ligand now exhibits upfield shifted triplet at 0.01 ppm whereas the quartet has been shifted downfield to 1.6 ppm (^{1}H NMR spectrum). We propose that the trifluoroacetate ligand dissociates ($\kappa^2 \rightarrow \kappa^1$) *trans*

to the ethyl ligand and aniline occupies the sixth site. Broad signals at 7.14, 7.03, and 6.35 ppm were observed in the ^{1}H NMR spectrum, supporting the coordination of aniline.

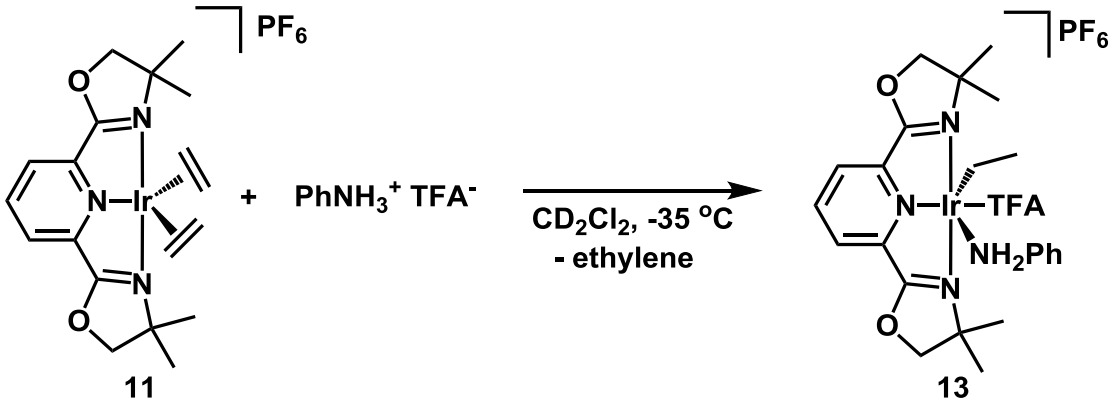

Figure 3.2: Protonation of **11** with anilinium trifluoroacetic acid to form **13**.

As complex **13** contains both an ethyl ligand and aniline, the possibility of promoting a direct C-N coupling reaction was considered. Unfortunately, thermolysis of **13** (in CD_2Cl_2) at 60 ˚C over several days resulted in the formation of multiple intractable Ir products as detected by ^{1}H NMR spectroscopy. Ethylene (5.40 ppm) and what appeared to be a new aniline based product based on a new set of aromatic resonances downfield of free aniline were also observed. The aniline based organic product was characterized by GC-MS as 2,2,2-trifluoro-*N*-phenylacetamide, likely formed by the known substitution reaction between amines and carboxylic acids.[6] However no resonances were observed in the ^{1}H NMR spectrum of the product mixture that corresponded to *N*-ethylaniline for which the ethyl signals show up at 3.14 (q) and 1.24 (t) ppm.

3.4 Reactivity of [(^{dm}Pybox)Ir(Et)(OAc)][PF_6] (12) with amines.

Although thermolysis of **13** did not lead to the desired C-N coupling, the acetate ligand in **12** would should be less susceptible to nucleophilic attack than the trifluoroacetate ligand in **13.** The reactivity of **12** was investigated with both aromatic and aliphatic amines. In all cases, no evidence of nucleophilic attack at the acetate ligand was observed.

Addition of an amine (amine = morpholine, piperidine, or aniline) (5 equiv.) to a CD_2Cl_2 solution **12** resulted in immediate quantitative formation of a new product. The product was characterized by ^{1}H NMR spectroscopy as the amine ligated complex (Figure 3.3). For the reaction of **12** with morpholine, the singlet indicative of the coordinated acetate group shifted from 2.11 ppm to 2.19 ppm. Additionally, the resonances corresponding to the oxazoline methylene protons were observed as a pair of doublets at 4.83 ppm, in contrast to the singlet observed in the starting material at 4.92 ppm, supporting the formation of the amine-ligated complex [(^{dm}Pybox)Ir(Et)(OAc)(morpholine)][PF_6] (**14-morpholine**). No further reaction was observed at room temperature. Thermolysis at 50 ˚C of the reaction mixture did not promote C-N bond formation, but rather led to the formation of ethylene. Qualitatively, ethylene was formed faster with more basic amines (piperidine (pK_a = 11.22)[7] and morphline (pK_a = 8.36)[7] reacted faster than aniline (pK_a = 4.19)[8]). This reactivity parallels the E2 elimination in organic chemistry and it is hypothesized that β-deprotonation (by the amine) of the ethyl group (Figure 3.4) is more favorable than nucleophilic attack at the α-carbon (Figure 3.5).

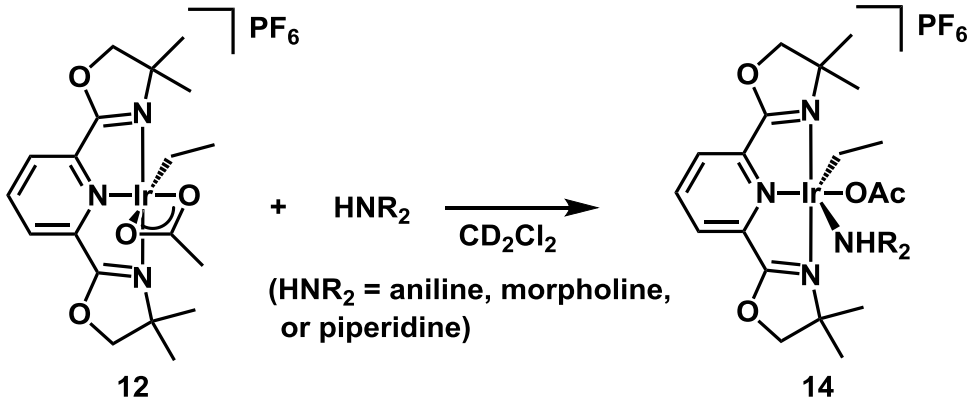

Figure 3.3. Reaction of **12** with amines to form the amine ligated complex, **14-amine**.

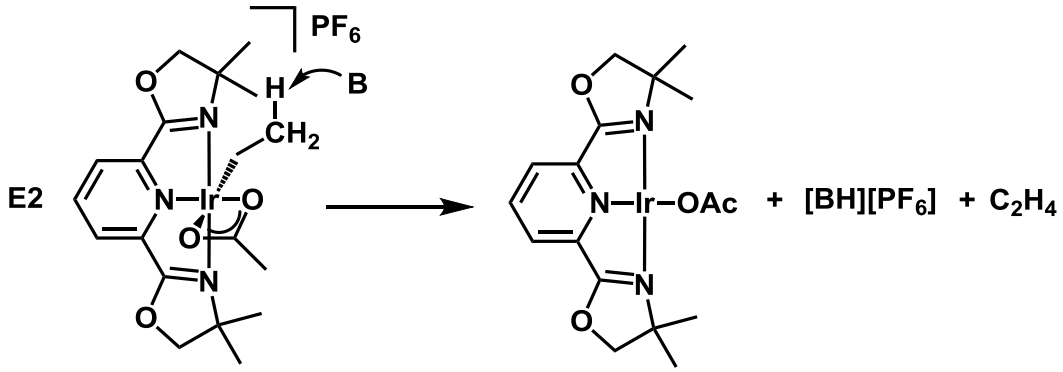

Figure 3.4. E2 type elimination of ethylene.

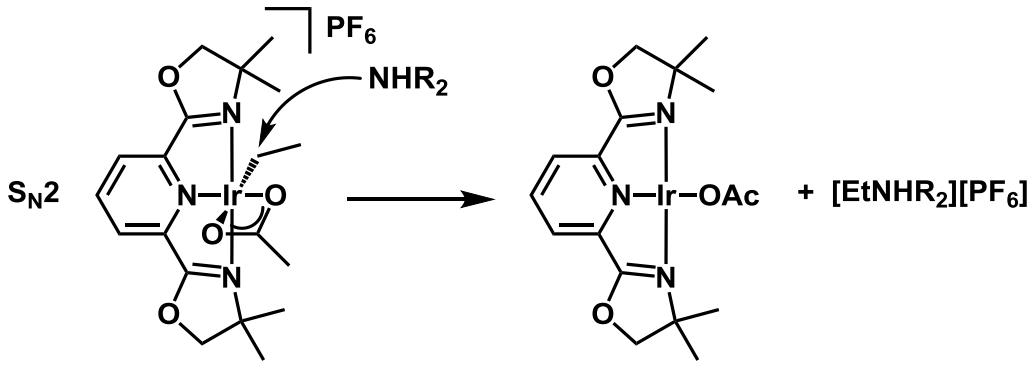

Figure 3.5. S_N2 attack the α-carbon of the Ir ethyl ligand.

To substantiate this proposal of the amine acting as a base in deprotonation of β-H of the alkyl, the reactivity of **12** was explored with other bases. Similar to the reactions with amines, thermolysis of **12** (in CD_2Cl_2) the presence of bases, such as Cs_2CO_3, $LiN(SiMe_3)_2$, and KO^tBu resulted in the formation of ethylene as determined by ^1H NMR spectroscopy. Attempts were made to explore the mechanism of this reaction, but despite screening many bases, multiple unidentifiable products were always formed, possibly due to the electrophilic sites on the Pybox ligand (*vide infra*).

Solvent effects were explored and provided further support for the β-deprotonation of the Ir-ethyl ligand. More polar solvents should favor S_N2 by stabilizing the transition state (Figure 3.5) and disfavor E2 (Figure 3.4).[9] Thermolysis of **12** in the presence of trimethylamine (5 equiv.) in acetone-d_6 gave markedly different results than thermolysis with the same amine in CD_2Cl_2. In acetone, almost no ethylene was observed by ^1H NMR spectroscopy. Furthermore, most of the starting material was retained along with the formation of a new product characterized by X-ray crystallography as the aquo complex, [(^{dm}Pybox)Ir(Et)(OAc)(aquo)][PF_6], **14-aquo** (Figure 3.6). The aquo ligand likely originated from adventitious water in the solvent. Consistent with our prediction for the amine complexes, the aquo ligand is *trans* to the ethyl ligand.

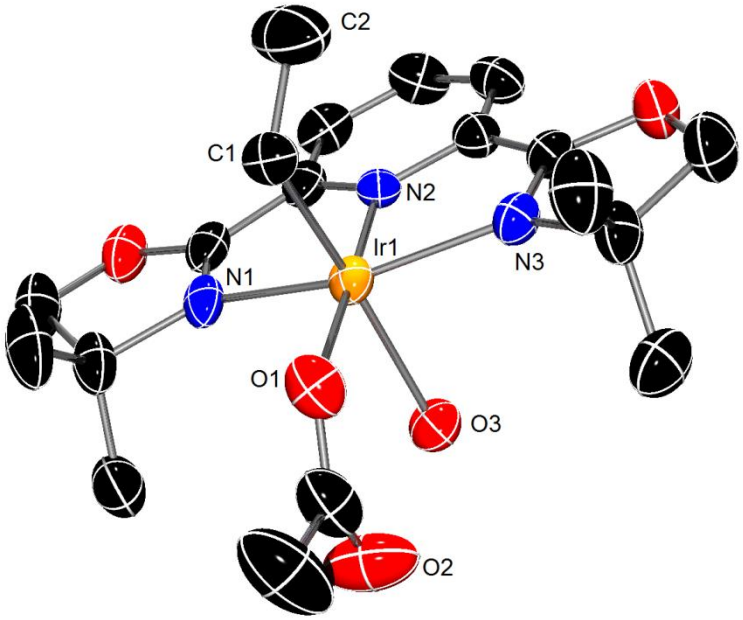

Figure 3.6. ORTEP of **14-aquo** shown with thermal ellipsoids at 50% probability level. The counter ion and hydrogen atoms have been omitted for clarity. Selected bond lengths (Å) and angles (˚): Ir(1)-N(1) = 2.054(4), Ir(1)-N(2) = 1.936(3), Ir(1)-N(3) = 2.048(4), Ir(1)-O(1) = 2.069(2), Ir(1)-O(3) = 2.244(3), Ir(1)-C(1) = 2.03(3), Ir(1)-C(1)-C(2) = 115(2).

3.5 Attempts to promote reductive elimination from 14 by oxidation

As thermolysis proved unsuccessful in promoting C-N bond formation under a variety of conditions, alternative methods to promote C-N bond formation from 14 were also explored. There is precedent for promoting reductive elimination reactions by oxidation of the metal center.[10,11,12] For example Hillhouse et al. reported the reductive elimination of C-N bonds from Ni promoted by oxidation.[13] Mayer, Sanford, et al. reported the oxidatively induced reductive elimination of ethane from Pd-Me complexes promoted by addition of ferrocenium hexafluorophosphate (Fc^+).[11] Furthermore, Periana et. al. reported the

oxyfunctionalization of an Ir-Me by addition of iodobenzene bis(trifluoroacetate).[12] Thus the reactivity of **14** was explored with both of these oxidants.

Complex **14-aniline** was prepared *in situ* (THF-d_8) and characterized by ^{1}H NMR spectroscopy. To this solution Fc^+ (1 eq.) was added. After 24 hours at room temperature, a resonance consistent with Fc was observed suggesting that an oxidation had occurred. No further reaction was observed after 10 days. At the end of the reaction, **14** remained (approximately 50 %) and there was a new upfield triplet at -0.07 ppm ($J_{H\text{-}H}$ = 7.5 Hz) suggesting a new Ir-ethyl had been formed (the quartet was obscured by other signals). Free acetic acid was also observed. This product was characterized by X-ray crystallography as [(^{dm}Pybox)Ir(Et)(Cl)(aniline)][PF_6] (**15**)[14] (Figure 3.7). There was a small amount of CH_2Cl_2 at the start of the reaction, which is likely where the Cl ligand originated. Notably, no C-N bonds were formed. This reaction was repeated with heat (80 ˚C), but still no C-N coupled products were observed (confirmed by GC-MS).

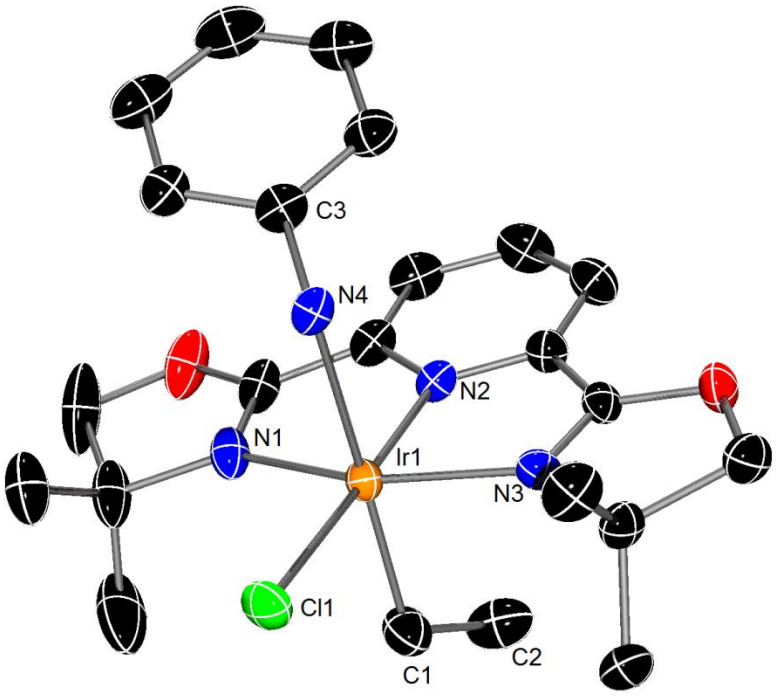

Figure 3.7. ORTEP of **15** shown with thermal ellipsoids at 50% probability level. The counter ion and hydrogen atoms have been omitted for clarity. Selected bond lengths (Å) and angles (˚): Ir(1)-N(1) = 2.046(5), Ir(1)-N(2) = 1.952(4), Ir(1)-N(3) = 2.045(4), Ir(1)-N(4) = 2.290(4), Ir(1)-Cl(1) = 2.3700(13), Ir(1)-C(1) = 2.088(6), Ir(1)-C(1)-C(2) = 119.1(4), Ir(1)-N(4)-C(3) = 115.3(3).

The reactivity of **14-aniline** was also explored with iodobenzene bis(acetate). **14-aniline** was prepared *in situ* (acetone-d_6) and characterized by ^{1}H NMR spectroscopy. Iodobenzene bis(acetate) (1 equiv.) was added resulting in the slow disappearance of the Ir-ethyl ligand. Over the course of 4 days at ambient temperature a multitude of products were formed by ^{1}H NMR spectroscopy, however, no C-N coupled products were detected.

3.6 Reactivity of 12 with other nucleophiles

Due to the undesirable reaction of **12** with basic amines, other nucleophiles were investigated. No reaction of **12** with NaN_3 was observed in CD_2Cl_2, presumably due to the insolubility of NaN_3. However, reaction of an acetone-d_6 solution of complex **12** with NaN_3 resulted in a color change from green to brown and a broadening of the ^{1}H NMR resonances. Thermolysis of a mixture of **12** and five equivalents of NaN_3 (acetone-d_6) at 80 $^\circ$C for 24 hours resulted in formation of multiple iridium products. At intermediate time points, there was evidence of an Ir hydride in the ^{1}H NMR spectrum at -25.05 ppm. The resonances corresponding to the ethyl ligand were completely absent by the end of the reaction and ethylene was observed. As the reaction proceeded, ethylene-d_1 was also observed. No C-N products were observed by ^{1}H NMR spectroscopy or GC-MS.

Addition of KI to an acetone-d_6 solution of **12** resulted in a significant upfield shift of the CH_3 resonance to -0.43 ppm in the ^{1}H NMR spectrum, consistent with the formation of (^{dm}Pybox)Ir(Et)(OAc)I (**16**) (Figure 3.8)[15]. Thermolysis of **16** and KI (5 equiv.) in acetone-d_6 at 80 $^\circ$C 24 hours resulted in the complete loss of the ethyl ligand and the formation of at least two new unidentified Ir containing species. Furthermore, ethylene and ethylene-*d* were observed in the ^{1}H NMR spectrum at the end of the reaction. No C-I coupling was observed by ^{1}H NMR spectroscopy.

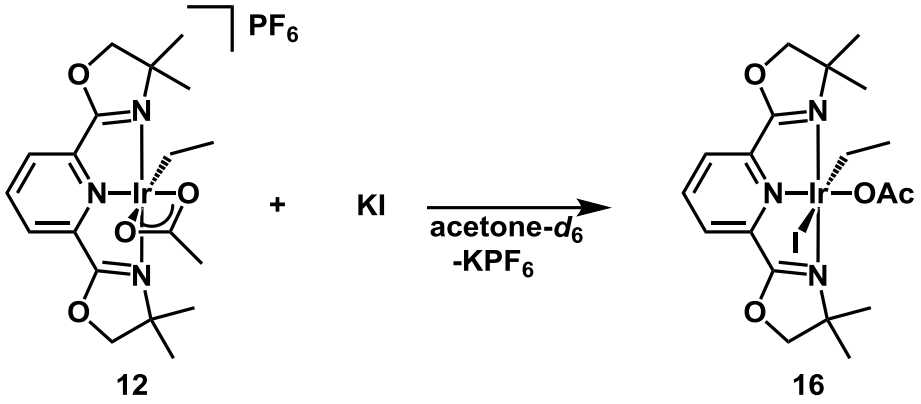

Figure 3.8. Reaction of **12** with KI to form **16**.

3.7 Synthesis of Rh analogues

The reactivity of the (Pybox)Rh analogues was also of interest. The presumably weaker rhodium carbon bond in these complexes could make them more amenable to C-X bond formation. However, these complexes were not known and initial attempts to prepare [(^{dm}Pybox)Rh(C_2H_4)$_2$][PF_6] using a similar procedure to the iridium complexes were unsuccessful and led only to decomposition. Additional attempts were carried out both in methanol (reported solvent for iridium) and THF as well as under ethylene atmosphere. Decomposition was observed in all cases.

While the complex [(^{dm}Pybox)Rh(C_2H_4)$_2$][PF_6] was not stable and decomposed at ambient temperature, protonation at low temperature (-40 °C) with acetic acid led to the formation of an isolable mixture upon warming to ambient temperature. This mixture was characterized by ^{1}H NMR spectroscopy and contained two Rh species. Both products appeared to contain an ethyl ligand as there were two upfield triplets and two quartets, both with Rh coupling ($J_{Rh\text{-}H}$ = 3.4 Hz). The products were formed in a 1:1.3 ratio and one

appeared to contain bound methanol as there was a peak in the ^{1}H NMR spectrum at 3.43 ppm that integrated to 3H compared to one of the ethyl resonances. Crystals suitable for X-ray diffraction were grown by vapor diffusion of pentane into a concentrated THF solution of the product mixture. Interestingly, the solid state structure (Figure 3.9) revealed one of the products had reacted further upon crystallization, and now contained an ethylene ligand bridging two Rh centers.

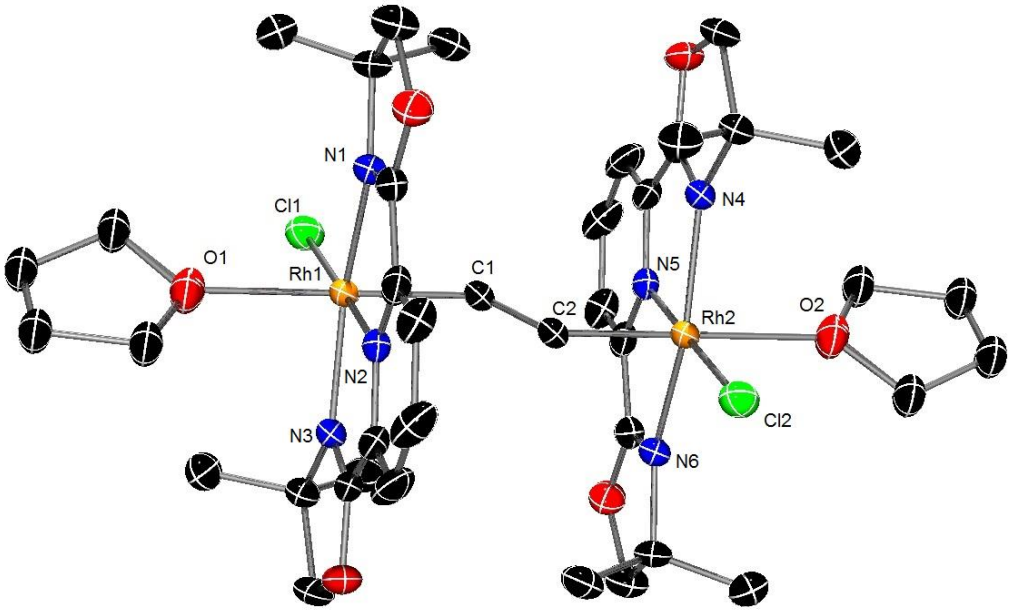

Figure 3.9. ORTEP of ethyl bridged Rh dimer shown with thermal ellipsoids at 50% probability level. The counter ion and hydrogen atoms have been omitted for clarity. Selected bond lengths (Å) and angles (˚): Rh(1)-O(1) = 2.316(7), Rh(1)-Cl(1) = 2.3343(12), Rh(1)-N(1) = 2.064(3), Rh(1)-N(2) = 1.957(3), Rh(1)-N(3) = 2.048(3), Rh(1)-C(1) = 2.072(4), Rh(1)-C(1)-C(2) = 115.5(4).

Notably, if protonation of the *in-situ* generated Rh ethylene complex at low temperature (-40 ˚C) (in MeOH) was performed using anilinium trifluoroacetate, the desired product, [(^{dm}Pybox)Rh(Et)(TFA)(MeOH)][PF_6] **17,** was formed as the sole product (Figure 3.10). This product was isolated upon warming to ambient temperature. The ^{1}H NMR spectrum for complex **17** (in CD_2Cl_2) exhibited a doublet of quartets at 2.86 ppm ($J_{H\text{-}H}$ = 7.5 Hz, $J_{Rh\text{-}H}$ = 2.6 Hz) and a triplet at 0.55 ppm. A sharp singlet at 3.3 ppm (that integrates to 3H) suggests that methanol was bound. Presumably the trifluoroacetate is κ^1 and methanol occupies the sixth. Free methanol was not observed, indicating an exchange reaction was not occurring.

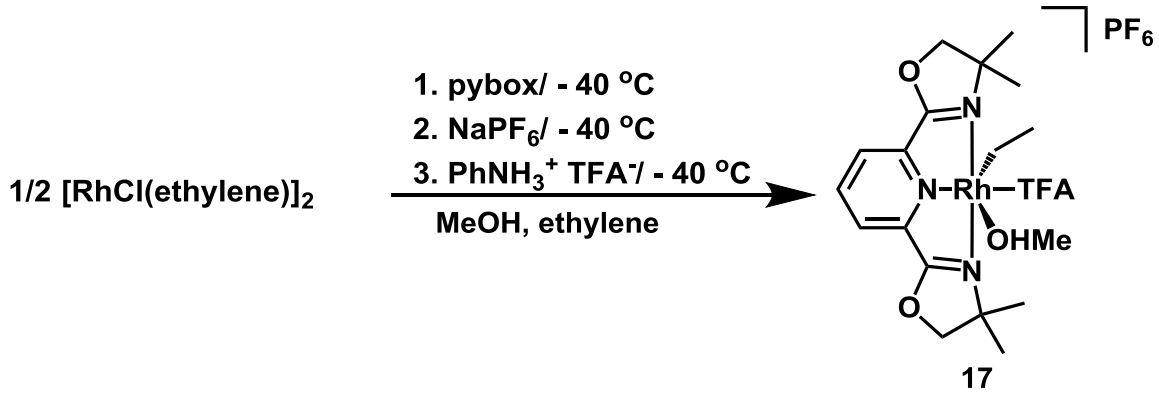

Figure 3.10. Synthesis of **17**.

The reactivity of complex **17** was investigated with aniline in both THF-d_8 and acetonitrile-d_3. Addition of aniline to a THF-d_8 slurry of complex resulted in displacement of the methanol ligand (free methanol observed in the ^{1}H NMR spectrum). It is presumed that a THF or aniline ligated complex is formed but due to the broadness of the signals, it is not clear if THF or aniline is bound. Thermolysis of this reaction mixture at 80 ˚C did not result in the formation of any coupled products, and similar to the reactions with **12**, the formation

of ethylene was observed in the ^{1}H NMR spectrum. Ethylene was also observed when the reaction of **17** with aniline was performed in acetonitrile-d_3.

3.8 Oxazoline ring opening by nucleophilic attack.

The reaction with sulfur nucleophiles provided some insight as to why so many products may be forming in the previous reactions with nucleophiles. Addition of five equivalents of NaSPh to complex **12** in acetone-d_6 at room temperature resulted in the formation of several new species as detected by ^{1}H NMR spectroscopy. However, this complex mixture reacted further at room temperature over the course of 24 hours to form a single product (90% NMR yield). The ^{1}H NMR spectrum reveals four distinctive resonances for the oxazoline methylene protons at 4.76, 4.73, 4.44, and 3.72 ppm, suggesting that the oxazoline methylene protons are in a different chemical environment. A single crystal suitable for X-ray crystallography was grown from vapor diffusion of pentane into an acetone solution containing the product. Analysis by X-ray crystallography (Figure 3.11) revealed the product to be [(NNNS)Ir(Et)(SPh)]Na, **18** (Figure 3.12). Notably, nucleophilic attack by the thiophenylate at the carbon of the oxazoline rings was observed resulting in ring opening. No reaction of thiophenylate with iridium ethyl ligand was observed. In this reaction, ring opening of the oxazoline rings occurred.

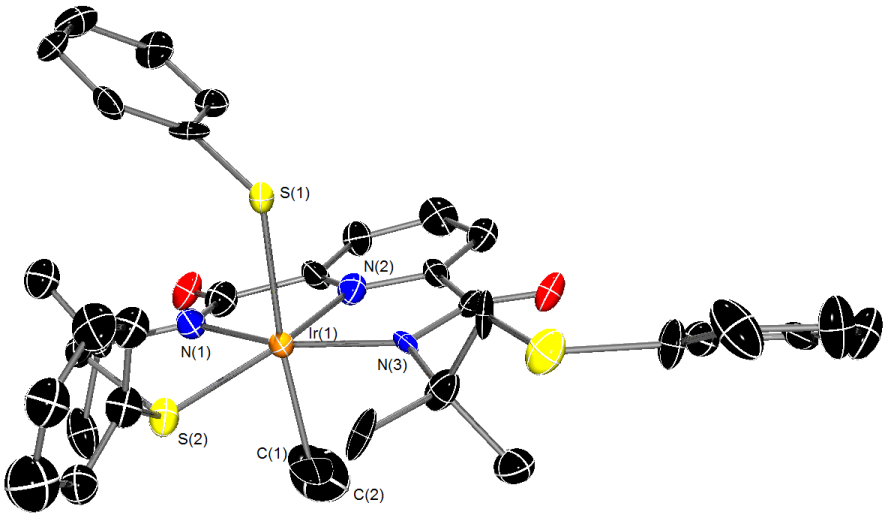

Figure 3.11. ORTEP of **18** shown with thermal ellipsoids at 50% probability level. The counter ion and hydrogen atoms have been omitted for clarity. Selected bond lengths (Å) and angels (˚): Ir(1)-N(1) = 2.032(17), Ir(1)-N(2) = 1.956(17), Ir(1)-N(3) = 2.067(15), Ir(1)-S(1) = 2.483(5), Ir(1)-S(2) = 2.324(6), Ir(1)-C(1) = 2.07(2), Ir(1)-C(1)-C(2) = 122(2).

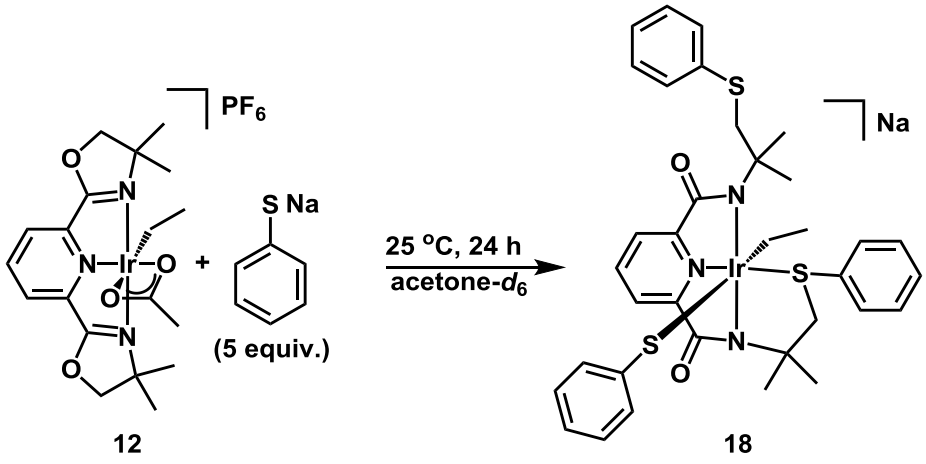

Figure 3.12. Reaction of **12** with sodium thiophenolate to form **18**.

Nucleophilic attack at the oxazoline rings of the Pybox pincer ligand has been previously reported by Vicic et al.[16] These authors observed nucleophilic attack at the oxazoline rings by acetate while attempting to synthesize (Pybox)Pd(OAc) from Pybox and $Pd(OAc)_2$. Two possible pathways were proposed for this reaction (Figure 3.13). In pathway 1, nucleophilic attack at the methylene carbon by acetate generated the ring opened product (top path). In pathway 2, nucleophilic attack at the imine carbon followed by nucleophilic attack at the carbonyl carbon of the acetate generated the ring opened product (bottom path). Because acetate was the nucleophile, it was difficult to determine the operative pathway.

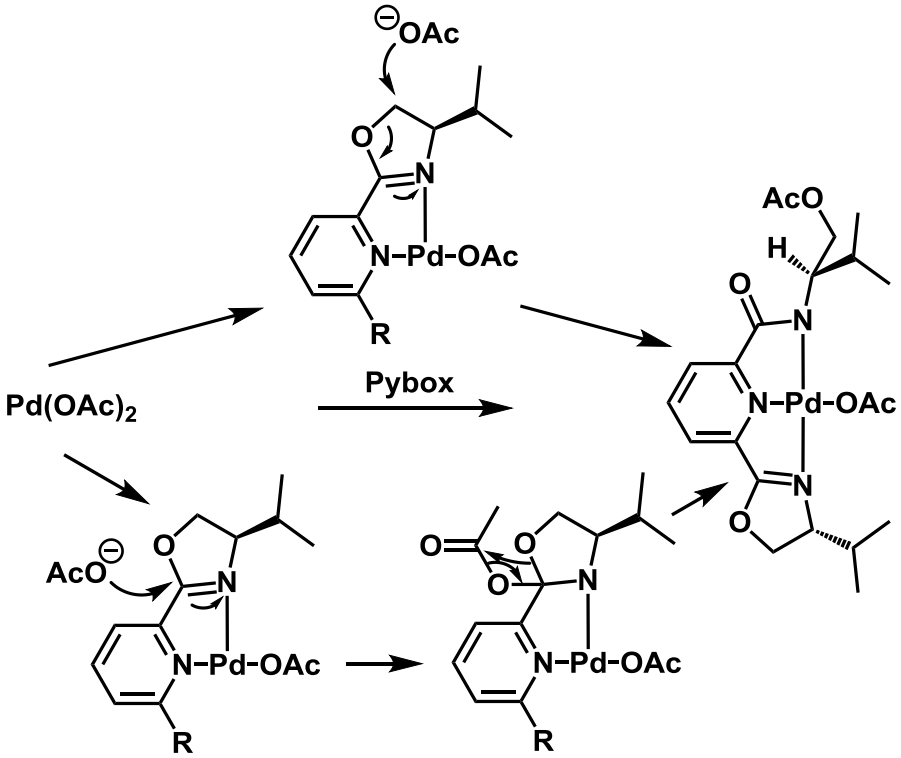

Figure 3.13. Possible pathways for nucleophilic attack reported by Vicic et al.[16]

If these same two pathways are considered for the reaction of complex **12** with thiophenylate, two distinctive products are possible (Figure 3.14). Only the top pathway is

consistent with the results obtained from the solid state structure. Thus, nucleophilic attack by thiopenolate occurs at the oxazoline methylene carbon to form the ring opened product.

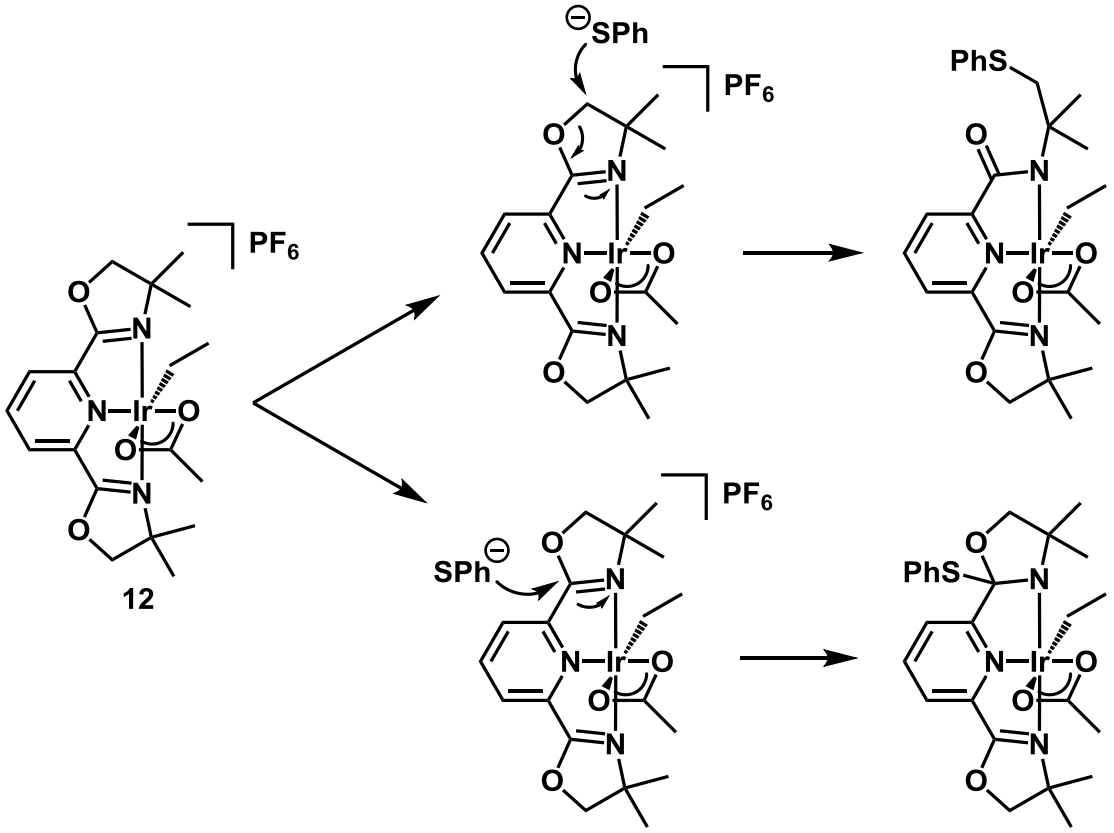

Figure 3.14. Possible pathways for nucleophilic attack at **12** by thiophenolate.

3.9 Summary

Thermolysis of [(^{dm}Pybox)Ir(Et)(OAc)][PF_6] (**12**) with a variety of amines led primarily to the formation of ethylene, consistent with an E2 elimination. Similar reactivity was observed when **12** was subjected to thermolysis conditions in the presence of base. Reaction of **12** with NaN_3 or KI resulted in the formation of many products. The reaction of **12** with NaSPh resulted in the ring opened product [(NNNS)Ir(Et)(SPh)]Na, **18** and similar

reactivity may be responsible for the large number of products that were formed in the reactions with other nucleophiles and bases.

Protonation of the Rh complex, [(^{dm}Pybox)Rh(C_2H_4)$_2$][PF_6], with anilinium trifluoroacetic acid at low temperature (-40 ˚C) in methanol resulted in the isolable complex, [(^{dm}Pybox)Rh(Et)(TFA)(MeOH)][PF_6] **17**. Similarly to the Ir analogues, no C-N coupling was observed when **17** was thermolyzed in the presence of aniline. Multiple products, possible due to ring opening of the pybox ligand, as well as ethylene were again observed by ^{1}H NMR spectroscopy, suggesting the barrier to nucleophilic attack had not been significantly reduced to out-compete the E2 elimination.

Experimental

General considerations. All manipulations were carried out under air-free conditions in a N_2 drybox or using standard Schlenk techniques. Solvents were dried by passage through two columns of activated alumina (THF) or passage through one column of alumina and one column of Q5 reactant (pentane). Iodobenzene was degassed and stored over 3 Å molecular sieves. Deuterated solvents were purchased from Cambridge Isotope Laboratories and dried over CaH_2 (dichloromethane-d_2), sodium/ benzophenone (THF-d_8) or 3 Å molecular sieves (bromobenzene-d_5). All other chemicals were purchased from Sigma-Aldrich and used as received. [Rh(COE)$_2$Cl]$_2$,[17] [Ir(COE)$_2$Cl]$_2$,[18] and ^{dm}Pybox[5] were synthesized according to published procedures. NMR spectra were recorded using Bruker AV300, DRX 499 or AV500

spectrometers. ^{1}H NMR and $^{13}C\{^{1}H\}$ NMR spectra were referenced to residual solvent signals relative to TMS and are reported in parts per million (ppm).

[(^{dm}Pybox)Ir(Et)(OAc)][PF$_6$] (12). This complex was prepared analogously to the published procedure for [(*S,S*-^{iPr}Pybox)Ir(Et)(OAc)][PF$_6$];[1] [(^{dm}Pybox)Ir(C_2H_4)$_2$][PF$_6$] **(11)** (31 mg, 0.05 mmol) was weighed into a 20 mL vial and dissolved in THF (2 mL). Acetic acid (2.6 µL, 0.046mmol) was added via syringe and the solution was stirred at room temperature for 14 hours. Pentane was added to precipitate the product, a brown solid, which was collected by filtration (25 mg, 78 %) ^{1}H NMR (CD_2Cl_2, 500 MHz, 298 K) δ 7.9 (3H, m, C_5H_3N), 4.9 (4H, s, O-CH_2), 2.11 (3H, s, Ir-OOCCH_3), 1.64 (6H, s, N-C-CH_3), 1.53 (6H, s, N-C-CH_3), 1.05 (2H, q, $J_{H\text{-}H}$ = 7.4 Hz, Ir-CH_2CH$_3$), 0.39 (3H, t, $J_{H\text{-}H}$ = 7.4 Hz, Ir-CH$_2$CH_3).

[(^{dm}Pybox)Ir(Et)(TFA)(NH_2Ph)][PF$_6$] (13). This complex was prepared on an NMR scale and not isolated. Complex **11** (3 mg, 0.005 mmol) and anilinium trifluoracetate (0.8 mg, 0.005 mmol) were weighed into a NMR tube fitted with a Teflon pin. CD_2Cl_2 was vacuum transferred into the tube (c.a. 0.4 mL), resulting a color change from orange to rust. ^{1}H NMR (CD_2Cl_2, 500 MHz, 298 K) δ 7.95 (1H, t, $J_{H\text{-}H}$ = 8 Hz, C_5H_3N), 7.78 (2H, d, $J_{H\text{-}H}$ = 8 Hz, C_5H_3N), 7.73 – 6.89, 6.44 – 5.92 (br, Ir-NH_2Ph), 4.76 (2H, d, $J_{H\text{-}H}$ = 8.8 Hz O-CH_2), 4.66 (2H, d, $J_{H\text{-}H}$ = 8.8 Hz, O-CH_2), 1.6 (2H, q, $J_{H\text{-}H}$ = 7.7 Hz, Ir-CH_2CH$_3$), 1.51 (6H, s, N-C-CH_3), 1.40 (6H, s, N-C-CH_3), 0.01 (3H, t, $J_{H\text{-}H}$ = 7.7 Hz, Ir-CH$_2$CH_3).

[(^{dm}Pybox)Ir(Et)(OAc)(amine)][PF$_6$] (14). This complex was prepared on an NMR scale and not isolated. Experimental is shown for **14-morpholine**. Complex **12** (3 mg, 0.0043 mmol) was weighed into a NMR tube fitted with a Teflon Pin. CD_2Cl_2 was vacuum transferred into the tube. Morpholine (1.9 µL, 0.021 mmol) was added via syringe resulting

in a green/ brown solution. ^{1}H NMR (CD_2Cl_2, 300 MHz, 298 K) δ 7.92 (3H, m, C_5H_3N), 4.89 (2H, d, J_{H-H} = 9 Hz O-CH_2), 4.82 (2H, d, J_{H-H} = 9 Hz, O-CH_2), 2.2 (3H, s, Ir-OOCCH_3) 1.71 (6H, s, N-C-CH_3), 1.58 (6H, s, N-C-CH_3), 1.37 (2H, q, J_{H-H} = 7.7 Hz, Ir-CH_2CH$_3$), -0.04 (3H, t, J_{H-H} = 7.7 Hz, Ir-CH$_2$CH_3). Note: The resonances for bound morpholine were not observed, likely due to the large excess. **14-piperidine.** ^{1}H NMR (CD_2Cl_2, 300 MHz, 298 K) δ 7.97 (1H, t, J_{H-H} = 8 Hz, C_5H_3N), 7.87 (2H, d, J_{H-H} = 8 Hz, C_5H_3N), 4.88 (2H, d, J_{H-H} = 8.8 Hz O-CH_2), 4.79 (2H, d, J_{H-H} = 8.8 Hz, O-CH_2), 2.19 (3H, s, Ir-OOCCH_3) 1.72 (6H, s, N-C-CH_3), 1.57 (6H, s, N-C-CH_3), 1.28 (2H, q, J_{H-H} = 7.6 Hz, Ir-CH_2CH$_3$), -0.04 (3H, t, J_{H-H} = 7.6 Hz, Ir-CH$_2$CH_3). Note: The resonances for bound piperidine were not observed, likely due to the large excess. **14-aniline** ^{1}H NMR (CD_2Cl_2, 300 MHz, 298 K) δ 7.86 (1H, t, J_{H-H} = 8 Hz, C_5H_3N), 7.70 (2H, d, J_{H-H} = 8 Hz, C_5H_3N), 4.75 (2H, d, J_{H-H} = 8.8 Hz O-CH_2), 4.68 (2H, d, J_{H-H} = 8.8 Hz, O-CH_2), 2.24 (3H, s, Ir-OOCCH_3) 1.55 (6H, s, N-C-CH_3), 1.53 (2H, obscured signal, Ir-CH_2CH$_3$)1.51 (6H, s, N-C-CH_3), -0.05 (3H, t, J_{H-H} = 7.7 Hz, Ir-CH$_2$CH_3). Note: The resonances for bound aniilne were not observed, likely due to the large excess.

Example of oxidation with Fc^+. Complex **12** (2 mg, 0.003 mmol), aniline (approximately 0.3 μL, 0.003 mmol) and hexamethylbenzene (internal standard) were transferred to a NMR tube fitted with a Teflon pin. THF-d_8 was vacuum transferred into the tube resulting in a green/ brown solution. Ferrocenium hexafluorophosphate (1 mg, 0.003 mmol) was added resulting in the darkening of the solution. [(^{dm}Pybox)Ir(Et)(Cl)(aniline)][PF_6] (**15**) was formed in approximately 50 % yield by ^{1}H NMR spectroscopy and characterized by X-ray diffraction. ^{1}H NMR (TFH-d_8, 500 MHz, 298 K) δ 8.01 (1H, t, J_{H-H} = 7.7 Hz, C_5H_3N), 7.85 (2H, d, J_{H-H} = 7.8 Hz, C_5H_3N), 4.84 (2H, O-CH_2), 4.73 (2H, d, J_{H-H} = 12.4 Hz, O-CH_2), 1.70

(Ir-CH_2CH$_3$ (obscured by solvent)), 1.65 (6H, s, N-C-CH_3), 1.64 (6H, s, N-C-CH_3), -0.07 (3H, t, $J_{H\text{-}H}$ = 7.9 Hz, Ir-CH$_2$CH_3). Note: bound aniline signals obscured by free aniline.

(^{dm}Pybox)Ir(Et)(OAc)I (16). This complex was prepared on an NMR scale and not isolated. Complex **12** (2 mg, 0.003 mmol) and KI (2.4 mg, 0.014 mmol) were weighed into a NMR tube fitted with a Teflon pin. Acetone-d_6 was vacuum transferred into the tube (c.a. 0.4 mL), resulting a green/ brown solution. ^{1}H NMR (acetone-d_6, 500 MHz, 298 K) δ 7.95 (3H, m, C$_5H_3$N), 4.94 (2H, d, $J_{H\text{-}H}$ = 8.6 Hz O-CH_2), 4.84 (2H, d, $J_{H\text{-}H}$ = 8.6 Hz, O-CH_2), 1.87 (6H, s, N-C-CH_3), 1.77 (6H, s, N-C-CH_3), -0.42 (3H, t, $J_{H\text{-}H}$ = 7.8 Hz, Ir-CH$_2$CH_3). Note: Ir-CH_2CH$_3$ and Ir-OOCCH_3 signals obscured by residual solvent peak.

[(^{dm}Pybox)Rh(Et)(TFA)(sol)][PF$_6$] (17). [RhCl(COE)$_2$]$_2$ (19 mg, 0.0048 mmol) was weighed into a 25 mL glass vessel containing a Teflon pin. Methanol (approximately 5 mL) was added. The Teflon pin was replaced with a rubber septum and the vessel was placed under an ethylene atmosphere. The solution was cooled to -40 ˚C. Under ethylene atmosphere a methanol solution (2 mL) of ^{dm}Pybox (26.7 mg, 0.097 mmol) was added. The solution was stirred, under ethylene atmosphere, at -40 ˚C for 30 minutes. A methanol solution (1 mL) of NaPF$_6$ (23.8 mg, 0.142 mmol) was added resulting in a cloudy yellow solution. The solution was stirred, under ethylene atmosphere, at -40 ˚C for 40 minutes. A methanol solution (2 mL) of anilinium trifluoroacetate was added. The solution was stirred, under ethylene atmosphere, at -40 ˚C for 40 minutes. Upon warming to ambient temperature, the solution darkened. Pentane (100 mL) was added to precipitate the product (brown solid). ^{1}H NMR (CD$_2$Cl$_2$, 500 MHz, 298 K) δ 8.39 (1H, t, $J_{H\text{-}H}$ = 8.1 Hz, C$_5H_3$N), 8.08 (2H, d, $J_{H\text{-}H}$ = 8.1 Hz, C$_5H_3$N), 4.82 (2H, d, $J_{H\text{-}H}$ = 8.8 Hz O-CH_2), 4.76 (2H, d, $J_{H\text{-}H}$ = 8.9 Hz, O-CH_2), 3.3 (3H, s,

Rh-OHC*H*$_3$), 2.86 (2H, dq, $J_{H\text{-}H}$ = 7.5 Hz, $J_{Rh\text{-}H}$ = 2.6 Hz, Rh-C*H*$_2$CH$_3$), 1.53 (6H, s, N-C-C*H*$_3$), 1.47 (6H, s, N-C-C*H*$_3$), 0.55 (3H, t, $J_{H\text{-}H}$ = 7.5 Hz, Rh-CH$_2$C*H*$_3$).

Attempted C-N coupling from 17 with aniline. Complex **17** (2 mg, 0.0026 mmol) and aniline (2.4 μL) were transferred to a NMR tube fitted with a Teflon pin. THF-d_8 (or CD_3CN) was vacuum transferred into the NMR tube. The solution was heated at 80 ˚C. Over time ethylene was observed along with multiple intractable products by ^{1}H NMR spectroscopy.

[(NNNS)Ir(Et)(SPh)]Na (18). Complex **12** (4 mg, 0.006 mmol) and sodium thiophenolate (3.8 mg, 0.03 mmol) were weighed into a NMR tube fitted with a Teflon pin. THF-d_8 was vacuum transferred into the tube resulting in a dark brown solution. The solution was left at ambient temperature for 1 week. The solution was filtered through a Teflon syringe filter into a vial. Crystals suitable for X-ray diffraction were grown by layering the THF solution with pentane. ^{1}H NMR (CD_2Cl_2, 500 MHz, 298 K) δ 8.48 (2H, br, Ar-*H*), 7.60 (1H, m, Ar-*H*), 7.34 (5H, m, Ar-*H*), 7.22 (3H, br, Ar-*H*), 7.15 (3H, t, $J_{H\text{-}H}$ = 7.8 Hz, Ar-*H*), 6.98 (1H, t, $J_{H\text{-}H}$ = 7.3 Hz, Ar-*H*), 6.78 (2H, d, $J_{H\text{-}H}$ = 6.9 Hz, Ar-*H*), 6.56 (1H, m, Ar-*H*), 4.20 (1H, d, $J_{H\text{-}H}$ = 9.3 Hz S-C*H*$_2$), 3.95 (1H, d, $J_{H\text{-}H}$ = 11.8 Hz, S-C*H*$_2$), 3.70 (1H, d, $J_{H\text{-}H}$ = 11.8 Hz, S-C*H*$_2$), 3.36 (1H, d, $J_{H\text{-}H}$ = 9.3 Hz, S-C*H*$_2$), 1.66 (2H, obscured by solvent, Ir-C*H*$_2$CH$_3$), 1.59 (3 H, br s, N-C-C*H*$_3$), 1.42 (3H, br s, N-C-C*H*$_3$), 1.39 (3H, br s, N-C-C*H*$_3$), 1.24 (3H, br s, N-C-C*H*$_3$), 0.31 (3H, t, $J_{H\text{-}H}$ = 7.2 Hz, Ir-CH$_2$C*H*$_3$).

X-ray crystallography methodology

Solution by direct methods (SHELXS, SIR97[19]) produced a complete heavy atom phasing model consistent with the proposed structures. The structures were completed by difference

Fourier synthesis with SHELXL97.[20,21] Scattering factors are from Waasmair and Kirfel[22]. Hydrogen atoms were placed in geometrically idealised positions and constrained to ride on their parent atoms with C---H distances in the range 0.95-1.00 Angstrom. Isotropic thermal parameters U_{eq} were fixed such that they were $1.2U_{eq}$ of their parent atom Ueq for CH's and $1.5U_{eq}$ of their parent atom U_{eq} in case of methyl groups. All non-hydrogen atoms were refined anisotropically by full-matrix least-squares.

Details for solid state structure determination of 15-aquo.

A red needle, measuring 0.45 x 0.04 x 0.03 mm^3 was mounted on a glass capillary with oil. Data was collected at 180K on a Bruker APEX II single crystal X-ray diffractometer, Mo-radiation.

Crystal-to-detector distance was 40 mm and exposure time was 30 seconds per frame for all sets. The scan width was 0.5^o. Data collection was 100% complete to 25^o in ϑ. A total of 66883 reflections were collected covering the indices, h = -34 to 34, k = -11 to 10, l = -15 to 15. 6360 reflections were symmetry independent and the R_{int} = 0.0345 indicated that the data was of better than average quality (0.07). Indexing and unit cell refinement indicated a primitive orthorhombic lattice. The space group was found to be P n a2_1 (No.33).

The data was integrated and scaled using SAINT, SADABS within the APEX2 software package by Bruker.[23]

The data was collected at 180 K instead of 100K because the crystals undergo a 1^{st} –order structural phase transition between 160K and 180K by which the diffraction pattern becomes low quality and indicates a domain structure. One tested, very thin crystals remained

untwinned in the orthorhombic space group at 100K for more than an hour, but eventually spontaneously transformed. A disordered PF_6^- anion and Ir-ethyl disorder is likely resolved into a lower symmetry space group in the low-T phase of the material.

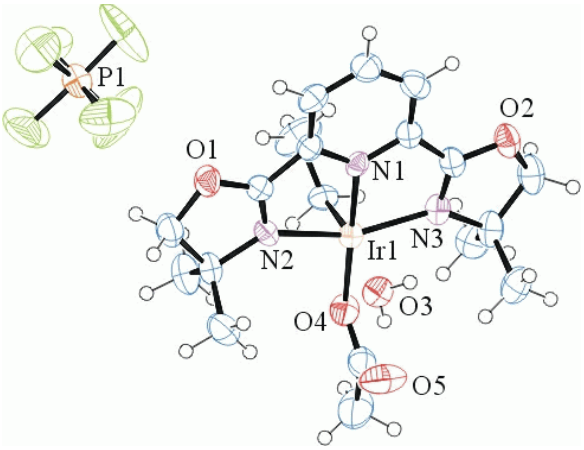

Figure 3.13. ORTEP of the structure with thermal ellipsoids at the 50% probability level. Disorder omitted for clarity.

Table 3.1: Crystallographic data for **14-aquo**.

Empirical formula	C19 H29 F6 Ir N3 O5 P	
Formula weight	716.62	
Temperature	180(2) K	
Wavelength	0.71073 Å	
Crystal system	Orthorhombic	
Space group	P n a 2_1	
Unit cell dimensions	a = 25.6875(13) Å	α= 90°.
	b = 8.2500(4) Å	β= 90°.
	c = 11.7240(6) Å	γ = 90°.
Volume	2484.6(2) $Å^3$	
Z	4	

Density (calculated)	1.916 Mg/m^3
Absorption coefficient	5.518 mm^{-1}
F(000)	1400
Crystal size	0.45 x 0.04 x 0.03 mm^3
Theta range for data collection	1.59 to 28.78°.
Index ranges	-34<=h<=34, -11<=k<=10, -15<=l<=15
Reflections collected	66883
Independent reflections	6360 [R(int) = 0.0354]
Completeness to theta = 25.00°	100.0 %
Max. and min. transmission	0.8519 and 0.1903
Refinement method	Full-matrix least-squares on F^2
Data / restraints / parameters	6360 / 35 / 393
Goodness-of-fit on F^2	1.096
Final R indices [I>2sigma(I)]	R1 = 0.0225, wR2 = 0.0462
R indices (all data)	R1 = 0.0281, wR2 = 0.0482
Absolute structure parameter	-0.001(6)
Largest diff. peak and hole	0.922 and -0.449 $e.Å^{-3}$

Details for solid state structure determination of 16.

A yellow prism, measuring 0.6 x 0.60 x 0.6 mm^3 was mounted on a loop with oil. Data was collected at -173°C on a Bruker APEX II single crystal X-ray diffractometer, Mo-radiation.

Crystal-to-detector distance was 40 mm and exposure time was 10 seconds per degree for all sets. The scan width was 0.5°. Data collection was 98% complete to 25° in ϑ. A total of 125039 reflections were collected covering the indices, h = -19 to 19, k = -20 to 20, l = -21

to 21. 14037 reflections were symmetry independent and the R_{int} = 0.0540 indicated that the data was of better than average quality (0.07). Indexing and unit cell refinement indicated a triclinic P lattice. The space group was found to be P $\bar{1}$ (No.2).

The data was integrated and scaled using SAINT, SADABS within the APEX2 software package by Bruker.[23]

The $PF6^-$ anion was found disordered. A second anion was identified as $H_2PO_4^-$. In addition, a THF solvent was found which does not coordinate with Ir.

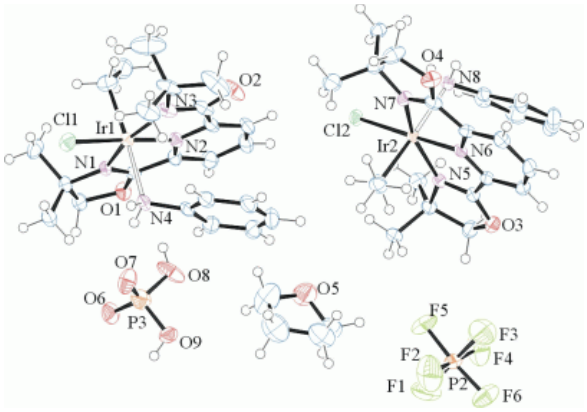

Figure 3.14. ORTEP of the structure with thermal ellipsoids at the 50% probability level. Disorder omitted for clarity.

Table 3.2: Crystallographic data for the structures provided.

Empirical formula	C50 H72 Cl2 F6 Ir2 N8 O9 P2
Formula weight	1560.40
Temperature	100(2) K
Wavelength	0.71073 Å

Crystal system	Triclinic	
Space group	P -1	
Unit cell dimensions	a = 14.6520(19) Å	α= 70.160(7)°.
	b = 15.277(2) Å	β= 66.663(7)°.
	c = 15.758(2) Å	γ = 64.061(7)°.
Volume	2852.9(6) $Å^3$	
Z	2	
Density (calculated)	1.816 Mg/m^3	
Absorption coefficient	4.890 mm^{-1}	
F(000)	1544	
Crystal size	0.60 x 0.60 x 0.60 mm^3	
Theta range for data collection	1.51 to 28.45°.	
Index ranges	-19<=h<=19, -20<=k<=20, -21<=l<=21	
Reflections collected	125039	
Independent reflections	14037 [R(int) = 0.0540]	
Completeness to theta = 25.00°	98.0 %	
Max. and min. transmission	0.1574 and 0.1574	
Refinement method	Full-matrix least-squares on F^2	
Data / restraints / parameters	14037 / 63 / 738	
Goodness-of-fit on F^2	1.093	
Final R indices [I>2sigma(I)]	R1 = 0.0350, wR2 = 0.0775	
R indices (all data)	R1 = 0.0617, wR2 = 0.0939	
Largest diff. peak and hole	3.309 and -1.348 $e.Å^{-3}$	

Details for solid state structure determination of ethyl bridged Rh dimer

A blue plate, measuring 0.35 x 0.03 x 0.02 mm^3 was mounted on a glass loop oil. Data was collected at -173^oC on a Bruker APEX II single crystal X-ray diffractometer, Mo-radiation.

Crystal-to-detector distance was 40 mm and exposure time was 60 seconds per frame for all sets. The scan width was 0.5^o. Data collection was 100% complete to 25^o in ϑ. A total of 68834 reflections were collected covering the indices, h = -22 to 22, k = -29 to 29, l = -21 to 21. 7625 reflections were symmetry independent and the R_{int} = 0.0853 indicated that the data was of slightly less than average quality (0.07). Indexing and unit cell refinement indicated a C-centered monoclinic lattice. The space group was found to be C 2/c (No.15).

The data was integrated and scaled using SAINT, SADABS within the APEX2 software package by Bruker.[23]

Extensive disorder of THF solvent is omitted in the ortep plot of the dimer, with each half related through a symmetry center located between the ethyl-carbon atoms C20 and C20'.

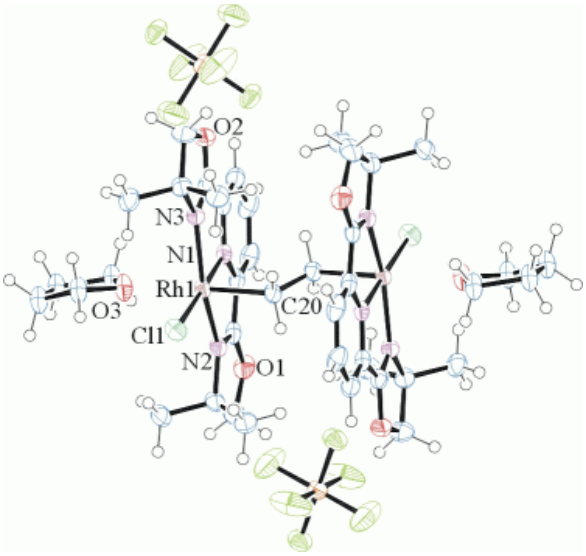

Figure 3.15. ORTEP of the structure with thermal ellipsoids at the 50% probability level. Disorder and some THF solvent omitted for clarity.

Table 3.3: Crystallographic data for ethyl bridged Rh dimer.

Empirical formula	C52 H82 Cl2 F12 N6 O9 P2 Rh2	
Formula weight	1501.90	
Temperature	100(2) K	
Wavelength	0.71073 Å	
Crystal system	Monoclinic	
Space group	C 2/c	
Unit cell dimensions	a = 17.062(4) Å	α= 90.000°.
	b = 22.108(4) Å	β= 92.586(13)°.
	c = 16.186(3) Å	γ = 90.000°.
Volume	6099(3) $Å^3$	
Z	4	
Density (calculated)	1.636 Mg/m^3	
Absorption coefficient	0.776 mm^{-1}	

F(000)	3080
Crystal size	0.35 x 0.03 x 0.02 mm^3
Theta range for data collection	1.84 to 28.40°.
Index ranges	-22<=h<=22, -29<=k<=29, -21<=l<=21
Reflections collected	68834
Independent reflections	7625 [R(int) = 0.0853]
Completeness to theta = 25.00°	100.0 %
Max. and min. transmission	0.9846 and 0.7729
Refinement method	Full-matrix least-squares on F^2
Data / restraints / parameters	7625 / 70 / 370
Goodness-of-fit on F^2	1.008
Final R indices [I>2sigma(I)]	R1 = 0.0478, wR2 = 0.0945
R indices (all data)	R1 = 0.0942, wR2 = 0.1128
Largest diff. peak and hole	1.383 and -1.129 e.$Å^{-3}$

Details for solid state structure determination of 19

A yellow chard, measuring 0.03 x 0.02 x 0.01 mm^3 was mounted on a loop with oil. Data was collected at -173°C on a Bruker APEX II single crystal X-ray diffractometer, Mo-radiation.

Crystal-to-detector distance was 40 mm and exposure time was 60 seconds per frame for all sets. The scan width was 1°. Data collection was 98.1% complete to 25° in ϑ. A total of 68727 reflections were collected covering the indices, h = -16 to 16, k = -18 to 18, l = -23 to 23. 13886 reflections were symmetry independent and the R_{int} = 0.268 indicated that the data

was of less than average quality (0.07). Indexing and unit cell refinement indicated a primitive triclinic lattice. The space group was found to be P $\bar{1}$ (No. 2).

The data was integrated and scaled using SAINT, SADABS within the APEX2 software package by Bruker.[23]

Sulfur of one and a ketone of another of two different Ir complexes are connected to sodium cations into a linear infinite chain. THF and water are binding as well leaving the sodium atoms tetrahedrally coordinated. Figure 1 shows an ORTEP[24] of the asymmetric unit.

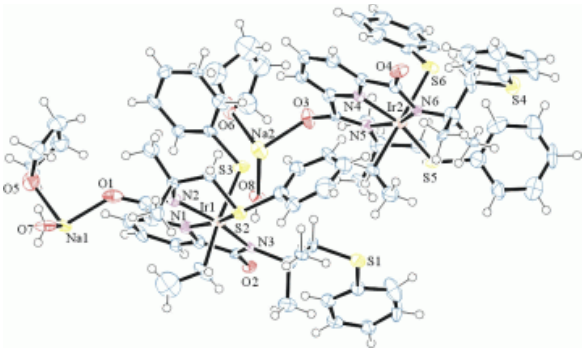

Figure 3.16. ORTEP of the structure with thermal ellipsoids at the 50% probability level.

Table 3.4: Crystallographic data for **18**.

Empirical formula	C39 H49 Ir N3 Na O4 S3
Formula weight	935.18
Temperature	100(2) K
Wavelength	0.71073 Å
Crystal system	Triclinic
Space group	P -1

Unit cell dimensions	a = 13.695(3) Å	α= 89.108(19)°.
	b = 15.271(4) Å	β= 89.925(16)°.
	c = 19.667(5) Å	γ = 69.930(17)°.
Volume	3862.7(17) $Å^3$	
Z	4	
Density (calculated)	1.608 Mg/m^3	
Absorption coefficient	3.674 mm^{-1}	
F(000)	1888	
Crystal size	0.03 x 0.02 x 0.01 mm^3	
Theta range for data collection	1.89 to 25.35°.	
Index ranges	-16<=h<=16, -18<=k<=18, -23<=l<=23	
Reflections collected	68727	
Independent reflections	13886 [R(int) = 0.2680]	
Completeness to theta = 25.00°	98.1 %	
Max. and min. transmission	0.9642 and 0.8978	
Refinement method	Full-matrix least-squares on F^2	
Data / restraints / parameters	13886 / 264 / 930	
Goodness-of-fit on F^2	1.006	
Final R indices [I>2sigma(I)]	R1 = 0.1030, wR2 = 0.1950	
R indices (all data)	R1 = 0.2172, wR2 = 0.2462	
Extinction coefficient	0.0021(2)	
Largest diff. peak and hole	7.440 and -2.228 $e.Å^{-3}$	

Notes to chapter 3.

(1) Díez, J.; Gamasa, M. P.; Gimeno, J.; Paredes, P. *Organometallics* **2005**, *24*, 1799.

(2) de Bruin, B.; Boerakker, M. J.; Verhagen, J. A. W.; de Gelder, R.; Smitts, J. M. M.; Gal. A. W. *Chem. Eur. J.* **2000**, *6*, 298.

(3) Pardes, P.; Díez, J.; Gamasa, M. P. *J. Organomet. Chem.* **2008**, *693*, 3681.

(4) (a) Goldberg, K. I.; Yan, J.; Winter, E. L. *J. Am. Chem. Soc.* **1994**, *116*, 1573. (b) Goldberg, K. I.; Yan, J. Breitung, E. M. *J. Am. Chem. Soc.* **1995**, *117*, 6889. (c) Williams, B. S.; Holland, A. W.; Goldberg, K. I. *J. Am. Chem. Soc*. **1999**, *121*, 252. (d) Pawlikowski, A. V; Getty, A. D.; Goldberg, K. I. *J. Am. Chem. Soc*. **2007**, *129*, 10382.

(5) Nishiyama, H.; Kondo, M.; Nakamura, T.; Itoh, K. *Organometallics*, **1991**, *10*, 500.

(6) Bender, M.L. *Chem. Rev*. **1960**, *60*, 53.

(7) Hall, H. K., Jr. *J. Am. Chem. Soc.* **1957**, *79*, 5441.

(8) Elliott, J. J.; Mason, S. F. *J. Chem. Soc.* **1959**, 2352.

(9) Smith, M. B.; March, J. *March's Advanced Organic Chemistry*, 5th ed.; John Wiley & Sons: New York, **2001**, 1299-1376.

(10) Diversi, P.; Ermini, V.; Ingrosso, G.; Lucherini, A.; Pinzino, C.; Simoncini, F. *J. Organomet. Chem*. **1998**, *555*, 135.

(11) Lanci, M. P.; Remi, M. S.; Kaminsky, W.; Mayer, J. M.; Sanford, M. S. *J. Am. Chem. Soc.* **2009**, *131*, 15619.

(12) Young, K. J. H.; Mironov, O. A.; Periana, R. *Organometallics*, **2007**, *26*, 2137.

(13) Lin, B. L.; Clough, C. R.; Hillhouse, G. L. *J. Am. Chem. Soc.* **2002**, *124*, 2890.

(14) Two compounds crystallized in the asymmetric unit with one PF_6 counter ion and one H_2PO_4 counter ion. It is not clear where this came from.

(15) Iodide is drawn trans to the ethyl ligand, but it is also possible that it is trans to pyridine.

(16) Kazi, A. B.; Jones, G. D.; Vicic, D. A. *Organometallics*, **2005**, *24*, 6051

(17) van der Ent, A.; Onderdelinden, A. L.; Schunn, R. A. *Inorg. Synth.* **1990**, *28*, 90.

(18) Herde, J. L.; Lamberg, J. C.; Senoff, C. V. *Inorg. Synth.* **1974**, *15*, 18.

(19) (a) Altomare A, Burla C, Camalli M, Cascarano G L, Giacovazzo C, Guagliardi A, Moliterni AGG, Polidori G, Spagna R. **(1999)** SIR97: a new tool for crystal structure determination and refinement *Journal of Applied Crysta*llography, ***32,*** 115-119.

(b) Altomare A, Cascarano G L, Giacovazzo C, Guagliardi A. **(1993)** Completion and refinement of crystal structures with SIR 92. *Journal of Applied Crysta*llography, ***26,*** 343-350.

(20) Sheldrick GM. **(1997)** SHELXL-97, Program for the Refinement of Crystal Structures. University of Göttingen, Germany.

(21) Mackay, S.; Edwards, C.; Henderson, A.; Gilmore, C.; Stewart, N.; Shankland, K.; Donald, A. **(1997)** *MaXus: a computer program for the solution and refinement of crystal structures from diffraction data*. University of Glasgow, Scotland.

(22) Waasmaier, D.; Kirfel, A. **(1995)** New Analytical Scattering Factor Functions for Free Atoms and Ions. *Acta Crystallographica* A., ***51***, 416-430.

(23) Bruker (**2007**) APEX2 (Version 2.1-4), SAINT (version 7.34A), SADABS (version 2007/4), BrukerAXS Inc, Madison, Wisconsin, USA.

(24) Farrugia LJ. **(1997)** Ortep-3 for Windows. *Journal of Applied Crysta*llography, ***30,*** 565.

Chapter 4

Carbon(sp^3)-Nitrogen Bond Formation from (BPA)Ir^{III}-Et Complexes

4.1 Introduction

$C(sp^3)$-N bond formation is a potential high vale reaction in catalysis. Thorough understanding of how to promote this fundamental reaction could lead to the development of new catalysts for selective and efficient syntheses of alkyl amines directly from olefins or alkanes. $C(sp^2)$-N coupling to form aryl amines is now well documented with the Buchwald-Hartwig amination protocol used extensively in academic and industrial laboratories.[1] In contrast $C(sp^3)$-N couplings have rarely been observed.[2] Furthermore, the few examples of stoichiometric $C(sp^3)$-N couplings have been limited to alkyls that have no β-hydrogens, such as *tert*-butylbenzene,[2e,f] or alkyls that are resistant toward β-H elimination, such as norbornane.[2d]

The challenge of developing a system where $C(sp^3)$-N coupling is possible became evident as we attempted to design new catalysts for anti-Markovnikov hydroamination (Figure 4.1). It was proposed that sterically bulky ligands would favor the formation of a linear metal alkyl upon protonation of a metal olefin precursor (Figure 4.1, step b). This was

realized using the complex, [(^{Me}TPA)Rh(C_3H_6)][BPh_4]. It was found that this protonation of this complex resulted in the formation of *n*-propyl complex, [(^{Me}TPA)Rh(C_3H_7)(OTf)][BPh_4].[3] If the methyl groups were not present on the pyridine moieties of the ligand, protonation of the propylene precursor resulted in the formation of the *iso*-propyl Rh complex, [(TPA)Rh(C_3H_7)][BPh_4] (Figure 4.2).

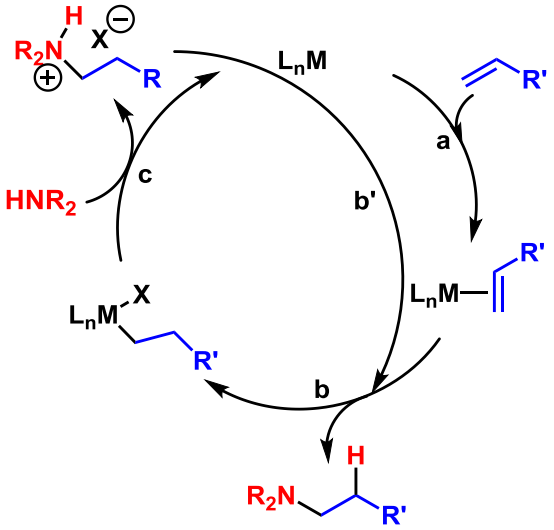

Figure 4.1. Proposed catalytic cycle for anti-Markovnikov hydroamination.

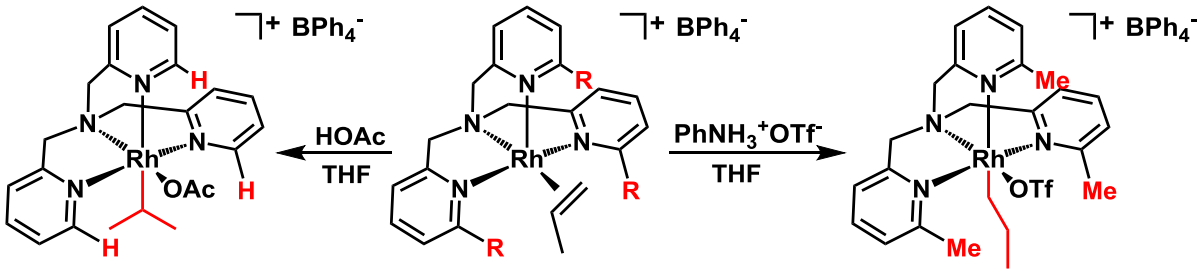

Figure 4.2. Steric controlled selectivity: protonation of (TPA)Rh-propylene$^+$.

While these Rh complexes were capable of the first two steps of our proposed catalytic cycle, the last step, C(sp^3)-N coupling, was not possible. Thermolysis of the complex [(^{Me}TPA)Rh(C_3H_7)(OTf)][BPh_4] (in the presence of amines or amides) resulted in the formation of a Rh-H and no C-N coupling was observed. The importance of five-coordinate metal alkyl species has become evident in examples of C(sp3)-X reductive elimination.[4] It was hypothesized that the facially coordinating TPA ligand dictates that the open site is cis to the alkyl ligand, which is not the proper orientation required for S_N2 nucleophilic attack. Protonation of the tridentate Rh propylene analogues (Figure 4.3) should result in Rh alkyl complexes with the correct geometry to undergo C-N reductive coupling. Unfortunately, the Rh propylene complexes were not thermally robust.[3] The tridentate Ir ethylene analogues, however, are known.[6,6]

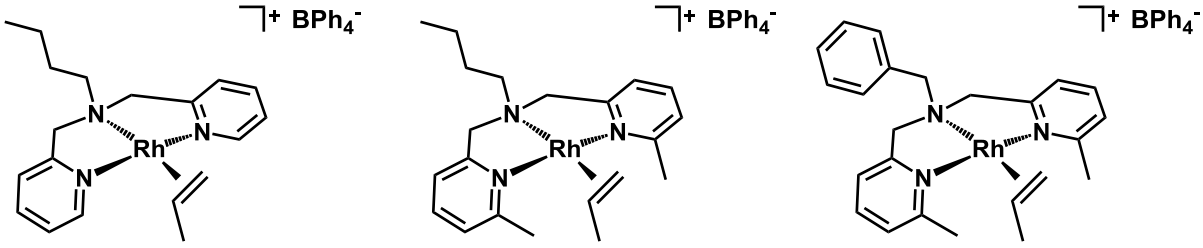

Figure 4.3 Proposed Rh propylene complexes with BPA ligand.

It was shown that the group on the nitrogen in the ligand backbone played an important role in the reactivity of the Ir *bis*-ethylene complexes.[5] N-H activation was observed when the group was hydrogen and C-H activation was observed for a phenyl group (Figure 4.4). Considering the reactivity of the *bis*-ethylene Ir complexes, we targeted complexes with alkyl groups on the nitrogen as these complexes did not undergo similar reactions. Notably, de Bruin et al. also reported the synthesis of the Ir *bis*-ethylene complex,

[(^{Me}BPA)Ir(C_2H_4)$_2$][PF_6].[6] This complex retains the methyl groups on the pyridine moieties (similar to the Rh system discussed above), thus protonation of the olefin complexes is expected to result in linear Ir alkyls. Reported in this chapter is a rare example of C-N bond formation from an isolated Ir^{III}-Et complex.

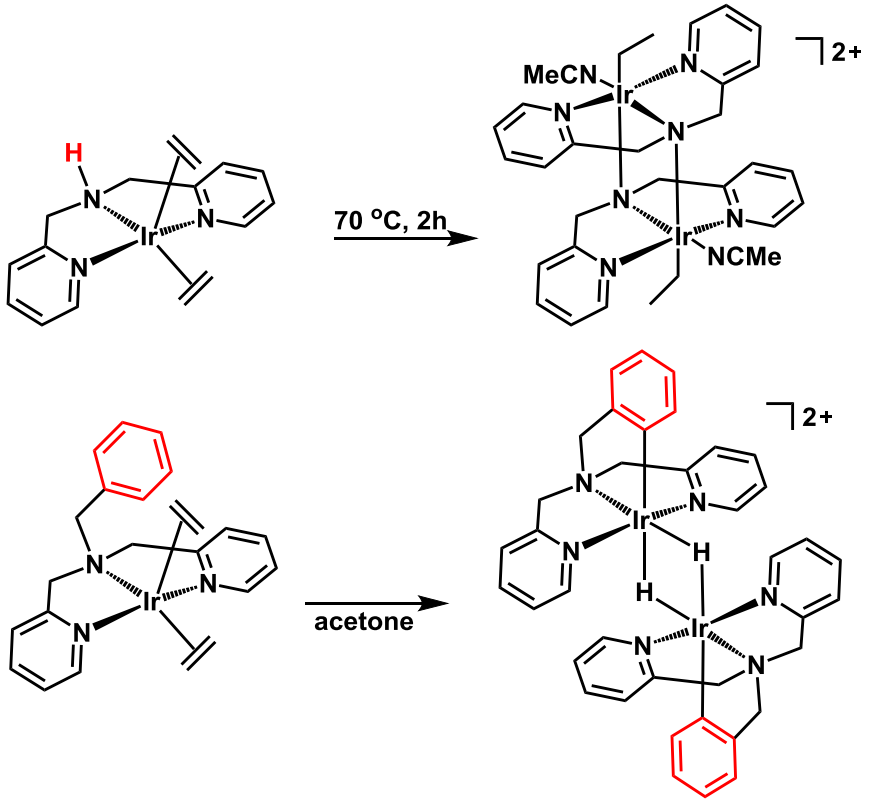

Figure 4.4 Reactivity of substituents on the amine in the BPA ligand.

4.2 Synthesis of [(^{Me}BPA)Ir(OAc)Et][PF_6]

The Ir^{III}-Et complex, [($^{Me,n\text{-}Bu}$BPA)Ir(OAc)Et][PF_6] (**20-OAc**) ($^{Me,n\text{-}Bu}$BPA = *N*,*N*-bis(6-methyl-2-pyridylmethyl)butylamine)) was prepared by addition of acetic acid to the Ir^{I} *bis*-ethylene compound, [($^{Me,n\text{-}Bu}$BPA)Ir(C_2H_4)$_2$][PF_6] (**19**). Complex **19** was modified from the known Ir^{I} *bis*-ethylene complex [(^{Me,Me}BPA)Ir(C_2H_4)$_2$][PF_6][6] to place a *n*-Bu on the nitrogen moiety in the ligand with the goal of increasing solubility. Upon protonation of

[($^{Me,n\text{-}Bu}$BPA)Ir(C_2H_4)$_2$][PF_6] (**19**) with acetic acid, the $^{Me,n\text{-}Bu}$BPA ligand undergoes a change in coordination mode from facial to meridional (Figure 4.5). The ^{1}H NMR spectrum for [($^{Me,n\text{-}Bu}$BPA)Ir(OAc)Et][PF_6] (**20-OAc)** (in CD_2Cl_2) exhibits a triplet and quartet for the Ir-Et at 0.52 and 2.70 ppm, respectively, and a singlet for the Ir-OAc at 2.12 ppm. The benzoate derivative was prepared by protonation of complex **19** with benzoic acid resulting in [($^{Me,n\text{-}Bu}$BPA)Ir(OBz)Et][PF_6] (**20-OBz**). The ethyl peaks were slightly downfield shifted compared to **20-OAc** at 0.65 (t) and 2.79 (q) ppm in the ^{1}H NMR spectrum.

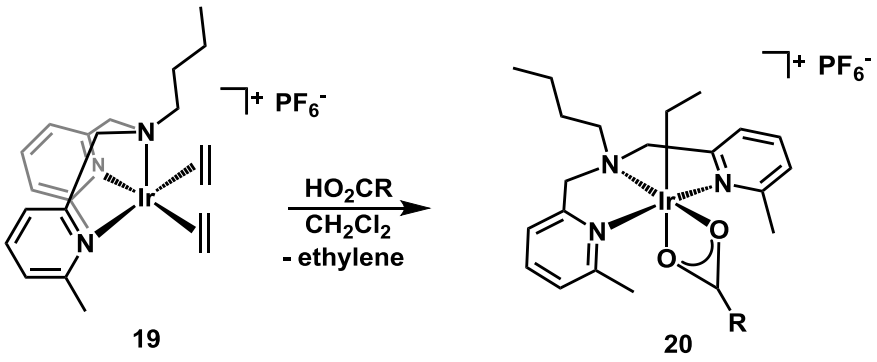

Figure 4.5 Protonation of **19** with carboxylic acids to form **20**.

Unfortunately, crystals of **20-OAc** that were suitable for X-ray diffraction could not be obtained. Crystals of [(^{Me,Me}BPA)Ir(OAc)Et][PF_6] (**21-OBz)** (^{Me,Me}BPA = *N*,*N*-bis(6-methyl-2-pyridylmethyl)methylamine)), however, were obtained by layering a concentrated methylene chloride solution of **21–OBz** with pentane. Notably, the ethyl group is trans to the oxygen moiety from the carboxylate ligand (Figure 4.6) with an elongated Ir-O distance of 2.298(4) Å. The Ir(1) – C(1) distance is the shortest reported for complexes containing an Ir ethyl ligand.[7] The Ir(1) – C(1) – C(2) angle is also on the low end for reported Ir ethyl ligands at 110.5° (118° average).

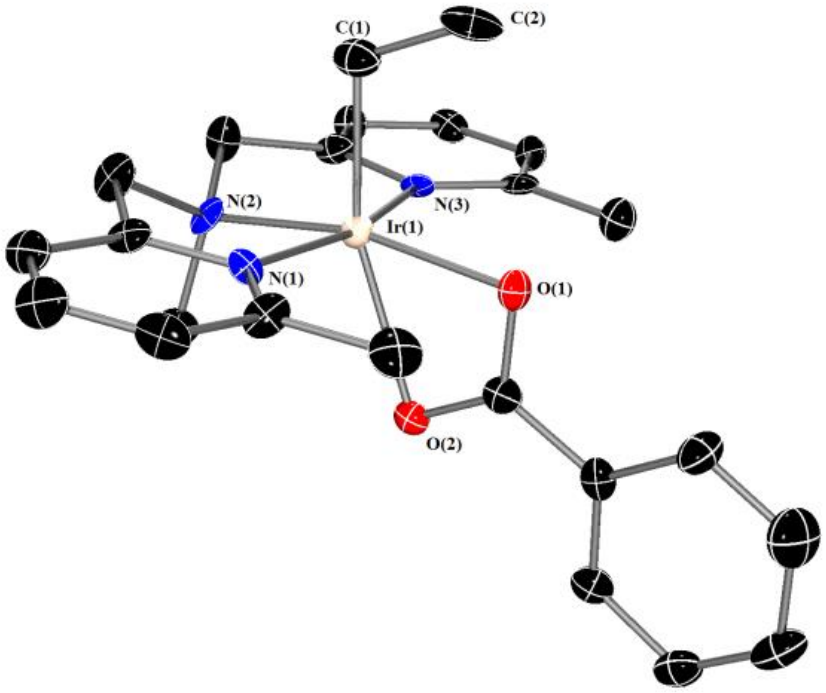

Figure 4.6. ORTEP of **21-OBz** shown with thermal ellipsoids at 50% probability level. The counter ion and hydrogen atoms have been omitted for clarity. Selected bond lengths (Å) and angles (˚): C(1)-Ir(1) = 2.055(7), C(1)-C(2) = 1.520(9), N(1)-Ir(1) = 2.112(4), N(2)-Ir(1) = 2.029(5), N(3)-Ir(1) = 2.090(4), O(1)-Ir(1) = 2.098(4), O(2)-Ir = 2.298(4), Ir(1)-C(1)-C(2) = 110.4(5).

Nucleophilic attack has been shown to occur at the carbon trans to an open site for C(sp^3)-X (X = N, O, I) reductive elimination reactions from Pt^{IV}.[4] We hypothesized that this dissociation of the oxygen moiety of the carboxylate ligand that is trans to the ethyl ligand would generate a five-coordinate species, placing the ethyl group trans to an open site. It was proposed that this five-coordinate geometry might facilitate the nucleophilic attack of an amine at the M-Et α-C to form the corresponding *N*-ethylamine.

4.3 C(sp^3)-N coupling from the reaction of 20 with amine

Excitingly, the thermolysis of **20-OAc** with aniline (5 equiv.) in CD_2Cl_2 at 80 ˚C resulted in the formation of *N*-ethylaniline in approximately 24 % yield (Figure 4.7). This was confirmed by spiking an authentic sample of *N*-ethylaniline into the reaction mixture as well as by GC-MS. Under the same conditions benzophenone hydrazone reacted with **20-OAc** to form *N*-ethylbenzophenone hydrazone in 41 % yield. In order further explore this reaction we transitioned to other solvents as more nucleophilic amines (i.e. piperidine) are known to react with methylene chloride.[8]

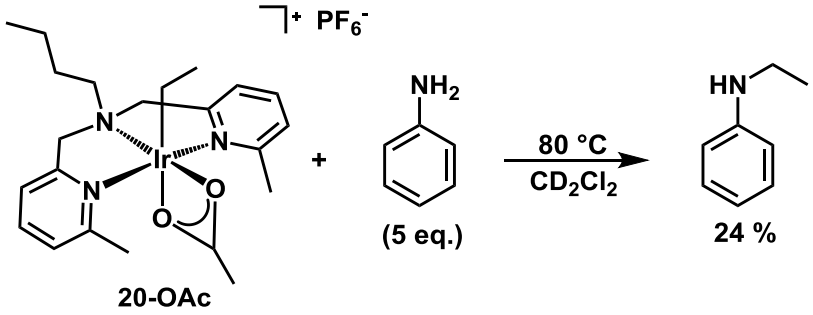

Figure 4.7. Reaction of **20-OAc** with aniline to form *N*-ethylaniline.

Thus, **20-OAc** and benzophenone hydrazone (5 equiv.) were thermolyzed at 80 ˚C in THF-d_8. This resulted in the formation of only trace *N*-ethylbenzophenone hydrazone in contrast to the 41 % obtained in CD_2Cl_2. This may indicate that the formation of a five-coordinate species is short lived due to coordination of THF to the open site.

Complex **20-OAc** was not soluble in benzene or toluene, therefore we used the less common solvent, *o*-dichlorobenzene-d_4. Notably, thermolysis of **20-OAc** and aniline (5 equiv.) in *o*-dichlorobenzene-d_4 at 80˚C resulted in the formation of *N*-ethylaniline in approximately 38 % yield with respect to **20-OAc (**Figure 4.8). The stoichiometric C-N

coupled yield could be increased further to 50 % by using a larger excess of aniline (20 equiv.).

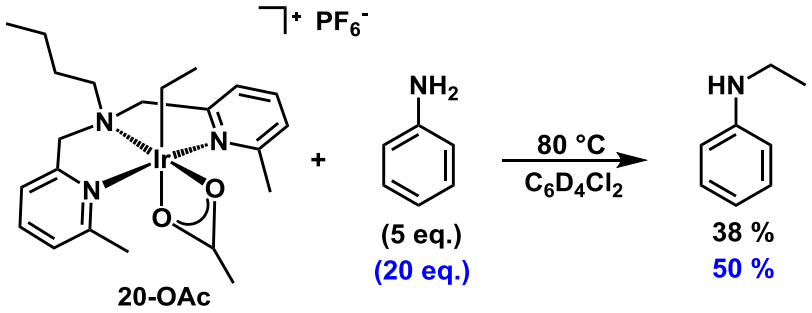

Figure 4.8. Reaction of **20-OAc** with aniline to form *N*-ethylaniline.

Higher C-N coupled yields were obtained with more nucleophilic amines. Thermolysis of **20-OAc** and benzophenone hydrazone (5 equiv.) in *o*-dichlorobenzene-d_4 at 80 ˚C again resulted in the C-N coupled product, *N*-ethylbenzophenone hydrazone, in 55 % yield (Figure 4.9).

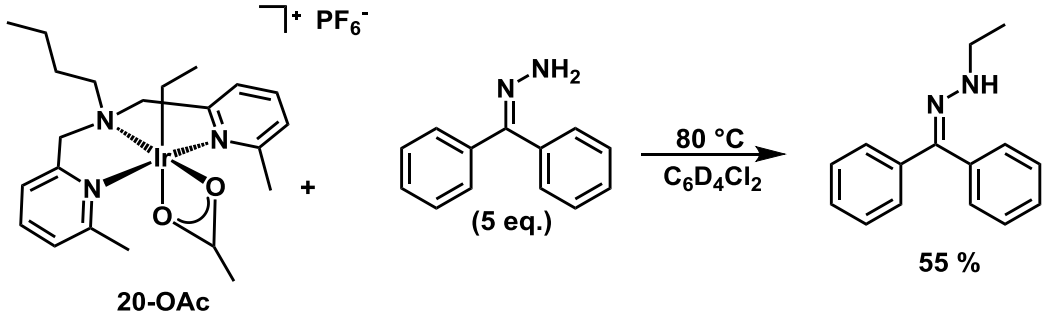

Figure 4.9. Reaction of **20-OAc** with benzophenone hydrazone to form *N*-ethylbenzophenone hydrazone.

The (Pybox)Ir-ethyl complexes that were examined and discussed in Chapter 3 appeared to undergo an E2 elimination rather than the desired S_N2 C-N coupling reaction

when treated with amine bases. E2 elimination is also a possibility for the reaction of **20** with basic amines (Figure 4.10) Notably, thermolysis of **20-OAc** with basic amines resulted in C-N coupled products in high yield. Thermolysis of **20-OAc** and morpholine (5 equiv.) in *o*-dichlorobenzene-d_4 at 80 ˚C resulted in *N*-ethylmorpholine in 58 % yield. Furthermore, reaction of **20-OAc** with piperidine under the same conditions resulted in *N*-ethylpiperidine in 72 % yield (Figure 4.11).

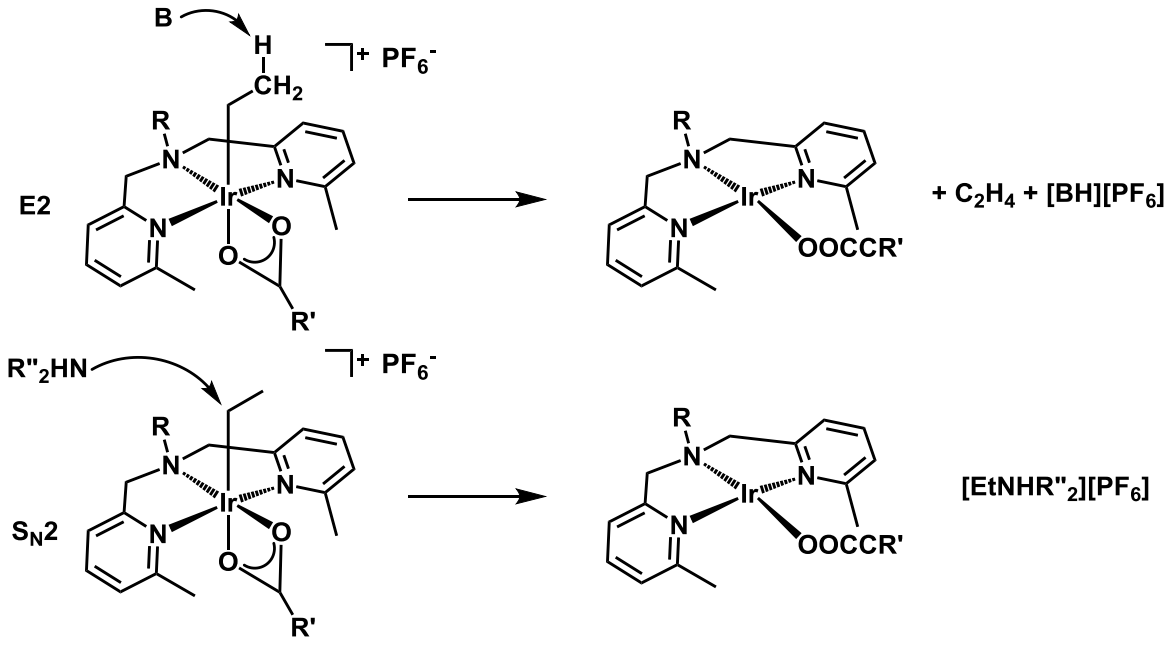

Figure 4.10. E2 elimination to form ethylene (top) and nucleophilic attack to form the desired C-N coupled product (bottom).

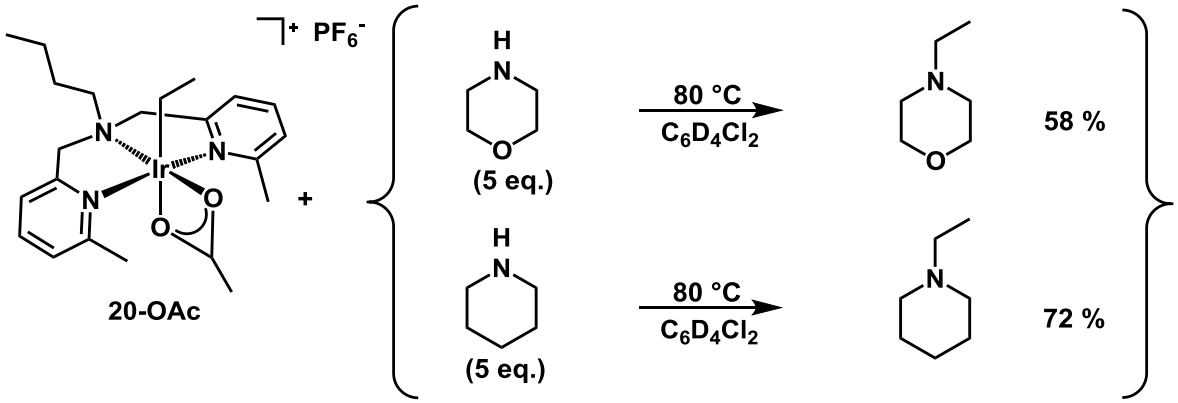

Figure 4.11. Reaction of **20-OAc** with morpholine and piperidine to form *N*-ethylmorpholine and *N*-ethylpiperidine, respectively.

C-N yields for the reaction of complex **20** with amines correlated with the nucleophilicity of the amine. The most nucleophilic amines (piperidine) resulted in the highest yield C-N yield. The nuclophilicity of the amines can be compared on the Swain-Scott nucleophilicity scale (*n*) (aniline, *n* = 12.64; morpholine, *n* = 15.65; piperidine, *n* = 17.35).[9]

As it is predicted that the acetate opens up (κ^2 to κ^1 coordination) prior to reaction, we hypothesized that a less donating carboxylate could improve the C-N yield. Thus, the reaction of **20-OBz** with benzophenone hydrazone was investigated. Thermolysis of **20-OBz** and benzophenone hydrazone (5 eq.) in *o*-dichlorobenzene-d_4 at 80 ℃ resulted in an increased C-N yield of 67 %, consistent with our prediction. A less donating carboxylate would also assist in the alternative pathway where β-H elimination to form an olefin precedes nucleophilic attack (*vide infra*).

We propose that the immediate Ir product from the C-N coupling reaction is (^{Me}BPA)Ir(OAc) or (^{Me}BPA)Ir(OBz). However, we were unable to directly observe this

product. Under the reaction conditions, it appears that this species reacts further to form multiple intractable products. Note that the Ir^{I} *bis*-ethylene precursor, [(^{Me}BPA)Ir(C_2H_4)$_2$][PF_6][6] is also unstable and decomposes to intractable products at ambient temperature. An example ^{1}H NMR spectrum for the reaction of **20-OBz** with benzophenone hydrazone is shown in Figure 4.12.

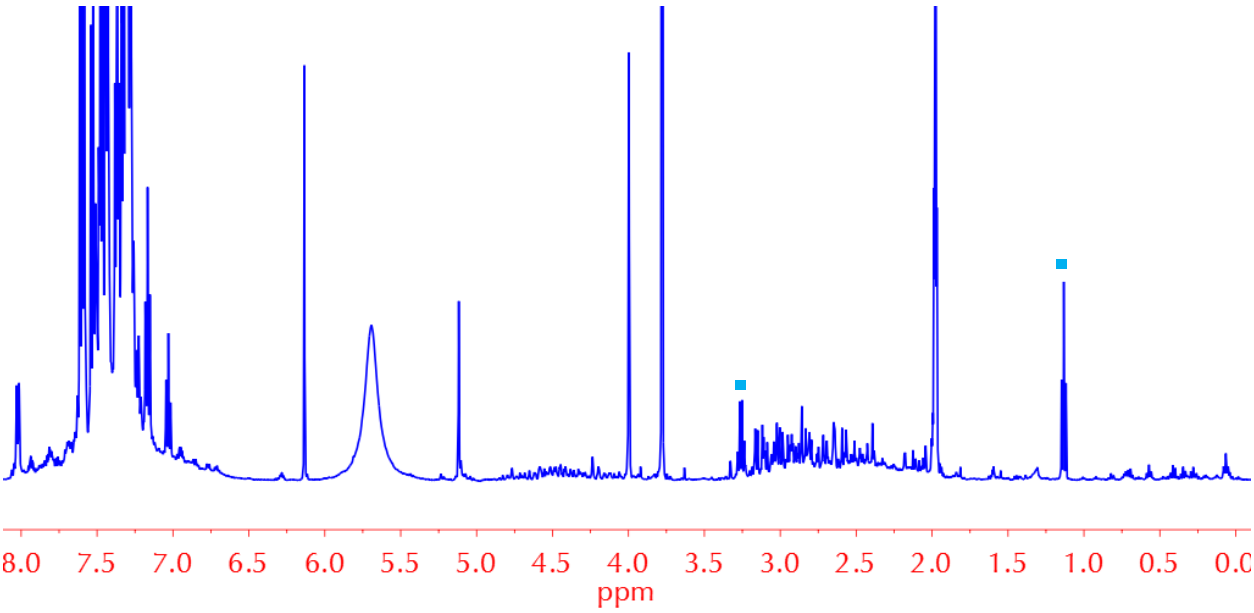

Figure 4.12. ^{1}H NMR of reaction of **20–OBz** with benzophenone hydroazone. *N*-ethylbenzophenone hydrazone indicated by blue square.

4.4 Attempted synthesis of (^{Me}BPA)Ir(OAc)

Independent synthesis of the proposed product, (^{Me}BPA)Ir(OAc), was attempted. Reaction of [($^{Me,n\text{-}Bu}$BPA)Ir(C_2H_4)$_2$][PF_6] with potassium acetate in CD_2Cl_2 led to the formation of **20–OAc** (Figure 4.13). This was unexpected; however, it is possible that the proton came from adventitious water in the solvent or reagents. Thus the same reaction was

attempted in THF-d_8. Surprisingly, this still led to the formation of **20-OAc**, even when rigorously dried potassium acetate was used. As the starting material, [($^{Me,n\text{-}Bu}$BPA)Ir(C_2H_4)$_2$][PF_6], decomposes in solution to form multiple unidentified products, it is possible that the proton was derived from one of the many products.

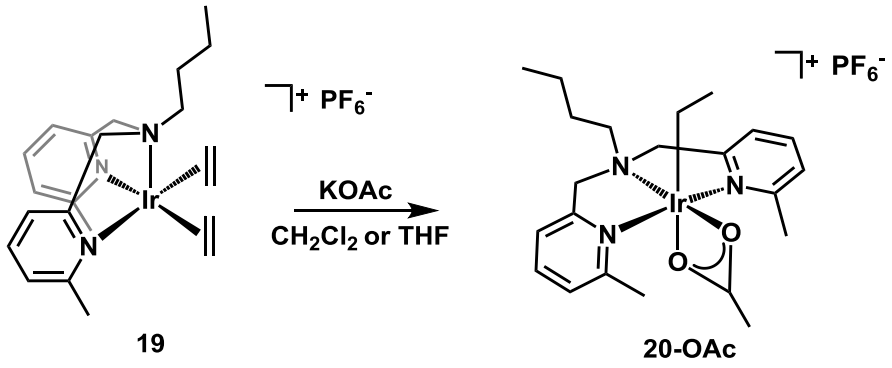

Figure 4.13. Reaction of complex **19** with KOAc to form **20-OAc**.

Thus, synthesis of (^{Me}BPA)Ir(OAc) was attempted by an alternative strategy as shown in Figure 4.14. The Ir acetate dimer [(COD)Ir(OAc)]$_2$ was prepared according to a published procedure.[10] Unfortunately the COD ligand could not be displaced by BPA. Furthermore, even heating at elevated temperatures (100 ˚C), starting material was still observed by ^{1}H NMR spectroscopy.

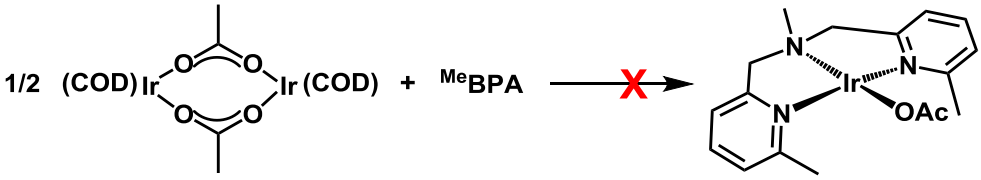

Figure 4.14. Attempted synthesis of (^{Me}BPA)Ir(OAc) by reaction of [(COD)Ir(OAc)]$_2$ with ^{Me}BPA.

4.5 Attempts to trap the proposed Ir^{I} species

If the proposed species, (^{Me}BPA)Ir(OAc), reacted further, one possibility considered was to attempt to trap it out with a donor ligand, such as a phosphine. Thermolysis of **21-OBz**, benzophenone hydrazone (5 equiv.), and triphenylphosphine (5 equiv.) at 80 ˚C in *o*-dichlorobenzene-d_4 resulted in no C-N coupling (Figure 4.15). Similarly, thermolysis of **21-OBz** and benzophenone hydrazone (5 equiv.) and carbon monoxide (1 atm) at 80 ˚C in *o*-dichlorobenzene-d_4 resulted in no C-N coupling. In both cases multiple intractable products were formed as well as ethylene (approximately 29 %) and ethane (approximately 4 %) by ^{1}H NMR spectroscopy. These results may indicate that formation of a five-coordinate species is necessary and coordination of triphenylphosphine or carbon monoxide limits its lifetime with the end result that no C-N coupling occurs.

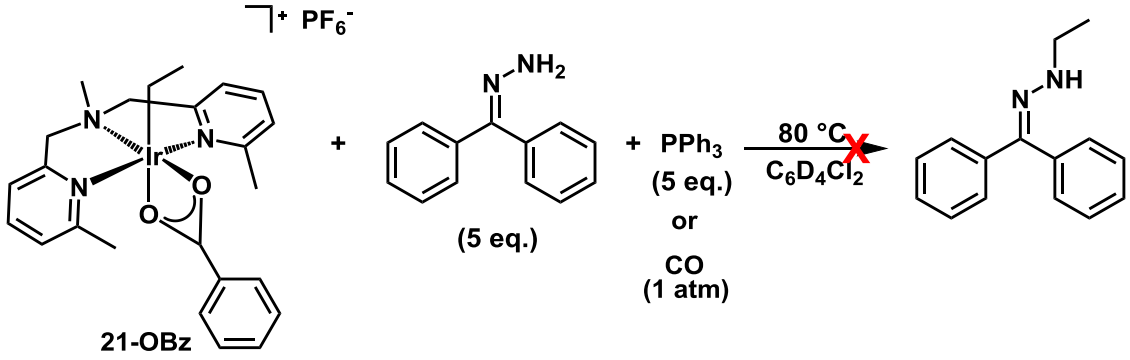

Figure 4.15. Reaction of **21-OAc** with benzophenone hydrazone in the presence of PPh_3 or CO. No C-N coupling was observed.

Solvent effects on the reaction of **21** with amines were also of interest. It is possible that the Ir product formed reacts with *o*-dichlorobenzene. In attempt to prevent this from occurring, the reaction of **21-OBz** with benzophenone hydrazone was performed in *o*-difluorobenzene. Thermolysis of **21-OBz** with benzophenone hydrazone (5 equiv.) in *o*-

difluorobenzene at 80 ˚C resulted in a C-N coupled yield of approximately 40 %. However, many species were still observed by ^{1}H NMR spectroscopy.

The reaction was also attempted in iodobenzene. If the Ir product reacts with the solvent, oxidative addition of iodobenzene should be more facile than *o*-dichlorobenzene. This may form a stable Ir^{III} species, thus preventing the Ir product from reacting further. Thermolysis of **21-OBz** with benzophenone hydrazone (5 equiv.) in iodobenzene at 80 ˚C resulted in the highest C-N yield (approximately 80 %), but again, led to the formation of a multitude of organometallic species as determined by ^{1}H NMR spectroscopy (Figure 4.16).

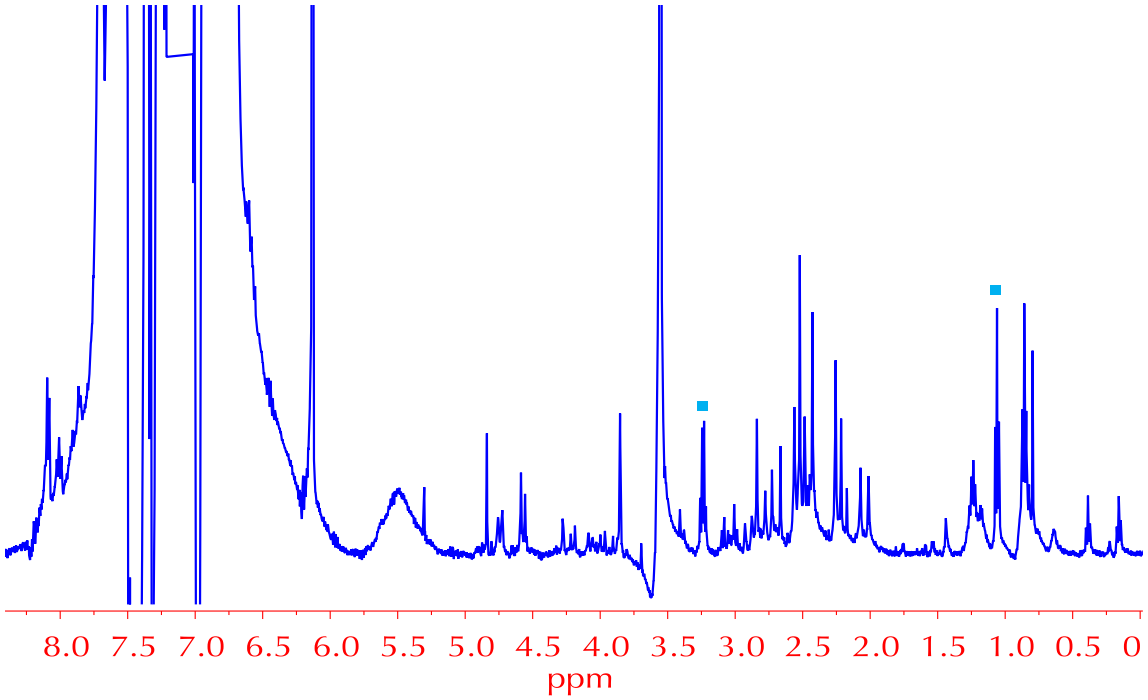

Figure 4.16. ^{1}H NMR of reaction of **21–OBz** with benzophenone hydroazone in iodobenzene. *N*-ethylbenzophenone hydrazone indicated by blue square.

4.6 Possible mechanisms

We have proposed three possible mechanisms for C-N bond formation. In pathway 1 (Figure 4.17), the carboxylate ligand dissociates ($\kappa^2 \rightarrow \kappa^1$) to generate a five-coordinate species. Nucleophilic attack by amine at the α C atom of the Ir-ethyl forms the C-N bond and Ir^{I}(OAc).

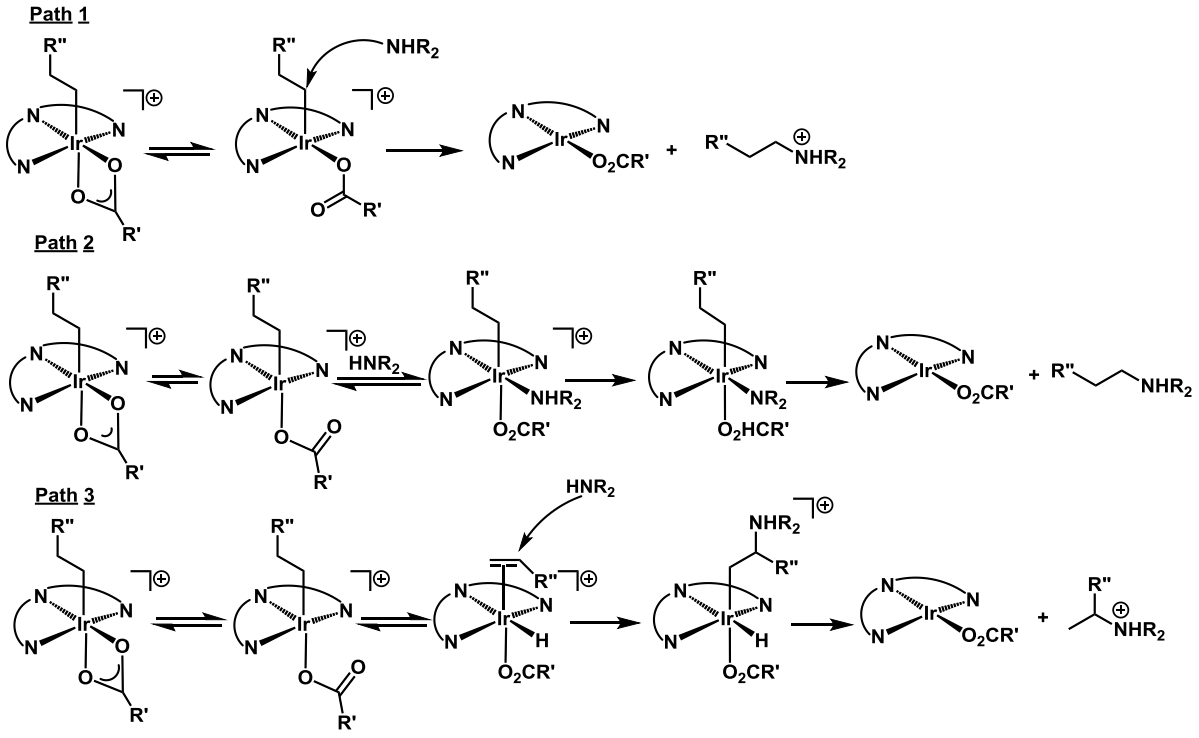

Figure 4.17. Possible pathways for C-N bond formation.

Alternatively the carboxylate ligand dissociates to κ^1 coordination followed by coordination of an amine to the open site (path 2). The amine ligand is subsequently deprotonated to form a metal amido. C-N reductive elimination would release the product.

In Pathway 3 (Figure 4.17), β-H elimination could occur to form an Ir ethylene hydride (Figure 4.17). Nucleophilic attack at the ethylene would form the C-N and

subsequent C-H reductive elimination would release the product. After β-H elimination to form the olefin complex, this mechanism looks similar to the olefin activation mechanism in hydroamination (see chapter 1, Figure 1.11).

All of these mechanisms are expected to be facilitated by less donating carboxylates. However, they should be distinguishable based on the regioselectivity obtained from the C-N coupling. In pathway 1, anti-Markovnikov selectivity is expected as nucleophilic attack should occur at the Ir α-C. Pathway 3 should also result in anti-Markovnikov selectivity. However, Markovnikov selectivity is expected for pathway 2 as nucleophilic attack at metal olefin complexes generally occur at the more substituted carbon. Thus, we attempted to synthesize the propylene and propyl complexes.

4.7 Attempted synthesis of propylene and propyl complexes: Allylic C-H activation.

In an attempt to synthesize [($^{Me,n\text{-}Bu}$BPA)Ir(C_3H_6)$_2$][PF_6], propylene was bubbled through a solution of [($^{Me,n\text{-}Bu}$BPA)Ir(C_2H_4)$_2$][PF_6] in CD_2Cl_2. This resulted in multiple intractable products as observed by ^{1}H NMR spectroscopy. [(^{Me}BPA)Ir(C_2H_4)$_2$][PF_6] decomposes in solution over the course of several hours.[6] It is possible that this complex simply decomposed, or that propylene first displaced the ethylene ligands to form [($^{Me,n\text{-}Bu}$BPA)Ir(C_3H_6)$_2$][PF_6] and then this complex decomposed.

An analogous synthesis to [(^{Me}BPA)Ir(C_2H_4)$_2$][PF_6] was also attempted as shown in Figure 4.20. The Ir starting material, $(COE)_4Ir_2Cl_2$ did not react with propylene. However, the *in situ* generated ethylene complex did undergo reaction with propylene. This again resulted in a multitude of products as determined by ^{1}H NMR spectroscopy. Two signals were observed in the hydride region of the ^{1}H NMR spectrum at -17.1 and -17.4 ppm in a 1:2

ratio, respectively. A signal at 4.94 ppm integrated to 4 protons compared to the hydride signal at -17.1 ppm. This data is consistent with the formation of an Ir(allyl)(hydride)[11] as one of the products.

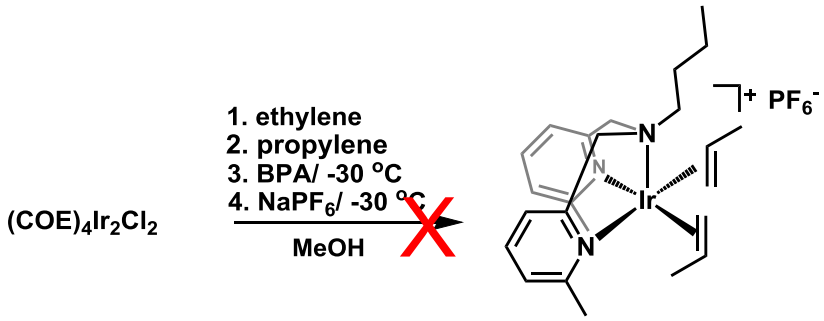

Figure 4.18. Attempted synthesis if the Ir propylene complex. Same procedure for complex **19**, with step 2 added.

Attempts to synthesize [($^{Me,n\text{-}Bu}$BPA)Ir(C_2H_4)$_2$][PF_6] were also made from the isolated Ir propylene precursor $Ir_2Cl_2(C_3H_6)_4$[15]. Addition of $^{Me,n\text{-}Bu}$BPA (2 equiv.) to a MeOD solution of $Ir_2Cl_2(C_3H_6)_4$ again resulted in the formation of a multitude of products as observed by ^{1}H NMR spectroscopy. The ^{1}H NMR spectrum had many unidentifiable peaks, however two hydride resonances were observed at -16.96 and -17.23 in a 1:2 ratio, respectively, similar to those observed in the spectrum of the reaction shown in Figure 4.20. As the propylene precursor could not be synthesized we were unable to determine the regioselectivity.

4.8 Fluorine labeled complex

Kinetic investigations could also give insight into the mechanism. Monitoring the starting material or product formation was not possible due to overlap of the ^{1}H NMR resonances. However, it was anticipated that adding in a fluorine moiety could give an NMR handle suitable for kinetic studies. Thus we synthesized the complex with a CF_3 group in the

ligand backbone [(^{Me,CF3}BPA)Ir(C_2H_4)][PF_6] (**22**). The ^{19}F spectrum for complex **22** exhibits a peak at -64 ppm.

Complex **22** was protonated with acetic acid or benzoic acid, analogously to **19,** to afford [(^{Me,CF3}BPA)Ir(OAc)Et][PF_6] **23-OAc** or [(^{Me,CF3}BPA)Ir(OBz)Et][PF_6] **23-OBz**, respectively (Figure 4.21). ^{19}F NMR spectra of both complex **24-OAc** and **24-OBz** contained a signal at -61 ppm.

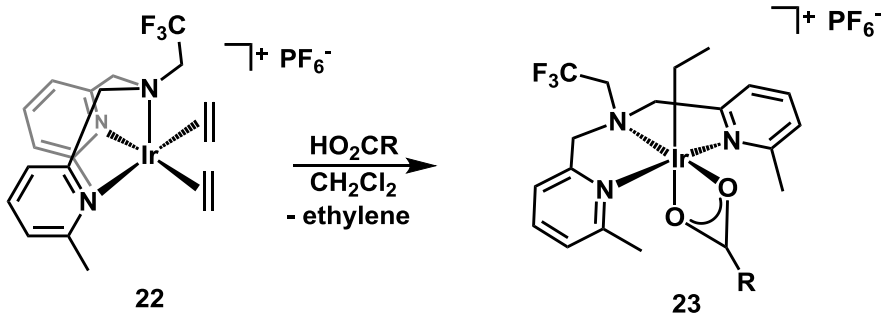

Figure 4.19. Protonation of **22** with carboxylic acids to form **23**.

Thermolysis of **23-OAc** and benzophenone hydrazone (5 eq.) in *o*-dichlorobenzene-d_4 at 80 ˚C resulted in only a trace (~1 %) of the C-N coupled product. Although one would expect addition of a CF_3 moiety to increase the rate of nucleophilic attack at the Ir-Et by increasing the electrophilicity of the Ir-Et, it may also prevent the carboxylate from opening. This would inhibit the formation of the five-coordinate species believed to be required for both nucleophilic attack and β-H elimination. If this is indeed the case, nucleophilic attack at the Ir α-C is not expected to readily take place. Similarly, if β-H elimination to form an Ir olefin does not occur, there is no route to C-N bond formation via pathway 2.

Similar to our observations with **20**, the benzoate derivative was expected to give higher C-N coupled yield as dissociation to κ^1 coordination should be more facile.

Thermolysis of **23-OBz** and benzophenone hydrazone (5 eq.) in in *o*-dichlorobenzene-d_4 at 80 ˚C resulted in a significantly higher yield (29 %), albeit not as high as **21-OBz** (67 %). This result further supports the mechanistic hypothesis that the acetate must open up to achieve the desired C-N coupling reaction. Although the CF_3 moiety provided a convenient NMR handle, these complexes were not investigated further due to the decreased C-N coupling yields.

4.9 Investigation of steric role on C-N coupling.

Previous studies at Rh^{III} have highlighted the importance of sterics in C-I reductive elimination.[12] It was shown that complexes with decreased steric bulk about the metal center did not undergo reductive elimination. This was observed for reductive elimination for both naphthyl based PCP Rh complexes (concerted C-I reductive elimination) as well as cationic PNP Rh complexes (concerted C-Cl reductive elimination, S_N2 attack at the Rh-Me by Br^- or I^-). Furthermore, sterically encumbered ligands were also shown to be important in C-C reductive elimination from Pt^{IV}.[13]

The role of sterics on the pyridine moieties of the ligand was investigated and found to be crucial for the observed C-N coupling reaction. The Ir^{III}-Et complex [(BPA)Ir(OAc)Et][PF_6] (**24-OAc**) (BPA = *N*,*N*-bis(2-pyridylmethyl)butylamine)) was prepared in a similar manner to that used to obtain **21-OAc**; acetic acid was added to [(BPA)Ir(C_2H_4)$_2$][PF_6] (Figure 4.22). The ^{1}H NMR spectrum for complex **24-OAc** (in CD_2Cl_2) exhibits a triplet and quartet for the Ir-Et at 0.3 and 2.31 ppm, respectively, and a singlet for the Ir-OAc at 2.25 ppm. The benzoate derivative was prepared by protonation of [(BPA)Ir(C_2H_4)$_2$][PF_6] with benzoic acid resulting in [(BPA)Ir(OBz)Et][PF_6] (**24-OBz**). The

ethyl resonances of the benzoate derivative were again downfield shifted at 0.43 (t) and 2.42 (q) ppm compared to acetate derivative.

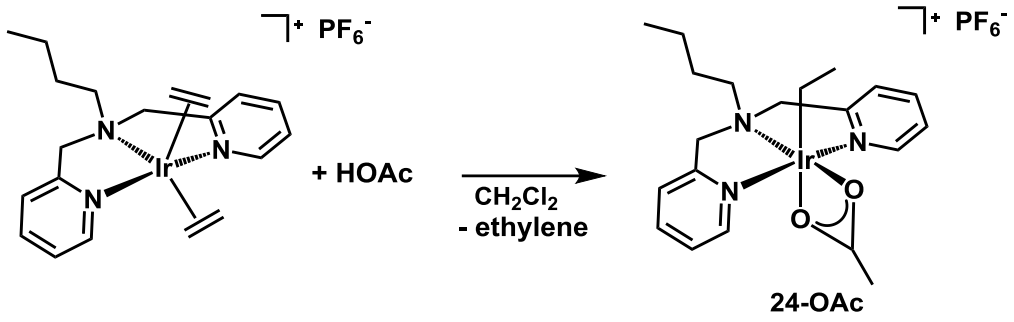

Figure 4.20. Protonation of $[(BPA)Ir(C_2H_4)_2][PF_6]$ with carboxylic acids to form **24**.

Surprisingly, thermolysis of **24-OAc** or **24-OBz** in the presence of benzophenone hydrazone (5 equiv.) in *o*-dichlorobenzene-d_4 at 80 ˚C did not result in any observable C-N coupled products by ^{1}H NMR spectroscopy. Furthermore, no C-O coupled products were observed. In both cases ethane was slowly liberated over time accompanied by the formation of a multitude of organometallic products as determined by ^{1}H NMR spectroscopy (Figure 4.23).

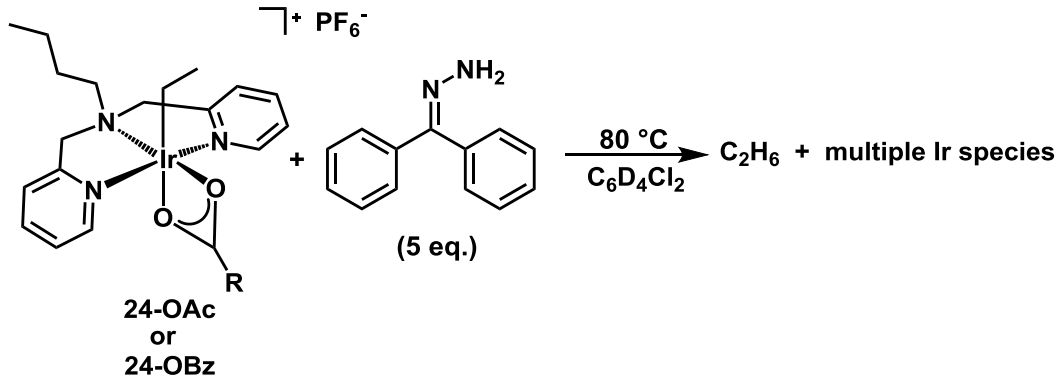

Figure 4.21. Removal of the methyl moieties resulted in complexes that did not undergo C-N coupling.

Similar to the C-I and C-C reductive elimination, sterics appear to be important in promoting the desired C-N coupling. One possibility for the role of the sterics in the C-N coupling reported above could be to promote dissociation of the acetate to generate a five-coordinate species, facilitating nucleophilic attack (or β-H elimination followed by nucleophilic attack). Alternatively, the sterically bulky ligand could favor Ir^{I}. In this case the square planar geometry should relieve the steric congestion of the octahedral Ir^{III} complex.

4.10 Computational investigation of possible mechanisms

As we were unable to rule out one of the proposed mechanisms experimentally, we turned to computation. Computations were performed using **21-OAc** with methyl amine. Single point geometry optimizations were performed to obtain ground energies. Nucleophilic attack at the Ir-Et in path 1 was found to have a transition state energy of 47.0 kcal mol^{-1}. This very high energetic barrier indicates that C-N coupling via path 1 is unlikely. The energy barrier for path 2 was also unreasonably high; the concerted C-N reductive elimination transition state energy was calculated to be 58.5 kcal mol^{-1}.

Path 3 was calculated to proceed via the lowest energy transition state. β-H elimination from **21-OAc** (blue) (**TS-1**) to form complex **A** was slightly uphill (ΔG = 8.5 kcal mol^{-1}) with a transition state energy of 14.3 kcal mol^{-1} (Figure 4.22). Nucleophilic attack at the olefin to generate complex **B** is uphill at 11.6 kcal mol^{-1} relative to **1-OAc**. The transition state energy for nucleophilic attack (**TS-2**) is 27.9 kcal mol^{-1} ($\Delta G^{\ddagger}$). Proton transfer from **B** to form an acetic acid ligand (complex **C**) results in a complex that lies at 20.9 kcal mol^{-1}. Dissociation of the acetic acid ligand to form a five-coordinate species results in complex **D** at 11.9 kcal mol^{-1}. Finally, C-H reductive elimination (**TS-3**) to release the amine product had a transition state energy of 35.0 kcal mol^{-1}.

Notably, the computed energies for the reaction of **24-OAc** (R = H) with methyl amine (red) are all higher in energy, consistent with the fact that no C-N product was observed experimentally. This highlights the importance of the sterics on the ligand. Significantly, β-H elimination is 6 kcal mol^{-1} lower for the with the complex with methyl groups (blue) and the product after C-H reductive elimination (**E**) is 11 kcal mol^{-1} lower in energy.

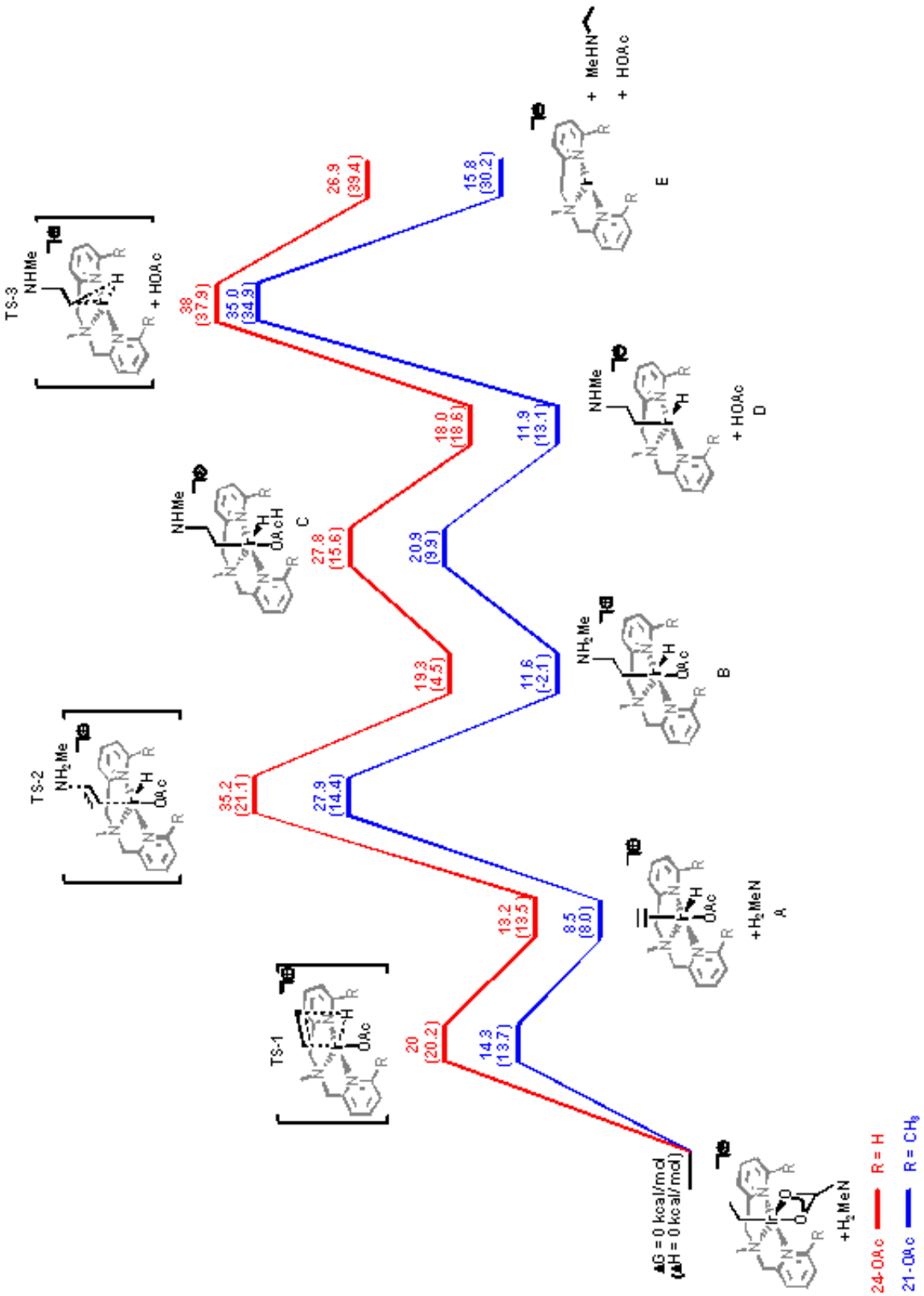

Figure 4.22. Computed reaction scheme.

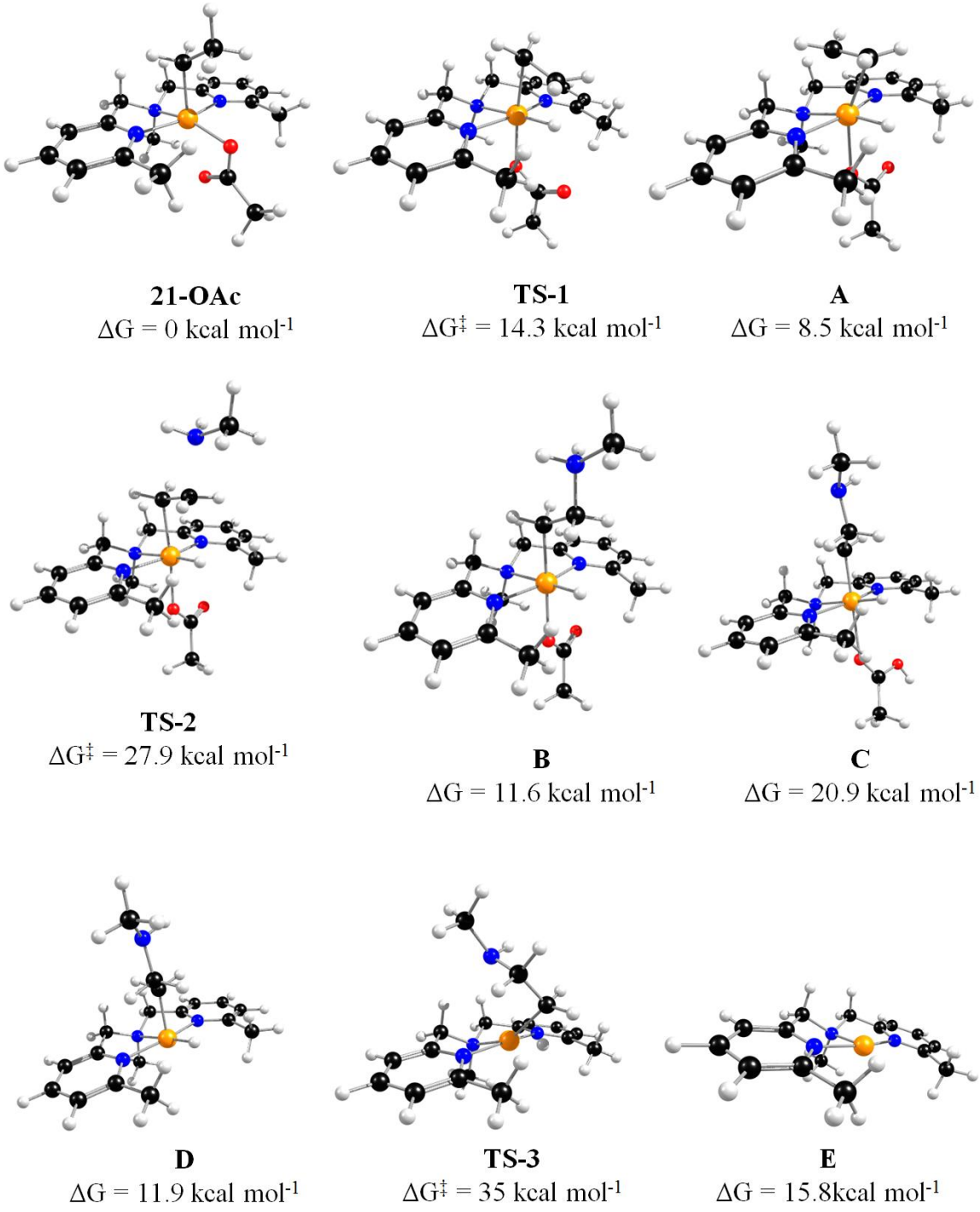

Figure 4.23. Optimized structures and transition states (blue).

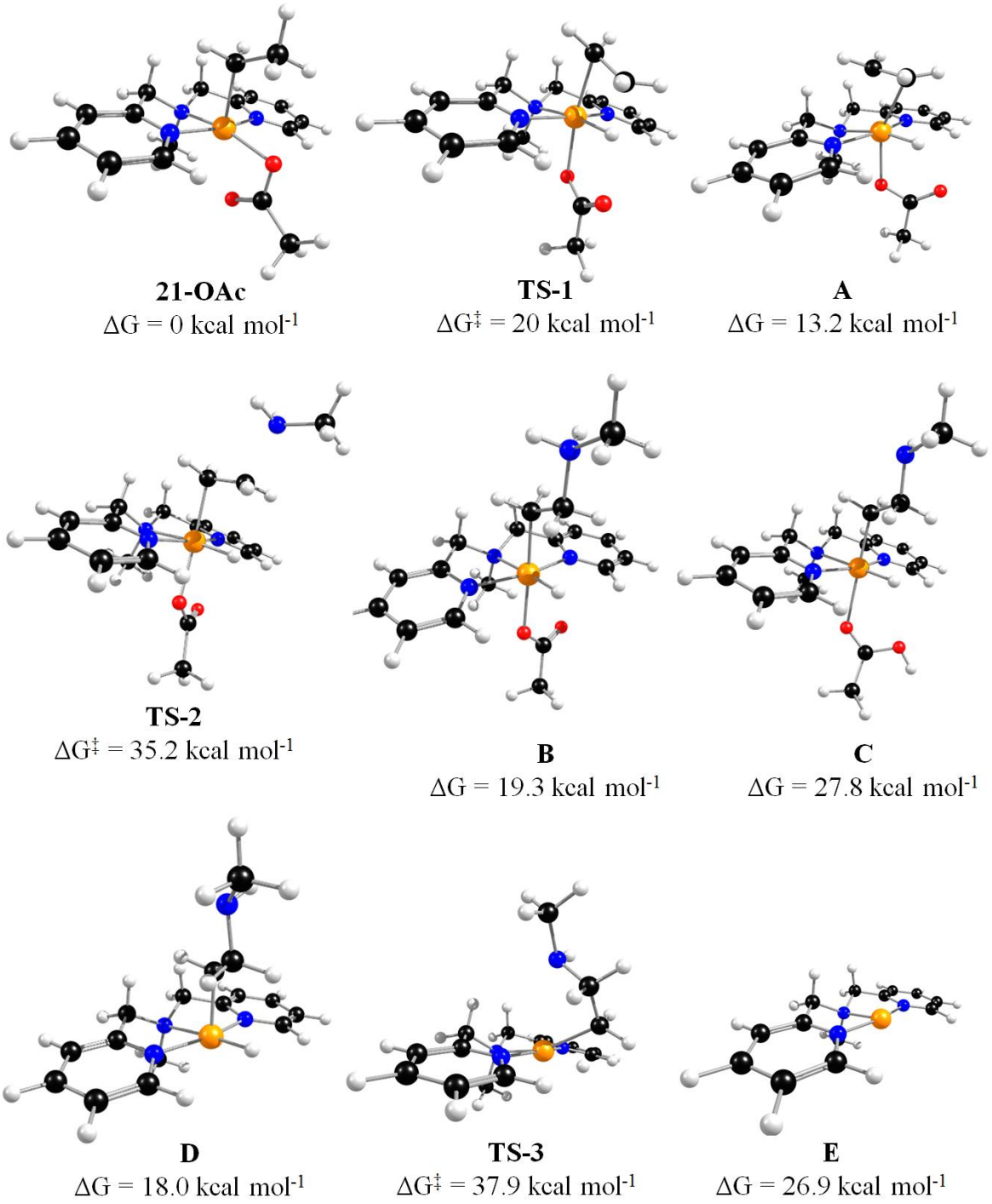

Figure 4.24. Optimized structures and transition states (red).

4.11 Summary

Several new Ir-ethyl complexes have been prepared by protonation of a cationic Ir *bis*-ethylene precursor. The complexes [($^{Me,n\text{-}Bu}$BPA)Ir(O_2CR)Et][PF_6] (**20**) and [(^{Me,Me}BPA)Ir(O_2CR)Et][PF_6] (**21**) both reacted with amines to form the corresponding C-N coupled products. More nucleophilic amines (i.e. morpholine/piperidine) give the highest yields, consistent with a mechanism involving nucleophilic attack. C-N coupling did not proceed in the presence of donor ligands such as PPh_3 or CO and only trace amounts of C-N products were observed in coordinating solvents, such as THF. These data are consistent with the necessity of the complex to form a five-coordinate species for the C-N coupling to proceed.

Both sterics and electronics were found to be important for the C-N coupling reaction. Reaction of the complex [(^{Me,CF3}BPA)Ir(O_2CR)Et][PF_6] (**23)** with benzophenone hydrazone resulted in greatly diminished C-N yields. In this case it is predicted that the carboxylate binds to the Ir more strongly, inhibiting the formation of a five-coordinate species. Furthermore, the less donating carboxylate, benzoate, which should facilitate dissociation to κ^1, resulted in increased C-N yields. Removal of the methyl groups on the pyridine moieties resulted in complexes that did not undergo any observable C-N coupling reactions. This result is consistent with previously reported reactions where sterics were shown to be essential for reductive elimination.[12,13]

The proposed mechanisms were investigated by computation. The lowest energy pathway (path 3) involves initial β-H elimination to form an olefin complex. Nucleophilic attack by amine at the Ir olefin forms the C-N bond. The product is released by subsequent

C-H reductive elimination. The formation of a five-coordinate species is key for this pathway as it is required for β-H elimination. This is in good agreement with experiment, where carboxylates that allowed for facile formation of five-coordinate species (by dissociation) gave the highest C-N yield.

This pathway is distinct from previously reported mechanisms for C(sp^3)-N reductive elimination where substrates resistant toward β-H elimination were employed.[2] In this work, where β-hydrides are available, the C-N coupling likely proceeds by β-H elimination to form an olefin followed by subsequent nucleophilic attack by an amine. We speculate that this may be a fundamental challenge for the development of C(sp^3)-N coupling reactions for alkyls higher than methyl, especially if selectivity for linear alkyl amines is desired.

Experimental

General considerations. All manipulations were carried out under air-free conditions in a N_2 drybox or using standard Schlenk techniques. Solvents were dried by passage through two columns of activated alumina (THF) or passage through one column of alumina and one column of Q5 reactant (pentane). Iodobenzene was degassed and stored over 3 Å molecular sieves. Deuterated solvents were purchased from Cambridge Isotope Laboratories and dried over CaH_2 (dichloromethane-d_2), sodium/ benzophenone (THF-d_8) or 3 Å molecular sieves (*o*-dichlorobenzene-d_4). All other chemicals were purchased from Sigma-Aldrich and used as received. $[Ir(COE)_2Cl]_2$[14], $[Ir(C_3H_6)_2Cl]_2$,[15] ^{Me,Me}BPA[6] and [(^{Me,Me}BPA)Ir(ethylene)$_2$][PF_6][6] were synthesized according to published procedures. NMR spectra were recorded using Bruker AV300, DRX 499, AV500, or AV700 spectrometers. ^{1}H NMR and ^{13}C{^{1}H} NMR

spectra were referenced to residual solvent signals relative to TMS and are reported in parts per million (ppm). Reaction of the Ir complexes **20** – **24** with amines were carried out in *o*-dichlorobenzene-d_4 at 80 ˚C unless otherwise specified. Yields were determined by integration of the *N*-ethylamine signals relative to the internal standard, trimethoxybenzene.

^{Me,CF3}BPA. This ligand was prepared analogously to the published procedure for the *N*-Me variant.[6] ^{1}H NMR ($CDCl_3$, 500 MHz, 298 K) δ 7.56 (2H, t, $J_{H\text{-}H}$ = 7.6 Hz, C_5H_3N), 7.32 (2H, d, $J_{H\text{-}H}$ = 7.7 Hz, C_5H_3N), 7.02 (2H, d, $J_{H\text{-}H}$ = 7.5 Hz, C_5H_3N), 3.97 (4 H, s, N-CH_2-pry), 3.33 (2H, q, $J_{F\text{-}H}$ = 9.4 Hz, NCH_2CF_3), 2.52 (6H, s, pyr-CH_3). ^{19}F NMR ($CDCl_3$, 470 MHz, 298 K) δ -68.8.

[($^{Me,n\text{-}Bu}$BPA)Ir(ethylene)$_2$][PF$_6$] (19). This complex was prepared according to the published procedure using $^{Me,n\text{-}Bu}$BPA.[6] ^{1}H NMR (CD_2Cl_2, 500 MHz, 298 K) δ 7.71 (2H, t, $J_{H\text{-}H}$ = 7.8 Hz, C_5H_3N), 7.34 (2H, d, $J_{H\text{-}H}$ = 8 Hz, C_5H_3N), 7.27 (2H, d, $J_{H\text{-}H}$ = 8 Hz, C_5H_3N), 4.71 (2H, d, $J_{H\text{-}H}$ = 16.2 Hz, N-CH_2-pyr), 4.07 (2H, d, $J_{H\text{-}H}$ = 15.9 Hz, N-C*H2*-pyr), 3.64 (2H, m, *n*-Bu), 3.32 (6H, s, pyr-CH_3), 1.97 – 1.66 (6H, br m, C_2H_4, *n*-Bu) 1.47 (2H, m, *n*-Bu), 1.03 (3H, t, $J_{H\text{-}H}$ = 7.3 Hz, *n*-Bu).

[($^{Me,n\text{-}Bu}$BPA)Ir(OAc)Et][PF$_6$] (20-OAc). Complex **19** (70 mg, 0.104 mmol) was weighed into a vial and dissolved in methylene chloride (approximately 3 mL). Acetic acid (6μL, 0.104 mmol) was added via a microliter syringe (10 μL). The reaction was stirred at ambient temperature for 14 h. The solution was filtered through a Teflon syringe filter into a vial containing pentane to precipitate the product which was collected by filtration yielding a brown solid (33 mg, 45 %). ^{1}H NMR (CD_2Cl_2, 500 MHz, 298 K) δ 7.81 (2H, t, $J_{H\text{-}H}$ = 7.7 Hz, C_5H_3N), 7.31 (2H, d, $J_{H\text{-}H}$ = 7.7 Hz, C_5H_3N), 7.22 (2H, d, $J_{H\text{-}H}$ = 7.7 Hz, C_5H_3N), 4.44 (2H, d,

$J_{H\text{-}H}$ = 16 Hz, N-CH_2-pry), 4.31 (2H, d, $J_{H\text{-}H}$ = 15.8 Hz, N-CH_2-pyr), 2.98 (2H, m, *n*-Bu), 2.7 (2H, q, $J_{H\text{-}H}$ = 7.2 Hz, Ir-CH_2CH$_3$), 2.64 (6H, s, pyr-CH_3), 1.63 (2H, m, *n*-Bu), 1.22 (2H, m, *n*-Bu), 0.85 (3H, t, $J_{H\text{-}H}$ = 7.3 Hz, *n*-Bu), 0.52 (3H, t, $J_{H\text{-}H}$ = 7.2 Hz, Ir-CH$_2$CH_3).

[($^{Me,n\text{-}Bu}$BPA)Ir(OBz)Et][PF$_6$] (20-OBz). Complex **19** (20mg, 0.029 mmol) and benzoic acid (3.6 mg, 0.029 mmol) were weighed into a vial and dissolved in CH_2Cl_2. The reaction mixture was stirred at ambient temperature for 14 h. The solution was filtered through a Teflon syringe filter into a vial containing pentane to precipitate the product. The brown solid was collected by filtration. Yield 11mg, 48 %. ^{1}H NMR (CD_2Cl_2, 300 MHz, 298 K) δ 8.07 (2H, d, $J_{H\text{-}H}$ = 7.9 Hz, Ir-OOCC$_6H_5$), 7.79 (2H, t, $J_{H\text{-}H}$ = 7.8 Hz, C$_5H_3$N), 7.59 (1H, d, $J_{H\text{-}H}$ = 7.6 Hz, Ir-OOCC$_6H_5$), 7.50 (2H, m, Ir-OOCC$_6H_5$), 7.34 (2H, d, $J_{H\text{-}H}$ = 7.4 Hz, C$_5H_3$N), 7.14 (2H, d, $J_{H\text{-}H}$ = 7.8 Hz, C$_5H_3$N), 4.50 (2H, d, $J_{H\text{-}H}$ = 15.9 Hz, N-CH_2-pry), 4.37 (2H, d, $J_{H\text{-}H}$ = 15.7 Hz, N-CH_2-pyr), 3.12 (3H, m, *n*-Bu), 2.80 (2H, q, $J_{H\text{-}H}$ = 7.03 Hz, Ir-CH_2CH$_3$), 2.53 (6H, s, pyr-CH_3), 1.71 (2H, m, *n*-Bu), 1.32 (2H, m, *n*-Bu), 0.91 (3H, t, $J_{H\text{-}H}$ = 7.4 Hz, *n*-Bu), 0.63 (3H, t, $J_{H\text{-}H}$ = 7.03 Hz, Ir-CH$_2$CH_3).

[(^{Me,Me}BPA)Ir(OBz)Et][PF$_6$] (21-OBz). (^{Me,Me}BPA)Ir(C$_2$H$_4$)$_2$][PF$_6$] (125 mg, 0.197 mmol) and benzoic acid (24 mg, 0.197 mmol) were weighed into a vial and dissolved in CH_2Cl_2. The reaction mixture was stirred at ambient temperature for 14 h. The solution was filtered through a Teflon syringe filter into a vial containing pentane to precipitate the product. The brown solid was collected by filtration. Yield 89mg, 62 %. ^{1}H NMR (CD_2Cl_2, 700 MHz, 298 K) δ 8.06 (2H, d, $J_{H\text{-}H}$ = 7.5 Hz, Ir-OOCC$_6H_5$), 7.80 (2H, t, $J_{H\text{-}H}$ = 7.7 Hz, C$_5H_3$N), 7.60 (1H, d, $J_{H\text{-}H}$ = 7.5 Hz, Ir-OOCC$_6H_5$), 7.50 (2H, m, Ir-OOCC$_6H_5$), 7.36 (2H, d, $J_{H\text{-}H}$ = 7.7 Hz, C$_5H_3$N), 7.25 (2H, d, $J_{H\text{-}H}$ = 7.8 Hz, C$_5H_3$N), 4.48 (2H, d, $J_{H\text{-}H}$ = 15.5 Hz, N-CH_2-pry), 4.39 (2H, d, $J_{H\text{-}H}$ = 15.5 Hz, N-CH_2-pyr), 3.04 (3H, s, N-CH_3), 2.78 (2H, q, $J_{H\text{-}H}$ = 7.3 Hz, Ir-

C*H*$_2$CH$_3$), 2.53 (6H, s, pyr-C*H*$_3$), 0.70 (3H, t, $J_{H\text{-}H}$ = 7.3 Hz, Ir-CH$_2$C*H*$_3$). ^{13}C{^{1}H} NMR (176 MHz, 298 K, CD$_2$Cl$_2$) δ 184.2 (s, Ir-OO*C*C$_6$H$_5$), 166.1 (s, *C*$_5$H$_4$N), 150.3 (s, *C*$_5$H$_4$N), 138.9 (s, *C*$_5$H$_4$N), 133.5 (s, Ir-OOC*C*$_6$H$_5$), 132.8 (s, Ir-OOC*C*$_6$H$_5$), 129.6 (s, Ir-OOC*C*$_6$H$_5$), 128.7 (s, Ir-OOC*C*$_6$H$_5$), 125.7 (s, *C*$_5$H$_4$N), 123.8 (s, *C*$_5$H$_4$N), 66.4 (s, N-*C*H$_2$-pyr), 65.4 (s, N-*C*H$_3$), 16.3 (s, Ir-CH$_2$*C*H$_3$), -12.1 (s, Ir-*C*H$_2$CH$_3$).

[(^{Me,CF3}BPA)Ir(C$_2$H$_4$)$_2$][PF$_6$] (22). This complex was prepared according to the published procedure using ^{Me,CF3}BPA.[6] ^{1}H NMR (CD$_2$Cl$_2$, 500 MHz, 298 K) δ 7.72 (2H, t, $J_{H\text{-}H}$ = 7.8 Hz, C$_5$*H*$_3$N), 7.36 (2H, d, $J_{H\text{-}H}$ = 7.5 Hz, C$_5$*H*$_3$N), 7.28 (2H, d, $J_{H\text{-}H}$ = 7.5 Hz, C$_5$*H*$_3$N), 4.96 (2H, d, $J_{H\text{-}H}$ = 16 Hz, N-C*H*$_2$-pry), 4.55 (2H, q, $J_{F\text{-}H}$ = 9.1 Hz, N-C*H*$_2$CF$_3$), 4.40 (2H, d, $J_{H\text{-}H}$ = 16 Hz, N-C*H*$_2$-pyr), 3.31 (6H, s, pyr-C*H*$_3$), 2.12 (4H, m, Ir-C$_2$*H*$_4$), 1.91 (4H, m, Ir-C$_2$*H*$_4$). ^{19}F NMR δ -63.6 (t, $J_{F\text{-}H}$ = 9.1 Hz), -73.9 (d, $J_{F\text{-}P}$ = 711 Hz).

[(^{Me,CF3}BPA)Ir(OAc)Et][PF$_6$] (23-OAc). Complex **22** (69.5 mg, 0.099 mmol) was weighed into a vial and dissolved in CH$_2$Cl$_2$. Acetic acid (5.7 μL, 0.099 mmol) was added via micro syringe. The reaction was stirred at ambient temperature for 14 h. The solution was filtered through a Teflon syringe filter into a vial containing pentane to precipitate the product which was collected by filtration. ^{1}H NMR (CD$_2$Cl$_2$, 500 MHz, 298 K) δ 7.88 (2H, t, $J_{H\text{-}H}$ = 7.9 Hz, C$_5$*H*$_3$N), 7.37 (2H, d, $J_{H\text{-}H}$ = 8 Hz, C$_5$*H*$_3$N), 7.31 (2H, d, $J_{H\text{-}H}$ = 8 Hz, C$_5$*H*$_3$N), 4.82 (2H, d, $J_{H\text{-}H}$ = 16 Hz, N-C*H*$_2$-pry), 4.50 (2H, d, $J_{H\text{-}H}$ = 15.5 Hz, N-C*H*$_2$-pyr), 3.84 (2H, q, $J_{F\text{-}H}$ = 8.8 Hz, N-C*H*$_2$CF$_3$), 2.80 (2H, m, Ir-C*H*$_2$CH$_3$), 2.63 (6H, s, pyr-C*H*$_3$), 2.14 (3H, m, Ir-OOCC*H*$_3$), 0.55 (3H, t, Ir-CH$_2$C*H*$_3$). ^{19}F NMR δ -61.0 (t, $J_{F\text{-}H}$ = 8.8 Hz), -71.7 (d, $J_{F\text{-}P}$ = 711 Hz).

[(^{Me,CF3}BPA)Ir(OBz)Et][PF$_6$] 23-OBz. Complex **22** (50 mg, 0.071 mmol) and benzoic acid (8.7 mg, 0.071 mmol) were weighed into a vial and dissolved in CH$_2$Cl$_2$. The reaction

mixture was stirred at ambient temperature for 14 h. The solution was filtered through a Teflon syringe filter into a vial containing pentane to precipitate the product. The brown solid was collected by filtration. Yield 27 mg, 48 %. ^{1}H NMR (CD_2Cl_2, 500 MHz, 298 K) δ 8.05 (2H, d, $J_{H\text{-}H}$ = 7.8 Hz, Ir-OOCC$_6H_5$), 7.87 (2H, t, $J_{H\text{-}H}$ = 7.8 Hz, C$_5H_3$N), 7.63 (1H, d, $J_{H\text{-}H}$ = 7.4 Hz, Ir-OOCC$_6H_5$), 7.51 (2H, m, Ir-OOCC$_6H_5$), 7.40 (2H, d, $J_{H\text{-}H}$ = 7.6 Hz, C$_5H_3$N), 7.22 (2H, d, $J_{H\text{-}H}$ = 7.8 Hz, C$_5H_3$N), 4.88 (2H, d, $J_{H\text{-}H}$ = 15.9 Hz, N-CH_2-pry), 4.58 (2H, d, $J_{H\text{-}H}$ = 15.6 Hz, N-CH_2-pyr), 4.0 (2H, q, $J_{F\text{-}H}$ = 8.4 Hz, N-CH_2CF$_3$), 2.87 (2H, m, Ir-CH_2CH$_3$), 2.53 (6H, s, pyr-CH_3), 0.68 (3H, t, $J_{H\text{-}H}$ = 7.1 Hz, Ir-CH$_2$CH_3). ^{19}F NMR δ -60.9, -71.8 (d, $J_{F\text{-}P}$ = 711 Hz).

[($^{n\text{-}Bu}$BPA)Ir(OAc)Et][PF$_6$] (24-OAc). [($^{n\text{-}Bu}$BPA)Ir(C$_2$H$_4$)$_2$][PF$_6$] (49 mg, 0.076 mmol) was weighed into a small vial and dissolved in CH_2Cl_2 (2 mL). Acetic acid (4.3, 0.076 mmol) was added via syringe resulting in an immediate color change from orange to yellow. The solution was filtered through a Teflon syringe filter into a vial containing pentane. The yellow solid (13 mg) was collected and dried in vacuo. Yield 13 mg, 25 %. ^{1}H NMR (CD_2Cl_2, 700 MHz, 298 K) δ 8.40 (2H, d, $J_{H\text{-}H}$ = 5.4 Hz, C$_5H_4$N), 8.00 (2H, t, $J_{H\text{-}H}$ = 7.8 Hz, C$_5H_4$N), 7.53 (2H, d, $J_{H\text{-}H}$ = 7.9 Hz, C$_5H_4$N), 7.50 (2H, m, C$_5H_4$N), 4.50 (2H, d, $J_{H\text{-}H}$ = 16 Hz, N-CH_2-pyr), 4.41 (2H, d, $J_{H\text{-}H}$ = 16 Hz, N-CH_2-pyr), 2.83 (2H, m, *n*-Bu), 2.31 (2H, q, $J_{H\text{-}H}$ = 7.3 Hz, Ir-CH_2CH$_3$), 2.26 (3H, s, Ir-OOCCH_3), 1.53 (2H, m, *n*-Bu), 1.18 (2H, h, $J_{H\text{-}H}$ = 7.4 Hz, *n*-Bu), 0.80 (3H, t, $J_{H\text{-}H}$ = 7.4 Hz, *n*-Bu), 0.30 (3H, t, $J_{H\text{-}H}$ = 7.3 Hz, Ir-CH$_2$CH_3). ^{13}C{^{1}H} NMR (176 MHz, 298 K, CD_2Cl_2) δ 189.4 (s, Ir-OO*C*CH$_3$), 166.1 (s, *C*$_5$H$_4$N), 150.1 (s, *C*$_5$H$_4$N), 138.9 (s, *C*$_5$H$_4$N), 125.8 (s, *C*$_5$H$_4$N), 123.8 (s, *C*$_5$H$_4$N), 66.3 (s, N-*C*H$_2$-pyr), 65.3 (s, *n*-Bu), 26.6 (s, *n*-Bu), 24.2 (s, Ir-OOC*C*H$_3$), 20.5 (s, *n*-Bu), 16.4 (s, Ir-CH$_2$*C*H$_3$), 13.7 (s, *n*-Bu), -12.6 (s, Ir-*C*H$_2$CH$_3$).

[($^{n\text{-Bu}}$BPA)Ir(OBz)Et][PF_6] (24-OBz) ($^{n\text{-Bu}}$BPA)Ir(C_2H_4)$_2$][PF_6] (34 mg, 0.052 mmol) and benzoic acid (6.4 mg, 0.052 mmol) were weighed into a vial and dissolved in CH_2Cl_2. The reaction mixture was stirred at ambient temperature for 14 h. The solution was filtered through a Teflon syringe filter into a vial containing pentane to precipitate the product. The yellow solid was collected by filtration. Yield 34 mg, 88 %. ^{1}H NMR (CD_2Cl_2, 700 MHz, 298 K) δ 8.36 (2H, d, $J_{H\text{-}H}$ = 5.5 Hz, C_5H_4N), 8.14 (2H, d, $J_{H\text{-}H}$ = 7.2 Hz, Ir-OOCC_6H_5), 7.98 (2H, t, $J_{H\text{-}H}$ = 7.8 Hz, C_5H_4N), 7.62 (1H, t, $J_{H\text{-}H}$ = 7.5 Hz, Ir-OOCC_6H_5), 7.56 (2H, d, $J_{H\text{-}H}$ = 7.8 Hz, C_5H_4N), 7.52 (2H, t, $J_{H\text{-}H}$ = 7.7 Hz, C_5H_4N), 7.41 (2H, m, Ir-OOCC_6H_5), 4.56 (2H, d, $J_{H\text{-}H}$ = 16 Hz, N-CH_2-pyr), 4.48 (2H, d, $J_{H\text{-}H}$ = 16 Hz, N-CH_2-pyr), 2.96 (2H, m, *n*-Bu), 2.42 (2H, q, $J_{H\text{-}H}$ = 7.3 Hz, Ir-C$H_2$$CH_3$), 1.63 (2H, m, *n*-Bu), 1.26 (2H, h, $J_{H\text{-}H}$ = 7.3 Hz, *n*-Bu), 0.86 (3H, t, $J_{H\text{-}H}$ = 7.4 Hz, *n*-Bu), 0.43 (3H, t, $J_{H\text{-}H}$ = 7.3 Hz, Ir-CH_2CH_3). ^{13}C{^{1}H} NMR (176 MHz, 298 K, CD_2Cl_2) δ 184.2 (s, Ir-OO*C*C_6H_5), 166.1 (s, *C*$_5H_4N$), 150.3 (s, *C*$_5H_4N$), 138.9 (s, *C*$_5H_4N$), 133.5 (s, Ir-OOC*C*$_6H_5$), 132.8 (s, Ir-OOC*C*$_6H_5$), 129.6 (s, Ir-OOC*C*$_6H_5$), 128.7 (s, Ir-OOC*C*$_6H_5$), 125.7 (s, *C*$_5H_4N$), 123.8 (s, *C*$_5H_4N$), 66.4 (s, N-*C*H_2-pyr), 65.4 (s, *n*-Bu), 26.7 (s, *n*-Bu), 20.6 (s, *n*-Bu), 16.3 (s, Ir-CH_2*C*H_3), 13.8 (s, *n*-Bu), -12.1 (s, Ir-*C*$H_2$$CH_3$).

X-ray crystallography methodology

The data was integrated and scaled using SAINT, SADABS within the APEX2 software package by Bruker.[16]

Solution by direct methods (SHELXS, SIR97[17]) produced a complete heavy atom phasing model consistent with the proposed structure. The structure was completed by difference Fourier synthesis with SHELXL97.[18,19] Scattering factors are from Waasmair and Kirfel[20]. Hydrogen atoms were placed in geometrically idealised positions and constrained to ride on

their parent atoms with C---H distances in the range 0.95-1.00 Angstrom. Isotropic thermal parameters U_{eq} were fixed such that they were $1.2U_{eq}$ of their parent atom Ueq for CH's and $1.5U_{eq}$ of their parent atom U_{eq} in case of methyl groups. All non-hydrogen atoms were refined anisotropically by full-matrix least-squares.

Details for solid state structure determination of 21-OBz.

A yellow plate, measuring 0.30 x 0.08 x 0.01mm^3 was mounted on a loop with oil. Data was collected at -183°C on a Bruker APEX II single crystal X-ray diffractometer, Mo-radiation.

Crystal-to-detector distance was 40 mm and exposure time was 30 seconds per frame for all sets. The scan width was 0.5°. Data collection was 96.4% complete to 25° in ϑ. A total of 37929 reflections were collected covering the indices, h = -9 to 9, k = -27 to 27, l = -23 to 23. 5954 reflections were symmetry independent and the R_{int} = 0.0897 indicated that the data was of average quality. Indexing and unit cell refinement indicated a primitive monoclinic lattice. The space group was found to be P $2_1/c$ (No. 14).

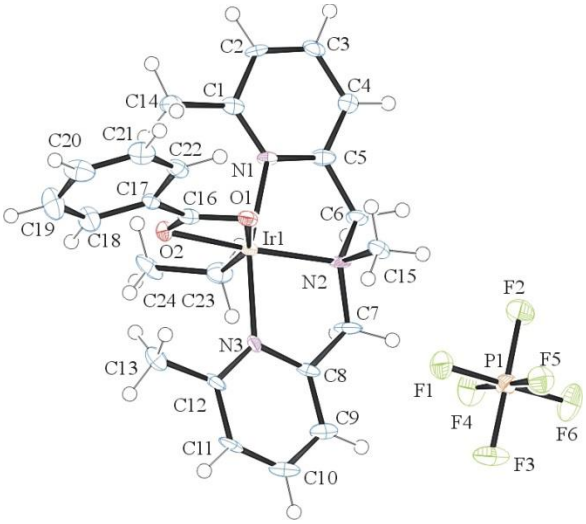

Figure 4.27. ORTEP of the structure with thermal ellipsoids at the 50% probability level. Disorder in phenyl C17 – C22 omitted for clarity.

Table 4.1: Crystallographic data for 21-OBz.

Empirical formula	C24 H29 F6 Ir N3 O2 P	
Formula weight	728.67	
Temperature	90(2) K	
Wavelength	0.71073 Å	
Crystal system	Monoclinic	
Space group	$P\ 2_1/c$	
Unit cell dimensions	a = 7.1262(7) Å	α= 90°.
	b = 20.627(2) Å	β= 91.346(6)°.
	c = 17.3329(16) Å	γ = 90°.
Volume	2547.0(4) $Å^3$	
Z	4	
Density (calculated)	1.900 Mg/m^3	
Absorption coefficient	5.377 mm^{-1}	
F(000)	1424	
Crystal size	0.30 x 0.08 x 0.01 mm^3	
Theta range for data collection	1.53 to 28.50°.	
Index ranges	-9<=h<=9, -27<=k<=27, -23<=l<=23	
Reflections collected	37929	
Independent reflections	5954 [R(int) = 0.0897]	
Completeness to theta = 25.00°	96.4 %	
Max. and min. transmission	0.9482 and 0.2954	
Refinement method	Full-matrix least-squares on F^2	
Data / restraints / parameters	5954 / 66 / 345	
Goodness-of-fit on F^2	1.028	

Final R indices [I>2sigma(I)]	R1 = 0.0488, wR2 = 0.0887
R indices (all data)	R1 = 0.0835, wR2 = 0.0989
Largest diff. peak and hole	1.765 and -2.418 e.Å^{-3}

Computational details

Computations were performed using Gaussian 09.[21] Complexes were modeled with the B3LYP functional with the 6-311++g(d,p) basis set. A solvent correction was added for *o*-dichlorobenzene. Minima and transition sate structures were confirmed by frequency calculations.

Ground state NH_2Me

6	0.708914000	-0.000027000	-0.017599000
1	1.116862000	-0.877417000	0.490143000
1	1.116208000	0.880849000	0.484566000
1	1.082810000	-0.003113000	-1.052511000
7	-0.749958000	-0.000022000	0.118135000
1	-1.159898000	-0.816500000	-0.321753000
1	-1.159763000	0.816498000	-0.321791000

Ground state NH_2MeEt

6	-1.554673000	-0.575471000	0.138118000
1	-1.648017000	-0.543342000	1.222100000
1	-1.100053000	-1.511118000	-0.176031000
1	-2.531600000	-0.459437000	-0.328553000
7	-0.675400000	0.567776000	-0.296950000
1	-1.150376000	1.447701000	-0.078715000
1	-0.579034000	0.547775000	-1.316570000
6	0.720490000	0.608952000	0.322998000
1	1.146563000	1.566300000	0.018880000
1	0.567833000	0.624854000	1.403024000
6	1.587791000	-0.554389000	-0.124203000

1	2.587077000	-0.414948000	0.292688000
1	1.220748000	-1.517630000	0.232565000
1	1.693016000	-0.589142000	-1.212218000

Ground state 21-OAc

77	0.001510000	0.085841000	0.116109000
6	3.140255000	0.656399000	0.180374000
6	2.393500000	-1.542606000	-0.108437000
6	4.460929000	0.212137000	0.035371000
6	3.682850000	-2.013698000	-0.275802000
6	4.744889000	-1.117535000	-0.209880000
1	5.258509000	0.938728000	0.120389000
1	3.850147000	-3.070444000	-0.442090000
1	5.766492000	-1.455389000	-0.334876000
6	-2.391518000	-1.542473000	-0.113385000
6	-3.137688000	0.658418000	0.162157000
6	-3.681178000	-2.014074000	-0.277469000
6	-4.458531000	0.213522000	0.021336000
6	-4.743115000	-1.117761000	-0.214302000
1	-3.848616000	-3.071484000	-0.439424000
1	-5.255759000	0.941112000	0.100848000
1	-5.764924000	-1.456281000	-0.335743000
7	0.001639000	-1.883435000	-0.557893000
6	1.242713000	-2.517717000	-0.046352000
1	1.477437000	-3.430528000	-0.601899000
1	1.070603000	-2.791052000	0.996355000
6	-1.241480000	-2.518736000	-0.052871000
1	-1.072459000	-2.798671000	0.988347000
1	-1.475558000	-3.428203000	-0.614117000
8	0.004732000	2.229255000	0.194159000
8	0.008806000	1.409968000	-1.837448000
6	0.008611000	2.415130000	-1.079337000

6	0.012702000	3.815207000	-1.622524000
1	0.891790000	3.958062000	-2.255543000
1	-0.862611000	3.961407000	-2.259990000
1	0.011954000	4.549889000	-0.819151000
7	-2.101418000	-0.217257000	0.071460000
7	2.103853000	-0.217912000	0.080984000
6	-0.001637000	-0.466953000	2.139009000
1	-0.858027000	-1.118940000	2.347752000
1	0.902916000	-1.043796000	2.364080000
6	2.906105000	2.111314000	0.453506000
1	2.697708000	2.647467000	-0.476756000
1	2.064383000	2.276397000	1.119429000
1	3.806518000	2.547674000	0.886465000
6	-2.903114000	2.116520000	0.417207000
1	-2.061640000	2.290588000	1.080977000
1	-2.694163000	2.639460000	-0.520604000
1	-3.803620000	2.559296000	0.843363000
6	0.005188000	-1.871195000	-2.055264000
1	0.886801000	-1.341772000	-2.410004000
1	-0.876237000	-1.344028000	-2.413843000
6	-0.062332000	0.739842000	3.074255000
1	-0.043540000	0.412139000	4.120634000
1	0.784070000	1.415734000	2.931050000
1	-0.975427000	1.323421000	2.935091000
1	0.007253000	-2.898527000	-2.432262000

Transition State 1 (blue)

77	-0.000006000	0.014253000	-0.414553000
6	-3.068040000	0.705815000	-0.393136000
6	-2.389148000	-1.461602000	0.230361000
6	-4.394272000	0.363025000	-0.088124000
6	-3.685630000	-1.828395000	0.554691000

6	-4.713227000	-0.900046000	0.384536000
1	-5.165026000	1.113158000	-0.223544000
1	-3.884517000	-2.824534000	0.934475000
1	-5.738775000	-1.159006000	0.626986000
6	2.389123000	-1.461633000	0.230335000
6	3.068031000	0.705785000	-0.393144000
6	3.685603000	-1.828442000	0.554654000
6	4.394262000	0.362978000	-0.088144000
6	4.713208000	-0.900101000	0.384502000
1	3.884483000	-2.824586000	0.934428000
1	5.165023000	1.113105000	-0.223560000
1	5.738755000	-1.159074000	0.626942000
7	-0.000010000	-1.768286000	0.786321000
6	-1.248709000	-2.450921000	0.335846000
1	-1.514886000	-3.271559000	1.012434000
1	-1.056780000	-2.876032000	-0.653813000
6	1.248672000	-2.450937000	0.335822000
1	1.056723000	-2.876036000	-0.653838000
1	1.514845000	-3.271587000	1.012399000
8	0.000096000	3.071843000	0.501420000
8	-0.000011000	1.031757000	1.468614000
6	0.000039000	2.337383000	1.497247000
6	0.000073000	2.916990000	2.903573000
1	-0.879834000	2.567916000	3.452544000
1	0.880421000	2.568491000	3.452212000
1	-0.000260000	4.005976000	2.863079000
7	2.079499000	-0.213971000	-0.238012000
7	-2.079515000	-0.213947000	-0.237998000
6	-0.000017000	-0.780011000	-2.391250000
1	0.910073000	-1.305589000	-2.675567000
1	-0.910118000	-1.305575000	-2.675559000

6	-2.758061000	2.082109000	-0.906747000
1	-1.836169000	2.489999000	-0.483481000
1	-2.660162000	2.068805000	-1.998580000
1	-3.583380000	2.757321000	-0.672173000
6	2.758063000	2.082089000	-0.906735000
1	2.660140000	2.068796000	-1.998566000
1	1.836186000	2.489991000	-0.483446000
1	3.583399000	2.757285000	-0.672173000
6	0.000008000	-1.609069000	2.268486000
1	-0.877739000	-1.042866000	2.572619000
1	0.877788000	-1.042908000	2.572602000
1	-0.000010000	-2.600507000	2.736890000
6	-0.000008000	0.664648000	-2.558177000
1	0.905126000	1.141522000	-2.923418000
1	-0.905139000	1.141534000	-2.923410000
1	0.000007000	1.425070000	-1.275931000

Ground State A (blue)

77	-0.066211000	0.032943000	-0.496910000
6	-3.106599000	0.740035000	-0.642735000
6	-2.483607000	-1.195399000	0.541986000
6	-4.444776000	0.509075000	-0.311266000
6	-3.797305000	-1.441368000	0.906891000
6	-4.798996000	-0.585626000	0.459305000
1	-5.195171000	1.209384000	-0.654077000
1	-4.028911000	-2.290140000	1.537992000
1	-5.834236000	-0.761848000	0.725909000
6	2.284310000	-1.348414000	0.476946000
6	3.019984000	0.487463000	-0.793199000
6	3.584020000	-1.694486000	0.804491000
6	4.345032000	0.144780000	-0.509386000
6	4.636941000	-0.941906000	0.294909000

1	3.765585000	-2.545143000	1.449235000
1	5.137427000	0.760917000	-0.913064000
1	5.663055000	-1.196076000	0.531832000
7	-0.096889000	-1.418899000	1.195996000
6	-1.379047000	-2.140113000	0.989750000
1	-1.692952000	-2.654540000	1.903936000
1	-1.226795000	-2.903376000	0.225564000
6	1.133857000	-2.216821000	0.960529000
1	0.913473000	-2.971769000	0.204687000
1	1.436963000	-2.746099000	1.869588000
7	2.003123000	-0.268296000	-0.311027000
7	-2.146822000	-0.128272000	-0.240269000
6	-0.088428000	-1.676853000	-1.891115000
1	0.823528000	-2.260679000	-1.845303000
1	-1.006801000	-2.248394000	-1.818750000
6	-2.717432000	1.964875000	-1.414963000
1	-1.995033000	2.548468000	-0.841678000
1	-2.255238000	1.708224000	-2.370214000
1	-3.595299000	2.578511000	-1.614546000
6	2.729909000	1.717651000	-1.596872000
1	2.051588000	1.519271000	-2.426246000
1	2.268246000	2.464144000	-0.947854000
1	3.655214000	2.130250000	-1.997910000
6	-0.057808000	-0.817431000	2.555737000
1	0.852424000	-0.231907000	2.667865000
1	-0.910705000	-0.157642000	2.690296000
1	-0.078499000	-1.616058000	3.305412000
6	-0.090676000	-0.492133000	-2.638524000
1	0.815259000	-0.158264000	-3.127777000
1	-1.005677000	-0.139999000	-3.098195000
8	-0.324649000	1.504966000	0.967817000

6	0.612322000	2.225166000	1.547656000
6	0.050333000	3.364922000	2.378036000
1	-0.161119000	4.210236000	1.716073000
1	-0.884865000	3.083772000	2.863263000
1	0.786050000	3.682892000	3.115168000
8	1.813550000	2.025930000	1.447100000
1	-0.018572000	1.289873000	-1.430415000

Transition State 2 (blue)

77	-0.074606000	0.097102000	0.142144000
6	-3.094323000	-0.076461000	0.881338000
6	-2.468550000	-0.616771000	-1.322536000
6	-4.424955000	-0.393371000	0.580130000
6	-3.773751000	-0.959017000	-1.651652000
6	-4.774791000	-0.829908000	-0.690081000
1	-5.171266000	-0.308873000	1.361910000
1	-3.996561000	-1.329740000	-2.646354000
1	-5.802889000	-1.086773000	-0.924360000
6	2.291725000	-0.404276000	-1.439946000
6	2.995702000	0.249373000	0.703410000
6	3.601755000	-0.604308000	-1.853932000
6	4.330093000	0.090686000	0.312442000
6	4.643835000	-0.339939000	-0.968126000
1	3.797257000	-0.965199000	-2.857958000
1	5.111719000	0.284168000	1.038106000
1	5.676672000	-0.483582000	-1.268582000
7	-0.073317000	-1.116177000	-1.732663000
6	-1.358985000	-0.724454000	-2.359231000
1	-1.659296000	-1.434436000	-3.141081000
1	-1.221895000	0.247815000	-2.840238000
6	1.147525000	-0.629208000	-2.418568000
1	0.906454000	0.316406000	-2.912147000

1	1.471576000	-1.327502000	-3.201108000
7	1.990543000	0.027373000	-0.180003000
7	-2.138037000	-0.157922000	-0.078459000
6	-0.116553000	1.968420000	-1.009292000
1	0.777442000	2.066774000	-1.626862000
1	-1.034175000	2.041041000	-1.596189000
6	-2.699283000	0.323786000	2.272591000
1	-1.929461000	-0.359413000	2.640105000
1	-2.275893000	1.332165000	2.292616000
1	-3.565231000	0.294898000	2.936819000
6	2.667772000	0.620534000	2.118818000
1	1.996618000	1.480143000	2.173735000
1	2.161483000	-0.222271000	2.596291000
1	3.580432000	0.844207000	2.674690000
6	-0.004815000	-2.585104000	-1.527547000
1	0.907538000	-2.824996000	-0.981140000
1	-0.855052000	-2.905359000	-0.926172000
1	-0.017230000	-3.099334000	-2.497748000
6	-0.107153000	2.772977000	0.169719000
1	0.815249000	2.903175000	0.721544000
1	-1.012470000	2.882023000	0.753662000
8	-0.293096000	-1.674991000	1.280995000
6	0.672887000	-2.484900000	1.638107000
6	0.219186000	-3.535070000	2.645688000
1	0.025181000	-3.057064000	3.611856000
1	-0.715423000	-4.002513000	2.323782000
1	0.994159000	-4.291681000	2.771632000
8	1.833358000	-2.444579000	1.228227000
1	-0.068740000	0.837480000	1.533655000
7	-0.136364000	4.784002000	-0.318438000
1	0.673069000	4.938383000	-0.916496000

1	-0.963334000	4.923044000	-0.895891000
6	-0.130277000	5.699855000	0.837642000
1	-1.007127000	5.499163000	1.457645000
1	0.765103000	5.515041000	1.435686000
1	-0.143371000	6.754520000	0.542810000

Ground State B (blue)

77	0.078869000	0.099105000	-0.175592000
6	3.087373000	-0.177579000	-0.913554000
6	2.476848000	-0.462582000	1.336237000
6	4.415315000	-0.472051000	-0.588289000
6	3.778469000	-0.777432000	1.692352000
6	4.771578000	-0.767923000	0.717000000
1	5.155031000	-0.483866000	-1.378394000
1	4.005273000	-1.038055000	2.718657000
1	5.797094000	-1.009137000	0.970227000
6	-2.276785000	-0.265178000	1.450313000
6	-2.987411000	0.151695000	-0.743542000
6	-3.579371000	-0.459431000	1.879261000
6	-4.316446000	-0.007795000	-0.342761000
6	-4.623081000	-0.318290000	0.970591000
1	-3.769000000	-0.728479000	2.910918000
1	-5.098798000	0.085003000	-1.084770000
1	-5.650613000	-0.467048000	1.280190000
7	0.091017000	-0.926150000	1.808019000
6	1.371052000	-0.447244000	2.379959000
1	1.678840000	-1.045925000	3.245666000
1	1.225193000	0.577535000	2.727120000
6	-1.127133000	-0.369310000	2.440511000
1	-0.887827000	0.629687000	2.810724000
1	-1.442971000	-0.968469000	3.302442000
7	-1.979274000	0.044155000	0.155130000

7	2.136253000	-0.145460000	0.052539000
6	0.129388000	2.058452000	0.656624000
1	-0.722549000	2.225357000	1.333918000
1	1.050166000	2.212853000	1.240586000
6	2.687081000	0.072288000	-2.335680000
1	1.916581000	-0.644781000	-2.625522000
1	2.257610000	1.069382000	-2.454609000
1	3.549488000	-0.023687000	-2.995846000
6	-2.663169000	0.397788000	-2.184838000
1	-2.022528000	1.271404000	-2.311663000
1	-2.117801000	-0.459588000	-2.583139000
1	-3.577882000	0.533023000	-2.762552000
6	0.041682000	-2.408595000	1.777848000
1	-0.866584000	-2.728708000	1.270239000
1	0.893790000	-2.786867000	1.215946000
1	0.066184000	-2.806734000	2.800147000
6	0.076078000	3.100634000	-0.430859000
1	-0.841326000	3.061383000	-1.017325000
1	0.930926000	3.062385000	-1.105239000
8	0.263133000	-1.797139000	-1.196086000
6	-0.668882000	-2.675529000	-1.414292000
6	-0.238166000	-3.813717000	-2.330724000
1	0.799665000	-4.096700000	-2.148190000
1	-0.896719000	-4.671432000	-2.199004000
1	-0.311032000	-3.480114000	-3.370623000
8	-1.810253000	-2.635703000	-0.951739000
1	0.071524000	0.791600000	-1.593678000
7	0.101263000	4.547940000	0.155818000
1	-0.676685000	4.619147000	0.815506000
1	0.948784000	4.631187000	0.721539000
6	0.035192000	5.659132000	-0.844955000

1	0.886855000	5.572054000	-1.517154000
1	-0.890252000	5.562486000	-1.409648000
1	0.061081000	6.619388000	-0.331068000

Ground State C (blue)

77	-0.013127000	0.083176000	-0.183629000
6	2.805083000	-1.119905000	-0.750679000
6	2.172276000	-0.799051000	1.488781000
6	4.016111000	-1.674943000	-0.327231000
6	3.354138000	-1.360327000	1.944294000
6	4.300017000	-1.799044000	1.022614000
1	4.725555000	-2.009515000	-1.073023000
1	3.531486000	-1.444510000	3.009220000
1	5.235308000	-2.233476000	1.354687000
6	-2.290676000	0.861523000	1.405247000
6	-2.904826000	1.048340000	-0.854245000
6	-3.561532000	1.221511000	1.822752000
6	-4.192184000	1.435151000	-0.469441000
6	-4.533271000	1.515268000	0.870370000
1	-3.779964000	1.282969000	2.881546000
1	-4.917139000	1.670785000	-1.237841000
1	-5.532482000	1.806407000	1.171488000
7	-0.227827000	-0.391384000	1.996935000
6	1.165264000	-0.234588000	2.479537000
1	1.309533000	-0.705992000	3.458503000
1	1.365521000	0.830793000	2.599133000
6	-1.178927000	0.661659000	2.424378000
1	-0.626590000	1.599929000	2.507078000
1	-1.613519000	0.444701000	3.407396000
7	-1.967864000	0.749485000	0.080677000
7	1.895385000	-0.678625000	0.155370000
6	0.631450000	2.044224000	0.112993000

1	-0.248978000	2.697980000	0.060588000
1	1.050316000	2.173216000	1.119360000
6	2.495400000	-1.006964000	-2.213330000
1	1.597383000	-1.575837000	-2.460139000
1	2.298174000	0.030077000	-2.489071000
1	3.329433000	-1.382374000	-2.806646000
6	-2.541388000	0.971747000	-2.306629000
1	-1.692489000	1.621328000	-2.526258000
1	-2.243985000	-0.042296000	-2.576458000
1	-3.388962000	1.269951000	-2.924335000
6	-0.750299000	-1.737262000	2.316112000
1	-1.740468000	-1.858402000	1.877302000
1	-0.089593000	-2.494457000	1.896432000
1	-0.820851000	-1.878224000	3.401976000
6	1.684568000	2.568443000	-0.863717000
1	1.286717000	2.553049000	-1.893273000
1	2.563101000	1.913904000	-0.858994000
8	-0.530055000	-2.214186000	-0.720161000
6	-1.426283000	-2.890082000	-1.179594000
6	-1.237795000	-4.295461000	-1.685012000
1	-0.204263000	-4.601653000	-1.542948000
1	-1.897241000	-4.986951000	-1.152495000
1	-1.484997000	-4.348865000	-2.749697000
8	-2.669142000	-2.375344000	-1.248297000
1	0.131820000	0.413373000	-1.714251000
7	2.142555000	3.898516000	-0.460375000
1	1.351160000	4.533389000	-0.422380000
6	3.176827000	4.453878000	-1.329883000
1	4.085456000	3.849983000	-1.248100000
1	2.892738000	4.491665000	-2.395085000
1	3.424043000	5.466406000	-1.004443000

1	-3.291313000	-3.006294000	-1.634295000

Ground State D (blue)

77	0.139244000	-0.029182000	0.452782000
6	-2.866343000	-0.365246000	1.222249000
6	-2.068815000	-1.521156000	-0.666095000
6	-4.127016000	-0.938491000	1.034741000
6	-3.300752000	-2.118620000	-0.870208000
6	-4.355005000	-1.815203000	-0.013054000
1	-4.920132000	-0.690086000	1.727917000
1	-3.431673000	-2.809825000	-1.693345000
1	-5.330287000	-2.264514000	-0.156513000
6	2.620831000	-0.684201000	-0.868842000
6	3.126772000	0.711719000	0.957461000
6	3.961134000	-0.826074000	-1.184147000
6	4.487695000	0.602881000	0.656959000
6	4.914487000	-0.165928000	-0.413061000
1	4.252495000	-1.441637000	-2.025943000
1	5.202066000	1.126318000	1.278918000
1	5.969334000	-0.257217000	-0.642501000
7	0.385986000	-1.753223000	-0.926163000
6	-0.919832000	-1.784367000	-1.628761000
1	-1.081808000	-2.737315000	-2.145172000
1	-0.914688000	-0.999233000	-2.387574000
6	1.550395000	-1.325729000	-1.739495000
1	1.200689000	-0.582129000	-2.459413000
1	1.982712000	-2.158668000	-2.305795000
7	2.202528000	0.070597000	0.194726000
7	-1.848440000	-0.647624000	0.365511000
6	-0.120226000	1.473409000	-0.968781000
1	0.855735000	1.956704000	-1.082770000
1	-0.373738000	1.005150000	-1.926784000

6	-2.620733000	0.560596000	2.375823000
1	-1.845915000	0.164309000	3.035674000
1	-2.272719000	1.534475000	2.028165000
1	-3.535662000	0.694151000	2.952832000
6	2.672280000	1.531909000	2.127617000
1	1.986971000	2.318662000	1.807918000
1	2.131316000	0.916226000	2.849244000
1	3.528873000	1.985607000	2.625922000
6	0.654156000	-3.033327000	-0.228767000
1	1.565265000	-2.946408000	0.363898000
1	-0.175009000	-3.269855000	0.438857000
1	0.775144000	-3.853036000	-0.947000000
6	-1.185532000	2.520968000	-0.660180000
1	-0.932000000	3.060382000	0.267092000
1	-2.151502000	2.035474000	-0.490516000
1	-0.022810000	1.144077000	1.488502000
7	-1.346858000	3.407228000	-1.812277000
1	-0.483208000	3.913512000	-1.979841000
6	-2.453531000	4.354182000	-1.677756000
1	-3.401015000	3.808237000	-1.660529000
1	-2.401989000	4.973638000	-0.767686000
1	-2.470573000	5.017263000	-2.544609000

Transition State 3 (blue)

77	0.129269000	-0.164228000	-0.295545000
6	-2.847540000	-0.185998000	-1.271316000
6	-2.195024000	1.404745000	0.325686000
6	-4.139796000	0.351305000	-1.269465000
6	-3.455861000	1.981100000	0.340900000
6	-4.459837000	1.430258000	-0.455379000
1	-4.883600000	-0.080900000	-1.929428000
1	-3.644471000	2.847222000	0.966003000

1	-5.460078000	1.850557000	-0.458075000
6	2.555807000	1.022727000	0.683223000
6	3.173294000	-0.730260000	-0.751750000
6	3.878131000	1.379690000	0.896378000
6	4.521334000	-0.416327000	-0.543267000
6	4.887700000	0.632468000	0.289405000
1	4.110722000	2.230917000	1.527225000
1	5.275501000	-0.998161000	-1.061419000
1	5.932424000	0.880799000	0.444076000
7	0.230098000	1.811590000	0.428574000
6	-1.064497000	1.928421000	1.179270000
1	-1.249592000	2.963510000	1.492550000
1	-0.979776000	1.294710000	2.067274000
6	1.418226000	1.771347000	1.340706000
1	1.113753000	1.239820000	2.247323000
1	1.729801000	2.783715000	1.626806000
7	2.192886000	-0.033842000	-0.110034000
7	-1.889713000	0.315897000	-0.443610000
6	-0.018549000	-2.395220000	0.009705000
1	-0.111689000	-3.194685000	-0.740986000
1	0.959843000	-2.546911000	0.470313000
6	-2.492056000	-1.299596000	-2.215543000
1	-1.589038000	-1.045882000	-2.777538000
1	-2.301629000	-2.237199000	-1.684756000
1	-3.308784000	-1.475709000	-2.918126000
6	2.795115000	-1.816020000	-1.719619000
1	2.467370000	-2.724114000	-1.204566000
1	1.978707000	-1.482082000	-2.364717000
1	3.652986000	-2.081605000	-2.340419000
6	0.369884000	2.892818000	-0.584440000
1	1.290657000	2.741713000	-1.148178000

1	-0.472933000	2.853923000	-1.274628000
1	0.396698000	3.872904000	-0.090833000
6	-1.145132000	-2.607058000	1.026571000
1	-1.170849000	-3.692232000	1.251922000
1	-2.115964000	-2.372351000	0.576368000
1	-0.005469000	-1.583079000	-1.096596000
7	-1.003450000	-1.802255000	2.239187000
1	-0.077044000	-1.968354000	2.626875000
6	-2.006316000	-2.145655000	3.250442000
1	-3.001205000	-1.862869000	2.889888000
1	-2.037350000	-3.218517000	3.506152000
1	-1.810767000	-1.581799000	4.166607000

Ground State E (blue)

77	0.000012000	-0.415032000	-0.085549000
6	2.984344000	-1.140790000	0.045331000
6	2.396708000	1.119425000	-0.211018000
6	4.332317000	-0.786469000	0.083120000
6	3.719096000	1.519045000	-0.154877000
6	4.708595000	0.546905000	-0.009077000
1	5.077783000	-1.563864000	0.191617000
1	3.973919000	2.568483000	-0.235551000
1	5.753618000	0.828498000	0.030867000
6	-2.396697000	1.119414000	-0.210966000
6	-2.984394000	-1.140776000	0.045424000
6	-3.719081000	1.519070000	-0.154882000
6	-4.332354000	-0.786419000	0.083192000
6	-4.708604000	0.546961000	-0.009074000
1	-3.973873000	2.568513000	-0.235582000
1	-5.077838000	-1.563787000	0.191745000
1	-5.753621000	0.828577000	0.030858000
7	0.000014000	1.575600000	0.185609000

6	1.257448000	2.076581000	-0.478084000
1	1.490546000	3.089741000	-0.138376000
1	1.065524000	2.102775000	-1.552275000
6	-1.257438000	2.076579000	-0.478030000
1	-1.065553000	2.102816000	-1.552228000
1	-1.490540000	3.089726000	-0.138285000
7	-2.028880000	-0.188628000	-0.096819000
7	2.028865000	-0.188620000	-0.096920000
6	2.516207000	-2.560253000	0.155382000
1	1.901304000	-2.694260000	1.050682000
1	1.912350000	-2.833087000	-0.717198000
1	3.357380000	-3.251121000	0.211182000
6	-2.516299000	-2.560276000	0.155144000
1	-1.916224000	-2.834289000	-0.719673000
1	-1.897668000	-2.693441000	1.048000000
1	-3.357456000	-3.250797000	0.215268000
6	0.000041000	1.946468000	1.638726000
1	-0.885351000	1.532041000	2.114719000
1	0.885430000	1.532010000	2.114697000
1	0.000061000	3.037695000	1.731827000

Ground State 24-0Ac

77	0.000004000	0.177738000	0.131516000
6	2.993593000	0.854075000	0.156199000
6	2.393569000	-1.386750000	-0.128995000
6	4.342382000	0.544869000	0.046911000
6	3.724273000	-1.752720000	-0.263853000
6	4.715426000	-0.776417000	-0.170864000
1	5.079234000	1.333266000	0.128758000
1	3.983142000	-2.790761000	-0.433131000
1	5.759623000	-1.047126000	-0.268871000
6	-2.393531000	-1.386777000	-0.129033000

6	-2.993591000	0.854039000	0.156167000
6	-3.724230000	-1.752770000	-0.263886000
6	-4.342374000	0.544810000	0.046882000
6	-4.715397000	-0.776484000	-0.170891000
1	-3.983083000	-2.790815000	-0.433167000
1	-5.079240000	1.333193000	0.128728000
1	-5.759591000	-1.047208000	-0.268898000
7	0.000029000	-1.765181000	-0.623800000
6	1.263065000	-2.401789000	-0.133304000
1	1.525919000	-3.273710000	-0.739283000
1	1.089485000	-2.739387000	0.889625000
6	-1.263013000	-2.401802000	-0.133340000
1	-1.089453000	-2.739416000	0.889587000
1	-1.525847000	-3.273713000	-0.739340000
8	-0.000069000	2.292608000	0.422288000
8	0.000004000	1.699465000	-1.688007000
6	-0.000048000	2.617453000	-0.827788000
6	-0.000044000	4.067917000	-1.213988000
1	0.878492000	4.279255000	-1.828077000
1	-0.877710000	4.278952000	-1.829409000
1	-0.000769000	4.709509000	-0.334652000
7	-2.037957000	-0.087496000	0.068546000
7	2.037973000	-0.087471000	0.068580000
6	-0.000012000	-0.472494000	2.125239000
1	-0.881876000	-1.094882000	2.317575000
1	0.881943000	-1.094744000	2.317607000
6	0.000050000	-1.716186000	-2.120001000
1	0.882476000	-1.180870000	-2.465147000
1	-0.882274000	-1.180717000	-2.465174000
6	-0.000125000	0.712570000	3.087858000
1	-0.000113000	0.360025000	4.126162000

1	0.878894000	1.347211000	2.954331000
1	-0.879250000	1.347057000	2.954304000
1	-0.000027000	-2.733062000	-2.524649000
1	2.642799000	1.863678000	0.324517000
1	-2.642809000	1.863647000	0.324479000

Transition State 1 (red)

77	0.038718000	0.072685000	-0.452071000
6	-2.968565000	0.655531000	-0.529930000
6	-2.283202000	-1.419915000	0.325678000
6	-4.303653000	0.357649000	-0.271570000
6	-3.596594000	-1.760258000	0.624116000
6	-4.624142000	-0.867539000	0.307676000
1	-5.068493000	1.087760000	-0.510549000
1	-3.812264000	-2.711597000	1.098808000
1	-5.655585000	-1.122535000	0.528020000
6	2.489509000	-1.179401000	0.372100000
6	2.990608000	0.924403000	-0.526951000
6	3.822742000	-1.380956000	0.707776000
6	4.341563000	0.770938000	-0.230782000
6	4.765658000	-0.398967000	0.394382000
1	4.118848000	-2.296441000	1.208836000
1	5.037079000	1.564203000	-0.480005000
1	5.811029000	-0.544430000	0.646022000
7	0.110491000	-1.547780000	0.955640000
6	-1.106292000	-2.343627000	0.588750000
1	-1.354022000	-3.070198000	1.371572000
1	-0.877460000	-2.893244000	-0.329460000
6	1.408840000	-2.215949000	0.623306000
1	1.259787000	-2.795505000	-0.293124000
1	1.713930000	-2.906246000	1.418579000
8	-0.721344000	3.025493000	-0.181117000

8	-0.022390000	1.406644000	1.232230000
6	-0.410076000	2.623782000	0.948580000
6	-0.445957000	3.553719000	2.149735000
1	0.568315000	3.692740000	2.537086000
1	-0.861492000	4.520846000	1.867756000
1	-1.039449000	3.111050000	2.954722000
7	2.087746000	-0.032847000	-0.245767000
7	-1.986723000	-0.225125000	-0.258607000
6	0.084034000	-0.869103000	-2.361010000
1	1.021567000	-1.360349000	-2.616617000
1	-0.794146000	-1.464204000	-2.607147000
1	-2.644227000	1.613970000	-0.920376000
1	2.601029000	1.824961000	-0.986817000
6	0.072142000	-1.172800000	2.398257000
1	-0.839685000	-0.614681000	2.602533000
1	0.913146000	-0.520174000	2.625513000
1	0.112482000	-2.079779000	3.013205000
6	0.000646000	0.563871000	-2.611071000
1	0.877592000	1.076961000	-3.000742000
1	-0.932182000	0.972362000	-2.995061000
1	-0.091369000	1.452695000	-1.345336000

Ground State A (red)

77	-0.052058000	0.049746000	-0.537444000
6	-3.018027000	0.819753000	-0.811086000
6	-2.504474000	-0.985435000	0.584494000
6	-4.367078000	0.732301000	-0.496646000
6	-3.839201000	-1.109435000	0.944765000
6	-4.786323000	-0.248973000	0.393358000
1	-5.064968000	1.430664000	-0.939791000
1	-4.132828000	-1.873375000	1.654182000
1	-5.830883000	-0.339199000	0.665778000

6	2.255683000	-1.280250000	0.583003000
6	2.985212000	0.477200000	-0.785367000
6	3.565664000	-1.586134000	0.922390000
6	4.314234000	0.198534000	-0.494196000
6	4.611036000	-0.848623000	0.368649000
1	3.764744000	-2.394335000	1.615429000
1	5.092422000	0.811123000	-0.930297000
1	5.637969000	-1.082106000	0.622774000
7	-0.131101000	-1.247292000	1.279622000
6	-1.441722000	-1.936459000	1.122020000
1	-1.780673000	-2.364505000	2.071116000
1	-1.315775000	-2.760506000	0.417842000
6	1.083651000	-2.094334000	1.117535000
1	0.855034000	-2.894597000	0.411905000
1	1.366990000	-2.563717000	2.065368000
7	1.979855000	-0.256205000	-0.274046000
7	-2.107351000	-0.024145000	-0.295622000
6	-0.131868000	-1.729834000	-1.833981000
1	0.755053000	-2.348915000	-1.752233000
1	-1.072629000	-2.262642000	-1.746218000
1	-2.635755000	1.577806000	-1.480819000
1	2.687503000	1.316681000	-1.397039000
6	-0.082514000	-0.538795000	2.586694000
1	0.840525000	0.030527000	2.659979000
1	-0.907471000	0.164586000	2.656904000
1	-0.135188000	-1.273657000	3.397824000
6	-0.080532000	-0.580230000	-2.640035000
1	0.842983000	-0.295653000	-3.129533000
1	-0.974891000	-0.214269000	-3.130376000
8	-0.079051000	1.602773000	0.857591000
6	0.587737000	2.723151000	0.654118000

6	0.372110000	3.743684000	1.755966000
1	-0.626800000	4.176354000	1.651512000
1	0.425553000	3.277245000	2.741144000
1	1.110199000	4.539184000	1.672994000
8	1.294470000	2.949726000	-0.316302000
1	0.052638000	1.249638000	-1.545337000

Transition State 2 (red)

77	0.086617000	0.116704000	-0.266745000
6	3.045586000	-0.113329000	-1.038575000
6	2.471319000	-0.651647000	1.166356000
6	4.373388000	-0.469004000	-0.823063000
6	3.781740000	-1.033076000	1.435233000
6	4.750277000	-0.932538000	0.434819000
1	5.086909000	-0.393049000	-1.635779000
1	4.037013000	-1.414099000	2.418501000
1	5.775598000	-1.227169000	0.633388000
6	-2.276421000	-0.300370000	1.328723000
6	-2.923483000	0.373825000	-0.812883000
6	-3.606443000	-0.457042000	1.703108000
6	-4.269984000	0.258401000	-0.488785000
6	-4.620062000	-0.167677000	0.789251000
1	-3.843219000	-0.808350000	2.701941000
1	-5.021458000	0.477460000	-1.238715000
1	-5.661546000	-0.287181000	1.069305000
7	0.070083000	-1.071996000	1.622450000
6	1.379152000	-0.714385000	2.228363000
1	1.669224000	-1.425448000	3.012923000
1	1.281694000	0.268846000	2.697364000
6	-1.138789000	-0.550427000	2.312694000
1	-0.873870000	0.392695000	2.799643000
1	-1.477839000	-1.237474000	3.098570000

7	-1.946951000	0.116923000	0.075197000
7	2.119063000	-0.182377000	-0.065048000
6	0.194330000	2.017313000	0.834117000
1	-0.681978000	2.150369000	1.470355000
1	1.126991000	2.089196000	1.397086000
1	2.686163000	0.225907000	-2.001930000
1	-2.593405000	0.659117000	-1.803426000
6	-0.038926000	-2.541650000	1.430358000
1	-0.962936000	-2.761950000	0.895356000
1	0.794872000	-2.888231000	0.820634000
1	-0.026384000	-3.045609000	2.405822000
6	0.169696000	2.781753000	-0.372299000
1	-0.762579000	2.905011000	-0.909688000
1	1.061735000	2.854388000	-0.982046000
8	0.221139000	-1.671059000	-1.377203000
6	-0.793421000	-2.432172000	-1.708645000
6	-0.442618000	-3.439024000	-2.796728000
1	0.513235000	-3.925005000	-2.583521000
1	-1.233649000	-4.184370000	-2.885320000
1	-0.333823000	-2.916737000	-3.753251000
8	-1.920605000	-2.382449000	-1.214908000
1	0.083251000	0.814734000	-1.691524000
7	0.240652000	4.807365000	0.039334000
1	-0.554755000	5.000854000	0.644776000
1	1.080558000	4.955874000	0.595350000
6	0.228424000	5.674357000	-1.153880000
1	1.090584000	5.433294000	-1.780055000
1	-0.680187000	5.479522000	-1.728326000
1	0.263534000	6.739972000	-0.903701000

Ground State B (red)

77	0.087058000	0.114226000	-0.292790000

6	3.040397000	-0.133731000	-1.063279000
6	2.491332000	-0.475060000	1.180330000
6	4.371523000	-0.452847000	-0.827797000
6	3.805406000	-0.813580000	1.471981000
6	4.764477000	-0.793788000	0.460646000
1	5.075777000	-0.445523000	-1.649760000
1	4.071533000	-1.102560000	2.481472000
1	5.792839000	-1.058129000	0.675437000
6	-2.257948000	-0.258581000	1.335522000
6	-2.930997000	0.182671000	-0.851248000
6	-3.575284000	-0.457998000	1.723256000
6	-4.267510000	0.016078000	-0.518394000
6	-4.598741000	-0.312727000	0.789592000
1	-3.794840000	-0.737121000	2.746625000
1	-5.024548000	0.116207000	-1.285299000
1	-5.630716000	-0.472013000	1.077889000
7	0.108654000	-0.921043000	1.684511000
6	1.403860000	-0.463391000	2.246784000
1	1.717901000	-1.076575000	3.099854000
1	1.274735000	0.559882000	2.605788000
6	-1.108877000	-0.368732000	2.329246000
1	-0.869216000	0.629049000	2.703198000
1	-1.421613000	-0.975034000	3.187250000
7	-1.943198000	0.062790000	0.051267000
7	2.120064000	-0.124895000	-0.083349000
6	0.136467000	2.087766000	0.514759000
1	-0.706189000	2.259647000	1.202625000
1	1.064691000	2.259865000	1.081857000
1	2.671196000	0.106681000	-2.050261000
1	-2.616885000	0.392864000	-1.863574000
6	0.047074000	-2.402980000	1.627567000

1	-0.861656000	-2.705880000	1.109903000
1	0.896301000	-2.777937000	1.059650000
1	0.065221000	-2.818760000	2.642780000
6	0.054691000	3.097906000	-0.601000000
1	-0.868649000	3.025550000	-1.175006000
1	0.900393000	3.050348000	-1.286191000
8	0.264344000	-1.776027000	-1.301377000
6	-0.694151000	-2.608828000	-1.577439000
6	-0.293956000	-3.691620000	-2.569898000
1	0.707347000	-4.068068000	-2.353056000
1	-1.018163000	-4.504978000	-2.553413000
1	-0.270163000	-3.261564000	-3.575681000
8	-1.831052000	-2.570507000	-1.103300000
1	0.068395000	0.782316000	-1.732405000
7	0.065511000	4.564300000	-0.060775000
1	-0.702923000	4.645211000	0.608735000
1	0.920678000	4.680708000	0.487124000
6	-0.035775000	5.639123000	-1.097753000
1	0.805522000	5.541894000	-1.781513000
1	-0.968764000	5.507626000	-1.642583000
1	-0.017123000	6.617023000	-0.618023000

Ground State C (red)

77	-0.015255000	0.024793000	-0.231580000
6	2.835085000	-0.925546000	-0.863031000
6	2.243177000	-0.741801000	1.388069000
6	4.097582000	-1.399982000	-0.535788000
6	3.486144000	-1.225770000	1.773116000
6	4.431056000	-1.556341000	0.804335000
1	4.799843000	-1.637521000	-1.324428000
1	3.713530000	-1.334316000	2.826655000
1	5.406511000	-1.927761000	1.093954000

6	-2.293781000	0.692671000	1.396857000
6	-2.919290000	0.824713000	-0.850023000
6	-3.584181000	1.013872000	1.795629000
6	-4.220384000	1.167632000	-0.508582000
6	-4.563341000	1.260160000	0.835288000
1	-3.816089000	1.078830000	2.851753000
1	-4.944794000	1.357183000	-1.290242000
1	-5.571694000	1.519454000	1.134326000
7	-0.171868000	-0.481987000	1.945491000
6	1.221033000	-0.278545000	2.419108000
1	1.401698000	-0.786797000	3.373083000
1	1.371083000	0.789765000	2.583949000
6	-1.168000000	0.517488000	2.408549000
1	-0.656516000	1.476406000	2.513379000
1	-1.586277000	0.253768000	3.387134000
7	-1.970935000	0.585818000	0.075319000
7	1.919325000	-0.603574000	0.070389000
6	0.585328000	1.997662000	0.093304000
1	-0.280701000	2.579296000	0.439649000
1	1.333560000	2.041429000	0.894848000
1	2.523652000	-0.784100000	-1.888508000
1	-2.599551000	0.726658000	-1.877332000
6	-0.631247000	-1.859310000	2.234485000
1	-1.616463000	-2.015671000	1.796558000
1	0.055813000	-2.575949000	1.787608000
1	-0.686239000	-2.029445000	3.316843000
6	1.193459000	2.712176000	-1.114659000
1	0.450941000	2.777477000	-1.928240000
1	2.031778000	2.129498000	-1.511389000
8	-0.515648000	-2.243222000	-0.776007000
6	-1.121017000	-2.744835000	-1.702966000

6	-1.009576000	-4.199231000	-2.074152000
1	-0.335183000	-4.704542000	-1.387229000
1	-1.991354000	-4.680196000	-2.038383000
1	-0.624201000	-4.298060000	-3.093565000
8	-1.937090000	-1.982382000	-2.448312000
1	0.073414000	0.359236000	-1.773932000
7	1.720076000	4.022105000	-0.728139000
1	0.973231000	4.586327000	-0.334590000
6	2.353782000	4.746961000	-1.827147000
1	3.248983000	4.207969000	-2.150919000
1	1.704297000	4.879410000	-2.708817000
1	2.669782000	5.733434000	-1.481597000
1	-2.343658000	-2.494365000	-3.160099000

Ground State D (red)

77	-0.120885000	-0.021061000	-0.597631000
6	2.851377000	-0.410694000	-1.273608000
6	2.037497000	-1.484406000	0.637886000
6	4.111236000	-0.964449000	-1.096791000
6	3.274924000	-2.072336000	0.856903000
6	4.330214000	-1.808580000	-0.014532000
1	4.899006000	-0.732872000	-1.801880000
1	3.411267000	-2.730143000	1.706603000
1	5.301351000	-2.259493000	0.149320000
6	-2.624843000	-0.501893000	0.740086000
6	-3.028249000	0.797362000	-1.163607000
6	-3.982438000	-0.546859000	1.021197000
6	-4.395214000	0.795009000	-0.922548000
6	-4.883112000	0.111423000	0.184844000
1	-4.331284000	-1.089552000	1.891305000
1	-5.056639000	1.321526000	-1.598296000
1	-5.945093000	0.086294000	0.396725000

7	-0.428373000	-1.645409000	0.892134000
6	0.875197000	-1.690552000	1.603965000
1	1.007978000	-2.631675000	2.149206000
1	0.888417000	-0.883075000	2.338913000
6	-1.591252000	-1.135802000	1.664204000
1	-1.226024000	-0.367694000	2.350212000
1	-2.061439000	-1.922811000	2.265146000
7	-2.154359000	0.162213000	-0.357430000
7	1.828863000	-0.658599000	-0.429968000
6	0.211902000	1.558672000	0.722824000
1	-0.775217000	1.948724000	0.994292000
1	0.678435000	1.157903000	1.629902000
1	2.625272000	0.249128000	-2.099664000
1	-2.593947000	1.309696000	-2.010796000
6	-0.735191000	-2.949170000	0.255283000
1	-1.638285000	-2.861671000	-0.349453000
1	0.090125000	-3.245475000	-0.392987000
1	-0.889009000	-3.727647000	1.011932000
6	1.092405000	2.689570000	0.196779000
1	0.621717000	3.164748000	-0.678041000
1	2.052247000	2.289440000	-0.143317000
1	0.074360000	1.060487000	-1.734584000
7	1.374463000	3.628105000	1.282324000
1	0.513250000	4.072576000	1.584197000
6	2.358488000	4.653684000	0.934296000
1	3.330093000	4.182648000	0.760902000
1	2.098016000	5.234614000	0.034910000
1	2.471715000	5.345983000	1.770532000

Transition State 3 (red)

77	-0.124821000	0.142958000	-0.443685000
6	2.847129000	0.015791000	-1.251622000

6	2.130510000	-1.371900000	0.482393000
6	4.131526000	-0.513793000	-1.194624000
6	3.389457000	-1.949606000	0.578307000
6	4.413586000	-1.511554000	-0.264487000
1	4.888903000	-0.149137000	-1.879419000
1	3.565563000	-2.734029000	1.306907000
1	5.404144000	-1.949223000	-0.200552000
6	-2.600888000	-0.754552000	0.700471000
6	-3.080178000	0.850673000	-0.926779000
6	-3.953705000	-0.976119000	0.919387000
6	-4.447965000	0.684399000	-0.739966000
6	-4.898171000	-0.242730000	0.197037000
1	-4.264171000	-1.714739000	1.651104000
1	-5.141209000	1.270458000	-1.332862000
1	-5.959062000	-0.401312000	0.358559000
7	-0.309455000	-1.672454000	0.622250000
6	0.978169000	-1.750975000	1.388323000
1	1.123745000	-2.747754000	1.822430000
1	0.918278000	-1.020211000	2.200830000
6	-1.515634000	-1.461620000	1.487442000
1	-1.211353000	-0.825561000	2.324834000
1	-1.880130000	-2.411488000	1.897278000
7	-2.160563000	0.155779000	-0.220925000
7	1.857585000	-0.387743000	-0.425710000
6	0.048305000	2.346450000	-0.834889000
1	0.160251000	2.835659000	-1.813918000
1	-0.932945000	2.662674000	-0.469819000
1	2.579488000	0.778534000	-1.972262000
1	-2.687723000	1.544595000	-1.659849000
6	-0.487990000	-2.872234000	-0.243418000
1	-1.394006000	-2.756561000	-0.838114000

1	0.361968000	-2.961568000	-0.919608000
1	-0.564446000	-3.774692000	0.377039000
6	1.173932000	2.881517000	0.055084000
1	1.178683000	3.984360000	-0.060868000
1	2.146762000	2.541506000	-0.319260000
1	0.024373000	1.180277000	-1.665964000
7	1.058737000	2.475947000	1.453189000
1	0.126356000	2.716319000	1.782635000
6	2.050035000	3.133288000	2.306389000
1	3.052963000	2.782818000	2.039066000
1	2.050784000	4.234169000	2.228765000
1	1.871122000	2.864209000	3.350909000

Ground State E (red)

77	0.000000000	-0.647796000	-0.061678000
6	2.986947000	-1.344921000	0.131497000
6	2.395433000	0.880440000	-0.233315000
6	4.334414000	-1.015636000	0.171082000
6	3.721249000	1.274943000	-0.181317000
6	4.712878000	0.313370000	0.016849000
1	5.067777000	-1.795908000	0.328381000
1	3.978657000	2.319976000	-0.303842000
1	5.756300000	0.600814000	0.052765000
6	-2.395433000	0.880440000	-0.233316000
6	-2.986947000	-1.344922000	0.131496000
6	-3.721249000	1.274943000	-0.181317000
6	-4.334413000	-1.015636000	0.171082000
6	-4.712878000	0.313371000	0.016849000
1	-3.978656000	2.319976000	-0.303841000
1	-5.067777000	-1.795908000	0.328381000
1	-5.756300000	0.600815000	0.052766000
7	0.000000000	1.350636000	0.146290000

6	1.257597000	1.827390000	-0.537828000
1	1.490222000	2.852636000	-0.236487000
1	1.064743000	1.811506000	-1.612036000
6	-1.257596000	1.827389000	-0.537829000
1	-1.064742000	1.811502000	-1.612038000
1	-1.490221000	2.852636000	-0.236491000
7	-2.023874000	-0.421694000	-0.069396000
7	2.023874000	-0.421693000	-0.069395000
1	2.648003000	-2.364234000	0.264913000
1	-2.648004000	-2.364234000	0.264912000
6	-0.000001000	1.772877000	1.585495000
1	-0.884906000	1.374576000	2.076068000
1	0.884905000	1.374578000	2.076069000
1	-0.000002000	2.866553000	1.640647000

Notes to Chapter 4

(1) (a) Hartwig, J. F. *Acc. Chem. Res.* **1998**, *31*, 852. (b) Wolfe, J. P.; Wagaw, S.; Marcoux, J.-F.; Buchwald, S. L. *Acc. Chem. Res.* **1998**, *31*, 805.

(2) (a) Lin, B. L.; Clough, C. R.; Hillhouse, G. L. *J. Am. Chem. Soc.* **2002**, *124*, 2890. (b) Pawlikowski, A. V.; Getty, A. D.; Goldberg, K. I. *J. Am. Chem. Soc.* **2007**, *129*, 10382. (c) Marquard, S. L.; Rosenfeld, D. C.; Hartwig, J. F. *Angew. Chem.* **2010**, *122*, 805. (d) Hanley, P. S.; Marquard, S. L.; Cundari, T. R. Hartwig, J. F. *J. Am. Chem. Soc.* **2012**, *134*, 15281. (e) Pérez-Temprano, M. H.; Racowski, J. M.; Kampf, J. W.; Sanford, M. S. *J. Am. Chem. Soc.* **2014**, *136*, 4097. (f) Camasso, N. M.; Sanford, M. S. *Science* **2015**, *347*, 6227.

(3) St. John, Anthony. PhD. Dissertation, University of Washington, **2011**.

(4) (a) Goldberg, K. I.; Yan, J.; Winter, E. L. *J. Am. Chem. Soc.* **1994**, *116*, 1573. (b) Goldberg, K. I.; Yan, J.; Breitung, E. M. *J. Am. Chem. Soc.* **1995**, *117*, 6889. (c) Williams, B. S.; Holland, A. W.; Goldberg, K. I. *J. Am. Chem. Soc.* **1999**, *121*, 252. (d) Frech, C. M.; Milstein, D. *J. Am. Chem. Soc.* **2006**, *128*, 12434. (e) Khusnutdinova, J. R.; Newman, L. L.; Zavalij, P. Y.; Lam, Y.-F.; Vedernikov, A. N. *J. Am. Chem. Soc.* **2008**, *130*, 2174. (f) Scott, V. J.; Labinger, J. A. Bercaw, J. E. *Organometallics* **2010**, *29*, 4090. (g) Crosby, S. H.; Thomas, H. R.; Clarkson, G. J.; Rourke, J. P. *Chem. Commun.* **2012**, *48*, 5775. (h) Crosby, S. H.; Clarkson, G. J.; Rourke, J. P. *Organometallics*, **2012**, *31*, 7256. (i) Feller, M.; Diskin-Posner, Y.; Leitus, G.; Shimon, L. J. W.; Milstein D. *J. Am. Chem. Soc.* **2013**, *155*, 11040. (j) O'Reilly, M. E.; Pahls, D. R.; Webb, J. R.; Boza, N. C.; Majumdar, S.; Hoff, C. D.; Groves, J. T.; Cundari, T. R. Gunnoe, T. B. *Dalton Trans.* **2014**, *43*, 8273. (k) O'Reilly, M. E.; Pahls, D. R.; Cundari, T. R.; Gunnoe, T. B. *Organometallics* **2014**, *33*, 6504.

(5) Thewissen, S.; Reijnders, M. D. M.; Smits, J. M. M.; de Bruin, B. *Organometallics* **2005**, *24*, 5964.

(6) de Bruin, B.; Peters, T. P. J.; Wilting, J. B. M.; Thewissen, S.; Smits, J. M. M.; Gal, A. W. *Eur. J. Inorg. Chem.* **2002**, 2671.

(7) Cambridge Structural Database, 9-5-2014.

(8) Mills, J. E.; Maryanoff, C. A.; McComsey, D. F.; Stanzione, R. C.; Scott, L. *J. Org. Chem.* **1987**, *52*, 1857.

(9) Kanzian, T.; Nigst, T. A.; Maier, A.; Pichl, S.; Mayr, H. *Eur. J. Org. Chem.* **2009**, 6379.

(10) Merola, J. S.; Husebo, T. L.; Matthews, K. E. *Organometallics* **2012**, *31*, 3920.

(11) Ortmann, D. A.; Gevert, O.; Laubender, M.; Werner, H. *Organometallics* **2001**, *20*, 1776.

(12) (a) Frech, C. M.; Milstein, D. *J. Am. Chem. Soc.* **2006**, *128*, 12434. (b) Feller, M.; Diskin-Posner, Y.; Leitus, G.; Shimon, L. J. W.; Milstein D. *J. Am. Chem. Soc.* **2013**, *155*, 11040.

(13) Lanci, M. P.; Remy, M. S.; Lao, D. B.; Sanford, M. S.; Mayer, J. M. *Organometallics* **2011**, *30*, 3704.

(14) van der Ent, A.; Onderdelinden, A. L.; Schunn, R. A.; *Inorg. Synth,* **1990**, *28*, 90.

(15) Onderdelinden, A. L.; van der Ent, A. *Inorg. Chim. Acta.* **1972**, *6*, 420.

(16) Bruker (**2007**) APEX2 (Version 2.1-4), SAINT (version 7.34A), SADABS (version 2007/4), BrukerAXS Inc, Madison, Wisconsin, USA.

(17) (a) Altomare A, Burla C, Camalli M, Cascarano G L, Giacovazzo C, Guagliardi A, Moliterni AGG, Polidori G, Spagna R. *Journal of Applied Crystallography* **1999**, *32*, 115-119. (b) Altomare A, Cascarano G L, Giacovazzo C, Guagliardi A. *Journal of Applied Crystallography*, **1993**, *26*, 343-350.

(18) Sheldrick, G.M. **(1997)** SHELXL-97, Program for the Refinement of Crystal Structures. University of Göttingen, Germany.

(19) Mackay, S.; Edwards, C.; Henderson, A.; Gilmore, C.; Stewart, N.; Shankland, K.; Donald, A. **(1997)** *MaXus: a computer program for the solution and refinement of crystal structures from diffraction data*. University of Glasgow, Scotland.

(20) Waasmaier, D.; Kirfel, A. *Acta Crystallographica A*. **1995**, *51*, 416-430.

(21) Gaussian 09, Revision D.01, M. J. Frisch, G. W. Trucks, H. B. Schlegel, G. E. Scuseria, M. A. Robb, J. R. Cheeseman, G. Scalmani, V. Barone, B. Mennucci, G. A. Petersson, H. Nakatsuji, M. Caricato, X. Li, H. P. Hratchian, A. F. Izmaylov, J. Bloino, G. Zheng, J. L.

Sonnenberg, M. Hada, M. Ehara, K. Toyota, R. Fukuda, J. Hasegawa, M. Ishida, T. Nakajima, Y. Honda, O. Kitao, H. Nakai, T. Vreven, J. A. Montgomery, Jr., J. E. Peralta, F. Ogliaro, M. Bearpark, J. J. Heyd, E. Brothers, K. N. Kudin, V. N. Staroverov, T. Keith, R. Kobayashi, J. Normand, K. Raghavachari, A. Rendell, J. C. Burant, S. S. Iyengar, J. Tomasi, M. Cossi, N. Rega, J. M. Millam, M. Klene, J. E. Knox, J. B. Cross, V. Bakken, C. Adamo, J. Jaramillo, R. Gomperts, R. E. Stratmann, O. Yazyev, A. J. Austin, R. Cammi, C. Pomelli, J. W. Ochterski, R. L. Martin, K. Morokuma, V. G. Zakrzewski, G. A. Voth, P. Salvador, J. J. Dannenberg, S. Dapprich, A. D. Daniels, O. Farkas, J. B. Foresman, J. V. Ortiz, J. Cioslowski, and D. J. Fox, Gaussian, Inc., Wallingford CT, 2013.

Chapter 5

Direct Formation of Carbon(sp^3)-heteroatom Bonds from Rh^{III} to Produce Methyl Iodide, Thioethers and Alkyl amines

5.1 Introduction

Reductive elimination, a fundamental organometallic reaction, is the product release step in numerous catalytic processes.[1] Reductive elimination reactions that form carbon-heteroatom (C-X) bonds are particularly valuable as new functionality is introduced into the product. For example, aryl amines are formed by C(sp^2)-N reductive elimination reactions from Pd^{II} in the product release step in Buchwald-Hartwig cross-coupling reactions.[2] Strikingly less prevalent in both catalytic and stoichiometric reactions are reductive eliminations involving alkyl groups to form C(sp^3)-X bonds,[3] and in particular C(sp^3)-N bonds.[4] Access to such couplings to form C(sp^3)-N bonds would be a tremendous asset in rational design efforts for catalytic systems. For example, a C(sp^3)-N bond forming reaction could be used to produce alkyl amines via olefin hydroamination or direct alkane oxidation.

In the few reported examples of C(sp^3)-X coupling reactions (X = N, O, S, halide), high valent metal centers such as Rh^{III} [3d,i-k] and Pt^{IV} [3a-c,e,g,h,4d] are primarily employed.

Recently, examples of C(sp^3)-N reductive elimination have also been observed from Pd^{IV} and Ni^{IV}. [4e,f] Sulfonamides have been employed for these reactions and C(sp^3)-N reductive elimination to produce alkyl amines has rarely been documented.[4d] Both concerted reductive elimination[4d] and S_N2 type mechanisms[4a-c] have been proposed for C(sp^3)-N coupling reactions with both pathways occurring through a coordinately unsaturated metal center.

Based on this knowledge, we sought to design a new system in which facile dissociation of one of the ligand moieties would allow for the formation of an unsaturated species. DPEphos was an ideal candidate as its flexible nature has allowed for both bidentate and tridentate coordination to Rh[5] as shown in Figure 5.1. We hypothesized this flexible binding may allow for the formation of a five-coordinate Rh^{III} species from which reductive elimination, to form Rh^{I}, would be facilitated.

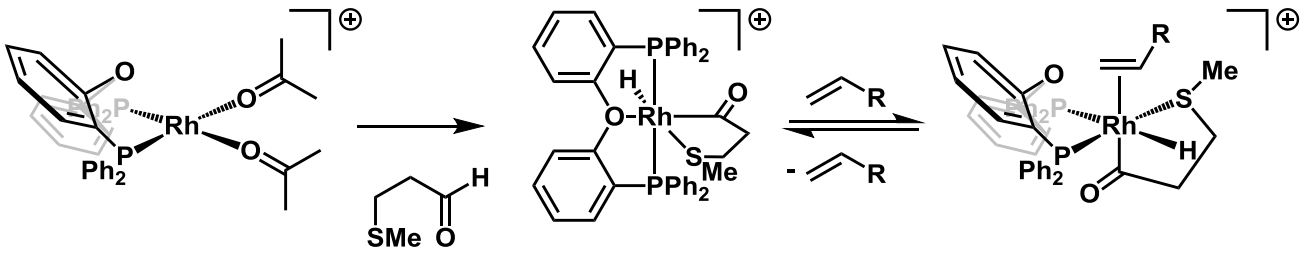

Figure 5.1. Binding modes of the DPEphos ligand.

Reported in this chapter is a well characterized example of C(sp^3)-I reductive elimination from Rh^{III} along with mechanistic studies that indicate the involvement of two competing pathways of S_N2 attack in the presence of excess iodide. Similar competitive behavior has not previously been observed in reductive elimination reactions and the presence of the second pathway provided access to incorporation of external nucleophiles. In this way, the formation of C(sp^3)-S and C(sp^3)-N bonds could be promoted in high yield.

Furthermore, mechanistic studies of the C(sp^3)-N coupling point to a path involving coordination of the amine to the metal center with C-N bond formation via external attack on the Rh^{III}-Me moiety by a second amine.

5.2 Synthesis of (DPEphos)RhMe(I)$_2$ (25)

The Rh^{III}-Me complex, (DPEphos)RhMe(I)$_2$ (**25**) was prepared in quantitative yield by addition of an excess of MeI to (DPEphos)$_2$Rh$_2$Cl$_2$[6] (Figure 5.2). Complex **25** (in THF-d_8) exhibits a doublet at 13.2 ppm (J_{Rh-P} = 103.8 Hz) in the ^{31}P NMR spectrum. The methyl group bound to Rh gives rise to a doublet of triplets in ^{1}H NMR spectrum at 2.22 ppm (J_{Rh-H} = 4.9 Hz, J_{P-H} = 2.6 Hz). The solid state structure of **25** (Figure 5.1) shows octahedral geometry about the Rh center with a meridional DPEphos ligand and trans iodide ligands. The Rh-Me (2.0769(19) Å) and Rh-I (2.6633(4) Å and 2.6379(4) Å) bond distances are similar in length to Rh-Me and Rh-I bonds, respectively, found in other Rh^{III} octahedral bisphosphine complexes.[3i,7]

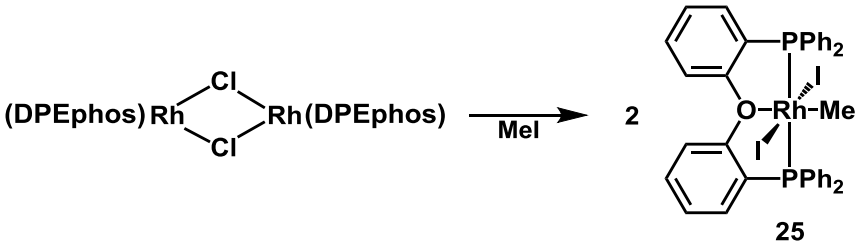

Figure 5.2 Synthesis of complex **25** by oxidative addition of MeI to (DPEphos)$_2$Rh$_2$Cl$_2$.

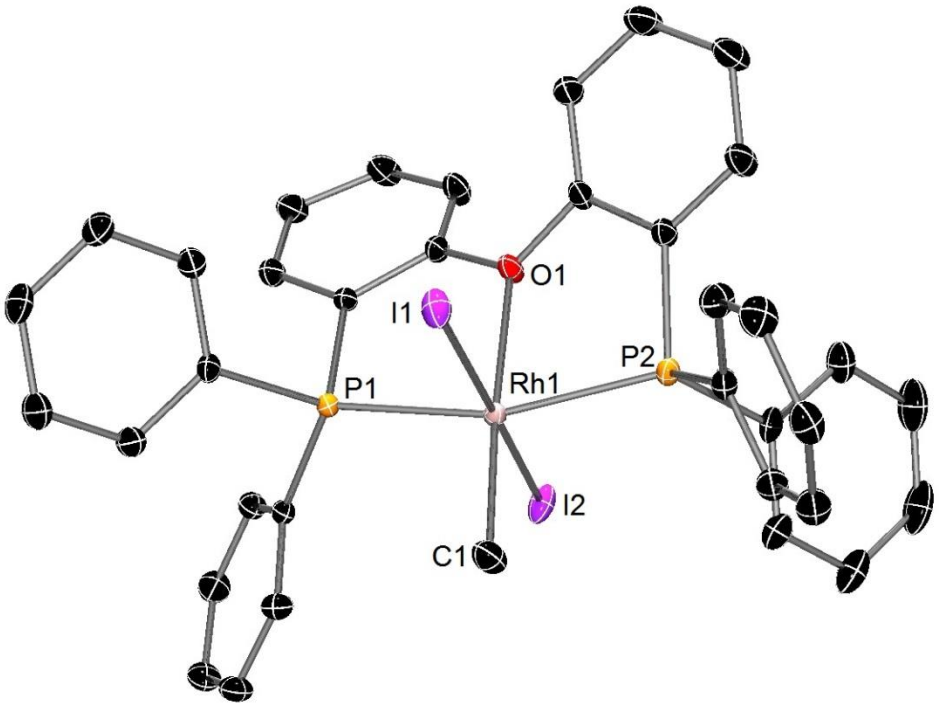

Figure 5.3 ORTEP of **25** shown with thermal ellipsoids at 50% probability level. The hydrogen atoms have been omitted for clarity. Selected bond lengths (Å): Rh(1)-C(1) = 2.0769(19), Rh(1)-I(1) = 2.6379(4), Rh(1)-I(2) = 2.6633(4), Rh(1)-O(1) = 2.2323(13), Rh(1)-P(1) = 2.3148(6), Rh(1)-P(2) = 2.3318(6).

5.3 Synthesis of a Rh methyl amido

We initially set out to synthesize a Rh methyl amido with the goal of promoting C(sp^3)-N reductive elimination. (DPEphos)RhMe$(OTf)_2$ (**26**) was prepared by chloride abstraction from **25** with AgOTf. The ^{31}P NMR spectrum for complex **26** exhibited a broad

peak around 34 ppm. This complex was not indefinitely stable in solution, so was generated *in situ* and then used immediately in subsequent reactions.

Addition of benzophenone hydrazone (5 equiv.) to a CD_2Cl_2 solution of **26** resulted in the immediate formation of a new species. This new species was fluxional on the NMR time scale at room temperature (broad peak at 33 ppm in the ^{31}P NMR spectrum). Upon cooling to 268 K, an ABX spin system was observed in the ^{31}P NMR spectrum (δ 35.1 (dd, $J_{Rh\text{-}P}$ = 157.9 Hz, $J_{P\text{-}P}$ = 43.6 Hz), 32.7 (dd, $J_{Rh\text{-}P}$ = 151.2 Hz, $J_{P\text{-}P}$ = 43.6 Hz)). The small P-P coupling constant of 43.6 Hz was consistent with *cis*-phosphines.[8] Thus we proposed the DPEphos ligand was now binding the Rh in κ^2 fashion and the product was (DPEphos)RhMe$(NR_2)_2$ (**27**) as shown in Figure 5.4.

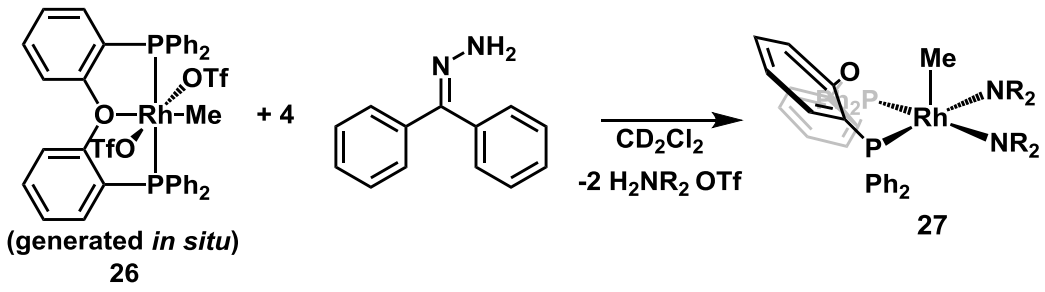

Figure 5.4. Synthesis of complex **27**.

Interestingly, the fluxionality observed in CD_2Cl_2 was not observed in C_6D_6. The ^{31}P NMR spectrum for complex **27** exhibited an ABX spin system (δ 35.0 (dd, $J_{Rh\text{-}P}$ = 158.9 Hz, $J_{P\text{-}P}$ = 43.6 Hz), 32.6 (dd, $J_{Rh\text{-}P}$ = 151.5 Hz, $J_{P\text{-}P}$ = 43.6 Hz) at room temperature in C_6D_6. Thermolysis of **27** in C_6D_6 at 80 ˚C resulted in the formation of a multitude of products as determined by ^{31}P NMR spectroscopy. The ^1H NMR spectrum had a peak at 3.12 ppm, consistent with the formation of *N*-methylbenzophenone hydrazone, albeit in low yield

(approximately 26 %). C-N coupling in quantitative yield was achieved by an alternative strategy (*vide infra*).

5.4 Reductive elimination of methyl iodide from 25

Thermolysis of **25** in iodobenzene at 80 ˚C resulted in quantitative formation of methyl iodide and a new Rh species. The ^{31}P NMR resonance of the new Rh product appeared only slightly downfield at 15.4 ppm with a similar coupling constant of J_{Rh-P} = 106.4 Hz. On this basis we speculated that it was also a Rh^{III} complex and considering the composition of the reaction mixture, we proposed that the product was (DPEphos)RhPh$(I)_2$ (**28**). Overlap of ^{1}H NMR resonances made characterization of the product challenging and attempts to obtain crystals were unsuccessful. To establish the identity of the Rh product, **25** was thermolyzed in *p*-bromotoluene (Figure 5.5). The ^{31}P NMR chemical shift and J_{Rh-P} coupling constant of the corresponding product (18.6 ppm, J_{Rh-P} = 105.5 Hz) were similar to that of the product from thermolysis in iodobenzene. Now, however, the ^{1}H NMR spectrum contained an upfield singlet (2.25 ppm, 3H), consistent with a bound *p*-tolyl moiety. Furthermore, a crystal suitable for x-ray diffraction was grown and the solid state structure (Figure 5.6) confirmed that the solvent had added to rhodium yielding (DPEphos)Rh(tolyl)IBr (**29**). The production of the tolyl complex **29** from the thermolysis of **25** in *p*-bromotoluene substantiates the proposal of the formation of the phenyl complex **28** from the thermolysis of **25** in iodobenzene. Thus, the overall thermolysis reaction involves the formation of a C(sp^3)-I bond with the reductive elimination of methyl iodide and the cleavage of a C(sp^2)-X bond with the oxidative addition of aryl halide.

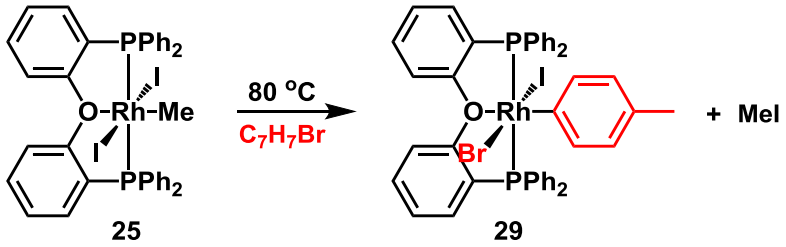

Figure 5.5 Thermolysis of **25** in *p*-bromotoluene to form **29** and MeI.

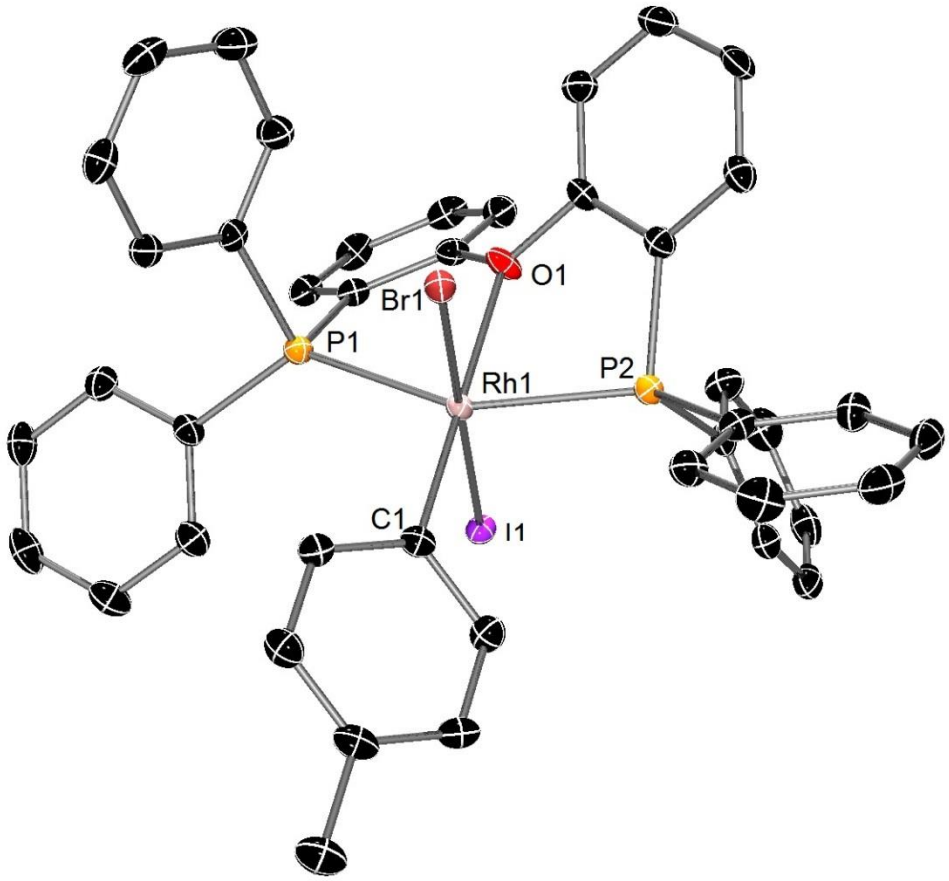

Figure 5.6. ORTEP of **29** shown with thermal ellipsoids at 50% probability level. The hydrogen atoms have been omitted for clarity. Selected bond lengths (Å): Rh(1)-C(1) = 2.014(4), Rh(1)-I(1) = 2.660(5), Rh(1)-Br(1) = 2.508(9), Rh(1)-O(1) = 2.250(2), Rh(1)-P(1) = 2.3513(7), Rh(1)-P(2) = 2.3513(7).

Considering literature precedent for mechanisms of reductive elimination, six potential pathways for MeI elimination from **25** are proposed in Figure 5.7. Routes (C_1 - C_3) involve concerted formation of the C(sp^3)-I bond. In path C_1, MeI eliminates directly from the six-coordinate complex **25**. In Path C_2, the formation of a five-coordinate species prior to concerted C-I coupling is proposed with the DPEphos ligand changing from κ^3 to κ^2 coordination. Dissociation of the oxygen group is pictured, however dissociation of a phosphine arm to generate a five-coordinate intermediate is also possible. In Path C_3 a cationic five-coordinate species is formed by iodide dissociation prior to concerted C-I reductive elimination involving the remaining Rh bound iodide. There is precedent for concerted C(sp^3)-I coupling from Rh^{III} upon thermolysis of the five-coordinate naphthyl-based (PCP)$Rh^{III}(CH_3)$I complex.[3d]

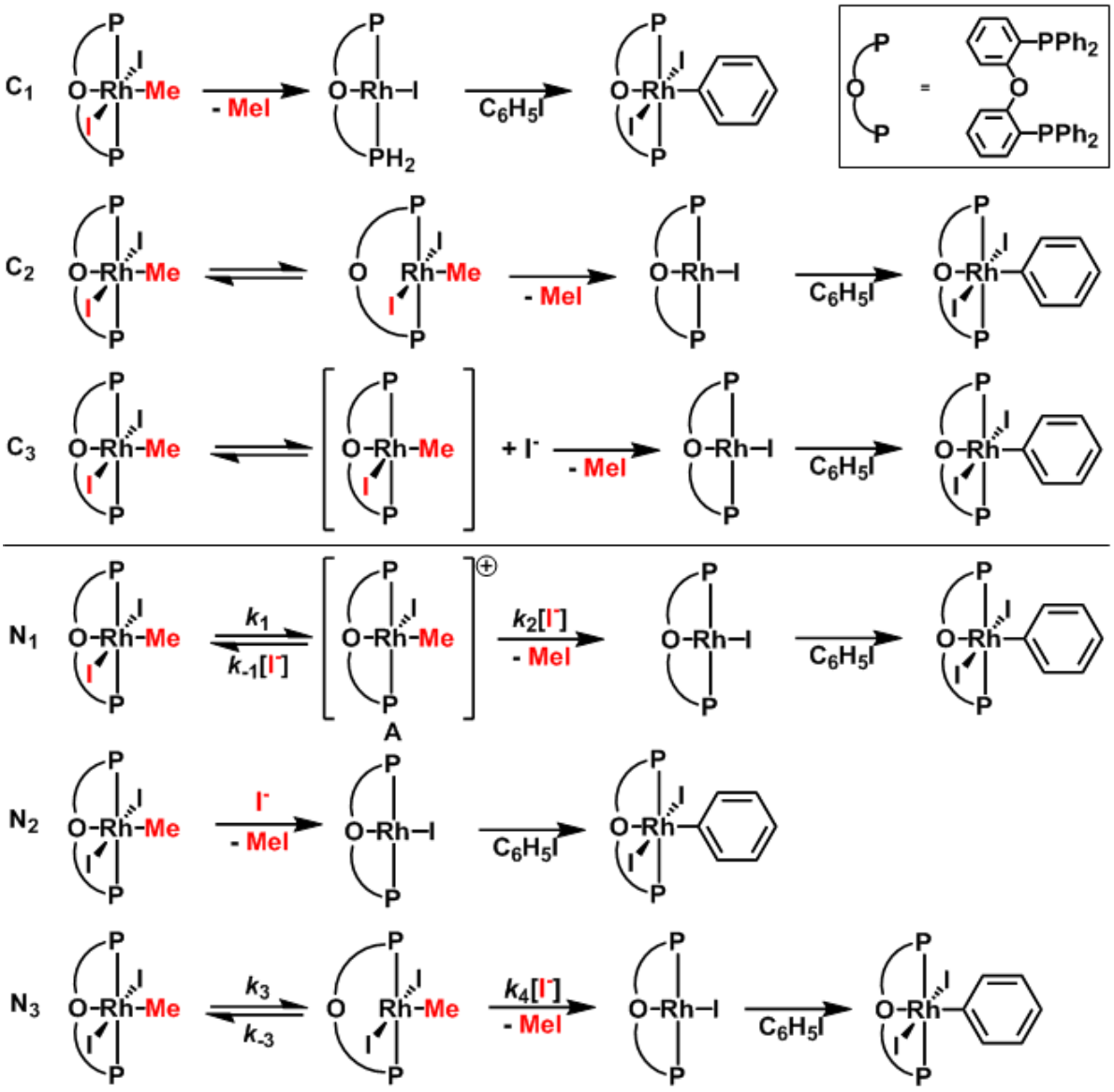

Figure 5.7. Possible mechanisms for the reductive elimination of MeI from **25**.

Three possible nucleophilic substitution paths for C(sp^3)-I bond formation are also shown in Figure 5.7 (N_1- N_3). In these reactions, C-I bond formation occurs via nucleophilic attack of iodide at a Rh^{III}–Me group. In path N_1, initial iodide dissociation generates a cationic five-coordinate species prior to S_N2 nucleophilic attack by iodide at the Rh^{III}-Me. Isomerization of the five-coordinate intermediate to place the Me group trans to the open site

prior to attack may also be necessary.[9] In path N_2, iodide attack occurs directly at the six-coordinate complex **25** and in path N_3, dissociation of the oxygen (κ^3 to κ^2 coordination of the DPEphos ligand) precedes nucleophilic attack by iodide. Ligand dissociation to generate a five-coordinate intermediate prior to nucleophilic attack (paths N_1 and N_3) should increase the electrophilicity of the methyl group. Furthermore, attack at the axial position of a square pyramidal metal center would be analogous to the well-established C(sp^3)-X bond formation step reported in reductive elimination reactions of Pt^{IV} complexes.[3a-c, 4b]

The thermolysis of **25** in iodobenzene at 80 °C was monitored by ^{1}H NMR spectroscopy. A first-order dependence on **25** was observed for this reaction (Figure 5.8) with a k_{obs} = 4.0 ± 0.1 x 10^{-4} s^{-1}). A first-order reaction was also observed when the reaction was carried out in the more polar bromobenzene solvent where the reaction was found to proceed approximately 1.7 times faster (k_{obs} = 6.6 ± 0.1 x 10^{-4} s^{-1}). The dielectric constants for bromobenzene and iodobenzene are ε = 5.45 and 4.59, respectively.[10] Only paths C_3 and N_1, where ionic intermediates are generated, are expected to be significantly affected by solvent polarity. Notably, similar solvent effects have been documented in other C-X couplings wherein initial X^- dissociation has been proposed.[3,4]

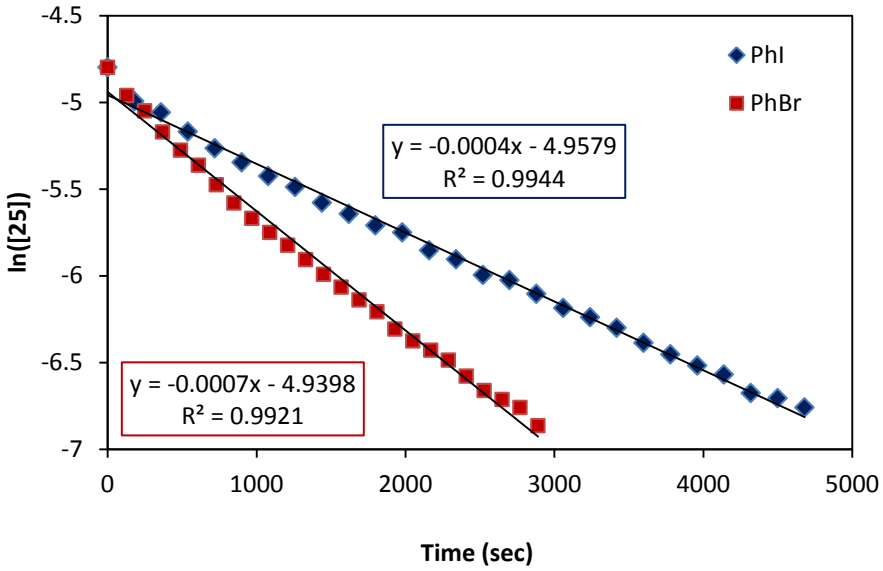

Figure 5.8. First order kinetic plot for the decomposition of **25**, 80 °C, C_6H_5I (blue diamonds), C_6D_5Br (red squares).

The dependence of the rate of the reaction on iodide concentration was also investigated. Complex **25** was thermolyzed in iodobenzene under pseudo-first order conditions in the presence of excess iodide added as [N(*n*-Bu)$_4$][I] (at constant ionic strength with added [N(*n*-Bu)$_4$][BF_4]). A plot of k_{obs} versus [I^-] shows a linear dependence of k_{obs} on [I^-] (Figure 5.9) The first order plots are shown in figure 5.10.

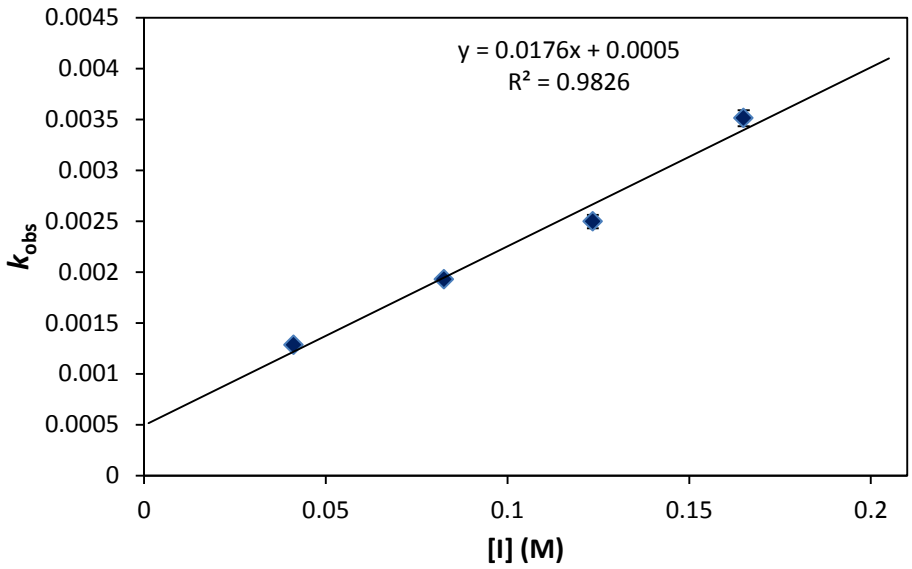

Figure 5.9. Plot of k_{obs} vs [iodide] for thermolysis of **25**, 80 °C, C_6H_5I. [29] = 0.00824 M, constant ionic strength.

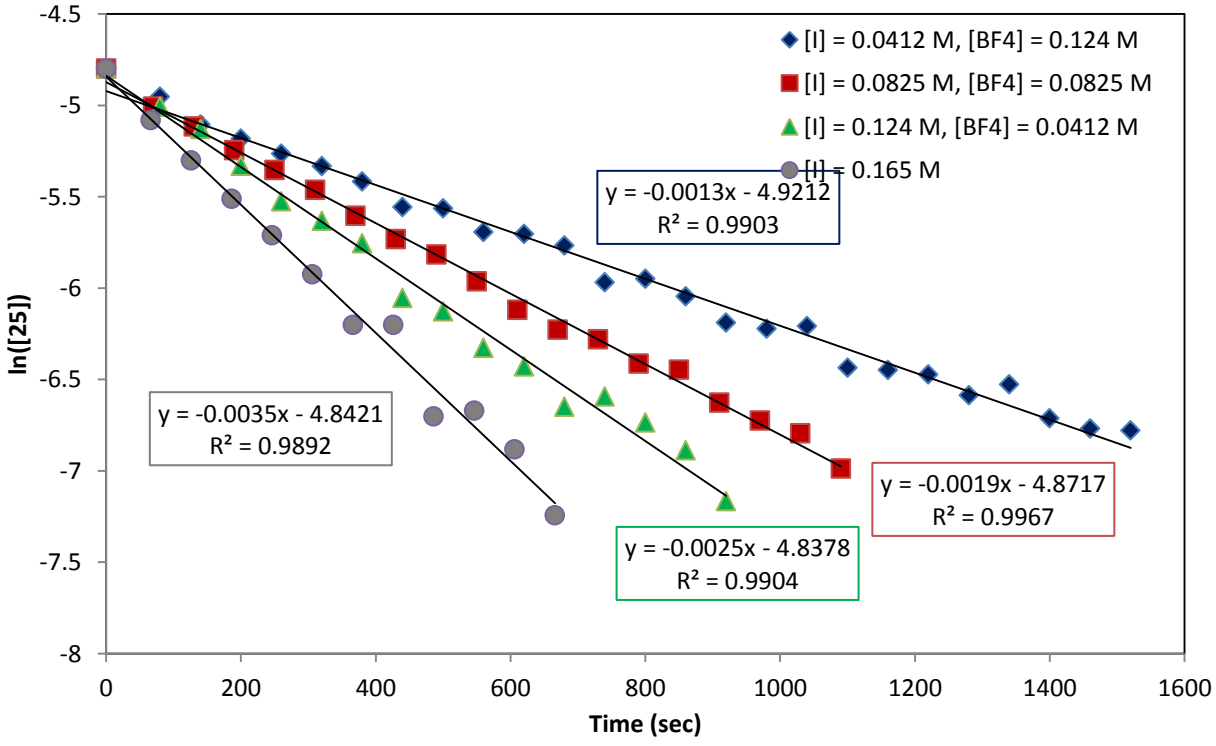

Figure 5.10. First order kinetic plot for the decomposition of **25** with added iodide (at constant ionic strength), 80 °C, C_6H_5I.

Notably the linear fit of k_{obs} versus iodide concentration exhibits a significant y intercept. This result implies that there are two distinct mechanistic paths to product ($k_{obs} = k_A + k_B[I^-]$). One of these paths shows a direct dependence on the iodide concentration ($k_B = 1.8 \pm 0.2 \times 10^{-2}$ M^{-1} s^{-1}) and the other is independent of iodide concentration ($k_A = 5 \pm 2 \times 10^{-4}$ s^{-1}). These data can be compared with the expected behavior of the paths shown in Figure 5.7. Path C_3 should be inhibited by iodide which is not consistent with either of the observed iodide dependences. In contrast, the rate of methyl iodide reductive elimination in the other path involving iodide dissociation, N_1, should be independent of iodide concentration. Application of the steady state approximation to intermediate A in path N_1 (Figure 5.7) results in rate equation (1).

Steady state approximation (SSA) on [A]: $k_1[25] - k_{-1}[A][I] + k_2[A][I] = 0$

$$[A] = \frac{k_1[25]}{k_{-1}[I] + k_2[I]}$$

$$\frac{-d[25]}{dt} = \frac{d[C]}{dt} = k_2[A][I]$$

Substituting [A]:

$$\frac{-d[25]}{dt} = k_{obs}[25] \quad \text{where } k_{obs} = \frac{k_1 k_2}{k_{-1} + k_2} \qquad (1)$$

Given that k_{-1} is simply ligand reassociation and k_2 is nucleophilic attack, it is likely that $k_{-1} >> k_2$ and in this case, $k_{obs} = K_1 k_2$. Paths N_2 or N_3 involve nucleophilic attack of iodide at either a six or five-coordinate intermediate, respectively. Either of these mechanisms (and none of the others) would be expected to result in a direct dependence of the rate on the iodide concentration. For example, the N_3 path would give rise to the rate expression shown as equation (2).

$$\frac{-d[28]}{dt} = k_{\text{obs}}[25][\text{I}] \quad \text{where } k_{\text{obs}} = K_3 k_4 \qquad (2)$$

Thus, the data in Figure 5.9 can be explained by a two path reaction consisting of N_1 and N_3 (or N_2). For the observed rate constant expression, $k_{obs} = k_A + k_B[I^-]$ implicated by the plot shown in Figure 5.9, $k_A = K_1k_2$ and $k_B = K_3k_4[I^-]$. Significantly, the k_A value determined in Figure 5.9 approximately matches the k_{obs} found in the absence of added $[I^-]$. Attempts to measure the dependence of k_{obs} versus $[I^-]$ in bromobenzene (and allow comparison of a solvent effect on k_A and k_B) were unsuccessful due to low solubility of both $[N(n\text{-Bu})_4]I$ and [(18-crown-6)K]I in bromobenzene.

It should be noted that if the iodide concentration is varied without maintaining constant ionic strength, a linear dependence is also observed but the intercept (k_A value) is approximately 4 times larger (Figure 5.11) (First order plots are shown in Figure 5.12). This suggests that added $[N(n\text{-Bu})_4]I$ also affects the reaction rate through increasing the ionic strength of the reaction solution. A more polar solution should increase the value of K_1 and decrease k_2.

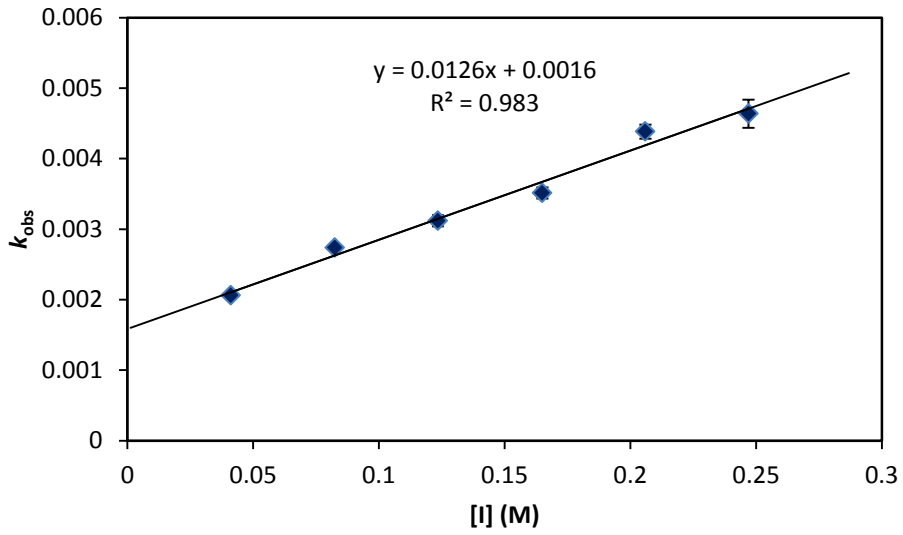

Figure 5.11. Plot of k_{obs} vs [iodide] for thermolysis of **25**, 80 °C, C_6H_5I. [29] = 0.00824 M.

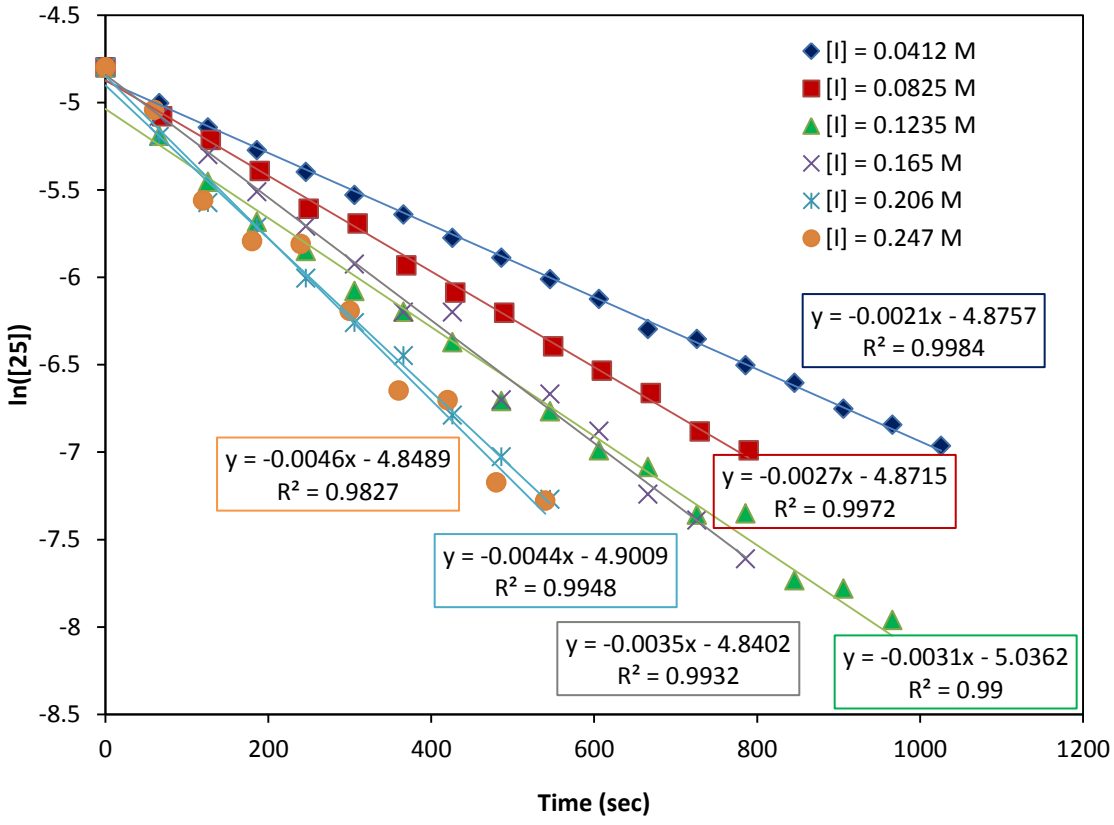

Figure 5.12. First order kinetic plot for the decomposition of **25** with added iodide, 80 °C, C_6H_5I.

When [N(*n*-Bu)$_4$][BF$_4$] was added without adding iodide ions, a second order kinetic dependence on **25** was observed (Figure 5.13). This kinetic behavior would result if under these conditions, the primary path of C-I bond formation is via N_3 (or N_2). Note that when iodide is not added to the reaction, it must come from **25** itself (the first step in path N_1). If we assume that k_4 [29'] >> k_2[A] under these conditions (k_2 decreases with increasing ionic strength), then nucleophilic attack is primarily at **25**' rather than A, giving the rate expression (3).

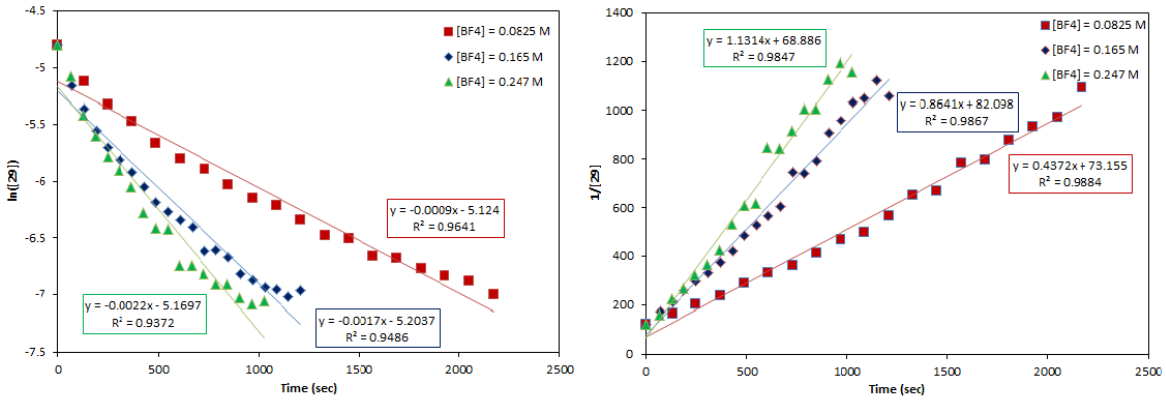

Figure 5.13. Comparison of fit for first order reaction (left) and second order reaction (right) for the reaction of **25** with [N(*n*-Bu)$_4$]BF$_4$, 80˚C, C_6H_5I .

SSA on [I]: $k_1[25] - k_{-1}[A][I] + k_4[25'][I] + k_2[A][I] = 0$

$$[I] = \frac{k_1[25]}{(k_{-1}[A] + k_4[25'] + k_2[A])}$$

$$\frac{-d[25]}{dt} = \frac{d[C]}{dt} = K_3k_4[25][I] \quad ([25'] = K_3[25])$$

Substituting [I]:

$$\frac{-d[25]}{dt} = \frac{k_1 K_3 k_4 [25]^2}{(k_{-1}[\mathrm{A}] + k_4[25'] + k_2[\mathrm{A}])}$$

If k_4[28'] >> k_2[A] (k_2[A] should be disfavored as polarity increases):

$$\frac{-d[25]}{dt} = \frac{k_1 K_3 k_4 [25]^2}{(k_{-1}[\mathrm{A}] + k_4[25'])}$$

$$\frac{-d[28]}{dt} = k_{\mathrm{obs}}[25]^2 \quad \text{where } k_{\mathrm{obs}} = \frac{k_1 K_3 k_4}{k_{-1}[\mathrm{A}] + k_4[25']} \qquad (3)$$

If reassociation of iodide is again much faster than nucleophilic (k_{-1}[A] >> k_4[28']), then the rate expression reduces that shown below thus explaining the second-order kinetics. Note that [A] is expected to be a small steady state value.

$$\frac{-d[25]}{dt} = k_{\mathrm{obs}}[25]^2 \quad \text{where } k_{\mathrm{obs}} = \frac{K_3 k_4}{k_{-1}[\mathrm{A}]} \qquad (4)$$

This analysis of the mechanism is important as it shows that C-I bond formation can occur by a path involving nucleophilic attack by external iodide (N_3 or N_2). This insight suggests that the coupling reaction should not be specific to iodide and that other C-X bonds (e.g. C-O, C-S, C-N, etc.) may be obtainable by the addition of suitable nucleophiles.

5.5 Reaction of 25 with KOAc

As C(sp^3)-OAc reductive elimination had previously been observed from Pt^{IV} systems,[3c] the thermolysis of **25** in the presence of added acetate ions was investigated. However, in contrast to the reaction of **25** with added iodide, no C-X coupling was observed. Instead the reaction of **25** with acetate at room temperature resulted in the displacement of one of the iodide ligands along with the central oxygen of the DPEphos ligand to generate complex **30** bearing a κ^2-acetate ligand (Figure 5.14).

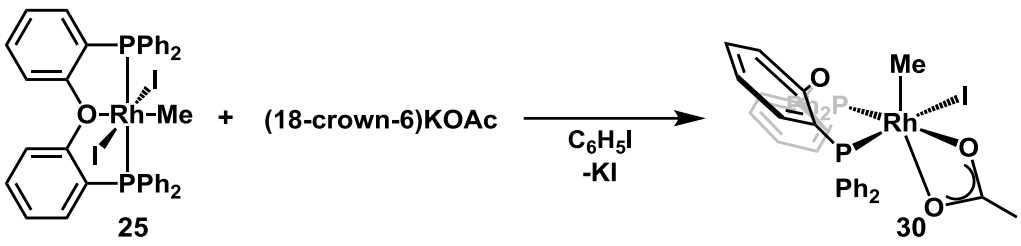

Figure 5.14. Reaction of **25** with KOAc resulting in the displacement of one iodide and the formation of complex **30**.

The ^{31}P NMR spectrum of **30** was markedly different than that of **25**, exhibiting an ABX spin system with $J_{Rh\text{-}P}$ = 135 Hz and 139 Hz and $J_{P\text{-}P}$ = 22 Hz. The small P-P coupling is consistent with two cis-phosphines,[8] suggestive that the DPEphos ligand is no longer binding Rh in a meridional fashion. The small phosphorus coupling to the methyl ligand in the ^{1}H NMR spectrum (C_6H_5I) (dt) ($J_{Rh\text{-}H}$ = 4.87 Hz, $J_{P\text{-}H}$ = 2.25) is consistent with the methyl ligand being cis to the two phosphines. Increasing the amount of acetate to 5 equiv. resulted in no further reaction; only one of the iodide ligands was substituted to yield **30**. A crystal suitable for X-ray diffraction was grown and the solid state structure (Figure 5.15) is consistent with the solution state structure. The oxygen moiety of the DPEphos ligand is no longer coordinated to Rh and the acetate ligand is bound in a κ^2-fashion. Thermolysis of **30** in iodobenzene up to 120 °C, with or without additional added acetate (5 equiv.), did not result in C-O coupling. However, the facile substitution of acetate for iodide at room temperature suggests that an iodide ligand in **25** is labile.

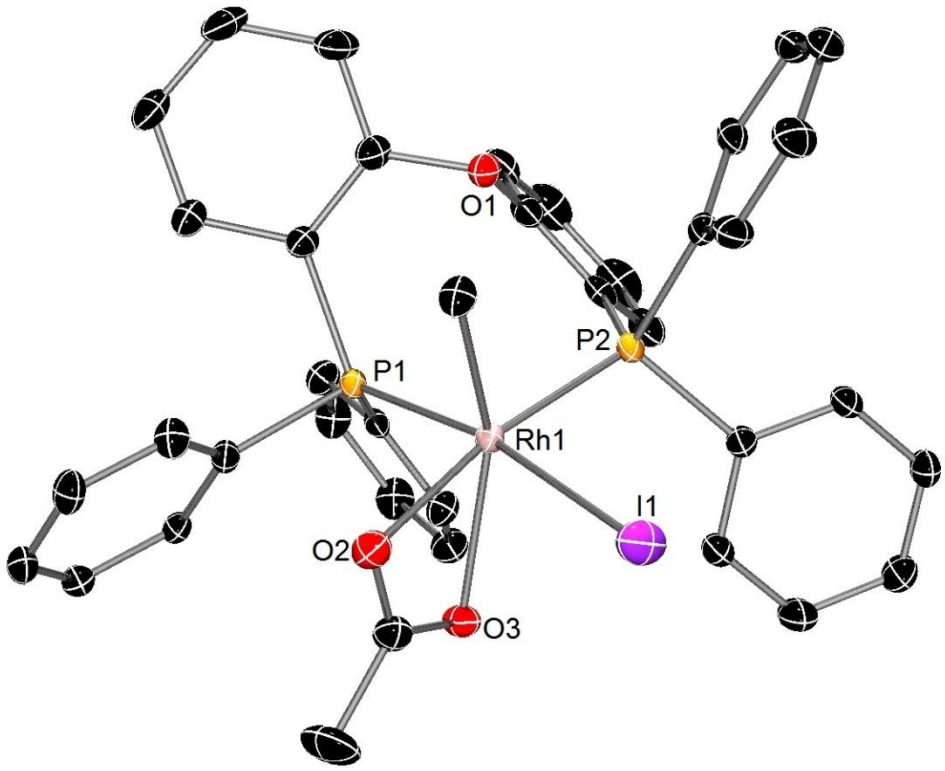

Figure 5.15. ORTEP of **30** shown with thermal ellipsoids at 50% probability level. The hydrogen atoms have been omitted for clarity. Selected bond lengths (Å) and angles (˚): Rh(1)-C(1) = 2.072(4), Rh(1)-I(1) = 2.7168(4), Rh(1)-O(2) = 2.123(3), Rh(1)-O(3) = 2.341(3), Rh(1)-P(1) = 2.29971(10), Rh(1)-P(2) = 2.2680(10). P(1)-Rh(1)-P(2) = 97.19(4), O(3)-Rh(1)-O(2) = 58.39(11).

5.6 C(sp^3)-N coupling

Notably, when nitrogen nucleophiles were added to solutions in C_6H_5I (or C_6D_5Br) of **25,** C(sp^3)-N coupling was observed**.** The addition of various amines resulted in quantitative formation of the *N*-methylamine product and **28** (or **28-Br**)[11] at *room temperature*. In

previous examples of reported C(sp^3)-N coupling, sulfonamides have generally been required,[3,4] but here, reaction of **25** with both piperidine and morpholine in bromobenzene-d_5 resulted in the corresponding *N*-methylamine product and **28-Br** (Figure 5.16).

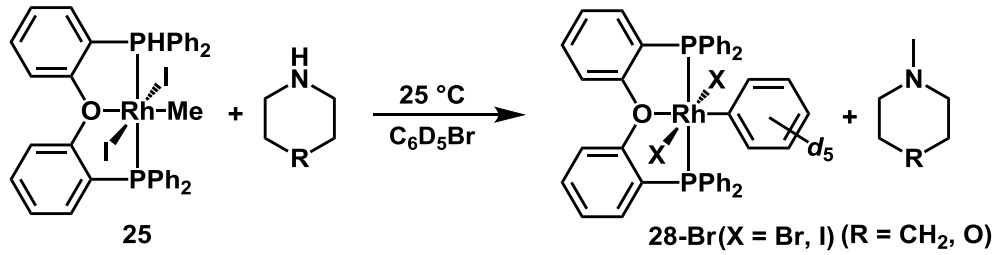

Figure 5.16. C(sp^3)-N coupling form **25** with morpholine and piperidine.

Reaction of **25** with less nucleophilic amines, such as isopropylamine, resulted in the observation of methyl iodide at intermediate time points (Figure 5.17). Over time, the methyl iodide was completely consumed to generate *N*-methylisopropylamine and *N*,*N*-dimethylisopropyl amine. It was surprising to see MeI formation from **25** at room temperature since our earlier experiments to achieve MeI reductive elimination without amine required heating. This led us to consider additional involvement of amine in promotion of the C-I coupling reaction.

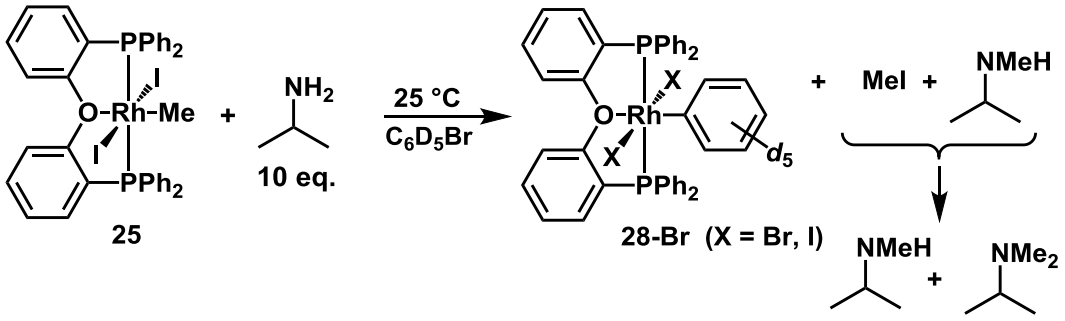

Figure 5.16. Reaction of **25** with isopropylamine forms methyl iodide which subsequently reacts to form the products shown.

Three mechanisms are proposed for the C(sp^3)-N bond forming reaction (Figure 5.17). Path N_3' represents the direct attack of amine at the rhodium methyl (this could happen with or without opening the chelating ligand) to form the C-N bond. Oxidative addition of aryl halide then forms the observed Rh product. In path N_4, the amine first replaces the iodide to form cationic intermediate **B** and then there are two potential paths from intermediate **B** depending on the nucleophilicity of the amine. More nucleophilic amines can attack the Rh-Me group of **B** directly whereas iodide can attack **B** in the presence of less nucleophilic amines to produce MeI.[12] Further reaction of the amine with MeI would generate methyl amine product.

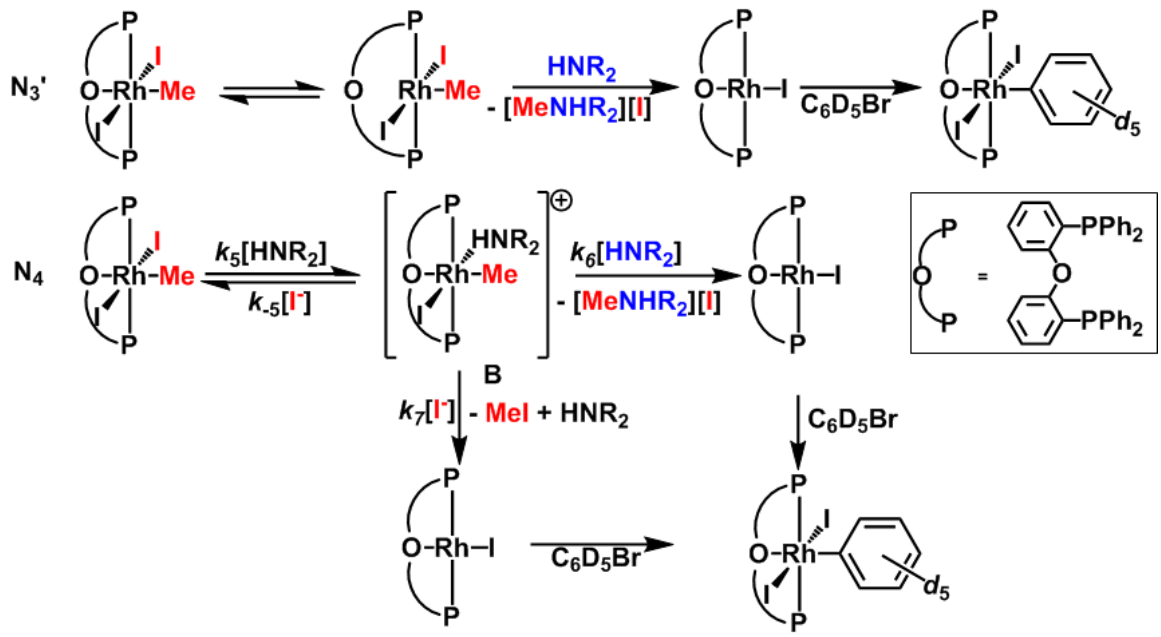

Figure 5.17. Possible pathways for C(sp^3)-N coupling from **25**.

The mechanisms shown in Figure 5.17 for C-N bond formation should exhibit different kinetic behavior. Thus, a kinetic investigation of the reaction of **25** with morpholine under pseudo-first order conditions ([morpholine] = 0.055 to 0.44 M; [**25**] = 0.011 M) was

performed. As shown in Figure 5.18 (first order kinetic plots are shown in Figure 5.19), the data are consistent with a second order dependence on morpholine. This kinetic behavior is inconsistent with N_3' (which should show a first-order dependence) but is expected for the pathway N_4, as shown in equation 5.

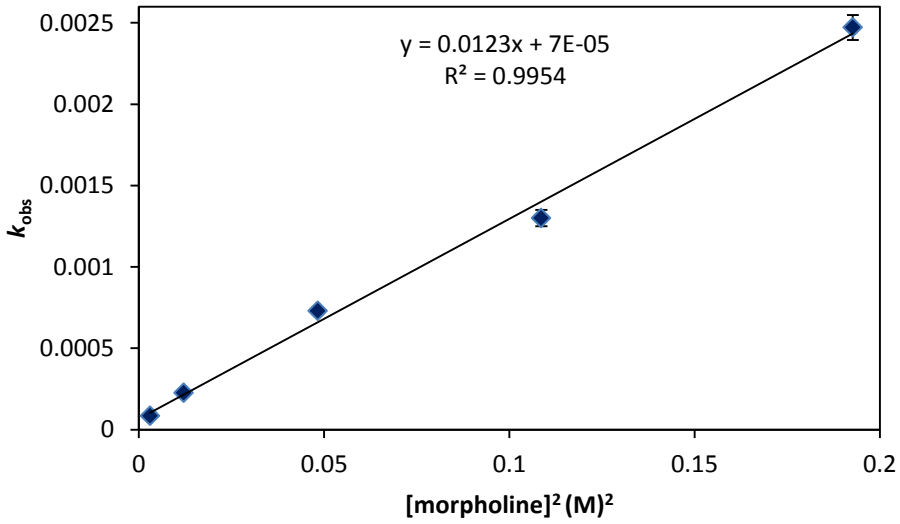

Figure 5.18. Plot of k_{obs} vs [morpholine]^2 for reaction of **25** with morpholine in C_6D_5Br. [1] = 0.01099 M.

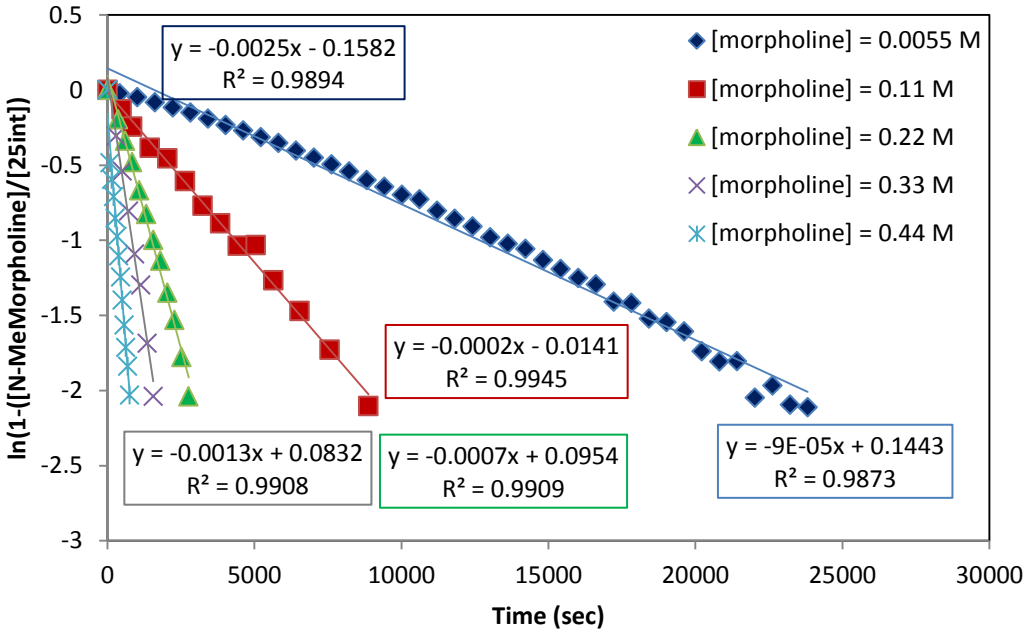

Figure 5.19. First order kinetic plots for reaction of **25** with morpholine, 25 ˚C, C_6D_5Br. Reaction progress was followed by the appearance of *N*-methylmorpholine in all cases except [morpholine] = 0.44 M. In this case the morpholine signal was too intense for accurate integration of the product and the disappearance of the Rh-Ar was monitored.

$$\frac{-d[25]}{dt} = \frac{d[\mathrm{C}]}{dt} = k_6[\mathrm{B}][\mathrm{HNR_2}]$$

$$K_5 = \frac{[\mathrm{B}][\mathrm{I}]}{[25][\mathrm{HNR_2}]}, [\mathrm{B}] = \frac{K_5[25][\mathrm{HNR_2}]}{[\mathrm{I}]}$$

Substituting [B]:

$$\frac{-d[25]}{dt} = k_{obs}[25][\mathrm{HNR_2}]^2 \quad \text{where } k_{\mathrm{obs}} = \frac{K_5 k_6}{[\mathrm{I}]} \qquad (5)$$

Mechanism N_4 also accounts for the acceleration in the MeI elimination in the presence of amine. With amine present, reductive elimination of methyl iodide was observed to occur at room temperature whereas elevated temperatures were required in the absence of

amine. Attack of iodide at the cationic intermediate **B** is faster than attack of iodide at **25** or **25'** (mechanism N_2 or N_3, respectively).

5.7 C(sp^3)-S coupling

The reaction of **25** with sulfur nucleophiles was also investigated and C(sp^3)-S coupling as shown in Figure 5.20 was observed. Addition of 10 equiv. of sodium thiophenolate (with 18-crown-6) to **25** in bromobenzene-d_5 resulted in a color change from orange to red. This was accompanied by a broadening of the ^{1}H NMR resonances. Thioanisole was formed over the course of 100 min at room temperature in high yield (85 %). The rhodium product was fluxional on the NMR time scale at room temperature. Upon cooling to 220 K, an ABX spin system was observed in the ^{31}P NMR spectrum, similar to that observed for the product of **25** with acetate. Based on this data, we propose the DPEphos ligand coordinates in a similar fashion as in **30**. Complex **31** was also prepared independently by reaction of **26** with excess NaSPh in THF.

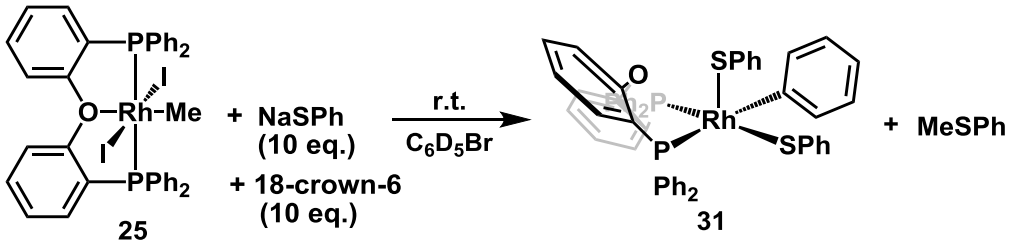

Figure 5.20. Reaction of **25** with NaSPh to form **31** and MeSPh.

5.8 Summary

The Rh^{III}-Me complex **25** undergoes methyl iodide reductive elimination via two competing mechanisms involving S_N2 attack by iodide at both cationic and neutral Rh^{III}-Me

species. The demonstration of bond formation via nucleophilic attack on the starting complex allowed the room temperature functionalization of the methyl ligand with both sulfur and nitrogen nucleophiles forming new C(sp^3)-S and C(sp^3)-N bonds, respectively. Notably, a second order dependence on morpholine was observed, consistent with the direct attack at the Rh^{III}-Me.

Experimental

General considerations

All manipulations were carried out under air-free conditions in a N_2 drybox or using standard Schlenk techniques. Solvents were dried by passage through two columns of activated alumina (THF) or passage through one column of alumina and one column of Q5 reactant (pentane). Iodobenzene was degassed and stored over 3 Å molecular sieves. Deuterated solvents were purchased from Cambridge Isotope Laboratories and dried over CaH_2 (dichloromethane-d_2), sodium/ benzophenone (THF-d_8) or 3 Å molecular sieves (bromobenzene-d_5). All other chemicals were purchased from Sigma-Aldrich and used as received. $[Rh(COE)_2Cl]_2$[13] was synthesized according to a published procedure. NMR spectra were recorded using Bruker AV300, AV500, or AV700 spectrometers. ^{1}H NMR and $^{13}C\{^1H\}$ NMR spectra were referenced to residual solvent signals relative to TMS and are reported in parts per million (ppm). $^{31}P\{^1H\}$ NMR spectra were referenced to H_3PO_4 (external) set to 0 ppm. Coupling constants are reported in Hz. Analytical data were obtained from the CENTC Elemental Analysis Facility at the University of Rochester, funded by NSF CHE-0650456. Reported data is an average of two samples.

(DPEphos)RhMe(I)$_2$ (25). [Rh(COE)$_2$Cl]$_2$ (199 mg, 0.147 mmol) and DPEphos (210 mg, 0.390 mmol) were weighed into a 10 mL sealable glass vessel and dissolved in THF (5 mL). The reaction mixture was stirred for one hour during which an orange solid precipitated. The volatiles were removed *in vacuo* and methyl iodide (c.a. 3 mL) was vacuum transferred into the flask. The reaction was stirred for 3 hours at ambient temperature. The volatiles were removed *in vacuo* yielding an orange solid (190 mg, 0.21 mmol) which was washed with pentane (3 x 5 mL). Crystals suitable for X-ray crystallography were grown by layering a concentrated solution of **25** in dichloromethane with pentane at -35 ℃. $^{31}P\{^1H\}$ NMR (283 MHz, 298 K, THF-d_8) δ 13.2 (d, $J_{Rh\text{-}P}$ = 103.8). ^1H NMR (700 MHz, 298 K, THF-d_8) δ 7.73 (2H, m, Ar-*H*), 7.70 – 7.65 (8H, bm, Ar-*H*), 7.63 (2H, m, Ar-*H*), 7.48 (2H, m, Ar-*H*), 7.35 – 7.29 (12H, Ar-*H*), 7.20 (2H, t, *J* = 7.5, Ar-*H*), 2.22 (3H, dt, $J_{Rh\text{-}H}$ = 4.9, $J_{Rh\text{-}P}$ = 2.6, Rh-CH_3). $^{13}C\{^1H\}$ NMR (176 MHz, 298 K, THF-d_8) δ 159.3 (t, *J* = 5.4) , 136.1 (bs), 135.6 (s), 134.8 (bs), 132.1 (s), 130.4 (s), 128.3 (t, *J* = 21.2), 127.9 (t, *J* = 5.0), 124.7 (s), 117.9 (s), -12.35 (dt, $J_{Rh\text{-}C}$ = 19.7 Hz, $J_{P\text{-}C}$ = 5.8, Rh-*C*H_3). Anal. Calcd. for $C_{37}H_{31}I_2OP_2Rh$: C, 48.82; H, 3.43. Found: C, 48.91; H, 3.51.

(DPEphos)RhMe(OTf)$_2$ (26). This complex was prepared on a NMR scale and not isolated. Complex **25** (4 mg, 0.0044 mmol) and AgOTf (2.3 mg, 0.009 mmol) were weighed into a NMR tube fitted with a Teflon pin. CD_2Cl_2 was vacuum transferred into the tube resulting in a faint yellow solution and with precipitate. $^{31}P\{^1H\}$ NMR (202 MHz, 298 K, CD_2Cl_2) δ 34 (bm).

(DPEphos)RhMe(NR$_2$)$_2$ (27). This complex was prepared on a NMR scale and not isolated. Complex **25** (5.9 mg, 0.006 mmol) and AgOTf (3.4 mg, 0.013 mmol) were weighed into a vial. CH_2Cl_2 (~2 mL) was added and the solution was stirred for 10 min. A solution change

from orange to yellow was accompanied by the precipitation of a white solid. The solution was filtered through celite and benzophenone hydrazone (5.1 mg, 0.026 mmol) was added. The volatiles were removed and C_6D_6 was vacuum transferred into the tube for NMR analysis. $^{31}P\{^1H\}$ NMR (202 MHz, 298 K, C_6D_6) δ 35.0 (dd, $J_{Rh\text{-}P}$ = 158.9 Hz, $J_{P\text{-}P}$ = 43.6 Hz), 32.6 (dd, $J_{Rh\text{-}P}$ = 151.5 Hz, $J_{P\text{-}P}$ = 43.6 Hz). ^1H NMR (500 MHz, 298 K, C_6D_6) δ 2.09 (3H, bm, Rh-C*H*$_3$).

(DPEphos)RhPh(I)$_2$ (28). Complex **25** (23 mg, 0.025 mmol) was dissolved in iodobenzene (c.a. 3 mL) and transferred to a sealable glass vessel. The solution was heated at 80 ˚C for 14 hours. The resulting orange solution was added dropwise to pentane to precipitate the product as an orange solid (22.2 mg, 0.0226 mmol). $^{31}P\{^1H\}$ NMR (283 MHz, 298 K, THF-d_8) δ 16.1 (d, $J_{Rh\text{-}P}$ = 106.9). ^1H NMR (700 MHz, 298 K, THF-d_8) δ 7.79 (2H, m, Ar-*H*), 7.65 (4H, m, Ar-*H*), 7.60 – 7.53 (8H, Ar-*H*), 7.48 (2H, m, Ar-*H*), 7.33 (4H, t, *J* = 7.3, Ar-*H*), 7.26 (8H, t, *J* = 7.5, Ar-*H*), 7.16 (2H, t, *J* = 7.5, Ar-*H*), 6.65 (1H, t, *J* = 7.3, Ar-*H*), 6.59 (2H, t, *J* = 7.4, Ar-*H*). $^{13}C\{^1H\}$ NMR (176 MHz, 298 K, THF-d_8) δ 159.2 (m), 146.4 (m), 137.2 (bs), 133.9 (s), 132.0 (s), 130.8 (s), 130.0 (t, *J* = 22.2), 128.0 (t, *J* = 5.1), 125.9 (s), 125.1 (s), 122.7 (s), 117.3 (s). Anal. Calcd. for $C_{42}H_{33}I_2OP_2Rh$: C, 51.88; H, 3.42. Found: C, 51.60; H, 3.34.

(DPEphos)Rh(*p*-tolyl)IBr (29). Complex **25** (23 mg, 0.025 mmol) was dissolved in *p*-bromotoluene and transferred to a sealable glass vessel. The solution was heated at 80 ˚C for 14 hours. The resulting orange solution was added dropwise to pentane to precipitate the product as an orange solid (23.5 mg, 0.025 mmol). Crystals suitable for X-ray crystallography were grown by layering a concentrated solution of **29** in *p*-bromotoluene with pentane. $^{31}P\{^1H\}$ NMR (283 MHz, 298 K, THF-d_8) δ 19.5 (d, $J_{Rh\text{-}P}$ = 107). ^1H NMR

(700 MHz, 298 K, THF-d_8) δ 7.81 – 7.65 (4H, Ar-*H*), 7.62 – 7.54 (8H, Ar-*H*), 7.52 – 7.47 (2H, Ar-*H*), 7.40 – 7.13 (16H, Ar-*H*), 6.44 (m, 2H, Ar-*H*), 2.17 (3H, Ar-CH_3). $^{13}C\{^1H\}$ NMR (176 MHz, 298 K, THF-d_8) δ 159.1 (m), 143.8 (m), 136.9 (bm), 136.1 (bm), 135.0 (s), 132.2 (s), 131.8 (s), 131.5 (s), 131.3 (s), 130.8 (s), 130.6 (s), 130.4 (s), 128.8 (t, J = 21.9), 128.0 (t, J = 5), 127.9 (t, J = 5), 127.1 (s), 125.0 (t, J = 2.7), 117.5 (t, J = 2.3), 20.5 (s). Anal. Calcd. for $C_{43}H_{35}BrIOP_2Rh$: C, 54.98; H, 3.76. Found: C, 54.57; H, 3.37.

(DPEphos)RhMeIOAc (30). Complex **25** (27 mg, 0.03 mmol) and potassium acetate (29 mg, 0.3 mmol) were transferred to a sealable glass vessel and dissolved in THF (5 mL). The reaction mixture was stirred at room temperature for 14 hours, during which time the solution became yellow. The solution was filtered through a Teflon syringe filter and the volatiles removed *in vacuo* yielding a yellow solid (25 mg, 0.03 mmol). Crystals suitable for X-ray crystallography were grown by layering a concentrated solution of **30** in benzene with pentane. $^{31}P\{^1H\}$ NMR (283 MHz, 298 K, THF-d_8) δ 36.2 (dd, $J_{Rh\text{-}P}$ = 133.7 Hz, $J_{P\text{-}P}$ = 22.5 Hz), 31.6 (dd, $J_{Rh\text{-}P}$ = 138.9 Hz, $J_{P\text{-}P}$ = 23.1 Hz). ^1H NMR (700 MHz, 268 K, THF-d_8) δ 8.89 (1H, m, Ar-*H*), 8.49 (1H, m, Ar-*H*), 7.69 (1H, t, J = 7.7, Ar-*H*), 7.60 (1H, m, Ar-*H*), 7.50 (1H, m, Ar-*H*), 7.48 – 7.40 (6H, Ar-*H*), 7.37 (2H, m, Ar-*H*), 7.30 (2H, m, Ar-*H*), 7.20 – 7.11 (4H, Ar-*H*), 7.06 (1H, m, Ar-*H*), 6.59 (1H, m, Ar-*H*), 6.88 (1H, m, Ar-*H*), 6.83 (1H, m, Ar-*H*), 6.50 (1H, dd, J = 8.1, 4.0, Ar-*H*), 6.40 (1H, m, Ar-*H*), 6.31 (1H, t, J = 7.6, Ar-*H*), 6.17 (1H, m, Ar-*H*), 5.92 (1H, m, Ar-*H*), 1.95 (3H, dt, $J_{Rh\text{-}H}$ = 5.1, $J_{P\text{-}H}$ = 2.5, Rh-CH_3), 1.00 (3H, s, Rh-OOCCH_3). $^{13}C\{^1H\}$ NMR (176 MHz, 298 K, THF-d_8) δ 184.90 (d, J = 4.7), 159.92 (d, J = 5.7), 158.55 (d, J = 6.8), 139.12 (bs), 138.56 (s), 137.75 (s), 137.69 (s), 137.42 (s), 136.19 (bs), 134.36 (t, J = 2.5), 133.60 (m), 133.23 (s), 133.20 (s), 133.05 (bs), 132.32 (bs), 130.96

(d, J = 2.5), 130.67 (bs), 130.45 (d, J = 2.5), 130.33 (s), 130.05 (s), 129.19 (s), 129.02 (s), 128.88 (s), 128.84 (s), 128.76 (s), 128.68 (s), 128.62 (s), 128.36 (d, J = 8.8), 128.24 (d, J = 10.62), 127.04 (d, J = 10.98), 126.76 (d, J = 6.4), 126.49 (d, J = 6.4), 125.58 (d, J = 5.3), 124.57 (d, J = 7.4), 122.57 (s), 122.35 (s), 119.48 (d, J = 4.5), 23.54 (d, J = 4.09, Rh-OOC*C*H_3), 3.79 (ddd, J = 22.1, 9.2, 4.7, Rh-*C*H_3). Anal. Calcd. for $C_{39}H_{34}I_2O_3P_2Rh$: C, 55.60; H, 4.07. Found: C, 56.01; H, 4.55.

Acquisition of kinetic data

Kinetic data was obtained by dissolving appropriate amounts of **25** and an internal standard (trimethoxybenzene or hexamethyldisiloxane) in iodobenzene (or bromobenzene-d_5) in a J. Young style NMR tube and following the reactions by ^{1}H NMR spectroscopy. For example, **25** (3 mg, 0.0033 mmol) was dissolved 0.4 mL of iodobenzene. A solvent suppression pulse program was used for samples in iodobenzene and samples were locked onto a capillary of C_6D_6 placed inside the NMR tube. An initial ^{1}H NMR spectrum was obtained at 298 K. For thermolysis reactions, the tube was removed from the NMR probe and the probe was heated to 253 K and allowed to equilibrate for 10 min. The tube was reinserted and spectra (1 pulse) were acquired at 60 second time intervals. For reaction of **25** (3 mg, 0.0033 mmol) with [N(*n*-Bu)$_4$]I and/or [N(*n*-Bu)$_4$]BF_4 (in 0.4 mL iodobenzene), the disappearance of the Rh-Me resonance was monitored. For reaction of **25** (4 mg, 0.0044 mmol) with amines (in 0.4 mL bromobenzene-d_5), the appearance of *N*-methylamine was monitored, as there was overlap between the Rh-Me resonance and the amine resonance.

Crystallographic information

Table 5.1. Crystal data and structure refinement for complexes **25**, **29**, and **30**.

	25	**29**	**30**
Empirical formula	C38 H33 Cl2 I2 O P2 Rh	C43 H35 Br I O P2 Rh	C42 H37 I O3 P2 Rh
Formula weight	995.19	939.37	881.47
Temperature	100(2) K	100(2) K	120(2) K
Wavelength	0.71073 Å	0.71073 Å	0.71073 Å
Crystal system	Monoclinic	Monoclinic	Monoclinic
Space group	*P* 2_1/c	*C* 2/c	*P* 2_1/n
Unit cell dimensions	a = 12.551(2) Å, α= 90°.	a = 12.6322(10) Å, α= 90°.	a = 13.8558(8) Å, α= 90°.
	b = 14.785(2) Å, β= 90.638(8)°.	b = 14.7078(14) Å, β= 94.445(4)°.	b = 16.7013(9) Å, β= 98.532(3)°.
	c = 19.348(3) Å, γ = 90°.	c = 19.7418(18) Å, γ = 90°.	c = 15.9056(9) Å, γ = 90°.
Volume	3590.2(10) $Å_3$	3656.8(6) $Å_3$	3640.0(4) Å3
Z	4	4	4
Density (calculated)	1.841 Mg/m_3	1.706 Mg/m_3	1.608 Mg/m3
Absorption coefficient	2.464 mm_{-1}	2.526 mm_{-1}	1.444 mm-1
F(000)	1936	1856	1764
Crystal size	0.16 x 0.11 x 0.05 mm_3	0.08 x 0.03 x 0.03 mm_3	0.18 x 0.15 x 0.09 mm3
Theta range for data collection	2.13 to 34.51°.	2.07 to 28.34°.	1.92 to 26.56°.
Index ranges	-20<=h<=19, -21<=k<=22, -30<=l<=30	-16<=h<=16, -19<=k<=19, -26<=l<=26	-17<=h<=17, -20<=k<=20, -19<=l<=19
Reflections collected	221659	143174	107563
Independent reflections	14207 [R(int) = 0.0438]	4550 [R(int) = 0.1074]	7520 [R(int) = 0.0413]
Completeness to theta = 25.00°	99.10%	100.00%	99.30%
Max. and min. transmission	0.8867 and 0.6939	0.9281 and 0.8235	0.8810 and 0.7810
Refinement method	Full-matrix least-squares on F_2	Full-matrix least-squares on F_2	Full-matrix least-squares on F2
Data / restraints / parameters	14207 / 31 / 458	4550 / 0 / 228	7520 / 0 / 444
Goodness-of-fit on F2	1.034	1.02	1.082
Final R indices [I>2sigma(I)]	R1 = 0.0260, wR2 = 0.0631	R1 = 0.0287, wR2 = 0.0547	R1 = 0.0408, wR2 = 0.1124
R indices (all data)	R1 = 0.0337, wR2 = 0.0672	R1 = 0.0485, wR2 = 0.0605	R1 = 0.0446, wR2 = 0.1149
Largest diff. peak and hole	1.883 and -0.957 $e.Å_{-3}$	0.472 and -0.641 $e.Å_{-3}$	1.804 and -2.208 e.Å-3

Methodology

Solution by direct methods (SHELXS, SIR97[14]) produced a complete heavy atom phasing model consistent with the proposed structures. The structures were completed by difference Fourier synthesis with SHELXL97.[15,16] Scattering factors are from Waasmair and Kirfel[17]. Hydrogen atoms were placed in geometrically idealised positions and constrained to ride on their parent atoms with C---H distances in the range 0.95-1.00 Angstrom. Isotropic thermal parameters U_{eq} were fixed such that they were $1.2U_{eq}$ of their parent atom Ueq for CH's and $1.5U_{eq}$ of their parent atom U_{eq} in case of methyl groups. All non-hydrogen atoms were refined anisotropically by full-matrix least-squares.

Data collection for 25

A red prism, measuring 0.16 x 0.11 x 0.05 mm^3 was mounted on a loop with oil. Data was collected at -173^{o}C on a Bruker APEX II single crystal X-ray diffractometer, Mo-radiation.

Crystal-to-detector distance was 40 mm and exposure time was 5 seconds per frame for all sets. The scan width was 0.5^o. Data collection was 99.1% complete to 25^o in ϑ. A total of 221659 reflections were collected covering the indices, h = -20 to 19, k = -21 to 22, l = -30 to 30. 14207 reflections were symmetry independent and the R_{int} = 0.0438 indicated that the data was of better than average quality (0.07). Indexing and unit cell refinement indicated a primitive monoclinic lattice. The space group was found to be P $2_1/c$ (No.14).

The data was integrated and scaled using SAINT, SADABS within the APEX2 software package by Bruker.[18]

One dichormethane solvent per Rh-complex is disordered over 6 positions showing now specific interactions with any other moiety which may explain why it appears disordered.

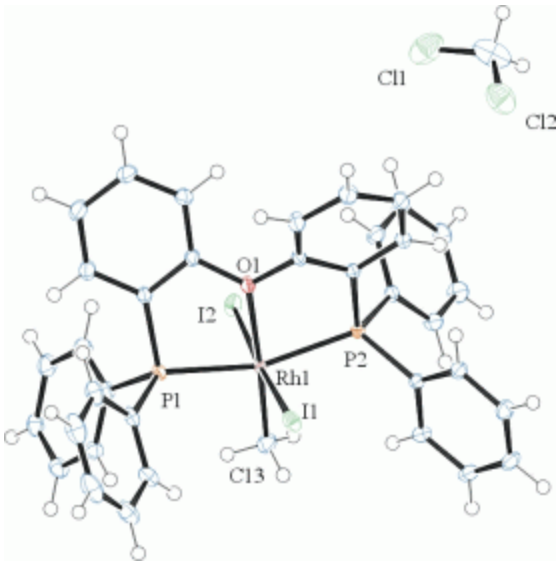

Figure 5.21. ORTEP of the structure with thermal ellipsoids at the 50% probability level. Disorder omitted for clarity.

Data collection for 29

An orange prism, measuring 0.08 x 0.03 x 0.03 mm^3 was mounted on a loop with oil. Data was collected at -173^{o}C on a Bruker APEX II single crystal X-ray diffractometer, Mo-radiation.

Crystal-to-detector distance was 40 mm and exposure time was 4 seconds per frame for all sets. The scan width was 0.5^o. Data collection was 100% complete to 25^o in ϑ. A total of 143174 reflections were collected covering the indices, h = -16 to 16, k = -19 to 19, l = -26 to 26. 4550 reflections were symmetry independent and the R_{int} = 0.1074 indicated appropriate data. Indexing and unit cell refinement indicated a C-centered monoclinic lattice. The space group was found to be C 2/c (No. 15).

The data was integrated and scaled using SAINT, SADABS within the APEX2 software package by Bruker.[6]

Iodine and Bromine are disordered at 1:1, indicating 3 possible molecular configurations: I/Br, Br_2, or I_2. The methyl hydrogen on the toluene are in the vicinity of the halides and disordered as well.

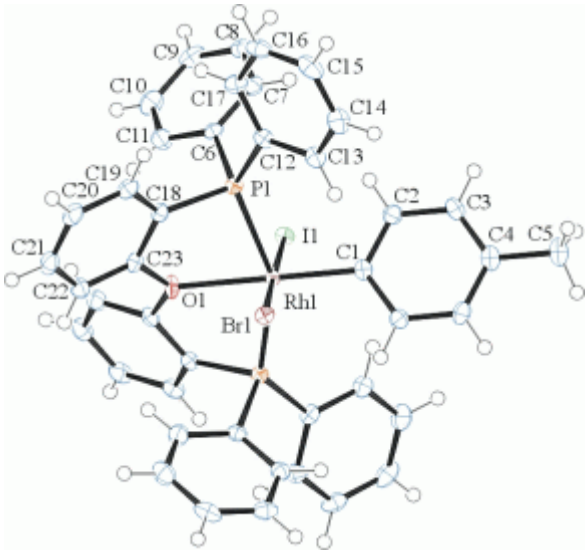

Figure 5.22. ORTEP of the structure with thermal ellipsoids at the 50% probability level. Disorder omitted for clarity.

Data collection for 30

A yellow piece measuring 0.18 x 0.15 x 0.090 mm^3 was mounted on a loop with oil. Data was collected at -153^oC on a Bruker APEX II single crystal X-ray diffractometer, Mo-radiation.

Crystal-to-detector distance was 40.00 mm and exposure time was 10 seconds per frame for all sets. The scan width was 0.5^o. Data collection was 99.3 % complete to 25^o in ϑ. A total of 107,563 reflections were collected covering the indices, h = -17 to 17, k = -20 to 20, l = -19 to 19. 7,520 reflections were symmetry independent and the R_{int} = 0.0413 indicated that the data was better than average quality (0.07). Indexing and unit cell refinement indicated a monoclinic lattice. The space group was found to be P 1 21/n 1 (No.14).

The data was integrated and scaled using SAINT, SADABS within the APEX2 software package by Bruker.[6]

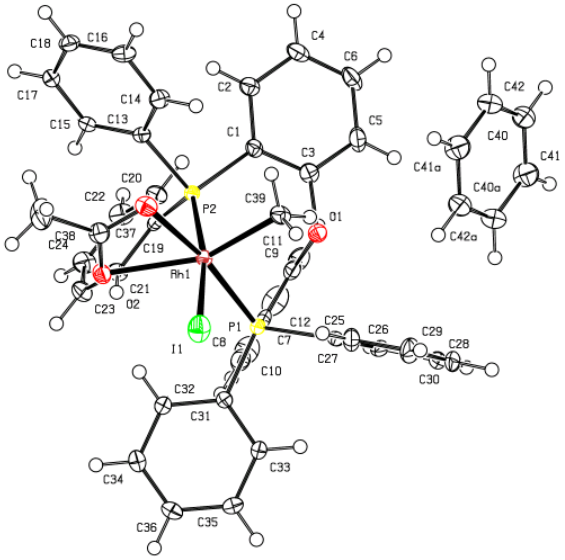

Figure 5.23. ORTEP of the structure with thermal ellipsoids at the 50% probability level.

Notes to Chapter 5

(1) (a) Cornils, B.; Herrmann, W. A. Applied Homogeneous Catalysis with Organometallic Compounds, VCH Publishers: New York, **1996**. (b) Hartwig, J. F. Organotransition Metal Chemistry: From Bonding to Catalysis, 1st ed.; University Science Books: California, **2010**.

(2) (a) Hartwig, J. F. *Acc. Chem. Res.* **1998**, *31*, 852. (b) Wolfe, J. P.; Wagaw, S.; Marcoux, J.-F.; Buchwald, S. L. *Acc. Chem. Res.* **1998**, *31*, 805.

(3) (a) Goldberg, K. I.; Yan, J.; Winter, E. L. *J. Am. Chem. Soc*. **1994**, *116*, 1573. (b) Goldberg, K. I.; Yan, J.; Breitung, E. M. *J. Am. Chem. Soc*. **1995**, *117*, 6889. (c) Williams, B. S.; Holland, A. W.; Goldberg, K. I. *J. Am. Chem. Soc*. **1999**, *121*, 252. (d) Frech, C. M.; Milstein, D. *J. Am. Chem. Soc*. **2006**, *128*, 12434. (e) Khusnutdinova, J. R.; Newman, L. L.;

Zavalij, P. Y.; Lam, Y.-F.; Vedernikov, A. N. *J. Am. Chem. Soc*. **2008**, *130*, 2174. (f) Scott, V. J.; Labinger, J. A. Bercaw, J. E. *Organometallics* **2010**, *29*, 4090. (g) Crosby, S. H.; Thomas, H. R.; Clarkson, G. J.; Rourke, J. P. *Chem. Commun*. **2012**, *48*, 5775. (h) Crosby, S. H.; Clarkson, G. J.; Rourke, J. P. *Organometallics*, **2012**, *31*, 7256. (i) Feller, M.; Diskin-Posner, Y.; Leitus, G.; Shimon, L. J. W.; Milstein D. *J. Am. Chem. Soc*. **2013**, *155*, 11040. (j) O'Reilly, M. E.; Pahls, D. R.; Webb, J. R.; Boza, N. C.; Majumdar, S.; Hoff, C. D.; Groves, J. T.; Cundari, T. R. Gunnoe, T. B. *Dalton Trans*. **2014**, *43*, 8273. (k) O'Reilly, M. E.; Pahls, D. R.; Cundari, T. R.; Gunnoe, T. B. *Organometallics* **2014**, *33*, 6504.

(4) (a) Lin, B. L.; Clough, C. R.; Hillhouse, G. L. *J. Am. Chem. Soc.* **2002**, *124*, 2890. (b) Pawlikowski, A. V.; Getty, A. D.; Goldberg, K. I. *J. Am. Chem. Soc.* **2007**, *129*, 10382. (c) Marquard, S. L.; Rosenfeld, D. C.; Hargwig, J. F. *Angew. Chem.* **2010**, *122*, 805. (d) Hanley, P. S.; Marquard, S. L.; Cundari, T. R. Hartwig, J. F. *J. Am. Chem. Soc.* **2012**, *134*, 15281. (e) Pérez-Temprano, M. H.; Racowski, J. M.; Kampf, J. W.; Sanford, M. S. *J. Am. Chem. Soc.* **2014**, *136*, 4097. (f) Camasso, N. M.; Sanford, M. S. *Science* **2015**, *347*, 6227.

(5) Pawley, R. J.; Moxham, G. L.; Dallanegra, R.; Chaplin, A. B.; Brayshaw, S. K.; Weller, A. S.; Willis, M. C. *Organometallics* **2010**, *29*, 1717.

(6) Prepared analogously to reported bisphosphine Rh^{I} complexes: Gellrich, U.; Meißner, A.; Steffani, A.; Kähny, M.; Drexler, H.-J.; Heller, D.; Plattner, D. A.; Breit, B. *J. Am. Chem.* **2014**, *136*, 1097.

(7) (a) Siedle, A. R.; Newmark, R. A.; Pignolet, L. H. *Organometallics* **1984**, *3*, 855. (b) Tulchinsky, Y.; Kozuch, S.; Saha, P.; Mauda, A.; Nisnevich, G.; Botoshansky, M.; Shimon, L. J. W.; Gandelman, M. *Chem. Eur. J.* **2015**, *21*, 7099.

(8) Pawley, R. J.; Huertos, M. A.; Lloyd-Jones, G. C.; Weller, A. S.; Willis, M. C. *Organometallics* **2012**, *31*, 5650.

(9) Grice, K. A.; Scheuermann, M. L.; Goldberg, K. I. *Top. Organomet. Chem.* **2011**, *35*, 1.

(10) W. M. Haynes, ed., *CRC Handbook of Chemistry and Physics*, 97th Edition (Internet Version **2017**), CRC Press/Taylor & Francis, Boca Raton, FL.

(11) At high concentration of morpholine (0.439 M) a new product was observed in the ^{31}P NMR spectrum in trace amounts. This product exhibited an ABX spin system, similar to **4** and **5**, suggesting one or both of the halides were replaced by morpholine.

(12) B' (κ^3 to κ^2 coordination of the DPEphos ligand) similar to 1' could also be involved.

(13) van der Ent, A.; Onderdelinden, A. L.; Schunn, R. A.; *Inorg. Synth*, **1990**, *28*, 90.

(14) (a) Altomare A, Burla C, Camalli M, Cascarano G L, Giacovazzo C, Guagliardi A, Moliterni AGG, Polidori G, Spagna R. *Journal of Applied Cryst*allography, **1999**, *32*, 115-119. (b) Altomare A, Cascarano G L, Giacovazzo C, Guagliardi A. *Journal of Applied Cryst*allography, **1993**, *26*, 343-350.

(15) Sheldrick GM. **(1997)** SHELXL-97, Program for the Refinement of Crystal Structures. University of Göttingen, Germany.

(16) Mackay, S.; Edwards, C.; Henderson, A.; Gilmore, C.; Stewart, N.; Shankland, K.; Donald, A. **(1997)** *MaXus: a computer program for the solution and refinement of crystal structures from diffraction data*. University of Glasgow, Scotland,.

(17) Waasmaier, D.; Kirfel, A. *Acta Crystallographica A.* **1995,** *51*, 416-430.

(18) Bruker (**2007**) APEX2 (Version 2.1-4), SAINT (version 7.34A), SADABS (version 2007/4), BrukerAXS Inc, Madison, Wisconsin, USA.